National Library of Canada
Canadian Theses Service
Ottawa, Canada
K1A 0N4

Bibliothèque nationale du Canada
Services des thèses canadiennes

CANADIAN THESES

THÈSES CANADIENNES

NOTICE

The quality of this microfiche is heavily dependent upon the quality of the original thesis submitted for microfilming. Every effort has been made to ensure the highest quality of reproduction possible.

If pages are missing, contact the university which granted the degree.

Some pages may have indistinct print especially if the original pages were typed with a poor typewriter ribbon or if the university sent us an inferior photocopy.

Previously copyrighted materials (journal articles, published tests, etc.) are not filmed.

Reproduction in full or in part of this film is governed by the Canadian Copyright Act, R.S.C. 1970, c. C-30. Please read the authorization forms which accompany this thesis.

AVIS

La qualité de cette microfiche dépend grandement de la qualité de la thèse soumise au microfilmage. Nous avons tout fait pour assurer une qualité supérieure de reproduction.

S'il manque des pages, veuillez communiquer avec l'université qui a conféré le grade.

La qualité d'impression de certaines pages peut laisser à désirer, surtout si les pages originales ont été dactylographiées à l'aide d'un ruban usé ou si l'université nous a fait parvenir une photocopie de qualité inférieure.

Les documents qui font déjà l'objet d'un droit d'auteur (articles de revue, examens publiés, etc.) ne sont pas microfilmés.

La reproduction, même partielle, de ce microfilm est soumise à la Loi canadienne sur le droit d'auteur, SRC 1970, c. C-30. Veuillez prendre connaissance des formules d'autorisation qui accompagnent cette thèse.

THIS DISSERTATION
HAS BEEN MICROFILMED
EXACTLY AS RECEIVED

LA THÈSE A ÉTÉ
MICROFILMÉE TELLE QUE
NOUS L'AVONS REÇUE

NL 339 (r. 88/01)

Canada

National Library of Canada
Canadian Theses Division
Ottawa, Canada
K1A 0N4

Bibliothèque nationale du Canada
Division des thèses canadiennes

0-315-24786-X

48

PERMISSION TO MICROFILM — AUTORISATION DE MICROFILMER

- Please print or type — Écrire en lettres moulées ou dactylographier

Full Name of Author — Nom complet de l'auteur
COLIN GEOFFREY KELLY

Date of Birth — Date de naissance
NOV. 5 1959

Country of Birth — Lieu de naissance
CANADA

Permanent Address — Résidence fixe
9135-143 ST. EDMONTON, ALTA.
T5R 0P5

Title of Thesis — Titre de la thèse
MULTILEVEL SIGNALLING AND DECISION-FEEDBACK EQUALIZATION FOR MULTIMODE OPTICAL FIBERS

University — Université
UNIV. OF ALTA.

Degree for which thesis was presented — Grade pour lequel cette thèse fut présentée
M.SC IN ELECTRICAL ENGINEERING

Year this degree conferred — Année d'obtention de ce grade
1984

Name of Supervisors — Nom du directeur de thèse
DR. P. GOUD / DR. C. ENGLEFIELD

Permission is hereby granted to the NATIONAL LIBRARY OF CANADA to microfilm this thesis and to lend or sell copies of the film.

The author reserves other publication rights, and neither the thesis nor extensive extracts from it may be printed or otherwise reproduced without the author's written permission.

L'autorisation est, par la présente, accordée à la BIBLIOTHÈQUE NATIONALE DU CANADA de microfilmer cette thèse et de prêter ou de vendre des exemplaires du film.

L'auteur se réserve les autres droits de publication; ni la thèse ni de longs extraits de celle-ci ne doivent être imprimés ou autrement reproduits sans l'autorisation écrite de l'auteur.

~~JUNE 12 198~~

Date
JUNE 12 1984

Signature
Colin G Kelly

NL-91 (4/77)

THE UNIVERSITY OF ALBERTA

MULTILEVEL SIGNALLING AND DECISION-FEEDBACK EQUALIZATION FOR MULTIMODE OPTICAL FIBERS

by

© COLIN G. KELLY

A THESIS

SUBMITTED TO THE FACULTY OF GRADUATE STUDIES AND RESEARCH

IN PARTIAL FULFILMENT OF THE REQUIREMENTS FOR THE DEGREE

OF MASTER OF SCIENCE

DEPARTMENT OF ELECTRICAL ENGINEERING

EDMONTON, ALBERTA

FALL 1984

THE UNIVERSITY OF ALBERTA

RELEASE FORM

NAME OF AUTHOR COLIN G. KELLY

TITLE OF THESIS MULTILEVEL SIGNALLING AND DECISION-FEEDBACK EQUALIZATION FOR MULTIMODE OPTICAL FIBERS

DEGREE FOR WHICH THESIS WAS PRESENTED MASTER OF SCIENCE

YEAR THIS DEGREE GRANTED FALL 1984

Permission is hereby granted to THE UNIVERSITY OF ALBERTA LIBRARY to reproduce single copies of this thesis and to lend or sell such copies for private, scholarly or scientific research purposes only.

The author reserves other publication rights, and neither the thesis nor extensive extracts from it may be printed or otherwise reproduced without the author's written permission.

(SIGNED) Colin G. Kelly

PERMANENT ADDRESS:

C/o D. H. KELLY........
...9135-143 ST.........
..EDMONTON, ALTA. CANADA
T5R 0P5

DATED ..June....11.....1984

THE UNIVERSITY OF ALBERTA

FACULTY OF GRADUATE STUDIES AND RESEARCH

The undersigned certify that they have read, and recommend to the Faculty of Graduate Studies and Research, for acceptance, a thesis entitled MULTILEVEL SIGNALLING AND DECISION-FEEDBACK EQUALIZATION FOR MULTIMODE OPTICAL FIBERS submitted by COLIN G. KELLY in partial fulfilment of the requirements for the degree of MASTER OF SCIENCE in ELECTRICAL ENGINEERING.

Paul A. Goud

Supervisor

Colin G. Englefield

Supervisor

G. D. Cormack

Wo-Sang Young

Date 84 06 04

Abstract

In this thesis, multilevel PAM signalling with decision-feedback equalization (DFE), for digital communication over a multimode optical fiber, is investigated. This investigation starts with a theoretical comparison of multilevel and binary signalling based on a derivation of the theoretical signalling capacities of a bandlimited channel possessing shot noise. A more applied comparison is then made through consideration of binary and 4 level signalling over hypothetical multimode fiber channels, both with and without DFE. This comparison indicates that 4 level signalling with DFE can offer bit rate - distance products with multimode fibers comparable to that obtainable with binary signalling over single-mode fibers. The choice of DFE is defended by a theoretical comparison to the linear zero-forcing and minimum mean-squared error equalizers. Also, an upper bound on the error propagation effect of DFE, for multilevel PAM systems, is derived; although this bound is pessimistic, it does indicate the strong dependence of this error propagation on the number of signal levels and the number of significant feedback taps. The potential data rate increase obtainable for a dispersion-limited fiber system, with feedback equalized multilevel signals, is demonstrated in an experimental 4 level PAM system having one tap of DFE. The system error rates, as a function of the received optical power and the data rate, are theoretically predicted through computer analysis, and these predictions are verified by their close agreement with the measured system performance. A data rate close to 5bits/Hz of channel bandwidth is demonstrated with the simple experimental system. Finally, concluding remarks summarize some of the concepts developed throughout the thesis, and recommendations for further research in this area are given.

Acknowledgements

I wish to express my appreciation and respect to the following:

- Dr. P. A. Goud and Dr. C. G. Englefield for their help in defining the project and their continuous support, advice, and interest.
- Mr. Bert Telder, for his competent technical assistance and helpful design suggestions throughout the experimental design stages of the project, as well as for his friendly support and interest throughout the whole of the project.
- The members of the examining committee for reviewing this work.
- All the members of the Optical and Microwave Communications group.
- The National Science and Engineering Research Council of Canada, as well as Alberta Government Telephones, for their support.

As well, I give my sincere thanks to my parents, family, and friends, for their encouragement and support. Thanks are also extended to my graduate course professors, particularily Dr. H. G. Schmidt-Weinmar, Dr. I. Filanovsky, and Dr. R. Rink, who kindled my interest in several thesis-related topics through their excellent tutoring.

TABLE OF CONTENTS

CHAPTER PAGE

1. INTRODUCTION..1
    1.1 Overview of Optical Fiber Communications............1
    1.2 Thesis Objectives....................................4
    1.3 Thesis Organization..................................6
    1.4 The General Optical Communication Link...............8
        1.4.1 The Data Encoder...............................9
        1.4.2 The Signal Filter..............................13
        1.4.3 The Driver and Source..........................13
        1.4.4 The Detector and Preamplifier..................14
        1.4.5 The Receiver Filter............................15
        1.4.6 The Main Amplifier.............................15
        1.4.7 Automatic Gain Control.........................16
        1.4.8 Timing Recovery................................16
        1.4.9 Equalization...................................16
        1.4.10 The Decoder...................................17
2. MULTILEVEL VS BINARY SIGNALLING...............................18
    2.1 Signal Capacities for Coded Signals..................18
        2.1.1 Dimensionality Theorem.........................19
        2.1.2 Basic System Definitions.......................19
        2.1.3 Information Coding.............................20
        2.1.4 Comparison of Code Formats.....................22
    2.2 Present Fiber Optic Device Technology................32
        2.2.1 Fiber Technology...............................33
        2.2.2 Source Technology..............................42

2.2.3 Detector Technology........................45

2.3 Optical Fiber Multilevel Systems....................47

2.3.1 Component Specifications....................48

2.3.2 System Power Requirements....................49

2.3.3 System Design....................................51

3. SIGNAL FILTERING AND EQUALIZATION........................58

3.1 Filtering..60

3.1.1 Choice of the Pulse Shape....................60

3.1.2 The Optimum Receiver Filter for PAM Systems..66

3.1.3 Joint Design of the Transmitter and Receiver Filters........................70

3.2 Equalization in PAM Systems........................71

3.2.1 The Zero-Forcing Equalizer..................73

3.2.2 The Minimum Mean-Squared Error Equalizer.....76

3.2.3 Decision-Feedback Equalization...............79

3.2.4 Residual Distortion in the Equalizer Designs............................83

3.2.5 Equalizer Design Procedure Examples..........85

4. THE EXPERIMENTAL 4 LEVEL PAM SYSTEM......................89

4.1 The Optical Fiber....................................91

4.2 The Transmitter......................................92

4.3 The Optical Receiver.................................93

4.3.1 The Optical Detector and Preamplifier........96

4.3.2 The Main Amplifier and AGC Circuitry........108

4.3.3 The Decoder and Decision-Feedback Equalizer.................110

5. THEORETICAL EVALUATION OF THE EXPERIMENTAL SYSTEM.......118

5.1 Signal and Noise Levels.............................119

5.2 Channel Pulse Response Modelling....................120

5.3 Completely Equalized Pulse Analysis................126

5.4 Inclusion of ISI in the System Analysis............130

5.5 Ideal One-Tap Decision-Feedback Equalization.......134

5.6 Non-Ideal One-Tap Decision-Feedback Equalization...136

5.7 Limitations of the Analysis Methods................140

6. THEORETICAL AND EXPERIMENTAL SYSTEM PERFORMANCE.........142

6.1 The Experimental System Setup.......................142

6.2 The Optical Detector and Preamplifier..............147

6.3 Transmitter Performance and Fiber Characteristics..151

6.4 The AGC Amplifier..................................154

6.5 The Decoder..157

6.6 The Channel Pulse Responses........................157

6.7 Summary of the Analytic and Measured System Performance..........................162

7. SUMMARY AND CONCLUSIONS..................................174

APPENDIX A Calculation of Channel Capacities in the Presence of Shot Noise...................181

APPENDIX B Design of the Transimpedance Preamplifier.......187

APPENDIX C Listing of the PAM System Analysis Program......202

APPENDIX D An Upper Bound on the Propagation Effect of DFE.......................221

REFERENCES..226

LIST OF TABLES

TABLE PAGE

1.1 A linear K=2, N=4 binary block code......................10

2.1 Maximum repeater spacing for various system types, data rates, and signalling formats.......................55

4.1 Overall transmitter and receiver signal coding.........117

6.1 Expected and measured preamplifier parameters..........149

6.2 Expected and measured transmitter and fiber characteristics..............................153

6.3 Summary of the AGC amplifier performance...............156

6.4 Summary of the sampled pulse vectors used in the system analysis program....................161

6.5 Performed system tests.................................162

LIST OF FIGURES

FIGURE PAGE

1.1 Block diagram of a digital optical communication link...8

1.2 Three common signal formats for the binary data stream "1 0 0 1 0"....................11

2.1 Channel capacity for additive white noise and for A-level PAM signalling..........................25

2.2 Channel capacity for additive white and shot noise as defined by Eqn. 2.6 and for A-level PAM signalling..27

2.3 Material dispersion bandwidth vs. LED source and spectral width and wavelength for 1 km of 1300 nm multimode fiber......................................37

2.4 Receiver sensitivity vs. data rate with various optical detectors - binary signalling, BER = 10^{-9}......46

2.5 Channel length and capacity limits for the 850 nm 2/4 level system using both LED and LD optical sources with and without DFE...........................52

2.6 Channel length and capacity limits for the 1300 nm 2/4 level system using both LED and LD optical sources with and without DFE...........................53

3.1 The Sinc pulse shape in the time and frequency domains.............................61

3.2 The Raised-Cosine pulse for β = 0, 0.5, and 1.........63

3.3 The Duobinary pulse shape...............................65

3.4 DFE for ISI cancellation in Duobinary pulses...........65

3.5 System model for the optimum receiver filter design....66

3.6 System model for the optimum receiver filter design for additive white gaussian noise......................67

3.7 System model for joint design of the transmitter and receiver filters...................70

3.8 The tapped delay line structure with length (2L-1).....73

3.9 Equivalent system model for equalizer design...........74

3.10 The Decision-Feedback equalizer with a leading linear equalizer........................80

4.1 The experimental 4-level PAM system....................90

4.2 Transmitter schematic and coding.......................94

4.3 Equivalent optical detector/preamplifier combinations for noise level considerations.........................101

4.4 AC-Equivalent circuit for the preamplifier............103

4.5 Experimental optical detector/preamplifier circuit diagram...................................105

4.6 Expected transimpedance preamplifier frequency response...................................106

4.7 Schematic diagram of the experimental main amplifier, peak detector, and automatic gain control circuits....109

4.8 Decoder and equalizer block diagram for the experimental system..........................111

4.9 Comparator board schematic and coding................113

4.10 Timing board schematic and coding...................114

4.11 Feedback board schematic and coding.................116

5.1 Sampled-time channel response representation..........121

5.2 Definition of the "half-interval" channel response vector H'...........................123

5.3 Individual error probabilities for the 4 level system...............................128

6.1 The experimental 4 level PAM system test setup........143

6.2 Measured Fiber/ODP pulse responses....................160

6.3 Theoretical system performance summary................164

6.4 Theoretical and experimental system performance with one-tap non-optimum DFE..........................165

6.5 Theoretical and experimental system performance with no equalization.................................166

6.6 Theoretical and experimental system performance at 30 Mb/s...167

6.7 Theoretical and experimental system performance at 40 Mb/s...168

6.8 Received signal eye diagrams....................172

A.1 Decoder threshold and adjacent signal level...........181

A.2 Normalized Gaussian PDF centered about b_i..............181

A.3 Equidistant signal levels and thresholds for a 4 level PAM system with no shot noise.................182

A.4 Signal level spacing with/without shot noise..........183

B.1 Computer-optimized modified hybrid-pi model for the BFR90 bipolar transistor......................188

B.2 Small-signal preamplifier circuit using hybrid-pi transistor models..........................190

B.3 Emitter-current controlled, hybrid-pi common-base transistor model.........................191

B.4 Simplified preamplifier circuit model.................193

B.5 Preamplifier circuit with the CC stage completely analyzed..................................195

LIST OF ABBREVIATIONS

AGC - automatic gain control

APD - avalanche photodiode

AWGN - additive white gaussian noise

BCH - Bose-Chaudhuri-Hocquenghem

BDP - bandwidth-distance product

BER - bit error rate

CB - common base

CC - common collector

CE - common emitter

DFE - decision-feedback equalization

ECL - emitter-coupled logic

FET - field-effect transistor

FWHM - full width at half maximum (power)

HI - high-impedance

ISI - intersymbol interference

LD - laser diode

LED - light-emitting diode

MMSE - minimum mean-squared error

MSE - mean-squared error

NRZ - non-return to zero

ODP - optical detector and preamplifier

PAM - pulse-amplitude modulation

PDF - probability density function

PE - probability of error

PED - desired probability of error

PIN	- P-type, Intrinsic, N-type semiconductor sandwich
P-P	- peak-to-peak
RF	- radio frequency
RMS	- root-mean-square
RZ	- return to zero
SNR	- signal to noise ratio
TDL	- tapped delay line
TI	- transimpedance
TTL	- transistor-transistor logic
ZF	- zero-forcing

CHAPTER 1. INTRODUCTION

1.1 Overview of Optical Fiber Communications

The past decade has witnessed major developments in the field of telecommunications. The emergence of optical fiber as a reliable, economically attractive transmission medium has been one such development. The principal advantages of optical fiber over other transmission media are by now well established. No other medium offers as large a bandwidth with such a low attenuation. Also, fiber systems are immune to electromagnetic interference, offer higher security, and weigh less than coaxial systems. They are much smaller than coaxial cables, resulting in installation cost reductions. This is especially true for buried communication networks with limited duct area, such as those found in urban telephone networks.

The technology involved in fiber systems is young [1]. Consider, for example, semiconductor lasers; these devices are usually employed as the optical source for long haul systems. The development of the first semiconductor laser dates back to 1962 (Hall, Nathan *et al.*) [2,3]; the first room temperature continuous wave semiconductor laser was developed in 1970 (Hayashi *et al.*) [4], but it lasted only a few hours. Present devices can have mean lifetimes exceeding 10^5 hours [5].

Actual fiber technology for communications started later than semiconductor laser technology. In 1966, Kao and Hockam [6] showed theoretically that the attenuation found in glass was mainly due to impurities and not due to the glass itself.

This spurred on fiber research and, in 1970, Corning Glass Works produced a single mode fiber with less than 20 dB/km attenuation at wavelengths around 830 nm [7]. In 1972, a multimode fiber with an attenuation of less than 4 dB/km was achieved [8]. In 1976, fibers with attenuations of 1.6 dB/km were reported, close to the theoretical limit for 830 nm [9]. By operating at longer wavelengths, values of 0.25 dB/km and less are increasingly being reported, the best result currently being 0.16 dB/km for a single-mode fiber at a wavelength of 1.55 um [10,11,12,13].

Another result of research efforts is the development of fibers with increasingly larger bandwidths. Although the best attenuation results for silica glasses have been achieved at 1.55 um, the best bandwidth results presently occur at a wavelength in the vicinity of 1.3 um, where the material dispersion of these glasses passes through zero. Using optical sources having a narrow linewidth and a center wavelength corresponding to this zero material dispersion wavelength, the material dispersion becomes quite small. In this situation, the bandwidth of multimode fibers is limited by modal dispersion. To-date, the highest modal bandwidth for a multimode fiber is 9.7 GHz-km, which is still an order of magnitude below the theoretical limit [14,15]. Single-mode fibers have no modal dispersion; hence, their bandwidth at this wavelength is extremely large and is in the order of 200 GHz-km or higher (depending on the spectral purity of the source) [16,17].

There exists, however, a demand for still longer range, higher capacity communication systems; an example of this is a trans-Atlantic fiber optic link with no underwater repeaters. Even with present fiber technology, most systems have a maximum data rate and repeater distance dictated by dispersion or attenuation limitations. Consequently, much research is being devoted to reducing these limitations. The last few years have seen a shift in emphasis from multimode to single mode fiber development because of the much higher bandwidth available from the latter. For a majority of fiber applications, however, single mode technology is neither required nor economically viable as yet. Source and detector technologies have advanced in step with fiber development in order to provide higher optical launch power, transmitter reliability, narrower source spectral width, higher receiver sensitivity, and longer wavelength operation.

Equalization is commonly used in the optical receiver to increase a system's signalling capacity. Extensive theoretical work has been done on this subject, and applied to relatively low speed systems such as telephone subscriber links. However, so far only the simplest equalization schemes have been used with high data rate fiber optic systems. The most common method used is linear equalization, either in the frequency or the time domain. Recently, decision feedback equalization (DFE) (in which a pulse's postcursor intersymbol interference (ISI) terms are cancelled by feedback based on the pulse's decoded value) has been applied to binary optical systems [18,19]. To the author's knowledge, more sophisticated equalization approaches than this have not been applied to fiber systems.

Another method of increasing the attainable data rate over a channel is to adopt a signalling method which realizes more of the channel's ultimate capacity. One way of accomplishing this is to trade optical power for an increased bit rate per available channel bandwidth, through the use of multilevel signalling. Although experimental multilevel pulse amplitude modulated (PAM) systems have been tested, they have not yet been used much in actual service. However, the potential of multilevel signals is well recognized, as will be shown in Chapter 2 [20,21,22]. The problem with multilevel signals is that any ISI that occurs has a more detrimental effect on the system's performance than upon that of a binary system. However, equalization techniques that can be applied to binary systems are useful for multilevel systems as well.

1.2 Thesis Objectives

DFE and multilevel signalling have each been studied fairly extensively. To the author's knowledge, however, they have not yet been applied together to a dispersive fiber optic link in order to realize more of the channel's capacity, as compared to conventional binary signalling. Consequently, this thesis has the following objectives in mind:

1. To qualitatively show the increase in signalling capacity obtainable on a dispersion limited optical fiber link with multilevel PAM signals, in contrast to binary signals.

2. To design a multilevel PAM system for an experimental dispersive fiber channel. This system will include the following:

   a) adjustable signal levels

   b) adjustable receiver thresholds

   c) adjustable one-tap DFE

3. To obtain the noise levels and pulse shapes from the experimental system. The pulse shapes will be measured at various data rates, and the thermal and shot noise values will be compared to the expected values derived from the receiver design.

4. To develop an accurate system model based on the experimental measurements of the noise and pulse shapes. Optimum signal levels and receiver thresholds are to be determined for this model. The theoretical error rate versus power characteristics for this model will be found for the cases of complete equalization, DFE, and no equalization. The resulting error behavior will include shot noise, ISI effects, and DFE error propagation effects (caused by erroneous equalization when a reception error is made), and should accurately represent the experimental system behavior.

5. To compare the theoretical results with actual system results and to demonstrate the improvement offered by the application of multilevel signalling and DFE.

1.3 Thesis Organization

The remainder of this chapter is a brief introduction to general optical digital communication systems. Chapter 2 is concerned with the theoretical and practical advantages of multilevel signalling in conjunction with PAM systems. In order to present the practical advantages offered in an unbiased manner, a brief summary of fiber optic technology that is presently viable is included. This summary is useful in determining the repeater - spacing dispersion and attenuation limits, as a function of the bit rate, for multimode fiber systems. These limitations are derived assuming that DFE is to be used. This choice is justified in Chapter 3, where some of the background theory concerning equalization and the closely related topic of signal filtering is covered .

Chapter 4 is concerned with the experimental four level system design, with flexibility being the paramount consideration. Emphasis is placed on the receiver preamplifier design because of its fundamental effect on overall system performance. The equalizer design is comparatively straightforward and, although only a single-tap equalizer is used, the design can be extended to include multiple taps.

The quality of a communication system is partially indicated by its bit error rate (BER). In Chapter 5, theory and computer programs are developed for characterizing and optimizing a multilevel PAM system with regard to its error behavior. These programs determine the theoretical received optical power requirements as a function of the desired error rate for various pulse shapes and noise levels. In doing so, optimum values for various system parameters are calculated. The programs also include the possibility of complete equalization as well as partial ISI cancellation through one or more tap DFE. Application of the programs to the experimental system is described in Chapter 6.

Chapter 6 also reports the performance of the designed system. System parameters are adjusted in order to minimize the error rate for various optical levels and bit rates for the cases of no equalization and single-tap DFE. Measurement of the preamplifier transimpedance and thermal noise, along with shot noise values, allows the system to be analyzed by the program developed in Chap. 5. These analytic results agree closely with the experimental results obtained, thus supporting the analytical methods used. The experimental results demonstrate that, through the use of a 4 level signal and DFE, a significant increase in the data handing capacity of the fiber link is obtained. In Chapter 7, the concluding chapter, recommendations are given for the investigation of problems with multilevel PAM signalling and DFE with regard to potential practical payoffs.

1.4 The General Optical Digital Communication Link

Figure 1.1 depicts an optical communication link for digital data transmission. The following sections briefly describe the purpose of each of the stages in the link.

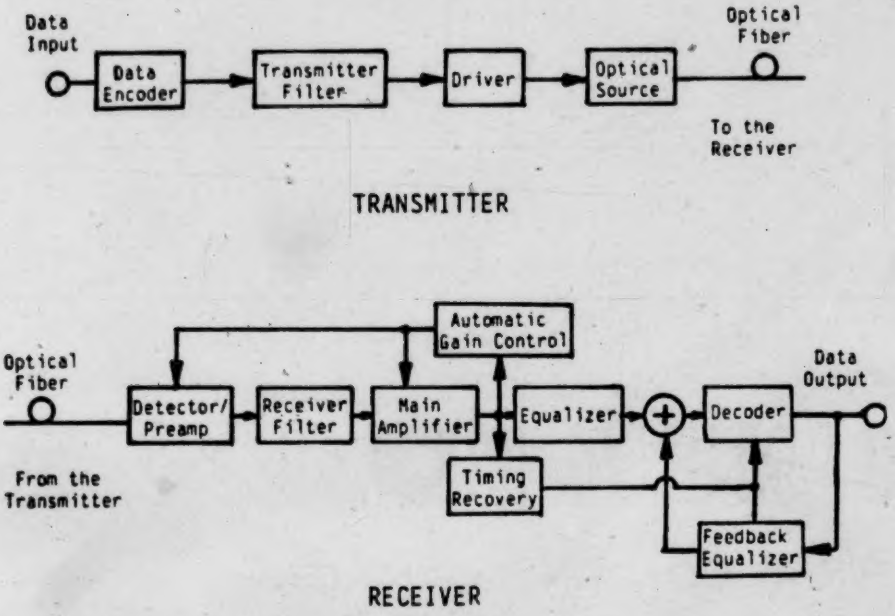
Data Input
Data Encoder
Transmitter Filter
Driver
Optical Source
Optical Fiber
To the Receiver
TRANSMITTER
Automatic Gain Control
Optical Fiber
Detector/ Preamp
Receiver Filter
Main Amplifier
Equalizer
Decoder
Data Output
From the Transmitter
Timing Recovery
Feedback Equalizer
RECEIVER

Fig. 1.1 Block Diagram of a digital optical communication link.

1.4.1 The Data Encoder

The encoder converts the outgoing data into a form more suitable for transmission over the desired channel. It usually includes some of the following functions:

a) Block or convolutional coding

b) Bit formatting

c) Bit coding

If a sequence of N data bits is transmitted without coding, and the probability of error per bit is p, then the probability of erroneous reception of one or more bits in the data stream, P_e, is given by [23]:

$$P_e = 1 - (1-p)^N$$

As an example, if $p = 10^{-5}$ and $N = 100$, then $P_e \cong 10^{-3}$. This error accumulation effect is eliminated through block or convolutional codes [23,24]. These codes add redundancy to the data, which increases the effective distance between individual code words. If the data rate is less than an appropriate bound [23] (which will be given in Chapter 2 for binary and multilevel signals) then, with appropriate coding, the error rate can be made arbitrarily small.

Block codes are a set of fixed length vectors (code words). Upon reception of a block of K data bits the coder produces an appropriate N bit output, where N is greater than K, by means of a look-up table or equivalent. An example of a K=2, N=4 linear binary block code is shown in Table 1.1:

Input Data	Output Data
00	1100
01	1001
10	0110
11	0011

Table 1.1 A linear K=2, N=4 binary block code.

Convolutional codes are generated by passing the data through a finite length shift register. The output data is obtained from algebraic combinations of the shift register data.

Both block and convolutional codes, in addition to adding redundancy, can add the capability to detect and possibly correct errors upon reception. Examples of binary block codes are Hamming, Golay, Hadamard, and Bose-Chaudhuri-Hocquenghem (BCH) codes. Nonbinary block and convolutional codes exist as well, an example being Reed-Solomon block codes.

Without proper bit formatting, two phenomena may occur due to poor data statistics:

1. In AC coupled systems, significant DC shifting may occur, causing an increase in the error rate for threshold crossing detectors.

2. In the reception of a data stream with few transitions from one level to another, timing information is lost and thus stable timing recovery becomes more difficult.

Three commonly used binary data formats are; return to zero (RZ), non-return to zero (NRZ), and Manchester or split-phase coding. Figure 1.2 illustrates each of these formats. [25]

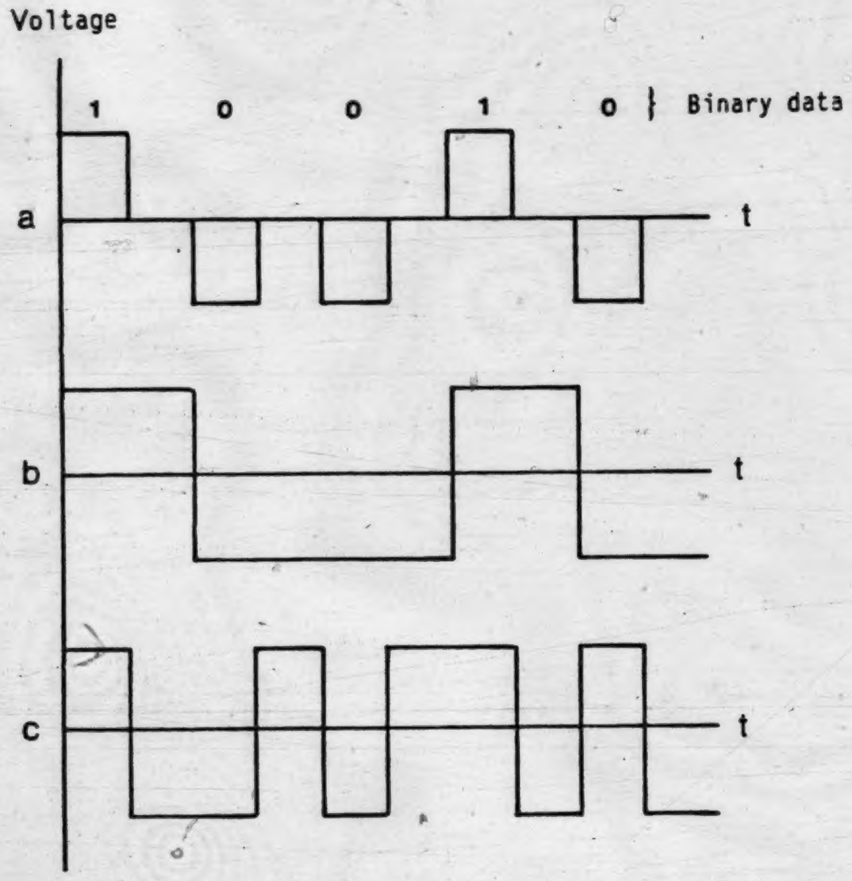
Voltage
1
0
0
1
0
Binary data
a
t
b
t
c
t

Figure1.2 Three common signal formats for the binary data stream " 1 0 0 1 0 ".

a) Return to zero format
b) Non - return to zero format
c) Manchester format

The NRZ format has the disadvantages of possible DC drift and loss of timing information. The RZ format ensures timing information, but still may have DC drift. Furthermore, it requires three levels and twice the bandwidth of the NRZ format. Manchester encoding overcomes both problems with a two level code, but again with a penalty in bandwidth requirements. Several other bit formats, such as alternate mark inversion, exist as well, with associated penalties.

Instead of converting from one bit format (usually NRZ) to another, a common practice is to scramble the data in a known fashion so that a certain amount of signal randomness is assured. Data scrambling results in no bandwidth or power penalty, and may be implemented in the block (or convolution) coder. In other words, proper block coding may ensure enough signal randomness so that a simple NRZ bit stream may be adequate for the particular system.

Bit coding may also be required in a system. In multilevel signalling, binary data is converted to multilevel data. Three level data is usually used, not to increase the bit rate for the given baud (symbol) rate, but to provide better data statistics, as discussed above. Other than this, most multilevel PAM systems use four or eight levels. Bit coding may also be used when signalling over dispersive channels, in order to help compensate for ISI. One such system involves duobinary signals, which will be discussed in Chapter 3. [26]

1.4.2 The Signal Filter

A signal filter may be used to shape and band-limit the signal before transmission in order to compensate for channel imperfections. Normally, it is designed for a particular channel, along with the receiver filter and, if present, the equalizer. Two different criteria for designing these filters are:

a) maximizing the received signal to noise ratio (SNR)

b) reducing the effects of ISI

Filtering is discussed in Chapter 3.

1.4.3 The Driver and Source

Conversion of an electrical signal to an optical signal occurs at the source. In fiber optic systems, the source is normally either a laser diode (LD) or a light emitting diode (LED). Performance of present LDs and LEDs is reviewed in Chapter 2.

The source obtains its power from the driver circuit. For optical sources, the driver usually consists of a medium to high power, low output impedance transistor array. LED drivers are relatively simple in comparison to LD drivers. Due to the thermal instability and degradation factors inherent in most LDs, stabilization of their optical output power must be provided by the driver circuitry. Also, LDs have a required threshold current before lasing starts; this threshold must be considered in the driver design.

The designs of the stages in the transmitter are interrelated. Obviously, the driver and source should match each other and the intended channel; less obvious is the effect of the source and channel on the data formatting, coding, and signal shape. As an example, for many sources, the maximum average power may be much lower than the maximum peak power, which implies that pulses shorter than the thermal time constant of the device are required for efficient use of the source. This requirement affects the signal shape and duty cycle, which in turn affects the proper filter and (if used) equalizer designs for the system.

1.4.4 The Detector and Preamplifier

The detector changes the optical power back into an electrical signal. For optical communication systems it is normally either a PIN (P-type, Intrinsic, N-type semiconductor sandwich) diode, avalanche photo-diode (APD), or phototransistor.

A preamplifier is needed when the received signal level is very low and hence requires level boosting with little noise penalty. To this end, preamplifiers are usually designed for a specified channel and detector. In optical receivers, from noise considerations, a silicon APD detector - bipolar transistor preamplifier typically has a superior performance compared to a PIN diode detector - field effect transistor (FET) preamplifier combination at short (0.83 um) wavelengths. At longer wavelengths (1.3, 1.5 um), however, silicon detectors are unusable, and other semiconductors such as Ge and InGaAs(P) must be used. A detailed discussion of optical detectors and preamplifiers is left to Chapter 4.

1.4.5 The Receiver Filter

As the bandwidth of a circuit is increased, its noise level also increases. Thus, receivers incorporate a filter to limit their bandwidth (with regard to the required signal bandwidth) and hence the noise. In some cases, enough filtering may be provided in the preamplifier through proper pole and zero placement in the preamplifier design. In other cases, more elaborate filtering is required to maximize the SNR as much as practicable. From noise considerations, the optimum filter is the matched filter. However, a matched filter, if realizable, requires an exact knowledge of the incoming signal characteristics; often, this information is not known. A more detailed consideration of the receiver filter design is left to Chapter 3.

1.4.6 The Main Amplifier

The preamplifier provides signal boosting with as low a noise penalty as is practicable. In the main amplifier design, control of signal distortion is more important than minimization of noise. It is usually assumed that enough gain has been provided by the preamplifier (if present), such that the main amplifier noise is negligible compared to the input signal and noise levels. Whereas a preamplifier is usually designed for a particular application, the main amplifier can normally be used for a much broader range of systems. Optical receiver amplifiers often incorporate automatic gain control to provide increased dynamic range.

1.4.7 Automatic Gain Control

In systems where the incoming signal level is not precisely known, automatic gain control (AGC) may be required. The gains of the amplifiers (and possibly the APD, if used, in an optical system) are adjusted to provide a constant output level. The AGC circuit includes a peak detector, comparator, and error amplifier. Through the use of AGC, receivers with a dynamic range of 40 dB or better have been realized [77].

1.4.8 Timing Recovery

In all but the simplest digital systems, timing recovery is required to provide a clock for the decoder and possibly the equalizer. Usually, timing information is derived from the data by means of very high-Q filters, phase-locked loops, or surface acoustic-wave devices. Timing recovery is a major consideration in system design, but is beyond the scope of this thesis. The experimental link outlined in Chapter 4 uses a delayed transmitter clock signal as the receiver clock.

1.4.9 Equalization

In systems where the baud (symbol) rate approaches the channel's Nyquist rate, significant ISI occurs. Proper transmitter and receiver filtering can help minimize this ISI. Complete elimination of ISI through filtering usually requires complicated and precise filters, as well as an exact knowledge of the channel characteristics. Often, the required filters are not physically realizable. Thus, for many systems, enough ISI still occurs that additional compensation measures are required. This compensation for ISI is termed equalization. Because of the importance of this topic to the thesis, it is covered in Chapter 3.

1.4.10 The Decoder

The decoder attempts to reconstruct the original data from the signal with as few errors as possible, and acts upon a signal which has been distorted and corrupted by noise. It usually involves some sort of decision making. In digital PAM systems these decisions are based on threshold detection, with the thresholds chosen to minimize the probability of error in decoding.

Besides decoding the received signal, the decoder may have the additional functions of error detection and monitoring. These functions are provided by the signal code and format - any violation of the coding rules upon reception indicates an error, and appropriate action can be taken.

The communication system discussed here is a typical model biased in design towards PAM systems. Specific aspects of this system will be considered in greater detail where they are germane to the thesis objectives.

CHAPTER 2. MULTILEVEL VERSES BINARY SIGNALLING

To appreciate the goals of the work presented in this thesis, it is important to understand the relative advantages and disadvantages of multilevel signalling compared to binary signalling. In certain situations, significant gains, in terms of the maximum data rate for a channel, may be achieved by adopting a multilevel transmission scheme; in other situations, multilevel signalling may offer no economic or practical advantages.

To clarify these situations, some fundamental communication theory is presented. Based on the results of this theory, the latter part of this chapter then indicates when it may be advantageous to use multilevel signalling in the light of present fiber optic technology.

2.1 Signal Capacities for Coded Signals

The reason for using multilevel signals is to increase the information handling capacity of a communication link. A brief study of maximum permissible data rates for a given channel and signalling method is needed to determine when the use of multilevel signals is justifiable. No attempt is made here to prove the stated results; proofs can be found in the references and tend to be tedious.

Wozencraft and Jacobs [23] cover the background communication theory pertaining to data rate limitations. This theory applies to a channel with a finite bandwidth (denoted by W, and for optical fiber systems, includes both the fiber bandwidth and the receiver bandwidth) and additive white gaussian noise (AWGN). Such a channel does not possess shot noise, which can have a larger variance than the background thermal noise in optical systems. Consequently, their results are presented here with appropriate extensions made to include the possibility of shot noise.

2.1.1 Dimensionality Theorem

The dimensionality theorem is based on theorems due to Shannon, Landau, and Pollak, with further work by Dollard.

Let the set of orthogonal waveforms that can be transmitted over the channel be designated $\{\varphi_j(t)\}$. Furthermore, limit each of these waveforms to:

a) duration T

b) have no more than η of its energy outside the frequency interval (-W,W). (Different bandwidth definitions result in different values for η.)

Then, the number of orthogonal waveforms, or dimensions, denoted by N, that can be accommodated by the channel is bounded by $2TW/(1-\eta)$.

2.1.2 Basic System Definitions

1. T, W, and η are defined in the dimensionality theorem.
2. D is the number of dimensions per second:

$D=N/T$, $D<2W/(1-\eta)$

3. Let the system data rate, in bits per second, be R. This data rate can be defined in bits per dimension, R_n, by the formula $R_n=R/D$. Defining the data rate in this manner allows comparison between different signal formats with regard to their potential ability in channel utilization.

4. The maximum signal energy per dimension is E_n.

5. The double-sided power spectral density and variance of the white noise is $N_o/2$.

6. The signal to noise ratio is E_n/N_o.

7. The set $\{\varphi_j(t)\}$ is the set of orthonormal waveforms used by the transmitter. An example, for T=2 and N=2, would be

$$\varphi_1 = u(t)-u(t-1)$$

$$\varphi_2 = u(t-1)-u(t-2)$$

where u(t) is the step function.

8. M is the total number of messages in the system. For example, if our information is either a binary 0 or 1 with no further coding, then M=2. If we group the binary data into 8 bit words, then $M=2^8$, or 256.

2.1.3 Information Coding

Chapter 1 mentioned some of the functions that may be performed by the transmitter encoder. Whatever the type of coding used to perform these functions, each possible message, M_i, is encoded by the transmitter into a signal S_i, which is eventually received and decoded. Thus, the $\{S_i\}$ has M members, each of which can be written in terms of the N orthogonal waveforms used by the transmitter:

$$S_i(t) = \sum_{j=1}^{N} b_{ij}(t) \text{ for } i=1 \text{ to } M.$$

With binary antipodal signalling, the b_{ij} are $\pm\sqrt{(E_n)}$. Also, $M < 2^N$. For antipodal multilevel signals with A levels (A=2 being the binary case), we define the b_{ij} to lie between $-\sqrt{(E_n)}$ and $+\sqrt{(E_n)}$. For example, a system with four equally spaced antipodal levels would have $b_{ij} = \pm\sqrt{(E_n)}$ or $\pm\sqrt{(E_n/3)}$. With multilevel signals, $M < A^N$.

Examples of two signal codes are:

a) Binary antipodal signals (A=2) with M=1, N=1:

M_1 = "yes" : $S_1(t) = +\sqrt{(E_n)}\,\varphi(t)$

M_2 = "no" : $S_2(t) = -\sqrt{(E_n)}\,\varphi(t)$

b) Multilevel signals, A=4, M=5, N=2:

M_1 = "a" : $S_1(t) = -\sqrt{(E_n)}\,\varphi_1(t) + \sqrt{(E_n)}\,\varphi_2(t)$

M_2 = "b" : $S_2(t) = -\sqrt{(E_n)}\,\varphi_1(t) - \sqrt{(E_n/3)}\,\varphi_2(t)$

M_3 = "c" : $S_3(t) = +\sqrt{(E_n/3)}\,\varphi_1(t) - \sqrt{(E_n)}\,\varphi_2(t)$

M_4 = "d" : $S_4(t) = +\sqrt{(E_n/3)}\,\varphi_1(t) + \sqrt{(E_n)}\,\varphi_2(t)$

M_5 = "e" : $S_5(t) = +\sqrt{(E_n)}\,\varphi_1(t) - \sqrt{(E_n/3)}\,\varphi_2(t)$

In general, there are many possible codes for a specified code format; the format for example b) being A=4, M=5, and N=2. Thus, when a code format is analyzed, this is done over the ensemble of possible codes following that format. When stating the probability of error for a code format, it is important to remember that it is an average; some codes will be superior and some worse.

2.1.4 Comparison of Code Formats

In this section, the theoretical error performance and signalling capacity of different code formats will be given, with the number of levels, A, being the variate. Wozencraft and Jacobs demonstrated that, for AWGN, the average probability of error for the ensemble of codes following a specific format is given by

$$P_e < 2^{-N(R_0-R_n)} \tag{2.1}$$

where R_0 is the exponential bound parameter for that format, and R_n is the data rate. For binary antipodal signals R_0 is:

$$R_0 = 1-\log_2[1+\exp(-E_n/N_0)] \tag{2.2}$$

For antipodal multilevel signals having A equidistant, equiprobable levels (which is a non-optimum situation, even for an AWGN channel), R_0 is:

$$R_0 = -\log_2[(1/A^2)\sum_{l=1}^{A}\sum_{n=1}^{A}\exp(-d_{lh}^2/4N_0)] \tag{2.3}$$

The parameter d_{lh} is the distance between the l^{th} and h^{th} levels. The situation corresponding to this expression is non-optimum because the probability of making an error,given the signal is either the maximum or minimum level,is half the probability of making an error for the other intermediate levels.

From expression 2.1, if the data rate, R_n, is less than the exponential bound R_0, the average probability of error can be made arbitrarily small for sufficiently large N. Tighter upper bounds than this have been derived, and consequently operation above the rate R_0 may be possible. However, it can be construed, for purposes of this discussion, to be an ultimate bound.

Equations 2.2 and 2.3 are for antipodal signals which lie between $\pm\sqrt{E_n}$. In optical systems, however, the signal levels are constrained to be one-sided. Extension of these equations to one-sided signalling can be done by shifting the signal levels so that they lie between 0 and $+2\sqrt{E_n}$. The associated distances between levels do not change with this translation. However, the maximum energy per dimension has increased from E_n to $4E_n$. This increase can be accounted for by inclusion of a 6 dB penalty when plotting R_o against E_n/N_o.

The R_o given by equations 2.2 and 2.3 can be compared to the ultimate channel capacity, which will be denoted by C_o, derived by Shannon [23]. Under the restriction of antipodal signalling with each signal having its maximum energy being N times E_n, this ultimate capacity (again for an AWGN channel), regardless of the coding scheme, is:

$$C_o = 0.5\log_2(1 + 2E_n/N_o) \tag{2.4a}$$

Extension of this result to one-sided signalling by including the associated 6 dB penalty produces:

$$C_o = 0.5\log_2(1 + E_n/(2N_o)) \tag{2.4b}$$

If the number of equally likely messages, M, is large, then:

1. If $R_n > C_o$, the probability of error is close to unity for every set of M transmitter signals.

2. If $R_n < C_o$, and optimum receivers are used, there exists a set of signals such that the probability of error can be made arbitrarily small.

Figure 2.1 depicts C_o and various R_o (for different number of signal levels) as a function of the maximum SNR per dimension. From this figure, the signal capacity of a binary system is less than that of a ternary system at a SNR of -12.0 dB or higher. In this region, the binary signalling capacity is "saturated". Below this region, it appears that multilevel signals are inferior to binary signals. This is true only for the case of multilevel signals incorporating equally probable, equidistant levels. By optimizing the probability of each level, multilevel signals can be optimized. Then, in no situation are they theoretically inferior to binary signalling. Of course, for low SNR's, the multilevel signals degenerate into binary signals. Graphically, inclusion of optimum level probabilities would result in the multilevel capacity curves shifting to the left and merging with the binary curve at low SNRs.

The results thus far are for systems having no shot noise. Optical systems, however, usually possess significant shot noise and thus have signal dependent noise variances. The overall noise variances for multilevel signals can be approximated by equation 2.5:

$$\sigma_i^2 = \sigma_o^2 + \xi b_i \qquad (2.5)$$

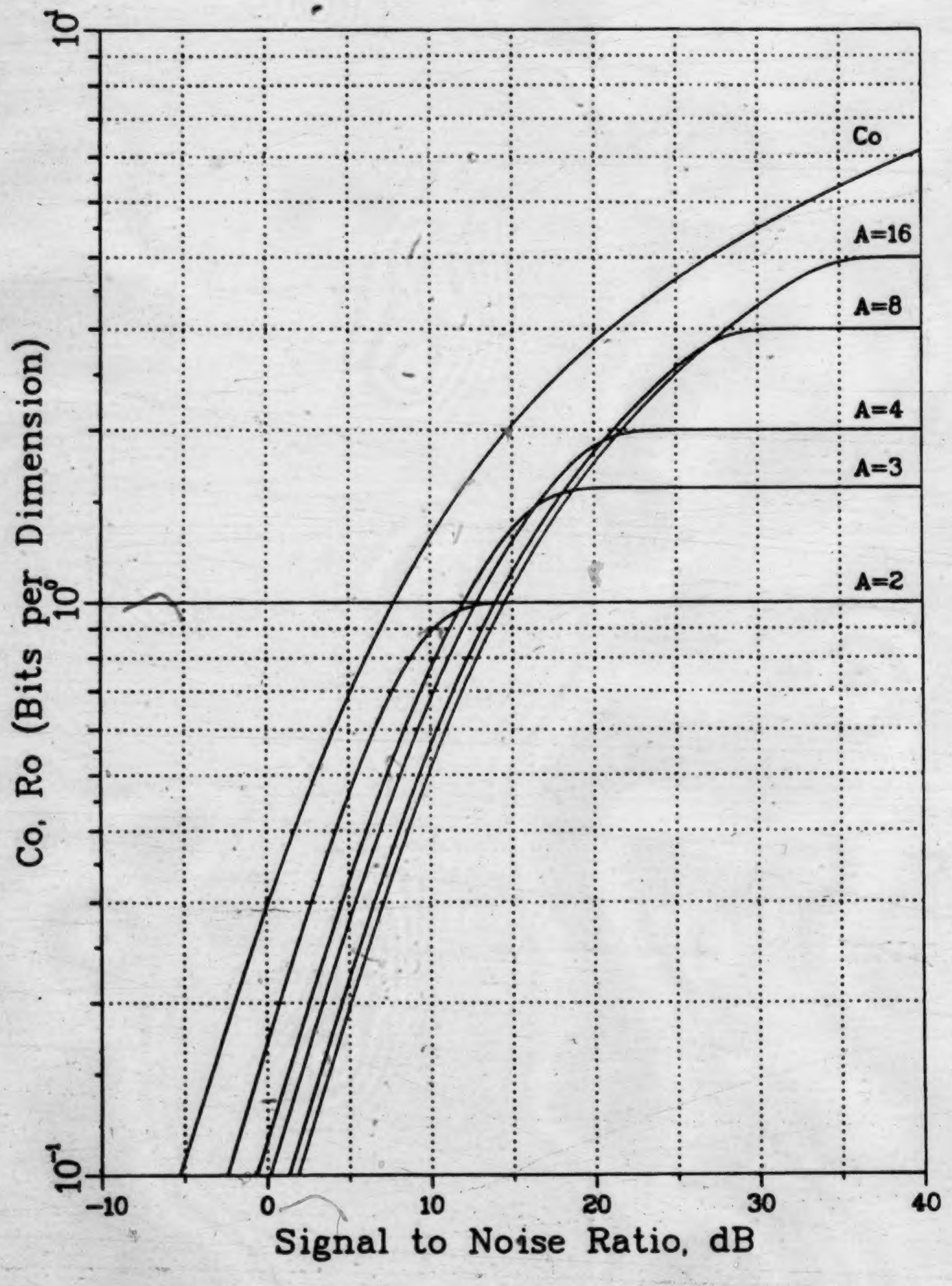

Fig. 2.1 Channel Capacity
for Additive White Noise
and for A-Level PAM Signalling

In this equation,

σ_i is the noise variance at the i^{th} signal level,
σ_0 is the noise variance in the absence of optical power (primarily due to thermal noise),
ξ is a shot noise parameter, and
b_i is the i^{th} signal level.

The derivation of (2.5) is left to Chapter 4 where the experimental preamplifier design is discussed. The equation shows that as the signal level is increased, the noise level also is increased. Obviously, this effect is detrimental to multilevel signalling and should be included in derivation of the signalling capacities. Finding comparable expressions to equations 2.3 and 2.4, however, is no simple task and well beyond the scope of this thesis. However, a point by point extension of equations 2.2 and 2.3 in order to include shot noise is fairly straightforward and is considered in Appendix A.

Chapter 6 includes measurements of the experimental preamplifier noise levels at various signal levels. Substitution of these results into equation 2.5 yields

$$\sigma_i^2 = (0.5\ \text{mV})^2 + 70\ \text{uV}\cdot b_i \qquad (2.6)$$

where σ_i and b_i are in volts. Figure 2.2 depicts the signal capacities equivalent to R_0 and C_0 for the noise defined by Eqn. 2.6. These capacities are designated by R_s and C_s in order to distinguish them from the R_0 and C_0 given for the case of no shot noise (Figure 2.1).

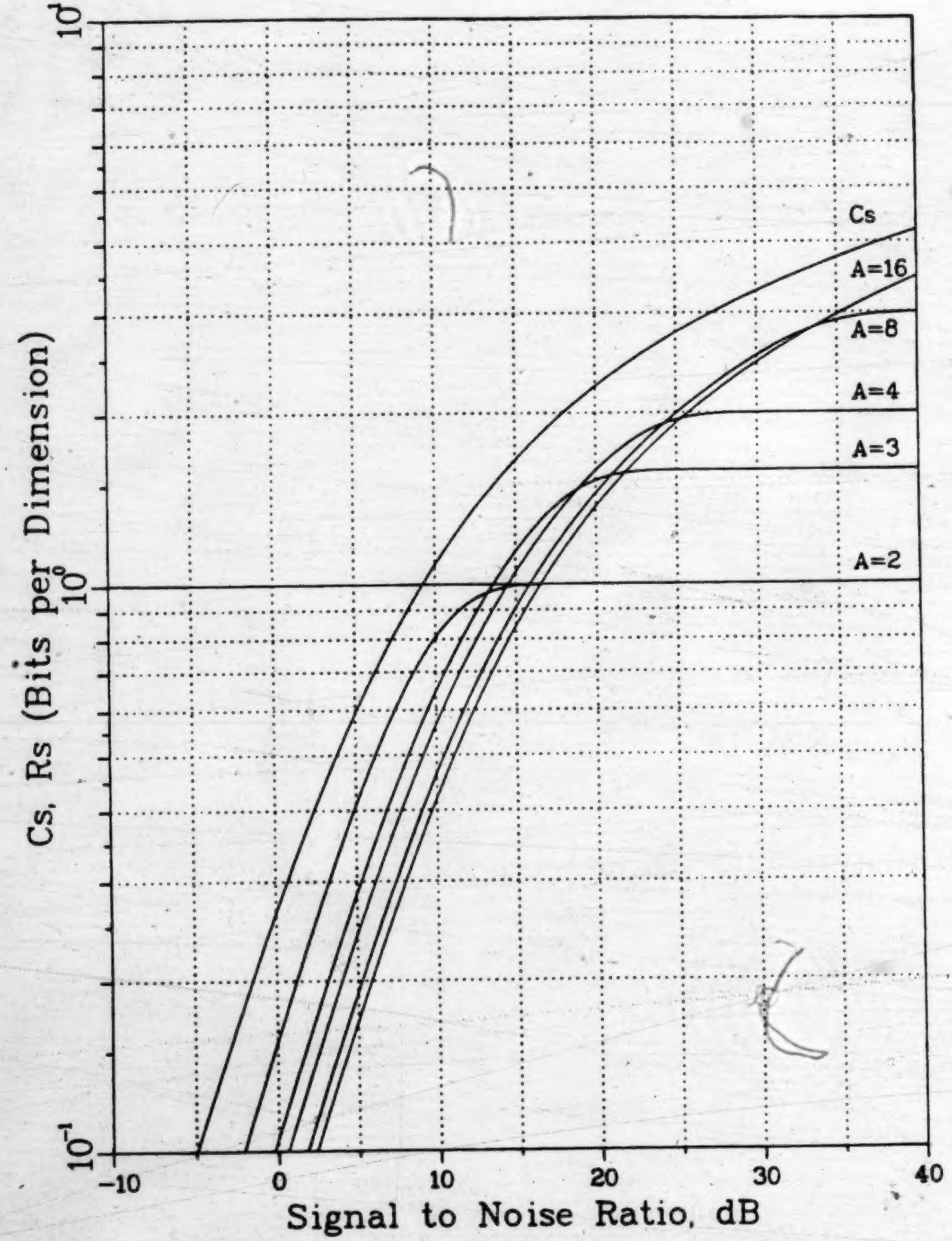

Fig. 2.2 Channel Capacity
for Additive White & Shot Noise
as defined by Equation 2.6
and for A-Level PAM Signalling

A comparison of Figures 2.1 and 2.2 indicates that the A - level capacity curves for the cases of shot noise and no shot noise are identical except at the knees of the curves. As the shot noise increases, the knees become rounder, and the corresponding signal capacities at the knees are reduced slightly. For the shot noise parameter ξ=70 uV, the tradeoff point between binary signalling and ternary level signalling is at a SNR figure of approximately 13 dB, as opposed to the 12 dB figure for the case of no shot noise.

The similarity between Figures 2.1 and 2.2 indicates that, for typical values of shot noise, the earlier comparisons between binary signalling and multilevel signalling based on Figure 2.1 still apply.

Figures 2.1 and 2.2 also indicate that the achievable signalling capacity with multilevel signals is close to the ultimate channel capacity. However, doubling the number of levels has less and less payoff as the number of levels increases. Because of this, economic considerations dictate that it is seldom worthwhile to go above 8 or 16 levels.

Often in the literature, a comparison is made between binary signalling with equalization and multilevel signalling as methods to increase a system's attainable bit rate. Salz [27] considered optimum (in the mean - squared sense) DFE for both binary and multilevel signals. Having derived the form of this equalizer, he then addressed the problem of signalling at faster than the channel's Nyquist baud rate by employing DFE and multilevel signalling. Specifically, the possible advantages of decreasing the number of signal levels (to a minimum of two for binary signalling) while increasing the signal baud rate in order to keep the data rate constant were investigated. Salz concluded that, for channels of practical interest, if the signal baud rate was increased above the channel's Nyquist rate, while the number of signal levels was decreased, the mean-squared-error (MSE) was increased.

Hence, from a MSE criterion, and for most practical channels, when the information rate is higher than the channel's Nyquist baud rate, multilevel signalling at the Nyquist baud rate with some equalization is superior to binary signalling above the Nyquist rate with more extensive equalization.

In contrast to this result are the conclusions made by Kasper [28]. Kasper's work indicates that, for multimode optical channels, the use of DFE in conjunction with binary signalling results in better system performance as compared to multilevel signalling at the same bit rate. For example, suppose we had a binary system capable of operating at half the Nyquist rate, but no higher, with negligible ISI. Neglecting shot noise, doubling the bit rate of this system and using ideal equalization would result in a 3 dB penalty. Doubling the bit rate by adopting a 4 level system would result in a 4.8 dB penalty in signal power (assuming the receiver sensitivity does not change) [28]. By this comparison, multilevel signalling is not as good as binary signalling with ideal equalization. However, this is a misleading and incomplete comparison, as will be shown:

1. The transmitter rate is given by $R=R_n \cdot D$. With equalization, R is increased by increasing D. With multilevel signalling, R is increased by increasing R_n. The basic difference is that multilevel signals take advantage of unused channel capacity, while equalization tries to compensate for channel restrictions.

2. If D can be increased by equalization, it can be increased for both binary and multilevel systems. A multilevel system can be equalized in the same way a binary system can. This possibility was not considered by Kasper.

3. There is a limit to the amount of equalization possible; if information is lost due to channel limitations, it is impossible to regenerate that information. This is reflected by the sharp increase in the equalization power penalty as the bit rate is increased. Linear equalization must compensate for the channel limitations in the presence of noise, and has inherent noise enhancement. This is especially true for channels having severe frequency attenuation characteristics or amplitude nulls in their time-domain impulse responses [18,26,27,28]. Nonlinear equalization methods such as DFE are better in this respect, as they do not enhance the signal noise. Experimental optical systems employing DFE have shown a "doubling" penalty of 3.5 dB [18]. However, DFE relies upon correct decisions being made by the receiver's decoder.

In all systems, errors are made occasionally. If the amount of feedback required for DFE is small, these decision errors have little effect on the system performance. However, if a large amount of feedback is necessary, these errors have a very serious effect on system performance. When an error occurs, the feedback value is wrong and hence may cause a decision error for the next bit. Thus, errors tend to propagate. With sufficiently large amounts of feedback, errors may substain themselves (analogous to oscillation in an amplifier), and the system becomes unusable.

4. If the baud rate of a system is increased sufficiently to cause significant ISI, pulse edges are rounded and hence timing information is lost. Thus, accurate clock extraction becomes more difficult to accomplish.

5. The power penalties mentioned above were under the assumption that all other system parameters remained constant as the baud rate was increased. For optical systems, this is not necessarily true, as will be shown in the next section. For example, the loss in receiver sensitivity when the baud rate is doubled may more than offset the power penalty differences between the two methods.

The above points show that the comparison between equalization and multilevel signalling is not a simple one; many factors have to be taken into account. The best method of increasing the bit rate in a dispersion-limited optical channel may involve both multilevel signalling and equalization.

Determination of the best compromise for typical fiber systems requires an examination of the state of present fiber optic technology.

2.2 Present Fiber Optic Device Technology

Section 2.1 defined the major difference between multilevel signalling and equalization as approaches to increase a system's bit rate. Equalization attempts to compensate for a channel's bandwidth restrictions and, although very useful when applied properly, has inherent limitations. This is especially true for linear equalization techniques, as will be shown in Chapter 3.

Multilevel signals, on the other hand, take advantage of more of the channel's capacity. The theoretical bound on the ultimate capacity of multilevel signals is very close to Shannon's bound for the channel.

In order to compare binary and multilevel signalling over fiber systems, the state of optical fiber communications has to be reviewed. This is done in the following sections. Although this thesis is concerned primarily with multimode fiber systems, a summary of single mode technology is also included here. Knowledge of both types of systems and devices is essential in realizing the relative advantages and limitations of the two system categories.

2.2.1 Fiber Technology

The ultimate capacity of a channel depends on its bandwidth and attenuation characteristics. For optical fibers, these characteristics depend on the type of fiber, manufacturing process, and source.

Attenuation in silica fibers is primarily due to material absorption and scattering, and is a function of certain fiber impurity concentrations as well as the operating wavelength. The bandwidth of fibers is limited primarily by modal, material, and waveguide dispersion. For multimode fibers, waveguide dispersion is negligible in comparison with the other two; in single mode fibers modal dispersion is eliminated and waveguide dispersion has to be considered.

In multimode fibers, modal dispersion is due to the difference in group velocity of different modes propagating along a fiber. Its effect is minimized by the use of graded index fibers. The pulse broadening caused by this mechanism is roughly proportional to the square root of the fiber length, for fiber lengths of 1 km or more (depending on the fiber characteristics).

Material dispersion (also called chromatic dispersion) for both single mode and multimode fibers is strongly dependent on the spectral linewidth and center wavelength of the optical source. The pulse broadening caused by material dispersion is proportional to the fiber length. At a wavelength of 850 nm, the material dispersion of silica per nanometer of spectral linewidth is typically 85 to 100 ps/km; at 1300 nm it passes through zero, and at 1550 nm it is roughly 20 ps/km for conventionally doped silica fibers [14,15,26,29].

The primary causes of attenuation in silica fibers are Rayleigh scattering, infrared and ultraviolet absorption, and the presence of OH ("water") radicals. The first three causes result in a theoretical wavelength - dependent minimum fiber attenuation. This attenuation limit is under 5 dB/km for wavelengths between 650 nm and 1900 nm [16, 30],with a minimum value, at 1550 nm, of approximately 0.1 dB/km (for single-mode fibers). The presence of OH ions, however, causes absorption peaks at 940, 1240, and 1380 nm [30]. The regions between these peaks, along with the theoretical attenuation minimum, results in 3 low - loss windows at the forenamed wavelengths of 850, 1300, and 1550 nm. Before the concentration of OH radicals could be reduced to levels obtainable today (10 ppb [14]), the lowest loss window was the 850 nm one. Systems operating at this wavelength are termed first generation systems. Reduction of the OH ion concentration opened up the other two windows; in fact, it is low enough in present fibers that the term "window" is no longer applicable. Fibers now have attenuations close to the theoretical minimum, and the 850 nm "window" is now the poorest one from a dispersion and attenuation viewpoint. However, source and detector technology is most advanced for this wavelength, and hence 850 nm systems are still commercially viable for many data communication links.

Typical attenuation values of present 850 nm multimode graded index fibers are from 2 to 4 dB/km, and values of 1.6 dB/km have been reported [29,30,31]. The material dispersion per kilometer of typical good quality 850 nm fiber length, τ_λ, is given by

$$\tau_\lambda = (85\ \mathrm{ps/km}) \cdot \Delta\lambda \tag{2.7}$$

where $\Delta\lambda$ is the source "full width at half maximum power" (FWHM) linewidth [15,26]. The material bandwidth-distance product (BDP) corresponding to this is:

$$f_\lambda = \ln(4)/(\pi \cdot \tau_\lambda) \cong 0.441/\tau_\lambda \tag{2.8}$$

A LED with a 30 nm FWHM linewidth results in a material BDP, f_λ, of 170 MHz-km; a LD having a 2 nm linewidth would have a 2.6 GHz-km material BDP. Values of 3.1 GHz-km have been reported [30].

Commercial 850 nm fibers with a modal BDP, f_m, of 800 to 1000 MHz-km have been produced. The overall fiber bandwidth, f_T, considering both material and modal dispersion, can be approximately predicted by the following formula [26]:

$$1/f_T = \sqrt{L/f_m{}^2 + (L/f_\lambda)^2} \tag{2.9}$$

L is the fiber length in kilometers. With values of $f_\lambda = 170$ MHz-km and $f_m = 800$ MHz-km, a 10 km fiber would have a bandwidth estimate of only 17 MHz.

An example of a current good quality 850 nm multimode fiber is Corning Glasswork's fiber #2410F. This fiber has a maximum attenuation of 2.4 dB/km and a modal BDP of 670 MHz-km [31].

Present attenuation values are around 0.6 - 0.7 dB/km for 1300 nm multimode fiber, and 0.4 dB/km for 1550 nm multimode fiber [14,15]. The 1300 nm window has the advantage of very low material dispersion. Typically, the material dispersion passes through zero with a slope of 0.1 ps/km-nm around this wavelength [15]. For an optical source having a center wavelength matched to a conventionally clad fiber's zero dispersion wavelength, the 3 dB optical (6 dB electrical upon reception due to the square-law nature of optical detectors) material BDP is approximated by [32,33]:

$$f_\lambda = 4f_o \quad \text{where} \quad f_o = 1.61\cdot 10^{12}\ \text{nm}^2/(\Delta\lambda_{rms})^2 \qquad (2.10)$$

If, however, the source center wavelength, λ, is different from the fiber zero-dispersion wavelength λ_o, the material BDP is sharply reduced from this maximum value. The appropriate formulas for the 3 dB optical material BDP are then:

$f_\lambda = x\cdot f_o$ where x satisfies the equation [32,33]:

$$0.5(1+x^2)^{0.25} = \exp[-(\lambda-\lambda_o)^2x^2/(2(1+x^2)\Delta\lambda^2_{rms}) \qquad (2.11)$$

Here, $\Delta\lambda_{rms}$ is the root-mean-square (RMS) source spectral width. This width is approximately $0.42\Delta\lambda$(FWHM) for sources having a gaussian or near gaussian spectral distribution. Figure 2.3 depicts f_λ for 1 km of typical multimode fiber for various LED source wavelengths and spectral widths.

Present 1300 nm edge-emitting LEDs have a FWHM linewidth around 70 nm. Assuming a wavelength mismatch of 25 nm between the fiber and source, the appropriate material BDP, from Fig. 2.3, is 3.75 GHz-km.

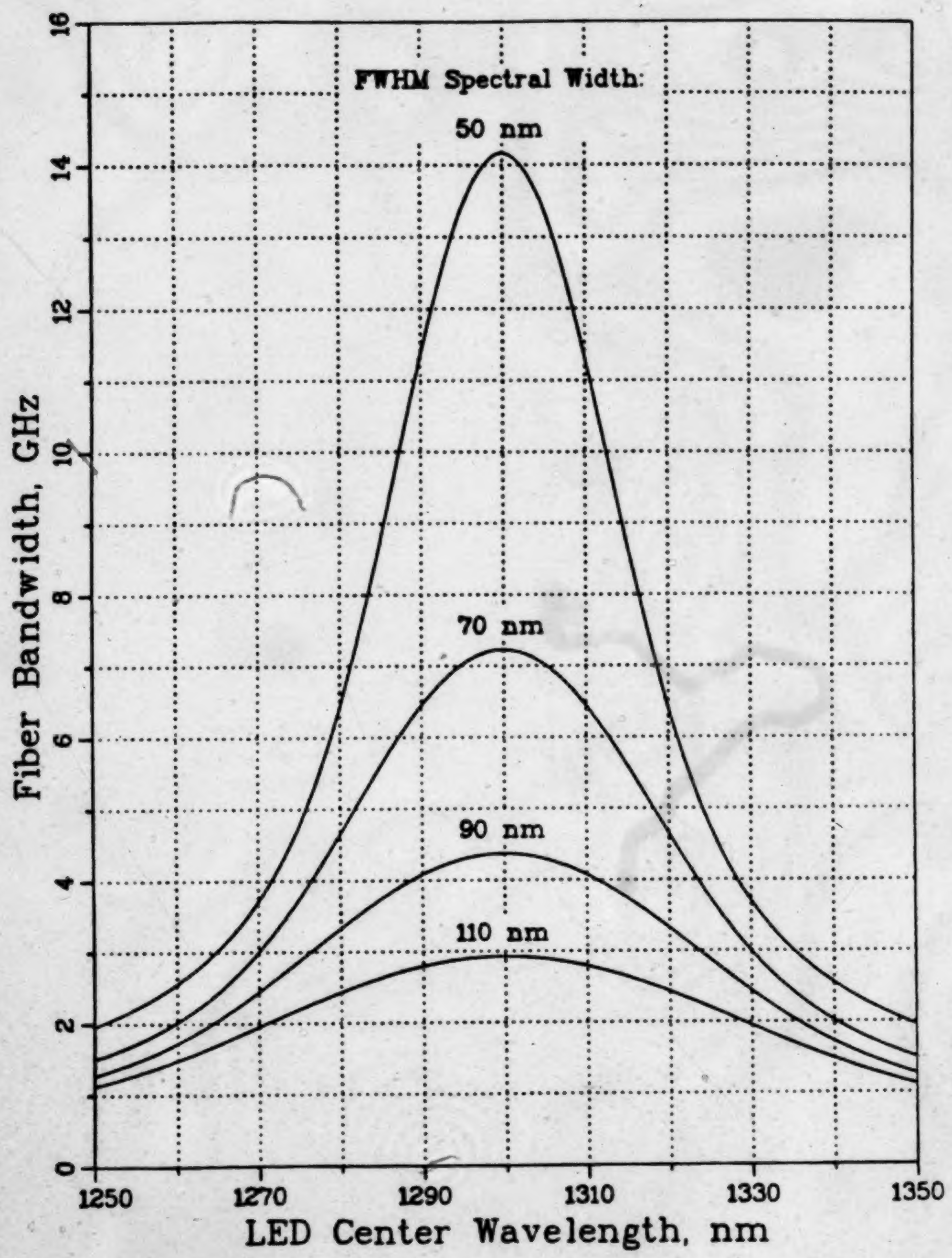

Fig. 2.3 Material Dispersion Bandwidth vs. LED Source Spectral Width and Wavelength for 1 km of 1300 nm Multimode Fiber

The modal bandwidth for 1300 nm fibers is higher than that obtainable with 850 and 1550 nm fibers. Recently, a median value of f_m= 1.83 GHz-km was reported for 1300 nm fibers mass produced under manufacturing conditions [14]. Experimental multimode fibers for this wavelength produced by the vapor-axial-deposition (VAD) process have been produced with average modal BDPs of 6 GHz-km, the highest value being 9.7 GHz-km [14].

Assuming that we have a LED source with a 70 nm FWHM linewidth and a center wavelength matched to the fiber's 1300 nm zero-dispersion point, a comparison of the modal and material BDPs for a conventional mass-produced 1300 nm fiber indicates that the overall fiber bandwidth is limited more by the modal dispersion than the material dispersion [13,29]. Thus, unlike 850 nm systems, transmission at medium data rates (100 Mb/s) over tens of kilometers may be possible at 1300 nm with a LED source, provided the source is closely matched to the fiber zero-dispersion wavelength. The major advantage offered by a laser-diode (LD) at 1300 nm would not be in available fiber bandwidth, but in power.

In order to further increase the fiber bandwidth, modal dispersion has to be reduced. In single-mode fibers, light propagates only in the HE_{11} mode, and hence no modal dispersion occurs. At 1300 nm, where the material dispersion may also vanish, waveguide dispersion remains. However, first-order cancellation of this waveguide dispersion is possible, and the attainable BDP with a highly coherent source may be over

100 GHz-km [13,14,16]. The ultimate bandwidth, $f_{maximum}$, of a single-mode fiber at its zero dispersion wavelength λ_o, for an ideal source, can be approximated with the following bandwidth - length relationship [13]:

$$(f_{maximum})^4 L = (3\ \mathrm{THz})^4\ \mathrm{km}. \qquad (2.12)$$

In addition to having a lower dispersion, single-mode fibers also have a slightly lower attenuation than multimode fibers. Typical values are 0.4 - 0.5 dB/km at 1300 nm and 0.2 dB/km at 1550 nm. The lowest value to date is 0.16 dB/km for a 1550 nm single-mode fiber.

While operation at 1550 nm. offers the lowest attenuation, the zero material dispersion wavelength is at 1300 nm. Hence, work is being carried out to shift the zero-dispersion wavelength to 1550 nm. The penalty for this is a slightly higher fiber attenuation [13,14,29,34].

Full utilization of single-mode fibers requires precise source characteristics and fiber manufacturing control. Near the zero-dispersion wavelength, the fiber BDP is not determined directly by the fiber dispersion, but by source mode-jumping for a single-mode source, and by mode-partition noise for a multi-mode source [16,35].

When multi-mode sources are used, mode-partition noise can be caused by power fluctuations between source spectral components. The BDP limitation caused by this phenomenon (for a power penalty of 1.5 dB at a 10^{-9} error rate) is

$$\mathrm{BDP} < (130\ \mathrm{Gb\text{-}km/ps})/(\Delta\lambda_{rms}|d\tau_{\lambda}/d\lambda|\cdot k^{0.5}) \qquad (2.13)$$

where k is a mode-partition noise-suppression factor ($0.1<k<1$). Typical experimental values for k are from 0.4 to 0.7 [16]. Equation 2.13 applies when the source center wavelength is different from the fiber zero-dispersion wavelength. For matched wavelengths, the appropriate formula is: [16]

$$BDP < (1173\ \mathrm{Gb\text{-}km/ps})/(\Delta\lambda_{rms}{}^{2}|d^{2}\tau_{\lambda}/d\lambda^{2}|\cdot k^{0.5}) \qquad (2.14)$$

For conventionally clad fibers, [15]

$$|d^{2}\tau_{\lambda}/d\lambda^{2}| \equiv 0.1\ \mathrm{ps/nm^{2}km} \qquad (2.15)$$

Mode-partition noise is eliminated by using single-mode optical sources. However, another limiting phenomenon arises. Temperature variations or drive variations may cause single-mode LD's to suddenly jump off their center wavelength to another wavelength. This behavior is called mode-jumping and also affects the BDP limitation of the fiber. Its effect is proportional to the material dispersion and the magnitude of the jump $\Delta\lambda_j$ [16]:

$$BDP < (225\ \mathrm{Gb/km\cdot s})/|\Delta\lambda_{j}(d\tau_{\lambda}/d\lambda)| \qquad (2.16)$$

To illustrate the effect of mode-partition and mode-hopping noise on a high capacity single-mode fiber system, consider the realization of a 20 km repeaterless link with a signalling capacity (at half the channel's Nyquist rate) of 1.6 Gb/s [34]. For a 1300 nm multimode LD source having an RMS spectral width of 2 nm and a mode-partition noise-suppression factor of 0.6, the fiber material dispersion, from (2.13), has to be less than 2.6 ps/km. From (2.15), this can be realized if the source center wavelength is within 26 nm of the fiber zero-dispersion wavelength. However, present source and fiber fabrication technology is not adequate to realize this condition commercially [34]. For a single-mode source having a mode hop of 3 nm, (2.16) indicates the material dispersion must be 2.3 ps/nm-km or less; an even tighter limit.

Reduction of these two limiting factors can be accomplished by providing

a) precise matching between the source center frequency and the fiber zero-dispersion wavelength.

b) minimization of the second derivative of the material dispersion with respect to the wavelength.

The first of these solutions is difficult to realize because of the high fiber impurity concentration tolerances, fiber dimension tolerances, and source composition tolerances required, not only for individual batches, but over many production batches. This is quite difficult to achieve, much as it is difficult to precisely control individual transistor parameters from batch to batch. (Common transistors usually have a manufacturer specified current gain range of 50 to 200 or more.) The second solution has spurred on developments of a fiber with low dispersion over a broad range of wavelengths. Bell Telephone Labs recently produced an experimental fiber with less than 1.5 ps/nm-km dispersion with wavelengths from 1.35 um to 1.63 um. The attenuation of this fiber averaged over a 119 km length, including splices, was 0.45 dB/km at 1300 nm and 0.27 dB/km at 1550 nm. This fiber was used to realize transmission of 420 Mb/s over the 119 km of fiber with no repeaters (a now broken record) [12]. However, this result is still far short of the theoretical capability of single-mode fibers, and involves some compromise in fiber characteristics due to source limitations.

2.2.2 Source Technology

Before fiber systems became commercially feasible, practical optical sources had to be developed. Much attention was paid to 850 nm sources (and detectors) and only recently has this attention shifted to longer wavelength devices.

LEDs and LDs for 0.85 um operation have been commercially available for many years. These short wavelength devices are made of AlGaAs; a semiconductor material that has been studied for many years and hence is readily available and understood. The better 850 nm LEDs have launch powers around -10 dBm, spectral FWHM linewidths of 30 nm, can be directly modulated to 100 Mb/s or higher, and have mean lifetimes in excess of 10^9 hours [14,36,37]. LDs for this wavelength have output powers of several milliwatts, RMS linewidths of <2 nm (for modulation at a few hundred Mb/s or less), can be modulated up to one Gb/s or higher, and have mean lifetimes of 10^6 hours [14,36].

LDs provide higher optical power outputs and have a narrower spectral width than LEDs. However, LEDs are more reliable, much simpler to operate due to their more stable output power with respect to temperature, and cheaper than LDs. They are also immune to coherency-related problems such as modal-noise, mode-jumping, and pulsations. Thus, LEDs are still very useful as sources for multimode systems, especially at

1300 nm where material dispersion is small [14,30,38].

Sources for longer wavelength operation are made of InGaAsP. LEDs operating at 1300 nm typically have launch powers of -12 dBm and FWHM linewidths of 70 nm for edge emitting designs, larger than that obtainable with 850 nm LEDs. (In general, the spectral width of a LED is proportional to the square of the LED wavelength [15].) Recently, a 1300 nm LED with an incorporated ridge waveguide was produced, resulting in a FWHM spectral width of 30 nm, higher modulation capability, and higher coupling efficiency; however, it was more temperature sensitive than conventional LEDs [14]. Thus far, the mean lifetimes of InGaAsP LEDs are typically from $5 \cdot 10^6$ to 10^8 hours, somewhat less than for 850 nm LEDs [35,38].

Present long wavelength LDs have some disadvantages compared to short wavelength LDs. Their output power is slightly lower, their spectral width is slightly higher, and they are much more temperature sensitive [14,27]. The first two disadvantages are more than offset by improved fiber characteristics at the longer wavelengths. The sensitivity problem has not yet been completely solved. Typical 1300 nm LDs have output powers of 0 - 3 dBm and RMS linewidths around 2 nm [14,34,35].

For single-mode fiber transmission, either single-mode or multimode sources may be used. Multimode sources, however, may cause mode-partition noise, as mentioned earlier. Thus, in order to achieve maximum bandwidth, single-mode sources are required. These sources also have their problems, some of which are:

1. LDs that exhibit single-mode operation under steady state conditions sometimes break into multimode operation when modulated. This problem can be solved through distributed feedback techniques [14,35].

2. LD linewidths need to be reduced to fully realize single-mode technology, especially for coherent detection [14].

3. As mentioned earlier, present fabrication technology is not adequate to match the LD center wavelength and the fiber zero-dispersion wavelength for Gb/s transmission [34].

Because of these problems, much source development for commercial single-mode systems is required.

Although single-mode fibers outperform multimode fibers, single-mode sources and fibers are much costlier than multimode sources and fibers. Since the capacity of single-mode systems is not required for almost all fiber optic applications, single-mode systems are generally used in only very long distance, high bit rate systems. As will be shown later, multimode fibers with either LDs or LEDs as an optical source, and with proper signal formatting and coding, are adequate for many data links, even at bit rates of 100 Mb/s or higher.

2.2.3 Detector Technology

The bandgap of silicon is close to 1 um. Hence, silicon is an ideal semiconductor for 850 nm optical detectors. Application of the mature silicon device technology to short wavelength detectors has resulted in cheap, high quality PIN diodes and APDs for first generation fiber systems. Silicon APDs have quantum efficiencies close to 100%, fast response times (≤1 ns), current gains of 100 with excess noise factors of about 5, and dark currents around 10 pA [14,30,36].

Unfortunately, silicon is useless as a semiconductor for long (> 1 um) wavelength detectors. Consequently, materials such as Ge, InGaAs, and InGaAsP are being used. Germanium has two major shortcomings compared to silicon - higher dark currents (- 100 nA) and, for APDs, higher excess noise. Even so, Germanium APDs are useful for long wavelength systems. One example APD has an excess noise factor of 7 at a gain of 10, a quantum efficiency of 80%, and a dark current of 1 uA at room temperature (for operation at 90% of its breakdown voltage) [14]. Newer devices such as InGaAs PIN diodes and InGaAsP APDs have better performance than Ge APDs; however, germanium devices are older and hence commercially more available. InGaAs PIN diodes have less stringent power supply requirements (possibly resulting in greater repeater reliability) and slightly higher sensitivities.

Figure 2.4 summarizes the best experimental 850 nm and 1300 nm repeater sensitivities (at a 10^{-9} BER and with binary signalling), as a function of the baud rate, for various

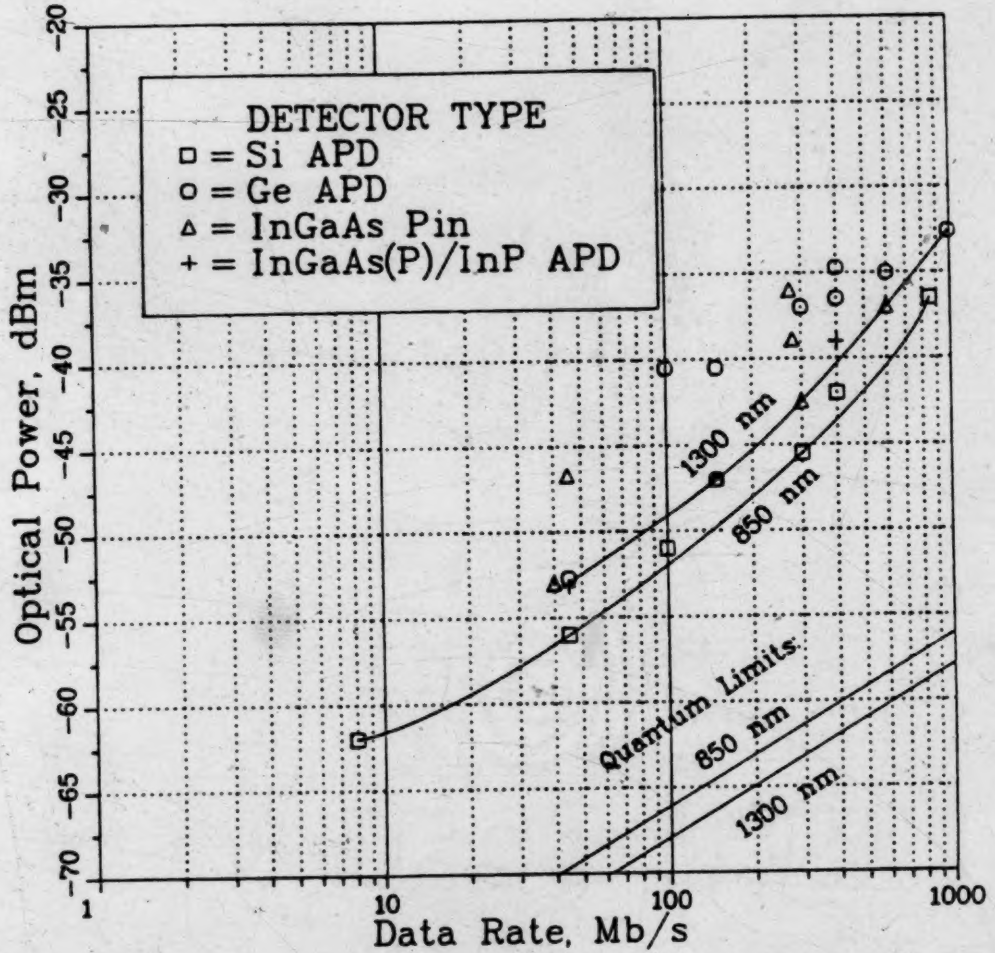

Fig. 2.4 Receiver Sensitivity vs. Data Rate
with various optical detectors
Binary signalling, BER=10E-9

optical detectors [14,29,30,35,39-44]. The two curved lines represent the achieved sensitivity limits, while the straight lines represent the quantum limits on receiver sensitivity for direct detection and binary signalling. From this graph, the sensitivity of 1300 nm receivers to date are about 3 db less than the comparable 850 nm receiver sensitivities, for bit rates in the vicinity of 20 Mb/s to 400 Mb/s.

2.3 Optical Fiber Multilevel Systems

Section 2.1 demonstrated the theoretical advantages of multilevel signalling. Section 2.2 discussed present fiber optic technology. In this section, the practical advantages of DFE and multilevel signalling for multimode fiber systems will be investigated. This will be done by deriving power and dispersion limits for the maximum repeater spacing in hypothetical 850 and 1300 nm multimode systems, using good quality commercially available or conceivable components. These limits will be formulated for both binary and four level signalling with and without decision feedback equalization. LED and LD optical sources will be used in derivation of these limits.

2.3.1 Component Specifications

The following is a summary of the assumed component specifications for the hypothetical systems.

Fiber

1. The 850 nm fiber is a multimode graded index fiber, with a numerical aperture of 0.2 and a 50 um core diameter, a material dispersion of 85 ps/nm-km, a modal bandwidth of 670 MHz/km, and an attenuation of 2.4 dB/km [31].

2. The 1300 nm fiber is a multimode graded index fiber with a numerical aperture of 0.2 and a 50 um core diameter, a material dispersion crossing through zero with a slope of 0.1 ps/km-nm^2, a modal bandwidth of 1.83 GHz-km, and an attenuation of 0.7 dB/km [14,15].

Sources

1. The 850 nm LED has a peak output power (launched into the fiber), OP, given by

$$OP_{peak} = -10 \text{ dBm} - 10\log(1+B/100 \text{ Mb/s}) \text{ dB} \qquad (2.17)$$

where B is the LED modulation frequency (or, equivalently, the data baud rate). This expression reflects the tradeoff between bandwidth and output power inherent to present LED (and LD) designs. The LED FWHM linewidth is 30 nm [15,29,30,35].

2. The 1300 nm LED has a FWHM linewidth of 70 nm, and a center wavelength 25 nm from the fiber's zero dispersion wavelength. The peak launch power of the LED is: [14,15,29,35,38]

$$OP_{peak} = -12 \text{ dBm} - 10\log(1+B/100 \text{ Mb/s}) \text{ dB}. \qquad (2.18)$$

3. The 850 nm (multimode) LD has a 3 nm FWHM linewidth and a peak launch power given by: [14,29]

$$OP_{peak} = 6 \text{ dBm} - 10\log(1+B/400 \text{ Mb/s}) \qquad (2.19)$$

4. The 1300 nm multimode LD has a 5 nm FWHM linewidth and a launch power given by: [15,35]

$$OP_{peak} = 3 \text{ dBm} - 10\log(1+B/400 \text{ Mb/s}) \qquad (2.20)$$

Detectors

1. The 850 nm detector is a silicon APD. The 850 nm receiver sensitivity for a given baud rate will be derived from experimental achievements to date, shown in Figure 2.4.

2. The 1300 nm detector is an InGaAs PIN diode. The receiver sensitivity using this device will also be derived from Figure 2.4.

2.3.2 System Power Penalties

The application of equalization and multilevel signalling requires additional receiver power. For proper system design this power penalty has to be included as an additional loss.

A multilevel system requires additional power over a binary system for the same error performance and receiver sensitivity. For additive gaussian noise, the additional penalty for using more than 2 levels is $10 \cdot \log(A-1)$, where A is the number of levels. For an ideal four level system, this penalty is 4.8 dB. However, an actual system would exhibit shot noise. Inclusion of shot noise results in the optimum levels being unequally spaced, as will be shown in Chapter 5. This increases the power penalty required; experimental results from the four level system used in this thesis indicate a 6.2 dB penalty is more appropriate.

The equalization penalty strongly depends on the amount of equalization required and the type of equalizer used. The reason that there is a penalty lies in the fact that when a signal is bandlimited, some of its spectral components are attenuated. Thus, for a given noise floor, the SNR of these attenuated components decreases, and this decrease is reflected in the power penalty. Although this penalty is not by any means constant, a penalty corresponding to a doubling of the achievable bit rate will be used. Above this rate, the equalization penalty increases drastically, and thus the assumption that further equalization beyond this rate is not practicable will be made. For DFE, a penalty of 3.5 dB for this condition is appropriate. The choice of DFE will be justified in Chapter 3 [18,28].

2.3.3 System Design

The dispersion and power limits for the maximum repeater spacing, as a function of the bit rate desired, are shown in Figures 2.5 and 2.6 for the 850 nm and 1300 nm systems respectively. The power limits were derived with the following formula:

$$L = (OP - M - P - R)/(F + I) \tag{2.21}$$

where

L is the maximum repeater spacing;

OP is the average launched optical power, and is 3 dB less than the peak launch power of the source;

M is a safety margin of 5 dB;

P is the power penalty if equalization, four level signalling, neither, or both are used and is 3.5 dB, 6.2 dB, 0 dB, or 3.5+6.2= 9.7 dB respectively;

R is the receiver sensitivity for the baud rate as given by Figure 2.4;

F is the fiber attenuation in dB/km; and

I is an additional loss of 0.2 dB/km for installation, cabling, and splices.

The dispersion limits for the repeater spacing are derived from the equations:

$$\begin{aligned} B &= 1.0 \cdot f_t \\ BE &= 2.0 \cdot f_t \\ M &= 2.0 \cdot f_t \\ ME &= 4.0 \cdot f_t \end{aligned}$$

B is the bit rate for a binary system with no equalization, BE is for a binary system with equalization, M is for a four level system, and ME is the bit rate for a four level system with equalization. The fiber bandwidth, f_t, is defined by f_λ, f_m, and L (Eqn. 2.9).

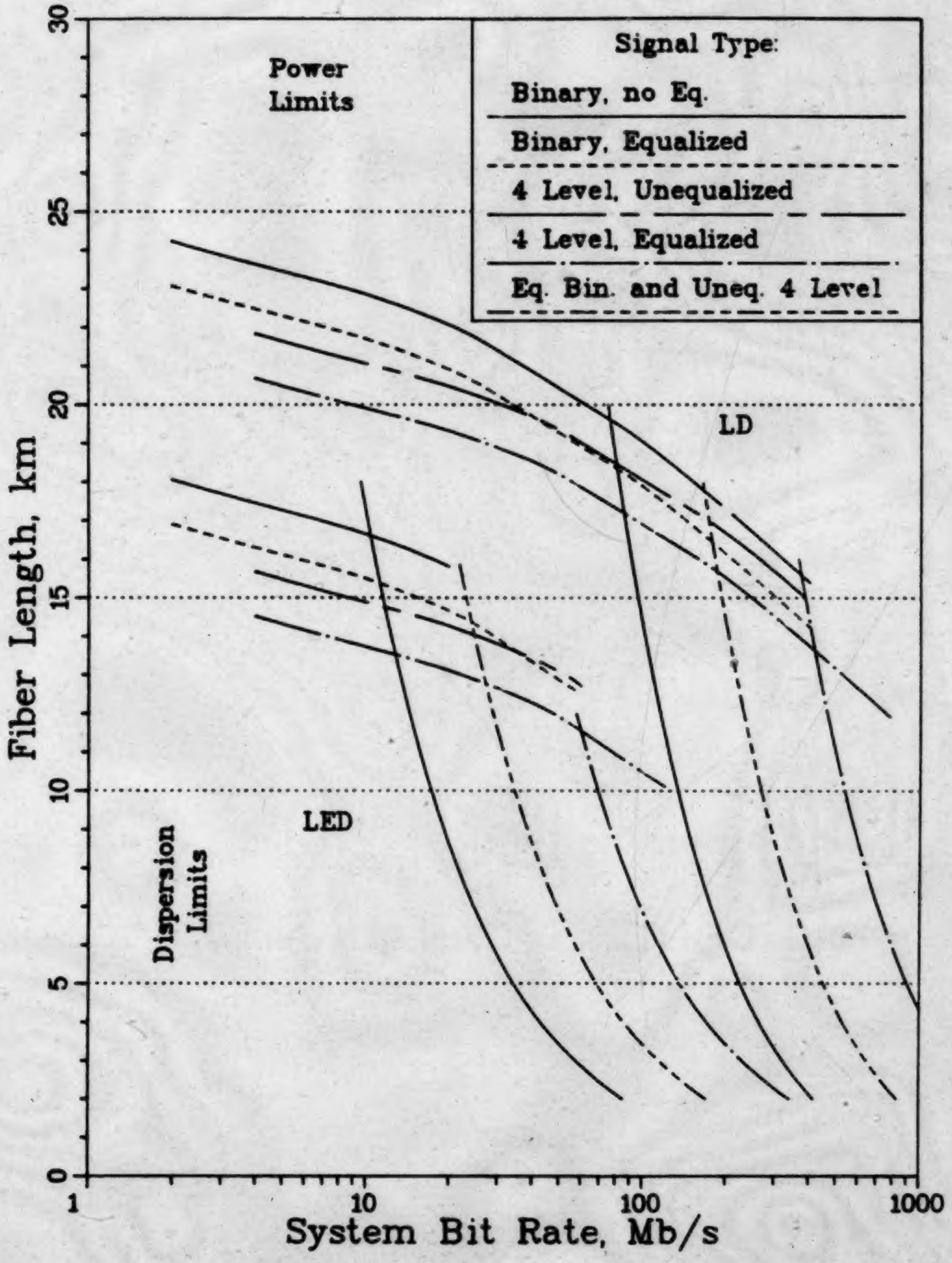

Fig. 2.5 Channel Length and Capacity Limits for the 850 nm 2/4 Level System using both LED and LD Optical Sources with and without DFE

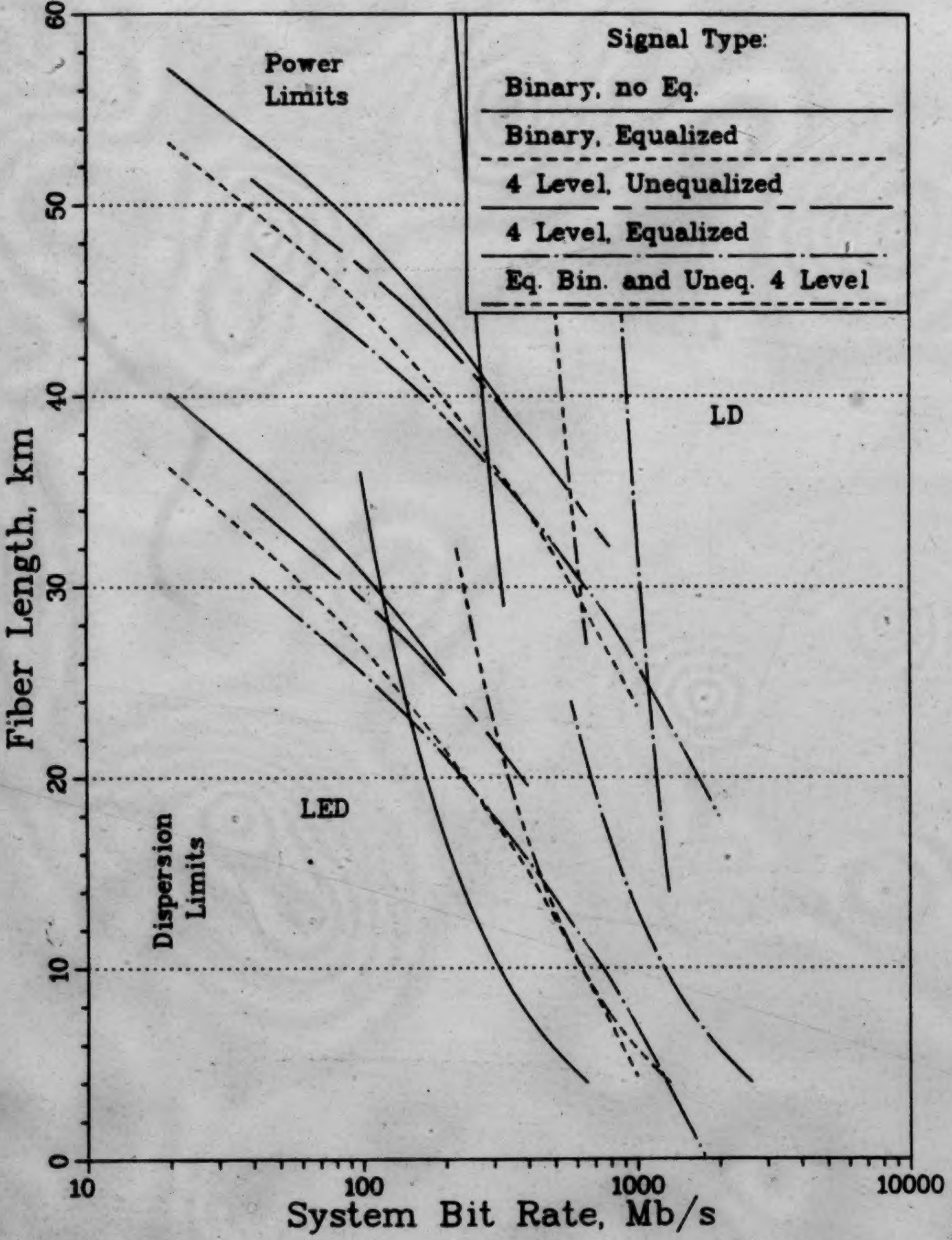

Fig. 2.6 Channel Length and Capacity Limits for the 1300 nm 2/4 Level System using both LED and LD Optical Sources with and without DFE

The difference between bit rate and baud rate should be clarified. The baud rate for PAM NRZ systems is the pulse rate; the bit rate is the baud rate multiplied by the number of bits represented by a pulse. For binary systems, they are the same; for a four level system the bit rate is twice the baud rate.

From Figures 2.5 and 2.6, it appears that the use of DFE lowers the attainable repeater spacing for power limited system operation. This, however, is not the case. The power limits for signalling with DFE were derived using a constant equalization penalty of 3.5 dB. The actual penalty will depend upon the amount of equalization required. Hence, the unequalized and equalized power limit curves are actually upper and lower bounds (assuming further equalization is not practical), with the transition between the two taking place between the unequalized and equalized dispersion limit curves.

Comparison between the different signalling formats can be facilitated by Table 2.1. This table shows the maximum attainable repeater spacing for the specified data rates and various signalling formats. Circled in the chart are the best signalling combinations for each source and data rate combination.

For the 850 nm system, with a LED optical source there is nothing to be gained through extensive equalization or multilevel signalling at DS-2 data rates, since the link is power limited. Of course, equalization may allow for a slightly lower receiver bandwidth and hence more receiver

System Type	Signal Format	Data Rate (Mb/s)					
		6.3 DS-2	45 DS-3	90 DS-3C	274 DS-4	560	1000
850 nm LED	Binary	$\boxed{17P}$	3.5P	2D	-	-	-
	Bin + DFE	17P	7.5P	4D	-	-	-
	4 Level	15.5P	7.5P	4D	-	-	-
	4 Level+DFE	15.5P	$\boxed{12.5P}$	$\boxed{7P}$	$\boxed{2.5D}$	-	-
850 nm LD	Binary	$\boxed{23P}$	$\boxed{20.5P}$	$\boxed{16P,D}$	4D	1.2D	-
	Bin + DFE	23P	20.5P	18.6P	9.5D	3.5D	1.7D
	4 Level	21P	19.5P	18P	9.5D	3.5D	1.7D
	4 Level+DFE	21P	19.5P	18P	$\boxed{15P}$	$\boxed{9.5D,P}$	$\boxed{4.5D}$
1300 nm LED	Binary	-	$\boxed{35.5P}$	$\boxed{31P}$	10.5D	4.5D	2D
	Bin + DFE	-	35.5P	31P	18.5D	10P,D	5P,D
	4 Level	-	34P	30P	22P,D	10.5P	5D
	4 Level+DFE	-	34P	30P	$\boxed{22P}$	$\boxed{13.5P}$	$\boxed{8P}$
1300 nm LD	Binary	-	$\boxed{54P}$	$\boxed{48.5P}$	38D,P	9D	3D
	Bin + DFE	-	54P	48.5P	$\boxed{40.5P}$	31D,P	13D
	4 Level	-	51P	47P	40.5P	34D,P	13D
	4 Level+DFE	-	51P	47P	40.5P	$\boxed{35P}$	$\boxed{26P,D}$

Table 2.1 Maximum repeater spacing for various system types, data rates, and signalling formats. (bit error rate = 10^{-9})

Legend

1. Each charted number is a maximum repeater spacing in km for the appropriate signalling format and data rate.

2. The D beside the repeater distance denotes the length is limited by the fiber dispersion. The P denotes the length is limited by power requirements.

3. The boxed in ($\boxed{}$) repeater distances correspond to the best signalling combination(s) for the given conditions.

sensitivity. However, the difference in the attainable maximum repeater spacing will be small. (The idea of trading receiver bandwidth for sensitivity will be mentioned in Chapter 4). At DS-3 or DS-4 bit rates, however, 4 level signalling with DFE allows a 3.5 times increase in the allowable repeater spacing; certainly this increase is substantial enough to warrant the extra repeater complexity. The 4 level signalling accounts for half of this increase. Using both DFE and 4 level signalling, a repeater spacing of 2.5 km with an 850 nm LED at DS-4 rates may be possible.

When an 850 nm LD is used, there is little advantage in going to 4 level signalling at DS-3 rates or lower. Also, equalization is not required, as the repeater spacings are power limited, not dispersion limited. At DS-4 rates, however, 4 level signalling with DFE is best, and the maximum repeater spacing is power limited, whereas for the other three signalling combinations the spacing is dispersion limited. The repeater spacing is increased by a factor of 3 over binary signalling without equalization. However, much of this improvement can be obtained with either 4 level signalling or DFE alone. The full potential of the 4 level signalling with DFE is realized at the European standard bit rate of 560 Mb/s; then, a repeater spacing of 13.5 km may be possible.

The 1300 nm system offers an order of magnitude increase in the available bandwidth - distance products. For example, the maximum repeater spacing with a LED at 850 nm and a DS-4 data rate is 2.5 km. At 1300 nm, the corresponding distance is

22 km. At 1 Gb/s and with a LD source, the maximum repeater spacing at 1300 nm is 26 km using both DFE and 4 level signalling, as compared to 4.5 km at 850 nm.

At 1300 nm and DS-4 bit rates or higher, four level signalling without equalization is usually better than binary signalling with DFE. This indicates that the 6.2 - 3.5 = 2.7 dB extra power required for unequalized 4 level signalling over binary signalling with DFE is more than offset by the decrease in receiver sensitivity and source launch power when the baud rate is doubled (for the same bit rate, the baud rate for binary signalling is double that of four level signalling). In fact, the power limits for four level unequalized signalling at 1300 nm surpass the binary unequalized signalling power limits, but at data rates where binary signalling is no longer useful.

At low data rates, where equalization or four level signalling is not required, the penalty for using 4 level signalling, in terms of the maximum repeater spacing is small (under 6% for the worst case in Table 2.1).

CHAPTER 3. SIGNAL FILTERING AND EQUALIZATION

In communication systems, filters and equalizers are often used to minimize or compensate for signal degradation. With PAM systems, the two types of degradation of concern are noise and ISI. Noise is an inescapable restriction in system design, and can only be minimized. Noise considerations determine the minimum received power required for a given error rate and thus ultimately define the attenuation limits for the maximum repeater spacing. Such limits were found in Chapter 2 for sample optical systems.

ISI, unlike noise, is deterministic. The noise variance in a received signal can be found, but the exact value of the interfering noise at any one time cannot be predicted. ISI, however, can be accurately predicted and consequently controlled or eliminated. A simple method of keeping the ISI to negligible levels involves restricting the maximum baud rate of a system to well below the system channel's Nyquist rate. For most communication systems, however, this is not an economically acceptable solution. If the need exists, a channel should be utilized as efficiently as possible within restrictions imposed by economic considerations and existing communication standards. The system design should also allow for the possibility of future growth. For many dispersive fiber systems, this implies that some amount of ISI is inescapable.

In practical systems, minimization of the ISI and noise has to be accomplished jointly. For example, receiver noise can be reduced by restricting the receiver bandwidth. However, this will also cause an increase in the ISI. Thus, filter and equalizer design should involve consideration of both sources of degradation.

For PAM systems, filters and equalizers are similar in design, and hence the two terms are sometimes used interchangably. The following definitions are adhered to throughout this thesis:

In digital communications, a filter is any device that performs one or more of the functions listed below:

1. It produces a desired pulse shape, usually for the purpose of minimizing ISI.

2. It reduces the noise level corrupting a signal through bandwidth restriction.

3. It aids in the extraction of timing information from the received signal.

An equalizer is any device designed to compensate for any ISI present in a signal. By this definition, the term equalizer is more specific than the term filter.

This chapter discusses three equalization methods useful in fiber optic systems; the linear zero-forcing equalizer, the linear minimum mean-squared-error equalizer, and the nonlinear decision-feedback equalizer mentioned earlier. The choice of a DFE, mentioned in Chapter 2, as the equalization method used throughout this thesis will be justified. The closely related topic of filtering, of concern in noisy channels, is covered for completeness, and serves as an introduction to the topic of equalization.

3.1 Filtering

The first two of the aforementioned functions of filters are pertinent to this thesis. In this section, the optimum filters for a given channel and desired pulse shape will be derived for the case of additive noise which may or may not be white. As it turns out, the inclusion of shot-noise does not change the structure of the optimum filters, and the results are applicable to a broad range of digital systems.

3.1.1 Choice of the Pulse Shape

In dispersive sampled-time systems, one design problem is that of choosing a pulse shape such that the ISI after sampling is minimized or controlled in some fashion.

In order to transmit at the Nyquist rate with no ISI, the pulse shape has to be rectangular in the frequency-domain. The time - domain representation of this is the sinc pulse given by

$$x(t)=\sin(\pi t/T)/(\pi t/T) = \mathrm{sinc}(t/T) \tag{3.1}$$

where T is the reciprocal of the data rate (= 1/2W for Nyquist signalling). Figure 3.1 depicts the time and frequency domain pulse shapes.

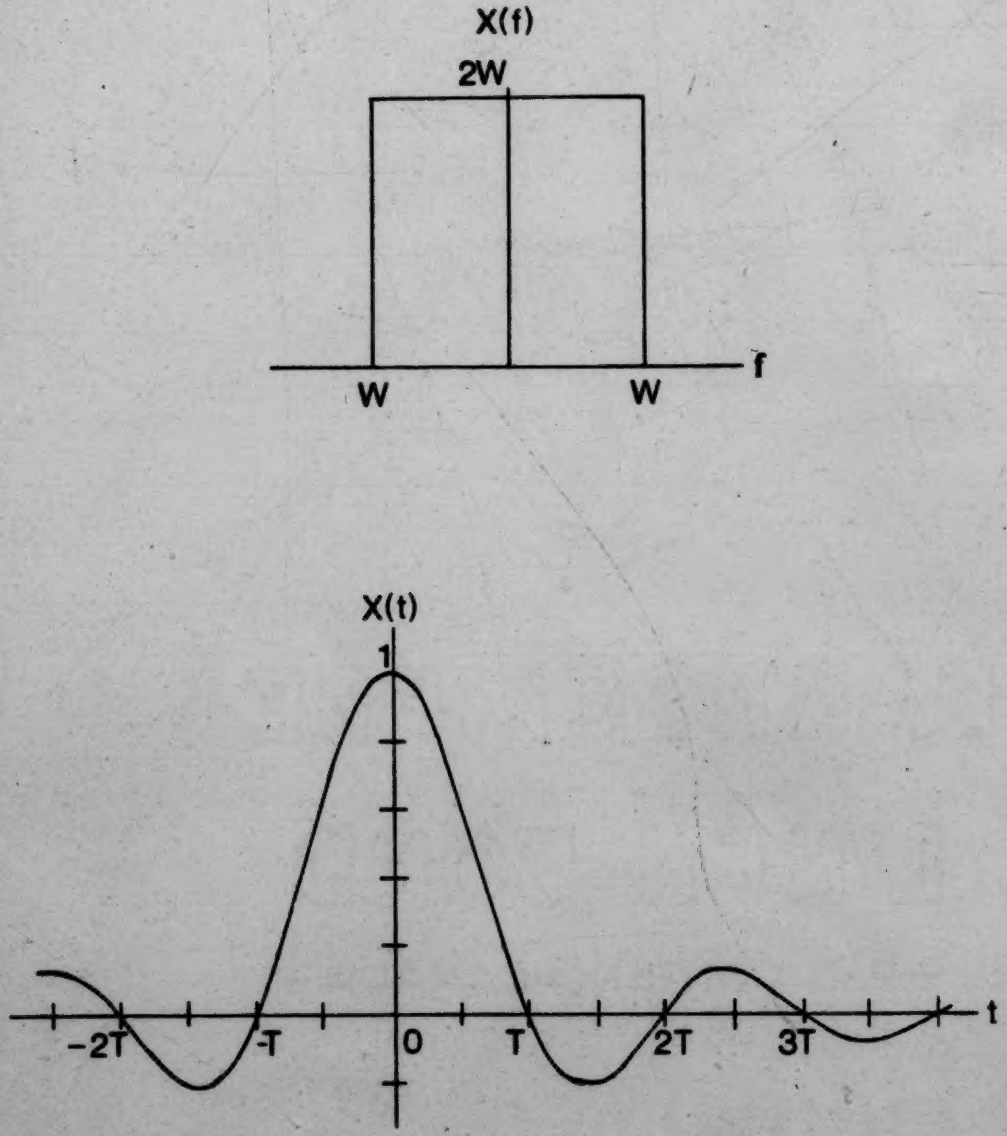

Fig. 3.1 The Sinc Pulse Shape in the Time and Frequency Domains.

The sinc pulse has two major problems:

1. Pulses with sharp discontinuities in the frequency domain are physically unrealizable. (However, they can often be approximated).

2. The tail of the sinc pulse decays as $1/t$. Hence, a timing error in sampling the received pulse may lead to a large or nonconverging ISI term. This also implies that even if the sinc pulse could be closely approximated, the resulting pulse would not be too useful. [45,46]

We are therefore restricted to transmission at less than the Nyquist rate, if the goal of no ISI at sampling instants is to be achieved or approached. This criterion is satisfied if the pulse shape in the frequency-domain is zero at the frequencies $-1/T$ and $+1/T$, and if the pulse has odd symmetry about the frequencies $-1/2T$ and $+1/2T$ [45].

One such pulse that is widely used in digital transmission is the raised-cosine, defined by the equations:

$$X(f)=\begin{cases} T, & 0 < |f| < (1-\beta)/2T \\ 0.5T[1-\sin(\pi t(f-1/(2T))/\beta)], & (1-\beta)/2T < |f| < (1+\beta)/2T \end{cases} \tag{3.2}$$

$$x(t) = \mathrm{sinc}(t/T)\cdot\cos(\beta\pi t/T)/(1-4(\beta t/T)^2) \tag{3.3}$$

The constant β is referred to as the rolloff parameter, and can have a value from 0 to 1. Figure 3.2 illustrates the raised-cosine shape for different values of β. For $\beta=0$, the shape degenerates into the sinc pulse. For other than this value of β, the tails of the raised - cosine pulse decay

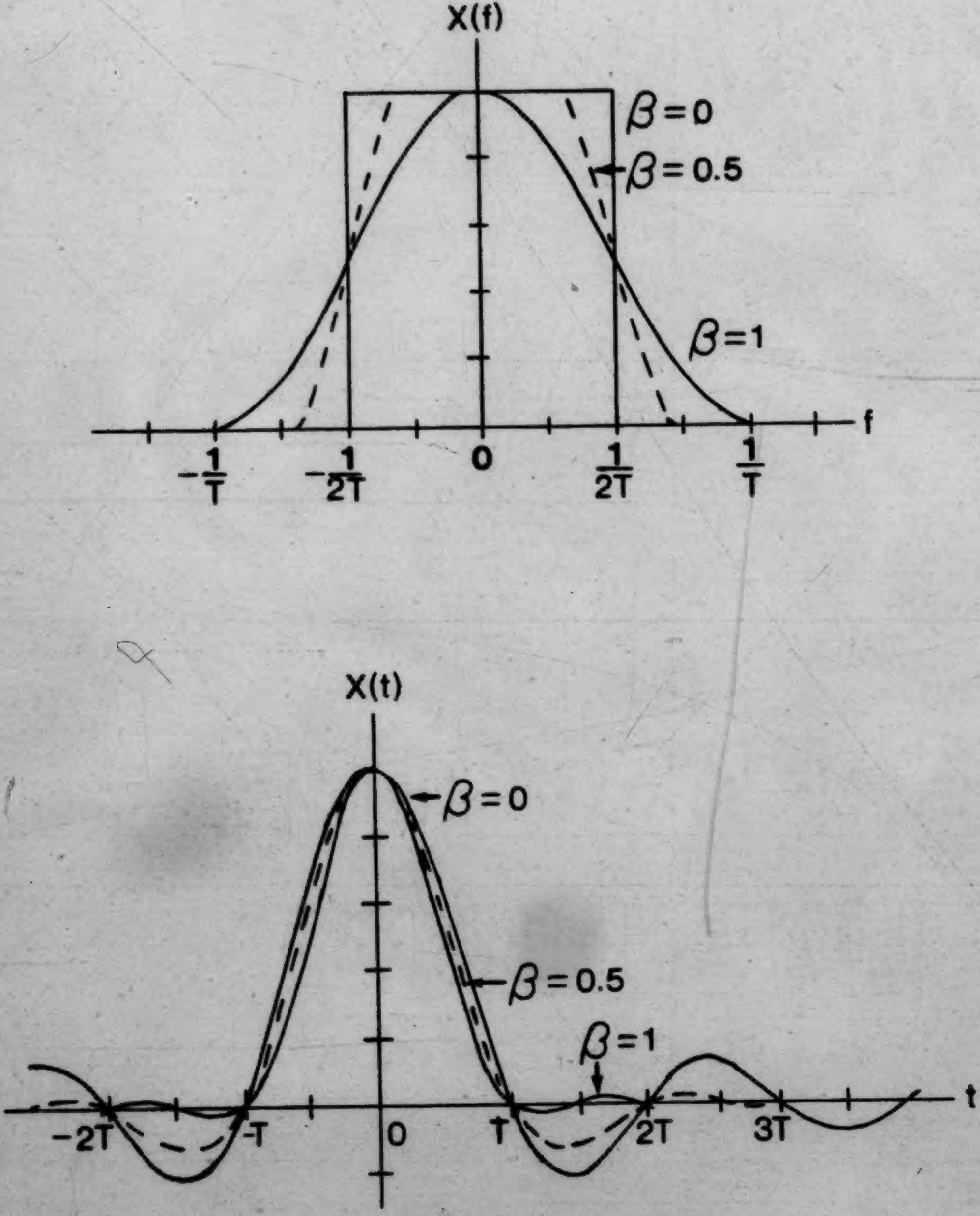

Fig. 3.2 The Raised - Cosine Pulse for β = 0, 0.5, and 1.
(The β = 0 shape is the sinc pulse)

more rapidly than the sinc pulse tails, and a timing error in sampling results in a converging ISI term. This also implies that the pulse does not have to be realized exactly, but may be approximated. The most useful raised-cosine shape is that for β=1. For this value of β, which corresponds to signalling at half the Nyquist rate, two other properties arise:

1. The half - amplitude pulse width (in the time domain) is equal to the pulse to pulse spacing, T.

2. There are additional zero crossings, as shown in Figure 3.2, at the times $t=\pm 3T/2, \pm 5T/2, \ldots$

These two features of the β=1 raised cosine greatly aid in timing extraction. In fact, Nyquist has shown that only this waveshape possesses all of the above features. The price, however, of these advantages is a bit rate equal to the bandwidth, or half the Nyquist rate. [46]

If signalling at or faster than the Nyquist rate is desired, we have to deal with ISI. Such signalling is termed partial-response signalling. Belonging to this category are duobinary signals, depicted in Fig. 3.3 and defined by [45,47]:

$$X(f) = \begin{cases} T(1+\exp(-j2\pi fT)) = 2T\cdot\exp(-j2\pi fT)\cdot\cos(\pi fT), & |f|<1/2T \\ 0, & |f|>1/2T \end{cases} \tag{3.4}$$

$$x(kT) = x_k = \begin{cases} 1, \text{ for } k=0,1 \\ 0, \text{ otherwise} \end{cases} \tag{3.5}$$

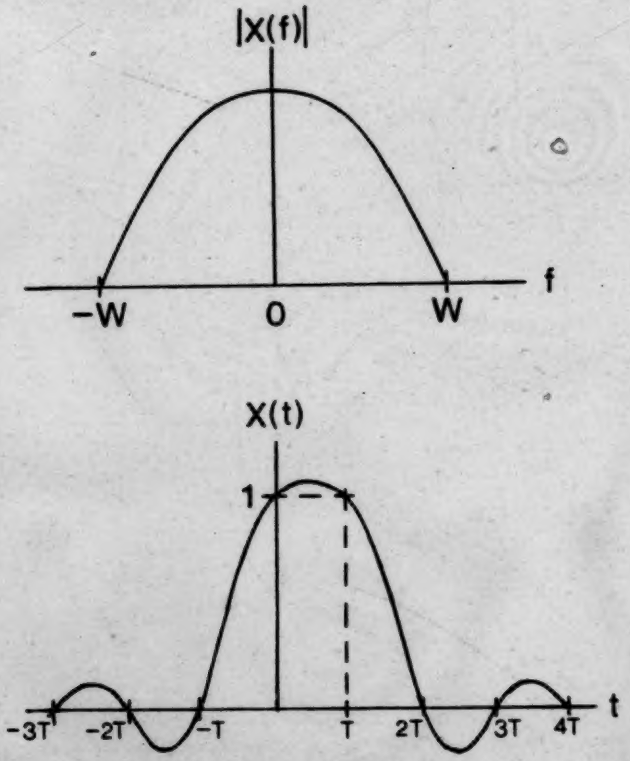

Fig. 3.3 The Duobinary Pulse Shape.

With this pulse, if the transmitted information is denoted by A_k (= A(kt)), and the received information by B_k, then B_k is given by $B_k = A_k + A_{k-1}$. DFE can be used to eliminate the A_{k-1} interference term in B_k:

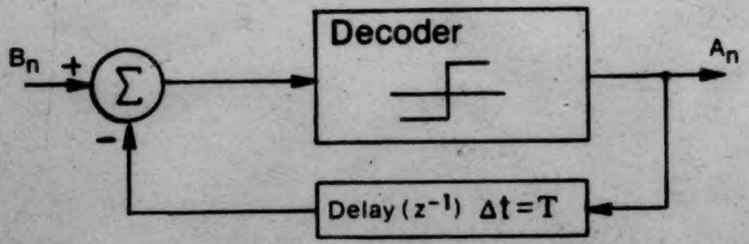
B_n
+
−
Σ
Decoder
A_n
Delay (z^{-1}) $\Delta t = T$

Fig. 3.4 DFE for ISI Cancellation in Duobinary Pulses.

This concept works well when all the decoder decisions are correct. However, incorrect decisions will propagate indefinitely, making the system unusable. This problem can be eliminated by coding the transmitted information in such a way as to pre-compensate for the ISI. This coding results in M signal levels being transmitted as 2M-1 levels. Upon reception, these 2M-1 levels appear as M levels due to the ISI.

3.1.2 The Optimum Receiver Filter for PAM Systems.

The previous section briefly discussed two pulse shapes useful in PAM systems. The design of the transmitter and receiver filters can now be considered. Once a particular pulse shape has been decided upon, we want the convolution of the transmitter filter, receiver filter, and the channel response to be that pulse shape. Furthermore, we would want to maximize the SNR of the received signal.

In this section, the design of the receiver filter will be discussed. This filter will be derived for a specified input pulse and will be optimum for that pulse shape.

The receiver portion of the communication system can be modelled as follows:

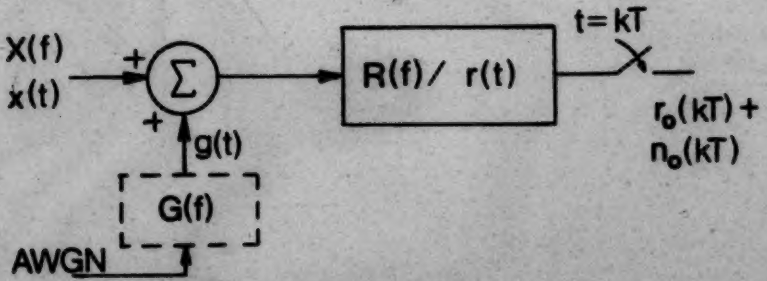

Fig. 3.5 System Model for the Optimum Receiver Filter Design.

The noise in this model, $g(t)$ is assumed to be additive and gaussian, but not necessarily white. The received signal shape is defined by $x(t)$ and $X(f)$. We would like to design $R(f)$, the receiver filter, such that the SNR after sampling is a maximum. Since it is more desirable to work with white noise, $R(f)$ can be broken into two parts, the first being a whitening filter with a transfer function given by:

$$R_w(f) = 1/|G(f)| \tag{3.6}$$

With this whitening filter known, Fig. 3.5 can be redefined for the white-noise case, where $G(f) = 1$. The sampled noise, $g(t)$, will become $n(t)$, to signify it is sampled white noise. The simplified model is thus:

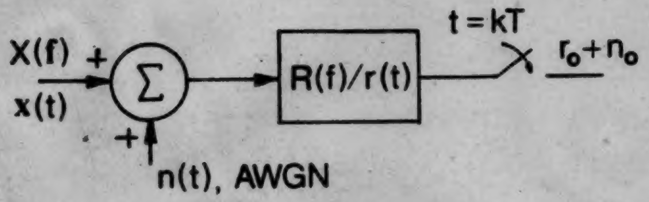

Fig. 3.6 System Model for the Optimum Receiver Filter Design for Additive White Gaussian Noise.

We denote σ_k to be the expected value of the output noise $n_o(kT)$:

$$\sigma_k^2 = E\{n_o(t)^2\} = (N_o/2)\int_{-\infty}^{\infty}|R(f)|^2 df \tag{3.7}$$

$N_o/2$ is the power spectrum of the AWGN. The SNR at the sampler output, S/N, is:

$$S/N = [r_o(kT)/\sigma_k]^2 \tag{3.8}$$

We wish to maximize the SNR. To do this, we make use of the inverse Fourier transform of $r_0(t)$:

$$r_0(t) = \mathcal{F}^{-1}\{R_0(f)\} * \delta(t-\mathcal{T}) = \int_{-\infty}^{\infty} R_0(f)\exp(j2\pi ft)df \tag{3.9}$$

Substituting $R_0(f) = \int_{-\infty}^{\infty} X(f)R(f)$ into Eqn. 3.9 results in

$$r_0(t) = \int_{-\infty}^{\infty} X(f)R(f)\exp(j2\pi ft)df. \tag{3.10}$$

Thus, the signal to noise ratio can be written:

$$S/N = \left|\int_{-\infty}^{\infty} X(f)R(f)\exp(j2\pi ft)df\right|^2 / \left[(N_0/2)\int_{-\infty}^{\infty} |R(f)|^2 df\right] \tag{3.11}$$

To maximize S/N, we rely upon Schwartz's inequality, stated here without proof:

$$\left|\int_{-\infty}^{\infty} Z^*(f)Y(f)df\right|^2 < \int_{-\infty}^{\infty} |Z(f)|^2 df \cdot \int_{-\infty}^{\infty} |Y(f)|^2 df \tag{3.12}$$

Equality occurs for $Z(f) = cY(f)$, where c is a constant.

If we denote $Z^*(f) = X(f)\exp[j2\pi fT]$ and $Y(f)=R(f)$, then S/N will be a maximum when $Z(f) = cY(f)$, or, substituting and letting $c=1$,

$$R(f) = [X(f)\exp(j2\pi fT)]^*. \tag{3.13}$$

The inverse fourier transform of this yields

$$\begin{aligned} r(t) &= \int_{-\infty}^{\infty} R(f)\exp(j2\pi ft)df \\ &= \int_{-\infty}^{\infty} X(f)^* \exp(-j2\pi fT) \cdot \exp(-j2\pi(-f)t)df \\ &= X(T-t). \end{aligned} \tag{3.14}$$

Thus, the optimum receiving filter for white noise is the time-reversed version of the received signal. Such a filter is therefore termed a matched filter. [16,45,46,48]

For the case of colored noise, the optimum filter[1] is the cascade of the whitening filter and the matched filter, with the matched filter matched to $W(f) = X(f)R_w(f) = X(f)^*/|G(f)|$:

$$R(f) = W(f)\exp(-j2\pi fT)/|G(f)| = X(f)^*\exp(-j2\pi fT)/|G(f)|^2 \tag{3.15}$$

For the majority of cases, however, the optimum receiver filter cannot be realized, or else is too complicated and hence expensive to justify. In these cases, other less optimal designs may be used. Often, sharp-cutoff lowpass filters are adequate in limiting the noise. One example in which the optimum filter can be realized is when the input signal, $y(t)$, is the rectangular pulse

$$y(t) = \pm A[u(t+kT) - u(t+(k+1)T)] + n(t) \tag{3.16}$$

and the additive noise is white. The constant A is the signal amplitude, and the $u(t)$ are unit step functions. Then, the matched filter is the well-known integrate and dump filter.

---

[1] This is not quite optimum because the whitening filter spreads the signal beyond the T - second sampling interval. This causes some ISI, as well as a discarding of some of the signal energy in the decision - making process [48].

3.1.3. Joint Design of the Transmitter and Receiver Filters

From section 3.1.2, the optimum receiver filter was found to be a matched filter. If the system model is expanded to include the transmitter filter and the channel, Figure 3.7 is obtained: [46,48]

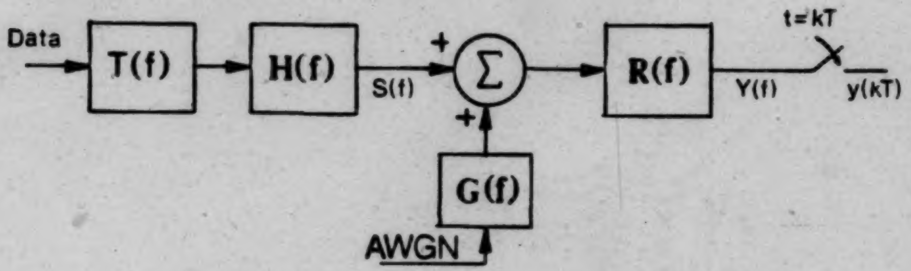

Fig. 3.7 System Model for Joint Design of the Transmitter and Receiver Filters.

$Y(f)$ is the desired pulse shape (for example, a raised cosine pulse), $R(f)$ is the receiver filter, $H(f)$ is the channel response, $T(f)$ is the transmitter filter, and $G(f)$ is the spectrum of the colored noise. Making $R(f)$ a matched filter, we have the relationship

$$R(f) = S(f)^{*}\exp(-j2\pi fT)/|G(f)|^{2}. \qquad (3.17)$$

Looking at only the signal component of the output, we want $S(f) = Y(f)/R(f)$. This yields

$$R(f) = Y(f)\exp(-j2\pi fT)/(R(f)|G(f)|^{2}) \qquad (3.18)$$

Ignoring phase shifts,

$$|R(f)|_{\text{optimal}} = Y(f)^{0.5}/|G(f)| \qquad (3.19)$$

Also, we have $S(f) = T(f)H(f) = Y(f)/R(f)$. Thus, $T(f) = Y(f)/R(f)H(f)$, or,

$$|T(f)|_{\text{optimal}} = \frac{|Y(f)|\cdot|G(f)|}{|Y(f)|^{0.5}\ |H(f)|} = \left|\frac{Y(f)^{0.5}G(f)}{H(f)}\right| \qquad (3.20)$$

For AWGN, these results reduce to:

$$|R(f)|_{optimal} = |Y(f)^{0.5}| \qquad (3.21)$$

$$|T(f)|_{optimal} = |Y(f)^{0.5}/H(f)| \qquad (3.22)$$

As mentioned in section 3.1.2, often these optimum filters are not realizable. These results, however, can serve as general guidelines in practical filter design. In many PAM systems, a transmitter filter is not used, and the transmitted signal is a series of rectangular pulses with some high frequency rolloff due to source bandwidth limitations.

When shot-noise is considered, the variance of the additive noise is dependent on the signal amplitude. However, the additive noise still has a mean of zero. Also, the correlation between noise samples and the signal level is zero (this will be shown in the derivation of the minimum mean-squared-error equalizer). Because of these properties, the optimum filters for the case of shot-noise are identical to the filters derived here and in section 3.1.2.

3.2. Equalization in PAM Systems

Often, it is not possible to eliminate ISI sufficiently through pulse shaping and filtering. Optimum filters, again, may not be realizable, and sometimes the exact channel characteristics are not known in advance. Hence, it is usually easier to compensate for ISI by equalization techniques than it is to eliminate its occurence completely.

Equalizers can be designed in both the frequency and time domain. For optical systems, the most common frequency-domain equalizer is found in conjunction with a high input impedance preamplifier and is essentially a differentiator. This preamplifier - equalizer combination will be mentioned in Chap. 4, where it will be compared with the transimpedance preamplifier design.

With sampled-time systems, equalizers designed in the time-domain tend to be more flexible and straightforward than frequency-domain designs. Consequently, this section will be limited to time-domain equalizer designs.

Three equalizer design approaches will be discussed in detail; the first based on a peak-distortion criterion, the second on minimizing the mean-squared error, and the last being the decision-feedback nonlinear equalizer. The noise will be taken as gaussian and white, but the possibility of shot-noise is included. Extension of the results to colored-noise involves the inclusion of a whitening filter as part of the channel response. In the derivation of the appropriate equalizers, the methods found in the stated references are followed, with appropriate changes to include multilevel signalling and shot-noise.

The zero-forcing (ZF) and minimum mean-squared-error (MMSE) equalizers are realized with a tapped delay line (TDL). The signal to be equalized is sampled at a rate related (usually equal) to the system baud interval T. These samples are fed into a chain of delay circuits, each with a delay equal to the sampling interval. The output signal from each delay circuit is multiplied, or weighted, by some value (weight), with all the weighted outputs going to a common summing amplifier. The output of this summing amplifier is the equalized signal, and the type of equalization is determined by the tap weights. Figure 3.8 shows the structure of the TDL.

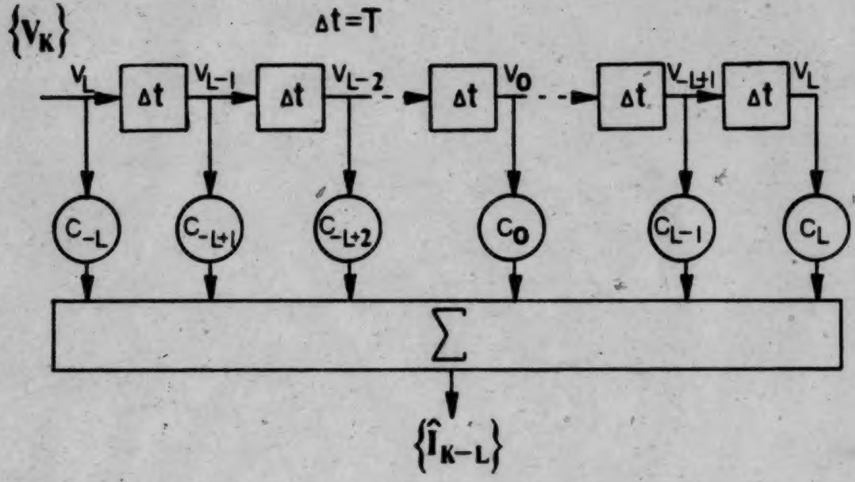

Fig. 3.8 The Tapped Delay Line Structure with Length (2L-1).

3.2.1 The Zero-Forcing Equalizer

Figure 3.9 is an appropriate model of a PAM communication link. Because we are working in the time-domain, it is more appropriate to use Z - transform representations than frequency domain representations for the various sections. R(z) now represents the convolution of the transmitter filter, channel response, and noise-whitening filter, after sampling at the rate 1/T. C(z) is the equalizer to be designed, and n_k is the value of the corrupting noise at the k^{th} sampling instant. I_k and I_k are the transmitted information and an estimate of the transmitted information, respectively.

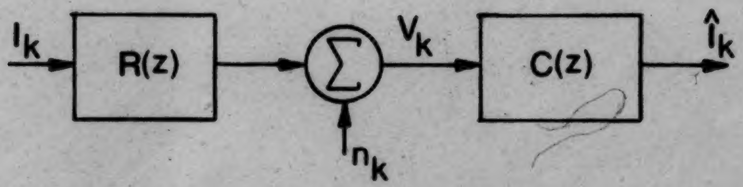

Fig 3.9 Equivalent System Model for Equalizer Design.

We define S(z) = R(z)C(z). In the time - domain, this is represented by:

$$s_k = s(kT) = \sum_{j=-\infty}^{\infty} c_j r_{k-j} \qquad (3.23)$$

From Figure 3.9, we have

$$I_k = r_o I_k + \underbrace{\sum_{j=-\infty}^{\infty} I_j s_{k-j}}_{\text{ISI Terms}} + \underbrace{\sum_{j=-\infty}^{\infty} c_j n_{k-j}}_{\text{Noise}}. \qquad (3.24)$$

The zero-forcing (ZF) criterion is not concerned with the corrupting noise; its aim is to reduce the peak distortion resulting from the ISI terms to zero at as many points as possible. In order to reduce the noise, the C(z) given by the zero-forcing algorithm should include a matched filter [45]. Minimization of the ISI distortion terms in Eqn. 3.24 is accomplished by setting

$$s_k = \begin{cases} 1, & k=0. \\ 0, & k\neq 0. \end{cases}$$

The Z - transform of the s_k yields S(z) = 1. Thus, S(z) = R(z)C(z) = 1, or C(z) = 1/R(z).

This ZF algorithm is attractive in its simplicity; however, because it does not consider noise it is not optimum except for the ideal case of no noise. If the folded spectral characteristic of R(z) contains any nulls, however, the zero-forcing equalizer attempts to compensate for this null by introducing infinite gain at that frequency. This results in infinite noise enhancement and the SNR going to zero. Adaptation of the above algorithm to a finite length equalizer involves a minimization problem with no general solution. (There is a global minima, but no relative minima). However, if the signal distortion defined as

$$D_0 = \sum_{n\neq 0} |r_n|/|r_0| \tag{3.25}$$

is less than unity, the solution to the finite length ZF equalizer is known. For an equalizer having (2L+1) taps, the solution is to set

$$s_k = \begin{cases} 1, & k=0 \\ 0, & k= -L, -L+1, \ldots, -1, 1, 2, \ldots, L. \end{cases} \tag{3.26}$$

This solution, however, is optimum (in terms of reducing the ISI) only if $D_0 = 1$.

The performance of the ZF equalizer strongly depends on the spectral characteristic of the unequalized signal. If the spectral response contains any nulls, the equalizer performance is very poor due to excess noise enhancement. If the distortion is too high ($D_0 > 1$), the appropriate equalizer tap weights become difficult to find, and the algorithm loses its simplicity. Furthermore, because the ZF algorithm does not consider noise, it is not optimum. Consequently, the minimum mean-squared-error algorithm is frequently used. [45]

3.2.2 The Minimum Mean-Squared-Error Equalizer

The zero-forcing algorithm was only concerned with minimizing the ISI terms in Eqn. 3.24. The MMSE algorithm, however, is concerned with minimizing the square of the estimation error, e_k, given by

$$e_k^2 = (I_k - \hat{I}_k)^2 \tag{3.27}$$

From Figure 3.9,

$$v_k = \sum_{n=-\infty}^{\infty} r_n I_{k-n} + n_k \tag{3.28}$$

and $$\hat{I}_k = \sum_{j=-\infty}^{\infty} (c_j v_{k-j})^2 \tag{3.29}$$

Thus, $$e_k^2 = (I_k - \sum_{j=-\infty}^{\infty} c_j v_{k-j})^2 \tag{3.30}$$

When e_k^2 is minimized, e_k is orthogonal to the received, unequalized data $\{v(k)\}$. Following Proakis [45], we want the correlation between the error and the data to be zero. With E denoting "the expected value of", we thus set

$$E\{e_k v_{k-1}^*\} = 0. \tag{3.31}$$

This expression is easier to solve than minimizing the e_k^2 expression, with the same results. Expanding this gives

$$\sum_{j=-\infty}^{\infty} c_j E(v_{k-j} v_{k-1}^*) = E(I_k v_{k-1}^*). \tag{3.32}$$

Substituting for v_k with Eqn. 3.28,

$$E(v_{k-j} v_{k-1}^*) = E\Big\{ \sum_{m=-\infty}^{\infty} r_m I_{k-j-m} \sum_{n=-\infty}^{\infty} r_n^* I_{k-1-n} + \sum_{m=-\infty}^{\infty} (r_m I_{k-j-m}) n_{k-1}^*$$
$$+ (\sum_{n=-\infty}^{\infty} r_n^* I_{k-1-n}) n_{k-j} + n_{k-j} n_{k-1}^* \Big\}. \tag{3.33}$$

Each of these terms can be reduced.

With uncorrelated data, $E(I_k I_l) = \overline{I^2}\delta_{kl}$. Thus, the first term is zero except when $j+m = l+n$. Hence, this term reduces to:

$$E\left(\sum_{m=-\infty}^{\infty} r_m I_{k-j-m} \sum_{n=-\infty}^{\infty} r_n^* I_{k-l-n}\right) = \overline{I^2} \sum_{n=-\infty}^{\infty} r_n^* r_{l+n-j} \tag{3.34}$$

The appropriate shot-noise model equivalent to Eqn. 2.5 is

$$\sigma_n^2 = \sigma_0^2 + \xi|b_n| = \sigma_0^2 + \xi\left|\sum_{k=-\infty}^{\infty} r_k I_{k-n}\right|. \tag{3.35}$$

While the noise variance is dependent on the information, the noise mean is not. Consequently, the second and third terms reduce to zero:

$$E\left(n_{k-l}\sum_{m=-\infty}^{\infty} r_m I_{k-j-m}\right) = E\left(n_{k-j}\sum_{n=-\infty}^{\infty} r_n^* I_{k-l-n}\right) = E(n_k)\sum_{p=-\infty}^{\infty} E(r_p I_{q-p}) = 0 \tag{3.36}$$

The noise samples in term 4 of Eqn. 3.33 are uncorrelated except when $j=l$. Thus,

$$E(n_{k-j} n_{k-l}^*) = E(\sigma_i^2) = \left(\sigma_0^2 + \xi\bar{I}\cdot\left|\sum_{n=-\infty}^{\infty} r_n\right|\right)\delta_{jl} \tag{3.37}$$

Equation 3.32 can now been reduced to Eqn. 3.38:

$$E(v_{k-j} v_{k-l}^*) = \overline{I^2}\sum_{n=-\infty}^{\infty} r_n^* r_{l+n-j} + \left(\sigma_0^2 + \xi\bar{I}\cdot\left|\sum_{n=-\infty}^{\infty} r_n\right|\right)\delta_{jl} \tag{3.38}$$

We now need to consider the right-hand term in Eqn. 3.32:

$$E(I_k v_{k-l}^*) = E\left(I_k \sum_{n=-\infty}^{\infty} r_n^* I_{k-l-n}\right) - E(I_k n_{k-l}) = \overline{I^2} r_{-l}^*. \tag{3.39}$$

Substituting Eqns. 3.38 and 3.39 into 3.32 results in:

$$c_j\left[\overline{I^2}\sum_{n=-\infty}^{\infty} r_n^* r_{l+n-j} + \left(\sigma_0^2 + \xi\bar{I}\cdot\left|\sum_{n=-\infty}^{\infty} r_n\right|\right)\delta_{jl}\right] = \overline{I^2} r_{-l}^* \tag{3.40}$$

By taking the Z - transform of this and defining

$$N = (\sigma_0^2 + \xi I \cdot | \sum_{n=-} r_n |)^2 / \overline{I^2}. \qquad (3.41)$$

the MMSE equalizer is given by

$$C(z) = R^*(z^{-1}) / (R(z) R^*(z^{-1}) + N \delta_{j1}). \qquad (3.42)$$

Notice that this equalizer includes a discrete-time matched filter. This result is expected, because of the inclusion of noise distortion in the equalizer design. For N = 0, the algorithm is identical to the zero-forcing algorithm. The above equalizer design is for an infinite length equalizer and channel memory. However, actual channels have a finite number of ISI precursor and postcursor terms.[1] The maximum number of precursor or postcursor terms will be called M. Also, all realizable equalizers have to be finite in length. The length will be defined as (2L-1) and represents the number of taps in the equalizer. With these restrictions, a more appropriate form for the equalizer than Eqn. 3.42 can be obtained. Defining

$$\Gamma_{j1} = \sum_{n=-M}^{M} r_n^* r_{1+n-j} + N \delta_{j1}, \quad 1, j = -L, -L+1, \ldots 0, \ldots, L \qquad (3.43)$$

and $\zeta_1 = r_{-1}^*$ (3.44)

the appropriate expression equivalent to Eqn. 3.40 is:

$$\Gamma C_{optimal} = \zeta \text{ , or, } C_{optimal} = \Gamma^{-1} \zeta. \qquad (3.45)$$

---

[1] If the received shape for an isolated pulse is drawn in the time domain and sampled at times t=kT, the "cursor" term refers to the pulse peak or near-peak sample. The terms sampled before and after this peak are precursor and postcursor terms respectively, and cause ISI with adjacent pulses.

3.2.3 Decision - Feedback Equalization

In linear equalizers, equalization is performed with a noise - enhancement penalty. A better approach would be to eliminate the interfering terms in such a way as not to incur noise enhancement.

DFE is a method of removing ISI terms arising from the tails (postcursors) of the past pulses without any subsequent noise penalty. To do this, the decoded data is used to estimate the ISI term affecting the present data. This estimate of the ISI is subracted from the incoming data, thereby removing any ISI caused by previous data. In the absence of decoder errors and with an accurate ISI model, the estimated ISI will be very close, if not equal to, the actual ISI caused by previous pulses. Because the decoded pulses are derived from the incoming pulses through a non-linear decision device, the resulting equalizer is non-linear. This non-linear decision process also means that the estimated ISI will be based on decoded and hence noiseless (except when a decoding error is made) data, as opposed to the noisy data entering the decision device.

DFE, however, cannot remove any ISI caused by pulse precursors, as the pulses contributing these precursors have not been decoded as yet. This ISI has to be removed through another equalization method, the most common being one - sided MMSE or ZF equalization. [27,45,50-52]

The overall equalizer, including a leading linear equalizer to remove any ISI caused by future data, is depicted in Fig. 3.10.

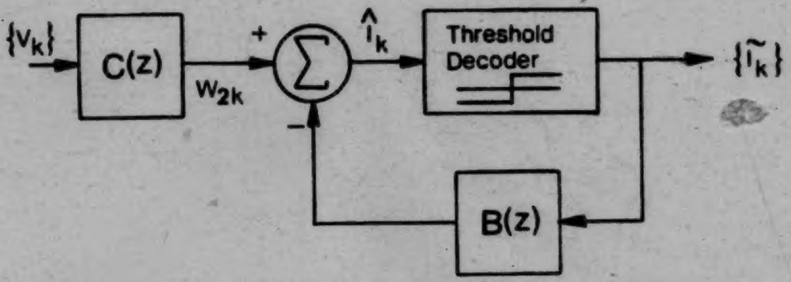

Fig. 3.10 The Decision - Feedback Equalizer with a leading Linear Equalizer.

Both C(z) and B(z) are based on TDL's, and their appropriate tap weights have to be found. The data stored in the B(z) delay circuits is previously decoded data, and the tap weights for B(z) are chosen to model the ISI caused by the data held in the delay line. C(z) only has to remove the ISI caused by future data, and hence is one - sided in its design. Letting the length of C(z) be L, the length of B(z) be infinite, and the channel memory be $\pm M$, we have

$$C(z) = \sum_{k=-L}^{0} c_k z^{-k}, \quad B(z) = \sum_{k=1}^{\infty} b_k z^{-k}, \text{ and } R(z) = \sum_{k=-M}^{M} f_k z^{-k}.$$

Defining $W(z) = C(z)*R(z)$, or, $w_p = \sum_{j=-L}^{0} c_j r_{p-j}$, we can write

$$\hat{I}_k = \sum_{p=-M}^{M} w_p I_{k-p} + \sum_{j=-L}^{0} c_j n_{k-j} - \sum_{n=1}^{\infty} b_n I_{k-n}. \qquad (3.46)$$

Thus,

$$e_k = (I_k-\hat{I}_k) = I_k - \sum_{j=-L}^{0} c_j n_{k-j} - \sum_{p=-M}^{0} w_p I_{k-p} - \sum_{p=1}^{M} w_p I_{k-p} - \sum_{n=1} b_n I_{k-n}$$

$$\text{or } e_k = I_k - \sum_{j=-L}^{0} c_j n_{k-j} - \sum_{p=-M}^{0} w_p I_{k-p} - \sum_{n=1}^{M} (w_n-b_n) I_{k-n} + \sum_{n=M+1} b_n I_{k-n}. \tag{3.47}$$

From this expression, it is evident that $E(e_k^2)$ will be minimized when [27]:

$$b_n = \begin{cases} w_n = \sum_{j=-L}^{0} c_j r_{n-j}, & n=1,2,\ldots\ldots,M. \\ 0, & n= M+1,\ M+2,\ldots, \quad . \end{cases} \tag{3.48}$$

Then, $e_k = I_k - \sum_{j=-L}^{0} c_j n_{k-j} - \sum_{p=-M}^{0} w_p I_{k-p}$. (3.49)

Substitution for w_p gives

$$e_k = I_k - \sum_{j=-L}^{0} c_j n_{k-j} - \sum_{p=-M}^{0} \sum_{j=-L}^{0} c_j r_{p-j} I_{k-p}. \tag{3.50}$$

Let u=p-j. Then, Eqn. 3.49 can be modified to read:

$$e_k = I_k - \sum_{j=-L}^{0} c_j \Big(\sum_{u=-M-j}^{-j} r_u I_{k-j-u} + n_{k-j} \Big). \tag{3.51}$$

Letting $z_{k-j} = \sum_{u=-M-j}^{-j} r_u I_{k-j-u} + n_{k-j}$ results in (3.52)

$$e_k = I_k - \sum_{j=-L}^{0} c_j z_{k-j}. \tag{3.53}$$

The input data stream, $\{v_k\}$, can be expressed as

$$v_k = \sum_{n=-M}^{M} r_n I_{k-n} + n_k. \tag{3.54}$$

As was the case for the MMSE equalizer previously considered in section 3.2.2, the optimum C(z) satisfies $E(e_k v_{k-1}^{*}) = 0$.

Substituting for e_k with Eqn. 3.53, this expression gives:

$E(v^*_{k-1}\sum_{j=-L}^{0} c_j z_{k-j}) = E(I_k v^*_{k-1})$, or, rewriting,

$$\sum_{j=-L}^{0} c_j E(z_{k-j} v^*_{k-1}) = E(I_k v^*_{k-1}). \qquad (3.55)$$

This equation is similar to Eqn. 3.32 derived for the MMSE equalizer alone. The right - hand side was evaluated to be $E(I_k v^*_{k-1}) = \overline{I^2} r^*_{-1}$.

The expression $E(z_{k-j} v^*_{k-1})$ can be reduced just as for the earlier MMSE equalizer. The result is

$$E(z_{k-j} v^*_{k-1}) = \overline{I^2} \sum_{n=-L-M} r^*_n r_{n+l-j} + \overline{I^2} N \delta_{jl}. \qquad (3.56)$$

where N is defined by Eqn. 3.41. We now have the result

$$\sum_{j=-L}^{0} c_j (\overline{I^2} \sum_{n=-L-M}^{-1} r^*_n r_{l+n-j} + \overline{I^2} N \delta_{jl}) = \overline{I^2} r^*_{-1} \qquad (3.57)$$

We can define $\Gamma_{jl} = \sum_{n=-L-M}^{-1} r^*_n r_{l+n-j} + N\delta_{jl}$, $j,l = -L, -L+1, \ldots 0$ (3.58)

and $\zeta_l = r^*_{-1}$. (3.59)

Again, M is the channel memory length. These expressions are very similar to Eqns. 3.43 and 3.44, the difference being due to the one-sided nature of C(z). As before, $C_{optimal} = \Gamma^{-1}\zeta$.

Again, the feedback equalizer tap weights, from Eqn. 3.48, are

$$b_n = \sum_{j=-L}^{0} c_j r_{n-j}, \quad n=1,2,3,\ldots M.$$

Notice that, although we started by allowing the length of B(z) be infinite, it only needs to be as long as the channel memory.

3.2.4 Residual Distortion in the Equalizer Designs

The performance of the three equalizer types discussed can be compared by determining the remaining signal distortion at the output of each equalizer. [45]

The distortion includes both noise and remaining ISI, and is denoted by J. Letting $J_{maximum} = 1$, for the linear equalizers we have $\overline{I^2}J = E|I_k-\hat{I}_k|^2 = E(e_kI_k^*) - E(e_k\hat{I}_k^*)$

$$= E(I_kI_k^*) - E(\hat{I}_kI_k^*) - E(I_k\hat{I}_k^*) + E(\hat{I}_k\hat{I}_k^*) \qquad (3.60)$$

The second term, upon substitution of Eqn. 3.28 and 3.29, with the constraint of a finite length equalizer, becomes

$$E(\hat{I}_kI_k^*) = E((\sum_{j=-L}^{L} c_j(\sum_{n=-M}^{M} r_nI_{k-j-n} + n_{k-j}))I_k^*)$$

$$= \sum_{j=-L}^{L} c_j[E(\sum_{n=-M}^{M} r_nI_{k-j-n}I_k^*) + E(n_{k-j}I_k^*)] = \overline{I^2}\sum_{j=-L}^{L} c_jr_{-j}. \qquad (3.61)$$

Likewise, the third term becomes

$$E(I_k\hat{I}_k^*) = \overline{I^2}\sum_{j=-L}^{L} c_j^*r_{-j}^*. \qquad (3.62)$$

The last term can also be reduced:

$$E(\hat{I}_k\hat{I}_k^*) = E(\sum_{j=-L}^{L} c_jv_{k-j}\sum_{l=-L}^{L} c_l^*v_{k-l}^*)$$

$$= \sum_{j=-L}^{L} c_j\sum_{l=-L}^{L} c_l^*\cdot E(v_{k-j}v_{k-l}^*)$$

$$= \sum_{j=-L}^{L} c_j\sum_{l=-L}^{L} c_l^*(\overline{I^2}\sum_{n=-M}^{M} r_n^*r_{l+n-j} + (\sigma_o^2 + \xi\overline{I}|\sum_{n=-M}^{M} r_n|)\delta_{jl}) \qquad (3.63)$$

Thus, the normalized distortion is

$$J = 1 - \sum_{j=-L}^{L} c_jr_{-j} - \sum_{j=-L}^{L} c_j^*r_{-j}^* + \sum_{j=-L}^{L}\sum_{l=-L}^{L} c_jc_l^*(\sum_{n=-M}^{M} r_n^*r_{l+n-j} + N\delta_{jl}). \qquad (3.64)$$

Substituting with ζ_l and Γ_{jl} (Eqns. 3.43 and 3.44),

$$J = 1 - \sum_{j=-L}^{L} c_j \zeta_j^* - \sum_{j=-L}^{L} c_j^* \zeta_j + \sum_{l=-L}^{L} c_l^* \Big(\sum_{j=-L}^{L} c_j \Gamma_{jl} \Big), \tag{3.65}$$

or, in matrix form, $J = 1 - C^T \zeta^* - (C^T)^* \zeta + (C^T)^* \Gamma C.$ (3.66)

For $C = C_{optimal} = \Gamma^{-1}\zeta$ and $C^T_{optimal} = \zeta^T (\Gamma^{-1})^T$,

$$J_{minimum} = 1 - \zeta^T (\Gamma^{-1})^T \zeta^* - (\zeta^T)^* ([\Gamma^{-1}]^T)^* \zeta + (\zeta^T)^* ([\Gamma^{-1}]^T)^* \Gamma \Gamma^{-1} \zeta$$

$$= 1 - C^T \zeta^* = 1 - \sum_{j=-L}^{L} c_j r_{-j}^*. \tag{3.67}$$

For real coefficients, $J = 1 + C^T (\Gamma C - 2\zeta)$ (3.68)

and $J_{minimum} = 1 - C^T \zeta = 1 - \zeta^T \Gamma^{-1} \zeta.$ (3.69)

The SNR can be related to J [17]: $SNR = (1-J)/J.$ (3.70)

Consequently, $SNR_{maximum} = (\zeta^T \Gamma^{-1} \zeta)/(1 - \zeta^T \Gamma^{-1} \zeta).$ (3.71)

For the decision-feedback equalizer, the above results apply when the one - sided expressions for Γ and ζ are used. The equivalent expression to Eqn. 3.65 is

$$J_{DFE} = 1 - \sum_{j=-L}^{0} c_j \zeta_j^* - \sum_{j=-L}^{0} c_j^* \zeta_j + \sum_{l=-L}^{0} c_l^* \Big(\sum_{j=-L}^{0} c_j \Gamma_{jl} \Big). \tag{3.72}$$

With the use of Eqns. 3.57 to 3.59, the minimum distortion for the DFE equalizer (with a leading MMSE equalizer) is

$$J_{min.,DFE} = 1 - \sum_{j=-L}^{0} c_j r_{-j}^* = 1 - C^T \zeta^*, \tag{3.73}$$

as for the MMSE equalizer.

3.2.5 Equalizer Design Procedure Examples.

The residual distortions found in the last section offer little physical insight into the performance differences between the three equalizers. Hence, the three design procedures derived in Sections 3.2.1 to 3.2.3, will be briefly outlined for a hypothetical channel.

The sampled channel response to a unit pulse is given by $R = [\ r_{-1},\ r_0,\ r_1\ ] = [\ 0.1,\ 0.8,\ 0.3\ ]$. This channel has only one precursor and one postcursor, and hence $M=1$. The postcursor term is larger than the precursor term, which is typical for fiber channels. This suggests that DFE should perform significantly better than the linear equalization methods.

The normalized noise, N, will be taken as 10^{-2}. The linear equalizers will be limited to 3 taps so that the design procedure is kept relatively simple. The decision - feedback equalizer will have two feedforward (linear equalization) taps and one feedback term.

1. The ZF Design.

First, the signal distortion term, D_0, has to be found. From Eqn. 3.25, $D_0 = (0.1 + 0.3)/0.8 = 0.5$. Since $D_0<1$, the solution to the equalizer design is given by Eqns. 3.23 and 3.26:

$$c_{-1}r_0 + c_0r_1 = 0.$$

$$c_{-1}r_1 + c_0r_0 = 1.$$

$$c_0r_1 + c_1r_0 = 0.$$

In matrix form, with r_{-1}, r_0, and r_1 substituted:

$$\underbrace{\begin{bmatrix} .8 & .1 & 0 \\ .3 & .8 & .1 \\ 0 & .3 & .8 \end{bmatrix}}_{\Gamma} \underbrace{\begin{bmatrix} c_{-1} \\ c_0 \\ c_1 \end{bmatrix}}_{C} = \underbrace{\begin{bmatrix} 0 \\ 1 \\ 0 \end{bmatrix}}_{\zeta}$$

The solution to this matrix is $c_{-1} = -0.1724$, $c_0 = 1.379$, and $c_1 = -0.5172$. (The numeric accuracy will be kept to ensure the equalizer distortion derived later will be accurate.)

2. The MMSE Design Procedure.

For this equalizer, we need to find the Γ_{jl} as defined by Eqn. 3.43, for j,l = -1, 0, 1:

$$\Gamma_{-1,-1} = \Gamma_{0,0} = \Gamma_{1,1} = r_{-1}^2 + r_0^2 + r_1^2 + N = 0.75$$

$$\Gamma_{-1,0} = \Gamma_{0,-1} = \Gamma_{0,1} = \Gamma_{1,0} = r_{-1}r_0 + r_0r_1 = 0.32$$

$$\Gamma_{-1,1} = \Gamma_{1,-1} = r_{-1}r_1 = 0.03$$

From these Γ_{jl} and from Eqns. 3.44 and 3.45:

$$\begin{bmatrix} 0.75 & 0.32 & 0.03 \\ 0.32 & 0.75 & 0.32 \\ 0.03 & 0.32 & 0.75 \end{bmatrix} \begin{bmatrix} c_{-1} \\ c_0 \\ c_1 \end{bmatrix} = \begin{bmatrix} 0.3 \\ 0.8 \\ 0.1 \end{bmatrix}$$

Solving this matrix gives the tap weights $c_{-1} = -0.1399$, $c_0 = 1.305$, and $c_1 = -0.4177$. Notice that these tap weights are close to the ones found for the ZF equalizer. This suggests that the system noise N is relatively small in comparison to the ISI distortion. The equalizer residual distortions for the two equalizers will be almost the same.

3. The DFE Design Procedure.

In order to keep the total number of taps to three (so that a valid comparison between the three equalizers can be made), the linear portion of this equalizer will have only two taps (j,l = -1,0). From Eqn. 3.58,

$$\begin{aligned}
\Gamma_{-1,-1} &= r_{-1}^2 + r_0^2 + r_1^2 + N = 0.75.\\
\Gamma_{-1,0} &= r_{-1}r_0 + r_0r_1 = 0.32.\\
\Gamma_{0,-1} &= r_0r_{-1} + r_1r_0 = 0.32.\\
\Gamma_{0,0} &= r_{-1}^2 + r_0^2 + N = 0.66.
\end{aligned}$$

The difference between these Γ_{jl} and the Γ_{jl} corresponding to a two-tap MMSE design is that $\Gamma_{0,0} = \Gamma_{-1,-1}$. The r_1^2 term is missing in $\Gamma_{0,0}$ as a consequence of the one-sided nature of this linear equalizer. The forward equalizer taps are given by:

$$\begin{bmatrix} 0.75 & 0.32 \\ 0.32 & 0.66 \end{bmatrix} \begin{bmatrix} c_{-1} \\ c_0 \end{bmatrix} = \begin{bmatrix} 0.3 \\ 0.8 \end{bmatrix}$$

Thus, $c_0 = 1.2838$ and $c_{-1} = -0.1478$. The feedback tap value, from Eqn. 3.48, is

$$b_1 = c_{-1}r_2 + c_0r_1 = 0.3851.$$

4. Residual Distortion in the Designed Equalizers.

The residual distortion for the ZF equalizer is derived from Eqn. 3.68, with $\Gamma = \Gamma_{MMSE}$, $\zeta = \zeta_{MMSE}$, and $C = C_{ZF}$:

$$J_{ZF} = 1 + [-0.172 \ \ 1.379 \ \ -0.517]\left(\begin{bmatrix} 0.75 & 0.32 & 0.03 \\ 0.32 & 0.75 & 0.32 \\ 0.03 & 0.32 & 0.75 \end{bmatrix}\begin{bmatrix} -0.172 \\ 1.379 \\ -0.517 \end{bmatrix} - 2\begin{bmatrix} 0.3 \\ 0.8 \\ 0.1 \end{bmatrix}\right)$$

$$= 0.0464.$$

The SNR corresponding to this, in dB, is

$$SNR_{ZF} = 20\log((1-J)/J) = 26.3 \text{ dB}.$$

For the MMSE equalizer, either the above expression, with $C = C_{MMSE}$, or the reduced Eqn. 3.69, gives $J_{MMSE} = 0.04008$. Thus, $SNR_{MMSE} = 27.6$ dB.

For DFE, from Eqn. 3.73, $J_{DFE} = 1 - c_{-1}r_1 - c_o r_o = 0.01732$. Thus, $SNR_{DFE} = 35.1$ dB.

For the same complexity (3 taps), the DFE equalizer SNR is 7.5 dB and 8.8 dB better than the SNR's for the ZF and MMSE equalizers respectively. If there were complete ISI cancellation with no penalty (ignoring the shot-noise that the ISI would cause), the SNR would be[1]:

$$SNR_{no\ ISI} = 20\log(r_o/N) = 38.1 \text{ dB}.$$

With this SNR as a reference, the decision-feedback equalizer has a penalty of 3 dB, the MMSE equalizer has a 10.5 dB penalty, and the ZF equalizer has a 11.8 dB penalty. This justifies the use of DFE in the experimental system over the other types of equalization.

---

[1] This is not the optimum SNR available with any form of equalization, as the signal information available from the precursor and postcursor terms is being discarded.

CHAPTER 4. THE EXPERIMENTAL 4 LEVEL PAM SYSTEM

In Chapter 2, the possible benefits of multilevel signalling and equalization for dispersive multimode fiber systems were investigated. In this investigation, the use of DFE, which would allow the system's maximum baud rate to be doubled with a 3.5 dB power penalty, was assumed. In Chap. 3, both optimum filtering and equalization were considered as methods of eliminating or controlling any ISI that may occur. For practical systems, the topic of optimum filtering is largely an academic topic, and some degree of equalization is necessary. For multimode fiber systems, DFE appears to be much superior to either ZF or MMSE equalization. In fact, for a typical 850 nm fiber response, it has been shown that DFE, even without a leading precursor equalizer, is superior to the optimum linear (Kalman filter) equalizer [49].

This chapter is concerned with the design of a 4 level PAM multimode fiber system with one - tap DFE. The objective of this experimental system is to demonstrate the thus far theoretical benefits of multilevel signalling and DFE discussed in Chapters 2 and 3. Figure 4.1 is a block diagram of the experimental system, which should be compared to Fig. 1.1, the more general optical system block diagram. Most of the differences between these two diagrams lie in the receiver sections, and hence will be discussed in conjunction with the experimental receiver design. Each of the components of Fig. 4.1 will be discussed below.

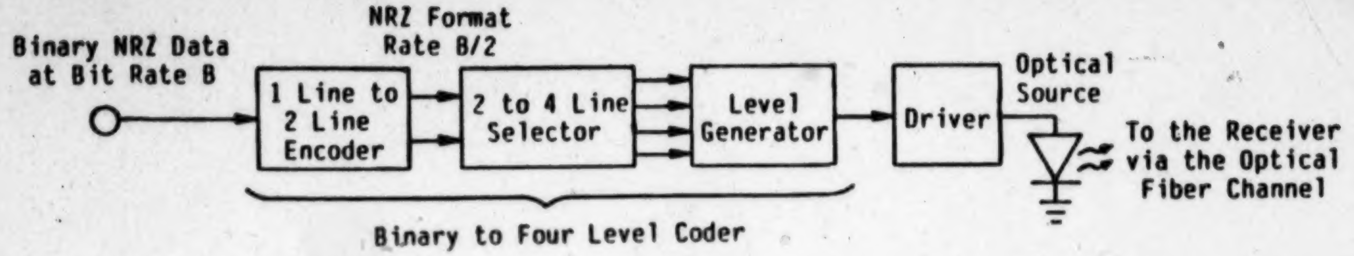
Binary NRZ Data
at Bit Rate B
NRZ Format
Rate B/2
1 Line to
2 Line
Encoder
2 to 4 Line
Selector
Level
Generator
Driver
Optical
Source
To the Receiver
via the Optical
Fiber Channel
Binary to Four Level Coder

a) Transmitter

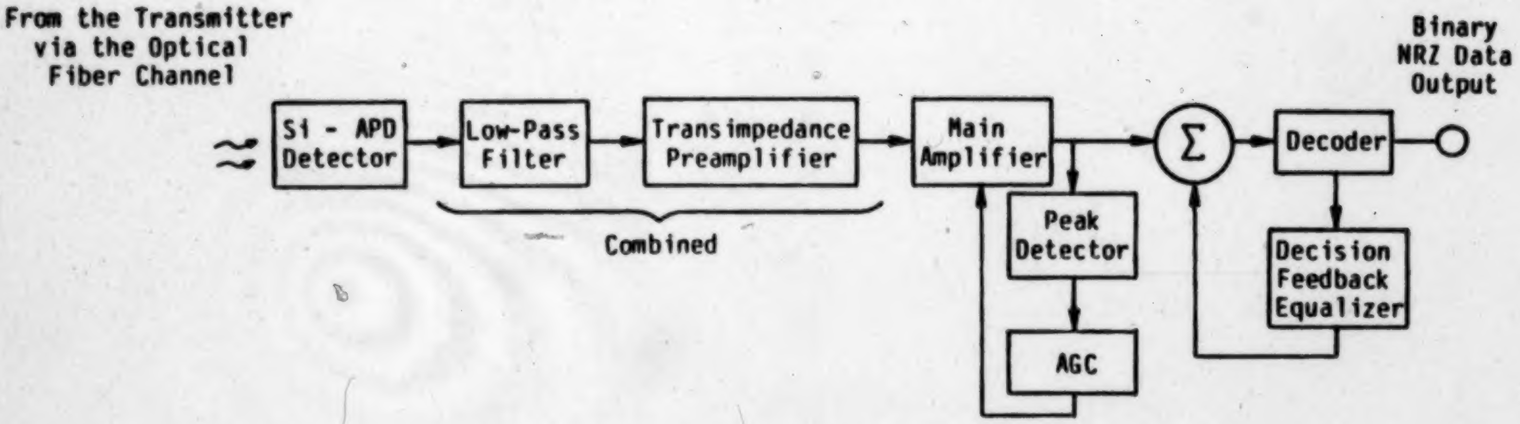
From the Transmitter
via the Optical
Fiber Channel
Si - APD
Detector
Low-Pass
Filter
Transimpedance
Preamplifier
Combined
Main
Amplifier
Peak
Detector
AGC
Σ
Decoder
Decision
Feedback
Equalizer
Binary
NRZ Data
Output

b) Receiver

Fig. 4.1 The Experimental 4 - Level PAM System.

4.1 The Optical Fiber

In order to have an affordable dispersion-limited system (as opposed to an attenuation-limited one), a fiber with a sufficiently low bandwidth to ensure significant ISI at moderate bit rates was chosen. The fiber selected was Siecor's Super-Fat Fiber Cable #155. This multimode fiber has the following properties [53]:

a) A high numerical aperature of 0.4.

b) An attenuation of 35 dB/km at 830 nm.

c) A minimum modal BDP of 5 MHz-km.

This fiber is intended for short-haul applications such as in power system communications; hence it has poor characteristics for medium-distance communications. The length used was 670 m; from the specifications, this length should result in a channel loss (excluding connector loss) of approximately 20 dB. Since this fiber has such a low modal bandwidth, and because the fiber length is under 1 km, the fiber bandwidth estimate is 5MHz·km/0.67 km = 7.5 MHz.

The maximum expected symbol rate for this channel, with no appreciable ISI and without elaborate filtering, is 7.5 to 10 Mbaud/s. With equalization, operation at baud rates above the channel's estimated Nyquist baud rate of 15 Mbaud/s may be possible, and consequently the system components should be capable of 20 Mbaud/s operation. For a 4-level signal, this translates into 40 Mb/s as an appropriate design value.

4.2 The Transmitter

The requirements for the transmitter are:

1. Compatability with a binary NRZ digital (TTL or ECL) input.

2. Conversion from 2 to 4 level coding, with adjustable level spacing and optical power output.

3. Capability of operation at up to 40 Mbit/second.

4. Optical output at a wavelength around 830 nm for compatability with the optical fiber.

Referring to Figure 4.1, the 1-line to 2-line encoder in the transmitter converts the incoming binary (NRZ format) data stream into two binary data streams. Each of these data streams has a bit rate half that of the input binary data stream. These two lines go to a 2-to-4 line selector, which activates an appropriate output line depending on the status of the two input lines. The level generator (which is a simple resistive divider) produces a 4 level signal whose amplitude is determined by the status of these 4 lines, and this 4 level signal controls the driver and hence the optical source intensity.

The optical source chosen is Northern - Telecom's high radiance LED #NT 40-3-30-3. The optical 3 dB bandwidth of this LED is 44 MHz (typically), its emission wavelength is 830 nm, and its FWHM spectral width is typically 40 nm [54].

In order to minimize the probability of error upon reception, Gray-coding [55] is used such that only one bit of the two represented by each of the four levels is changed in transitions between adjacent levels. With Gray coding, the erroneous decoding of a received signal level as being an adjacent level results in only a one bit error, as opposed to a possible two erroneous bits with another coding scheme.

Figure 4.2 shows the transmitter schematic, along with the associated coding. The division of the input stream into two data streams is accomplished with flip-flops and gates (IC1 to IC4). IC5 is the 2-to-4 line selector, and the potentiometers P1 to P4 generate the 4 level signal. These potentiometers allow for adjustment of each signal level. The transistor driver stage converts the 4 level voltage signal into an appropriate LED current.

4.3 The Optical Receiver

Comparing Fig. 4.1 to Fig. 1.1, the following differences are evident:

1. The problem of clock recovery was not considered in this thesis, although in a practical system it would have to be included. Much literature is available on this topic [56-58].

2. Automatic-gain-control was used in conjunction with the main amplifier, but not with the optical detector and preamplifier. Rather, the detector bias voltage could be externally controlled for maximum system flexibility. (For most of the measurements, the recommended operating voltage for the optical detector was used because the characteristics of the detector are stated for this voltage.)

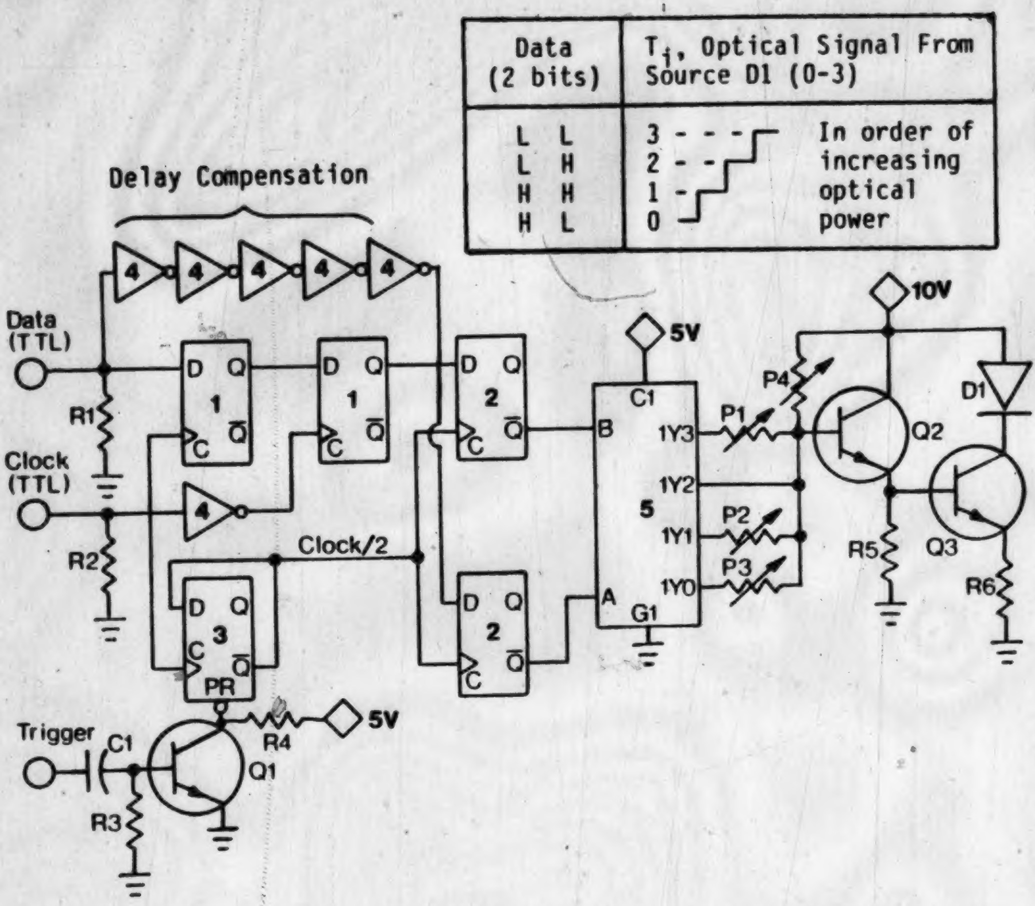
Delay Compensation
4
Data
(TTL)
Clock
(TTL)
Trigger
R1
R2
R3
R4
C1
Q1
5V
D
Q
C
Q̄
1
2
3
PR
Clock/2
B
A
C1
G1
5
1Y3
1Y2
1Y1
1Y0
P1
P2
P3
P4
10V
Q2
Q3
R5
R6
D1

Data (2 bits)	T_i, Optical Signal From Source D1 (0-3)	
L L	3	In order of increasing optical power
L H	2	
H H	1	
H L	0	

Optical Output P_i

R1,2,3	- 50 ohms
R4	- 1.0 kilo-ohms
R5	- 390 ohms
R6	- 15 ohms, 2 watts
P1	- 5.0 kilo-ohm trimpot
P2,3,4	- 10 kilo-ohm trimpots
C1	- 100 to 200 pF
D1	- NT 40-3-30-3 LED
Q1	- 2N4401
Q2,3	- 2N5943
IC1,2,3	- SN74S74
IC4	- SN74S04
IC5	- SN74156

Fig. 4.2 Transmitter Schematic and Coding.

3. In order to evaluate the effectiveness of DFE alone, linear equalization was not used in the receiver. This decision was made with regard to the results of Kasper [28], who showed that, for simulated binary PAM systems, DFE with optimum timing and no precursor equalizer was almost as effective as "pulse-peak timed" DFE with a leading equalizer. The subject of optimum timing will be explained in Chapter 6.

4. The filter used in the experimental system was incorporated into the preamplifier design; it can be controlled somewhat through the DC biasing of the preamplifier. Although optimum signal filters in both the transmitter and receiver would have increased the overall receiver sensitivity, enough information on the channel's dispersion characteristics was not known in advance to design proper filters. An integrate-and-dump filter in the receiver would have been feasible, but would have complicated the decoder and equalizer design, especially for operation at varying baud-rates.

Hence, the overall receiver design was relatively straightforward, except for the preamplifier. Although much attention has been given to optical preamplifier design in the literature, emphasis will be placed on the experimental preamplifier in this chapter because it is the most critical and, in terms of design, most complex portion of the system. The design details, however, are left to Appendix B.

4.3.1 The Optical Detector and Preamplifier.

To approach the maximum baud rate that can be supported by a fiber channel without incurring excessive ISI, the receiver's optical detector/preamplifier (ODP) combination has to have a much higher bandwidth than the channel. However, noise considerations require that the ODP bandwidth be as small as possible; consequently, a compromise must be made. This tradeoff manifests itself as a decrease in receiver sensitivity as its bandwidth is increased, as illustrated by Fig. 2.2.

Proper preamplifier design and detector choice therefore involves both sensitivity and bandwidth considerations. Furthermore, for economic reasons, the receiver has to be applicable to as many systems as practicable. A design that is optimum for one power level may saturate at a slightly higher level, thus making the device useful for only a narrow range of applications. For both commercial applications and experimental ones such as this, the received power may vary over such a range that a large receiver dynamic range is essential.

The bandwidth associated with an ODP is primarily determined by the time-constant associated with the preamplifier's input capacitance and the resistance seen by this capacitance. The input capacitance consists of the parallel combination of the detector capacitance, the capacitance of the first amplifying device, and the wiring capacitance. Usually, it is not under designer control (with the exception of Miller capacitance) save through device selection and circuit construction practices. The resistance seen by this capacitance, however, can be controlled by the designer. With this in mind, two broad categories of optical receiver preamplifiers have emerged, one based on a high input impedance design, and the other with a relatively low effective input impedance.

Again, of the two types of signal degradation that are of concern here (noise and ISI), ISI is deterministic. Stochastic noise, on the other hand, is random and cannot be compensated for in any fashion. The high-impedance (HI) design recognizes this and, by making the preamplifier input resistance large, reduces the thermal noise associated with this resistance. The resulting time-constant is large relative to the baud-interval, and severe ISI occurs. Equalization is therefore required to compensate for the partial signal integration performed by the preamplifier input network. The philosophy is that this equalization can be performed after amplification of the detected signal, so that the overall noise figure of the preamplifier is minimized. Although the required equalization, which is often in the form of a differentiator, results in noise enhancement, the preamplifier noise is still kept small in comparison to the signal shot noise, and some net sensitivity gain is achieved.

In contrast with the above type of preamplifier is the design aproach resulting in a sufficiently low input impedance such that the associated time-constant is comparable to or smaller than the baud interval. This results in a higher input thermal noise level than the HI design; however, because little or no signal distortion is introduced by the receiver, no compensating equalization is required. (Of course, some may be required to correct for the channel distortion incurred.)

Most optical detectors are current sources, whereas signal decoders usually compare voltage levels. Consequently, the majority of low input impedance preamplifiers perform a current to voltage conversion and are aptly called transimpedance (TI) preamplifiers. Feedback is usually added to lower the effective input resistance while keeping the actual physical resistance high. Thus, feedback increases the ODP bandwidth without increasing its thermal spot noise. Feedback also increases the dynamic range of the ODP; often this consideration, and not noise and bandwidth ones, determines the amount of feedback used. If noise were the only consideration, enough feedback could be applied to provide a physical input resistance as high as in the HI design while keeping the effective input resistance low, so that noise-enhancing equalization is not required. However, to do this the preamplifier must possess a high open-loop voltage gain, leading to instability.

A comparison of the two designs shows that the HI preamplifier has a slightly greater sensitivity than the TI design, for comparable bandwidths. However, the HI design requires careful equalization to accurately compensate for its introduced signal distortion. Because of device manufacturing variations, this equalization usually has to be tailored to individual units; obviously, this is not commercially feasible. Also, because of the partial integration in the HI preamplifiers, the first stage of the design can saturate easily, resulting in a low dynamic range. The TI preamplifier, in contrast, does not have this inherent problem.

Thus, HI preamplifiers are used only for applications requiring the utmost sensitivity; for most systems, a TI preamplifier is preferred. Furthermore, with the TI preamplifier, the designer has enough control over the input resistance so that some front-end signal integration can occur if desired. A TI preamplifier was chosen for this system because of the needed dynamic range and bandwidth flexibility [5,7,39,59-65].

The optical detector can be either a PIN diode or an APD. APDs require much higher bias voltages than PIN diodes. This higher bias allows for signal amplification through avalanche gain, and hence less external amplification is required. However, this avalanche gain, being a quantum effect, is not constant and results in excess shot noise because of its random nature.

For a complete analysis of the noise characteristics of optical detectors in conjunction with a preamplifier, several factors involving, for example, device characteristics and the optical pulse shape, have to be considered. The resulting expressions, although accurate, have little obvious physical meaning, and are not required to make a simple comparison between PIN ODPs and APD ODPs. Personick and others have considered this subject in more depth [5,59,60,66]. The elementary results that will be derived below, although not complete, provide enough physical insight to allow a proper choice of optical detector.

Figure 4.3 illustrates the input and output noise and signal levels for a PIN detector/preamplifier and an APD detector/preamplifier. P_i refers to the received optical power, Si to the preamplifier input signal, σi to the noise corrupting this signal, and So and σo to the amplifier output signal and noise. The gain, G, for the PIN diode detector is one; for the APD its average value is denoted by $\overline{G}$. The amplifier introduces noise σ_{amp}, and this input-referred noise, being essentially independent of the amplifier gain and the detector used, is assumed to be the same for both the PIN and APD preamplifiers. The output of the PIN-diode ODP is:

$$(So + \sigma o)_{PIN} \equiv A\cdot Si_{PIN} + A(\sigma i^2_{PIN} + \sigma^2_{amp})^{0.5} \qquad (4.1)$$

For the APD ODP,

$$\begin{aligned}(So + \sigma o)_{APD} &\equiv (A/\overline{G})\cdot(Si_{APD} + (\sigma i^2_{PIN} + \sigma^2_{amp})^{0.5}) \\ &= A\cdot Si_{PIN} + (A/\overline{G})\cdot(\sigma i^2_{APD} + \sigma^2_{amp})^{0.5}. \qquad (4.2)\end{aligned}$$

These equations have the same output signal level, So; however, their noise levels are different. If the detector noise is broken into a signal shot-noise component and a dark-current shot-noise component, the detector noises can be related:

$$\sigma i^2_{PIN} \equiv \sigma^2_{shot} + \sigma^2_{dark} \qquad (4.3)$$

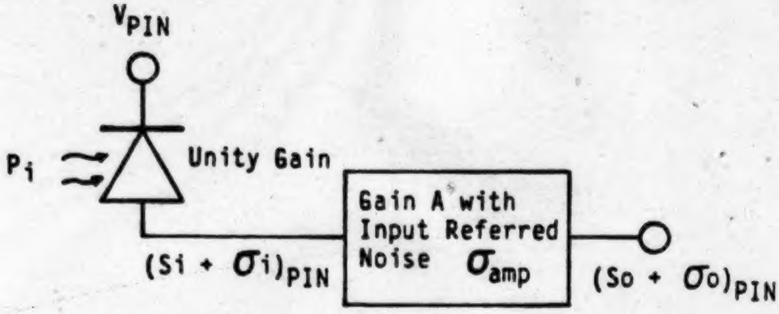
V_{PIN}
P_i
Unity Gain
Gain A with Input Referred Noise σ_{amp}
$(Si + \sigma i)_{PIN}$
$(So + \sigma o)_{PIN}$

a) Pin Diode Detector and Preamplifier

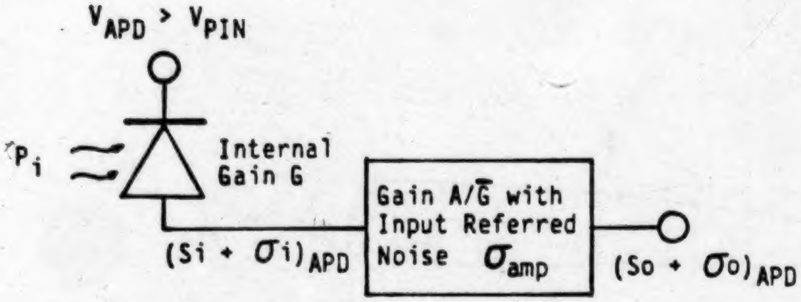
$V_{APD} > V_{PIN}$
P_i
Internal Gain G
Gain $A/\bar{G}$ with Input Referred Noise σ_{amp}
$(Si + \sigma i)_{APD}$
$(So + \sigma o)_{APD}$

b) APD Detector and Preamplifier

Fig. 4.3 Equivalent Optical Detector/Preamplifier Combinations for Noise Level Comparisons.

For σi^2_{APD}, the signal component is multiplied by the expected value of G^2, whereas the dark-current noise is not. (The assumption that the dark current is primarily surface current, as opposed to bulk current, is made here. The bulk dark current does undergo avalanche multiplication, but is negligible.) [26,66]

$$\sigma i^2_{APD} \equiv G^2\sigma^2_{shot} + \sigma^2_{dark}. \tag{4.4}$$

The expected value of G^2 is not $(\overline{G})^2$. A simple expression for G^2 will be used here; a more accurate one is given in [66]. This expression is [26,62]

$$G^2 \equiv (\overline{G})^{2+x}. \tag{4.5}$$

The parameter x is from 0.3 to 0.5 for typical silicon APDs; for germanium APDs it is close to unity. Substitution of equations 4.3, 4.4, and 4.5 into 4.1 and 4.2 results in:

$$\sigma o_{PIN}{}^2 \equiv A^2(\sigma^2_{shot} + \sigma^2_{dark} + \sigma^2_{amp}) \tag{4.6}$$

$$\sigma o_{APD}{}^2 \equiv A^2[(\overline{G})^x\sigma^2_{shot} + (\sigma^2_{dark} + \sigma^2_{amp})/(\overline{G})^2] \tag{4.7}$$

The PIN -diode expression (Eqn. 4.6) is identical to the APD noise expression (Eqn. 4.7) with $\overline{G} = 1$. Thus, a valid comparison between the two can be made by finding the optimum avalanche gain. If this gain is close to unity, the use of an APD is not justified. If, however, it is much larger than one, a more sensitive receiver could be realized with an APD detector. Differentiating Eqn. 4.7 with respect to the gain and setting the result to zero yields:

$$\overline{G}_{optimum} \equiv [2(\sigma^2_{dark} + \sigma^2_{amp})/x\,\sigma^2_{shot}]^{1/(2+x)} \tag{4.8}$$

This is identical to the result derived by Pearsall [66], except for the APD excess-noise factor expression used. When appropriate values are substituted in the above expressions, the optimum gain for a silicon APD is usually much larger than one; often, the optimum gain is around 100. Because of the large value of this gain (for 850 nm systems), receivers incorporating silicon APDs are more sensitive than PIN-diode receivers [39,66, Chap. 2]. Hence, a silicon APD was chosen as the detector for the experimental receiver. The particular device used is RCA's #C30908E APD. This detector has a high responsivity of 77 amps per watt of optical power at 830 nm operation and at the recommended operating voltage.

With the above choices for the optical detector and preamplifier type, the preamplifier design can now be attended to. Its first stage should exhibit good frequency response, high current gain, and low noise. The cascode (common-emitter, common base) transistor pair meets these requirements, and is often found in high-frequency amplifiers. In order to drive an external 50 ohm amplifier, a additional common-collector (CC) stage is used as a buffer. With the addition of voltage-shunt feedback, the ac equivalent preamplifier circuit, including stray capacitances, becomes as shown in Figure 4.4.

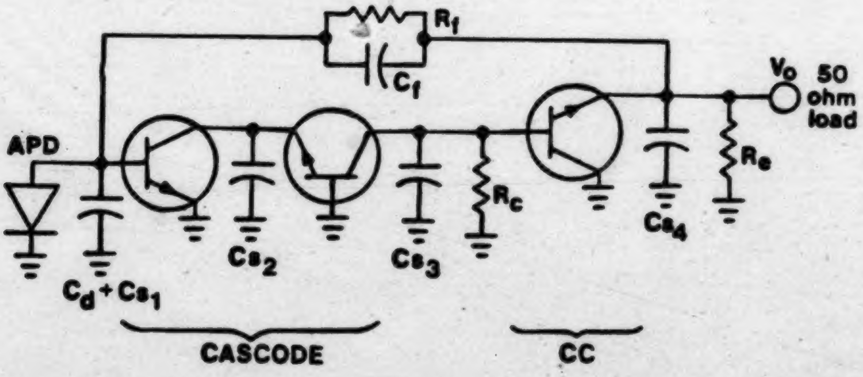

Fig. 4.4 AC-Equivalent Circuit for the Preamplifier.

The design procedure must determine the optimum or near-optimum resistors (Rf,Rc,Re) and dc bias conditions for the desired signal bandwidth and load (50 ohms). This optimization is with respect to the input referred circuit noise, under the restraints imposed by stability requirements. El-Diwany *et. al.* [64] considered this problem, and have derived the optimum circuit parameters by approximating the amplifier's frequency response with a two pole transfer function and through the use of a hybrid-pi model for the transistors. Their results were used to determine the component values and currents for the final circuit. Application of El-Diwany's results to the preamplifier design is left to Appendix B. The final circuit can be more accurately characterized (but still as a two-pole model) using the zero time-constant approach outlined by Gray and Meyer [68]. Instead, final circuit analysis was carried out using COMPACT [69], a computer circuit-analysis program. The modified hybrid-pi transistor model used for this program is given in Appendix B. Figure 4.5 shows the final preamplifier circuit derived in Appendix B, with dc biasing arrangements shown. Figure 4.6 is a graph of the expected preamplifier frequency response, for two different values of cascode dc bias currents, as determined by the computer analysis.

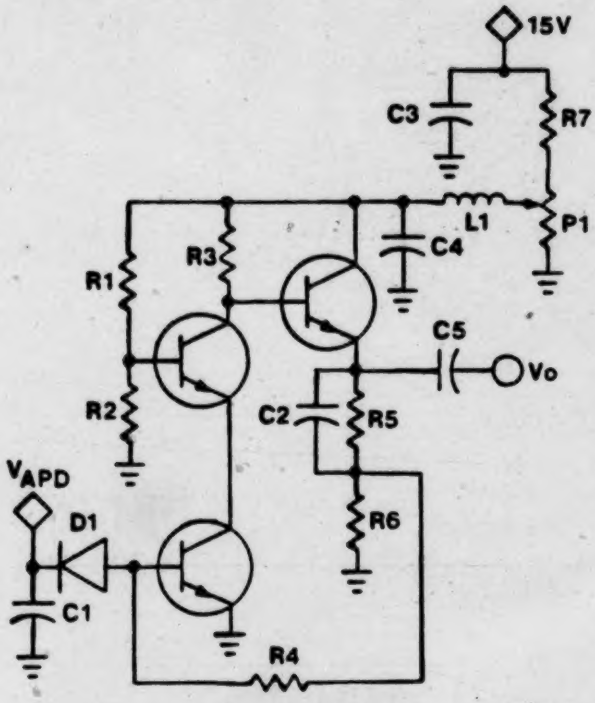
15V
C3
R7
L1
P1
R3
C4
R1
C5
Vo
R2
C2
R5
V_{APD}
D1
R6
C1
R4

R1,2,3 - 2.7 kilo-ohms
R4 - 20 kilo-ohms
R5 - 470 ohms
R6 - 120 ohms
R7 - 220 ohms, 1 watt
P1 - 5.0 kilo-ohms
L1 - 2 uH
C1,3,4 - 0.1 uF
C2 - 22 uF/16V
C5 - 0.01 uF
Q1,2,3 - BFR90

$Ic_1 \equiv 0.2$ mA
$Ic_2 \equiv 6.0$ mA
$Vc_E \equiv 5.0$ V

Fig. 4.5 Experimental Optical Detector/Preamplifier Schematic.

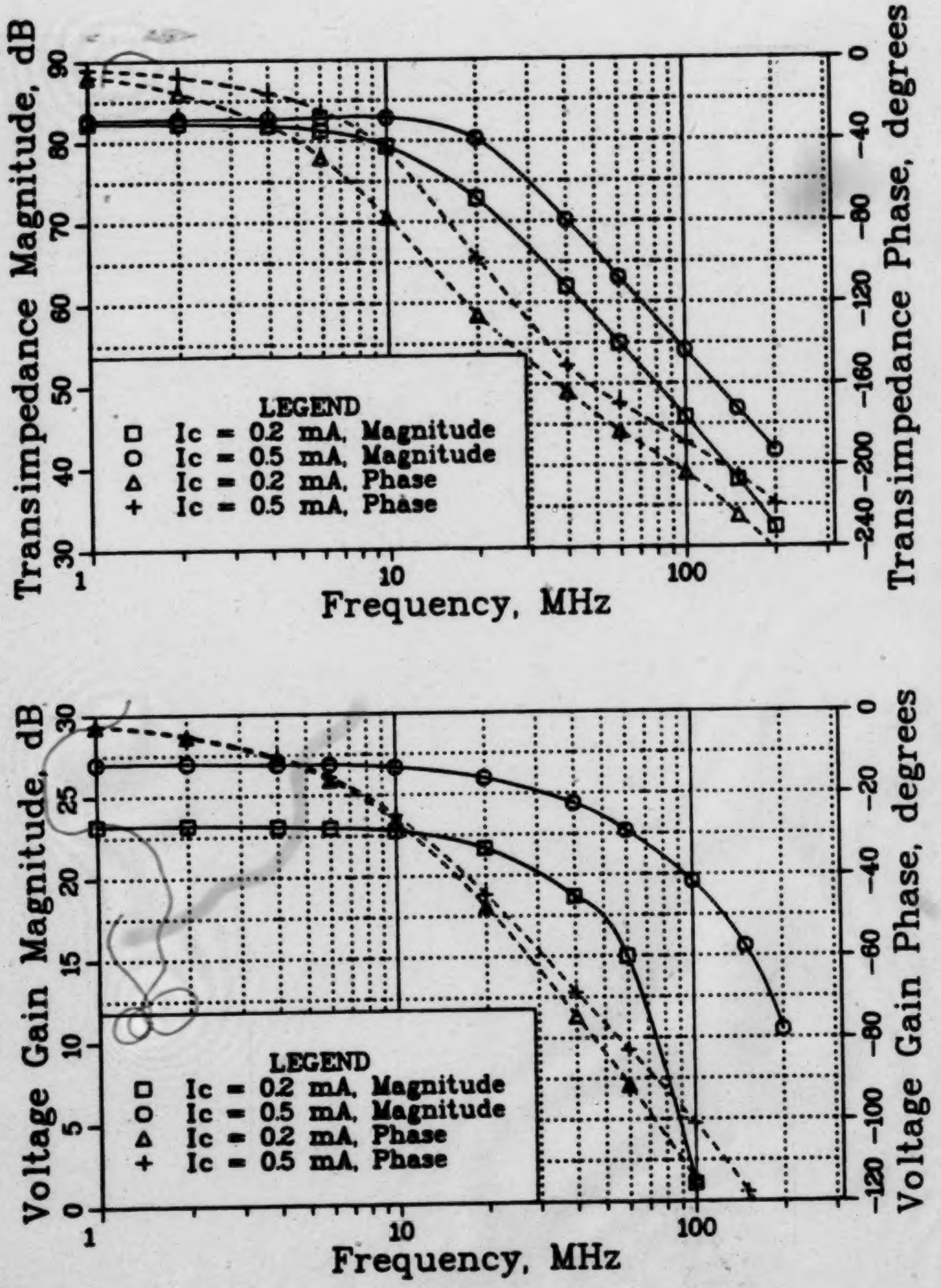

Fig. 4.6 Transimpedance Preamplifier Frequency Response (Computer Estimation)

At a cascode bias current of 0.2 mA, the expected transimpedance is 13 kilo-ohms, and the expected bandwidth is 9.35 MHz. This bandwidth is slightly higher than the expected fiber bandwidth. From the voltage-gain phase and magnitude curves shown in Fig. 4.6, the phase-margin for the preamplifier is approximately 65 degrees at a cascode bias current of 0.2 mA. For the 0.5 mA bias current, the phase-margin is smaller, indicating that the preamplifier may become unstable if the cascode current is increased further without component value changes. Finally, the difference in signal bandwidths for the two operating currents indicates the sensitivity of the circuit to the bias conditions.

From Appendix B, the expected ODP output signal and noise levels are given by

$$S_i = TR \cdot R_\lambda \cdot P_i \cong 10^6 P_i \qquad (4.9)$$

$$\sigma_i^2 \cong \sigma_o^2 + \xi S_i \cong (0.1\ \text{mV})^2 + (70\ \text{uV}) \cdot S_i \qquad (4.10)$$

where

S_i is the ODP output signal in volts,

P_i is the optical power incident on the APD in watts,

TR is the preamplifier transimpedance in ohms,

R_λ is the APD responsivity in amps/watt,

σ_i is the ODP output referred noise level in volts

σ_o is the ODP output referred stationary noise level (primarily thermal noise) in volts,

and ξ is the ODP shot noise parameter in volts.

4.3.2 The Main Amplifier and AGC Circuitry

Following the preamplifier is the main signal amplifier. This amplifier must have the following characteristics:

a) 50 ohm input and output impedance

b) provision for automatic gain control (AGC)

c) a large signal bandwidth

AGC is required because the average input optical power to the APD will vary, possibly over a range of 20 dB. The main amplifier should exhibit little output signal level variance with varying input signal strength.

The bandwidth of the circuit should be made larger than the preamplifier and channel bandwidth in order to minimize signal distortion. Noise is no longer a major consideration, as it was for the preamplifier.

Motorola's MC1590 RF amplifiers [70] are well suited as amplifiers in this application. In order to ensure a high dynamic range with good AGC control, two of these devices are cascaded together in the main amplifier. The output of the second amplifier is followed by a common-collector (CC) transistor buffer to drive the 50 ohm output load. Figure 4.7 shows the main amplifier and AGC circuitry. IC1 and IC2 in this diagram are the MC1590 RF amplifiers.

R1 - 50 ohms
R2,14 - 4.7 kilo-ohms
R3,5 - 100 ohms
R4,7 - 10 kilo-ohms
R6 - 470 ohms
R8,18 - 1.0 kilo-ohms
R9 - 2.7 kilo-ohms
R10,15,16 - 20 kilo-ohms

R11,12 - 39 kilo-ohms
R13 - 390 kilo-ohms
R17 - 270 kilo-ohms
P1 - 1.0 kilo-ohms
P2 - 5.0 kilo-ohms
C1,5,10,11 - 0.1 uF
C2 - 1.0 uF
C3,4,7,8 - 22 uF/16V tant.

C6 - 2.2 uF tant, 0.1 uF
C9 - 470 uF/16V, 1 uF
D1,2 - 1N4148
Q1 - 2N5943
IC1,2 - MC1590
IC3,4 - MC741

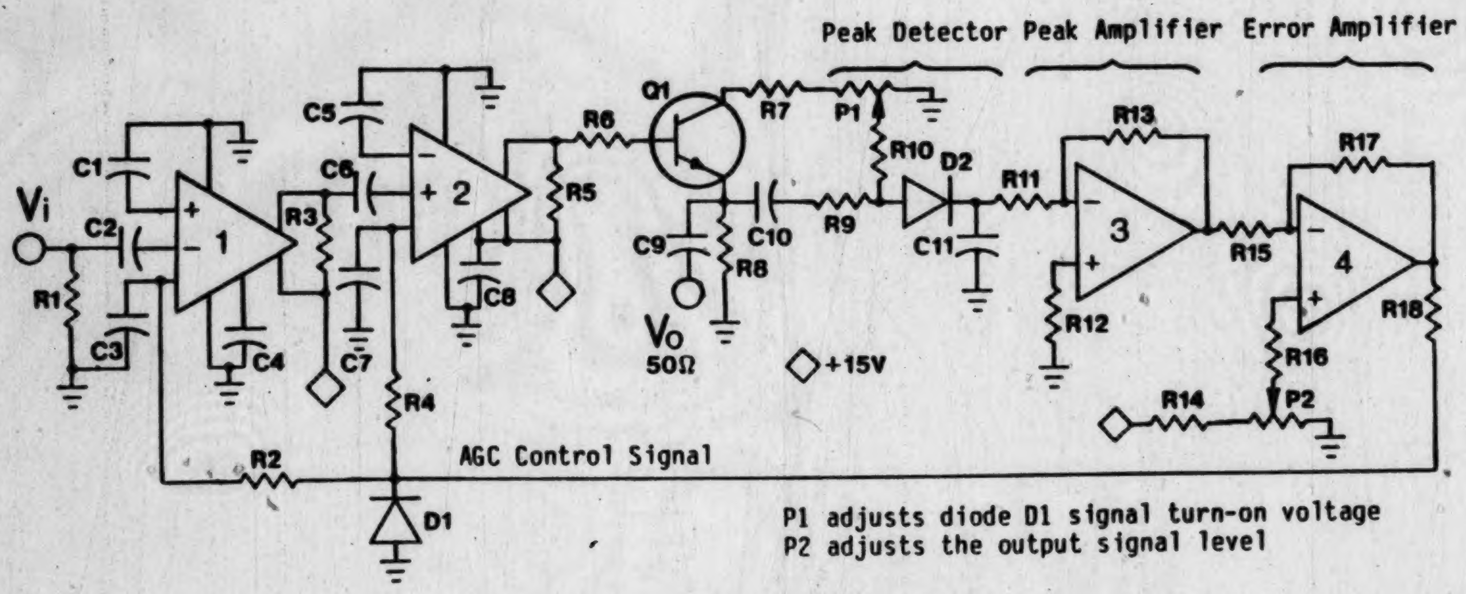
Peak Detector
Peak Amplifier
Error Amplifier
Vi
C1
C2
C3
R1
1
C4
R3
C5
C6
+ 2
C7
C8
R4
R5
R6
Q1
R7
P1
R10
D2
R11
R13
C9
C10
R9
C11
Vo
50Ω
R8
+15V
3
R12
R15
R17
4
R18
R16
R14
P2
R2
AGC Control Signal
D1

P1 adjusts diode D1 signal turn-on voltage
P2 adjusts the output signal level

Fig. 4.7 Schematic Diagram of the Experimental Main Amplifier, Peak Detector, and Automatic Gain Control Circuit

The peak detector in the AGC control loop consists of diode D1 and capacitor C11, with the diode biased to just below its turn-on point for increased detection sensitivity. The diode allows the capacitor to charge quickly, but prevents its fast discharge. Thus, the capacitor charges to the signal peak. Following the peak-detector is a low-frequency amplifier (IC3) that provides a voltage gain of 10. The input impedance of this amplifier, along with the size of the peak-detection capacitor, determines the AGC time-constant. This time-constant is made long in comparison to the baud-interval of the system, but short compared to the expected signal fluctuations in the system under steady-state conditions. The output from the peak amplifier is compared to a preset level, and the error is amplified by IC4 to form the AGC signal.

4.3.3 The Decoder and Decision-Feedback Equalizer

Figure 4.8 outlines the overall decoding and equalizing network for the 4-level receiver. It is sectioned into three boards, and each board is shielded so that clock noise is minimized. Clock noise considerations, as well as speed, dictated the use of ECL logic, which does not possess switching spikes. Transmission line techniques were followed in construction of the circuits. Consequently, the overall decoder and equalizer should be capable of operation at much higher rates than the channel is capable of supporting, even with extensive equalization.

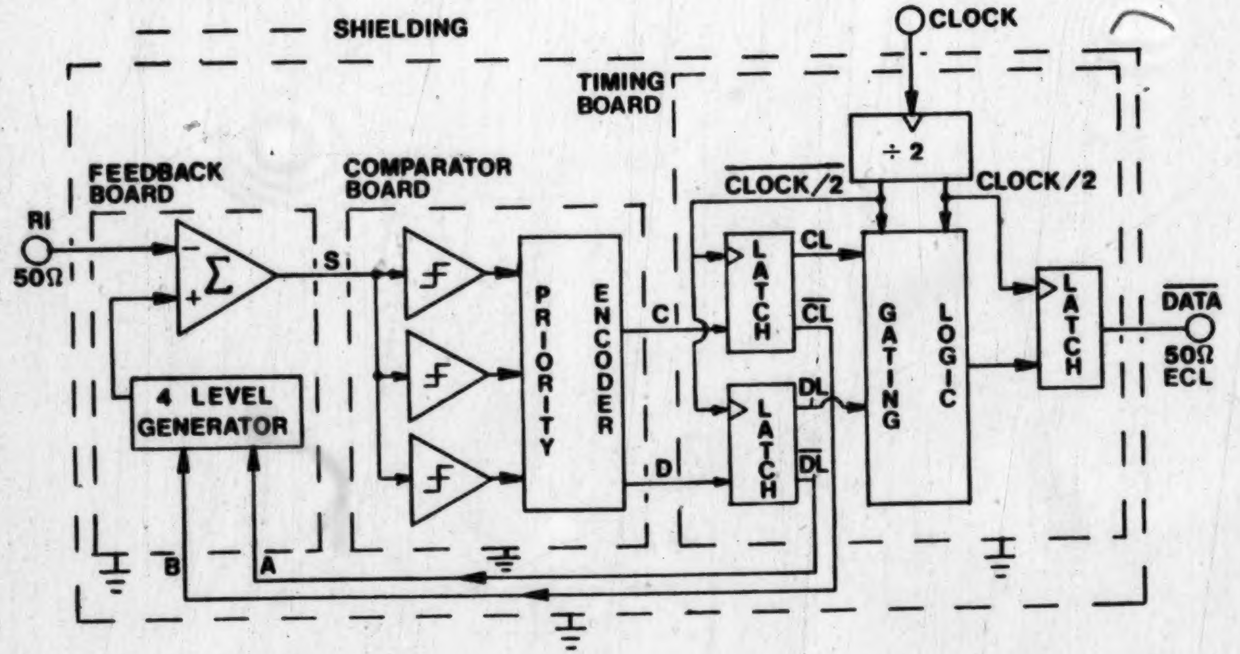
SHIELDING
TIMING BOARD
FEEDBACK BOARD
COMPARATOR BOARD
RI
50Ω
S
Σ
−
+
4 LEVEL GENERATOR
PRIORITY ENCODER
C
D
CLOCK
÷ 2
$\overline{\text{CLOCK/2}}$
CLOCK/2
LATCH
CL
$\overline{\text{CL}}$
DL
$\overline{\text{DL}}$
GATING LOGIC
LATCH
$\overline{\text{DATA}}$
50Ω
ECL
B
A

Fig. 4.8 Decoder and Equalizer Block Diagram For the Experimental System.

The comparator board, illustrated in Fig. 4.9, uses high speed ECL comparators (IC1 and IC2) and an 8 bit priority encoder (IC3) to decode the equalized 4-level input signal (denoted as S on Fig. 4.8) into 2 binary signals. The comparator thresholds are determined through potentiometers. Their optimum values, along with the optimum signal levels, can be analytically determined; this is done in the next chapter. The output of the comparator board is unclocked, and only indicates the quantized level of the present input signal.

The timing board, shown in Fig. 4.10, samples the two output signals from the comparator. This sampling is accomplished by flip-flops (IC2) and should be done at such a time as to minimize the probability of reception error. Kasper [28] considered this timing in conjunction with binary signals and DFE. An adequate, but generally non-optimal, timing would result in sampling when the received signal eyes are fully open. The optimum timing phase is slightly before this "centered timed" (pulse peak timed) point, as will be explained in Chapter 6.

The two resulting clocked binary signals are used by the feedback board to generate the feedback signal. They are also multiplexed (through NOR gates - IC3) into one bit stream, this final bit stream being a logical inversion of the data fed into the transmitter. Negation of this output was not required for the test setup used. Proper clock synchronization is required to multiplex the two bit streams in the right order; on the experimental system, this was done by toggling

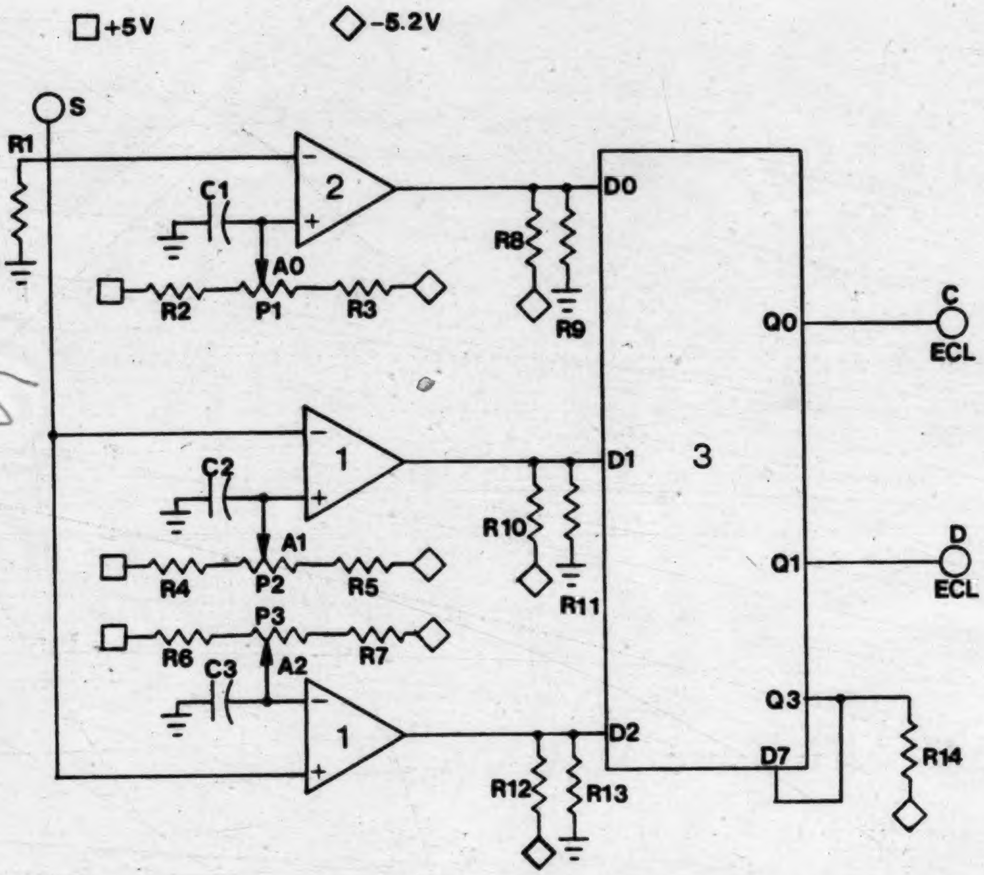
□+5V
◇-5.2V
S
R1
C1
2
A0
R2
P1
R3
R8
R9
D0
Q0
C
ECL
C2
1
A1
R4
P2
R5
R10
R11
D1
3
Q1
D
ECL
P3
R6
R7
C3
A2
1
R12
R13
D2
Q3
D7
R14

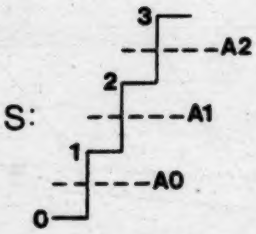
S:
3
A2
2
A1
1
A0
0

S	D0	D1	D2	C	D
0	H	H	L	L	L
1	L	H	L	L	H
2	L	L	L	H	H
3	L	L	H	H	L

R1 - 50 ohms
R2-R7 - 10 kilo-ohms
R8,10,12 - 180 ohms
R9,11,13 - 110 ohms
R14 - 560 ohms
P1 - P3 - 10 kilo-ohms
C1 - C3 - 0.1 uF
IC1 - MC1650
IC2 - MC1650
IC3 - MC10165

Fig. 4.9 Comparator Board Schematic and Coding.

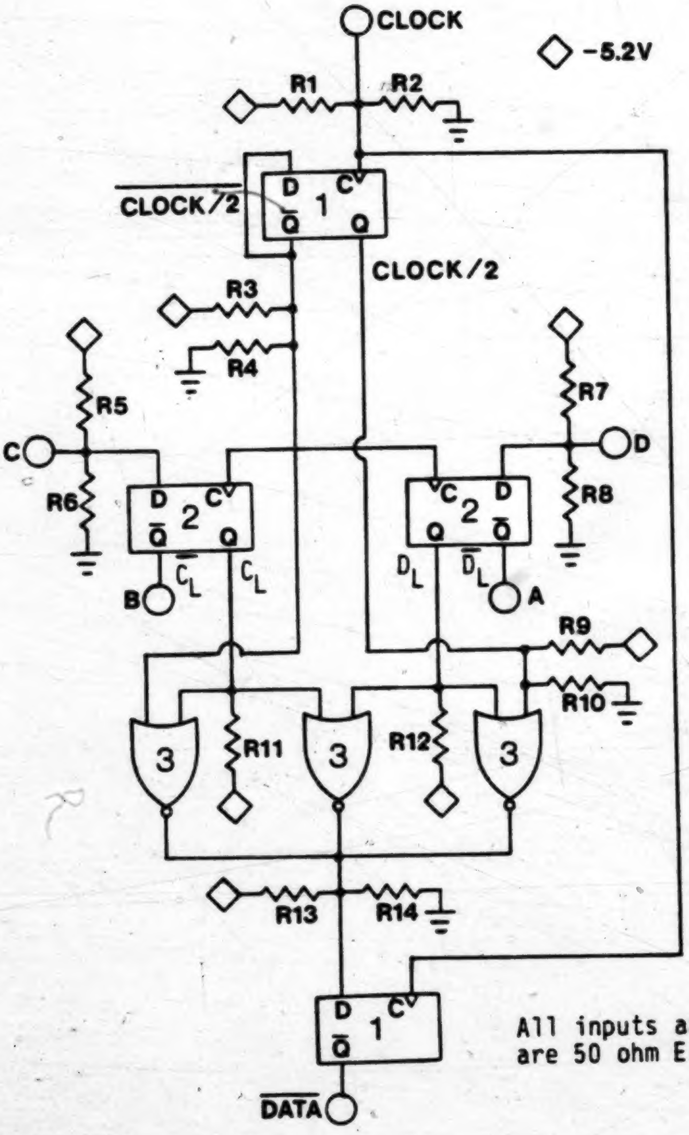
CLOCK
-5.2V
R1
R2
$\overline{\text{CLOCK/2}}$
D
C
$\overline{Q}$
1
Q
CLOCK/2
R3
R4
R5
R6
R7
R8
C
D
2
$\overline{C_L}$
C_L
D_L
$\overline{D_L}$
B
A
R9
R10
R11
R12
3
R13
R14
$\overline{\text{DATA}}$

R1,5,7 - 130 ohms
R2,6,8 - 82 ohms
R3,9,13 - 220 ohms
R4,10,14 - 150 ohms
R11,12 - 510 ohms
IC1,2 - MC10131
IC3 - MC10102

C_L D_L	Clock/2	$\overline{\text{Data}}$
L L	L H	H H
L H	L H	L H
H L	L H	H L
H H	L H	L L

All inputs and outputs are 50 ohm ECL signals

Fig. 4.10 Timing Board Schematic and Coding.

the clock source until synchronization was obtained. In an actual link with clock recovery, synchronization is usually accomplished through coding techniques and data correlators. This subject, though, is not of concern here.

The feedback board, shown in Fig. 4.11, uses NOR gates (IC1, IC2) to generate a 4-level signal from the 2 clocked binary streams produced by the timing board. This 4 level signal, which approximates the decoded data's first postcursor ISI contribution, is subtracted from the incoming unequalized signal (denoted as R on Fig. 4.8) by the difference amplifier IC3. Thus, one-tap DFE is accomplished. Control of the amount of feedback, and of the individual levels in the generated fedback signal, is accomplished through potentiometers. Extension of the feedback to include more taps can be done through inclusion of additional data latches (on the timing board), 4 level generators, and difference amplifiers.

The ECL 4-level generator on the feedback board is conceptually equivalent to the one used in the transmitter. Hence, if a higher speed multilevel transmitter is required, ECL logic can easily be used.

The overall system coding is summarized in Table 4.1.

B A	Feedback
H H	3
H L	2
L L	1
L H	0

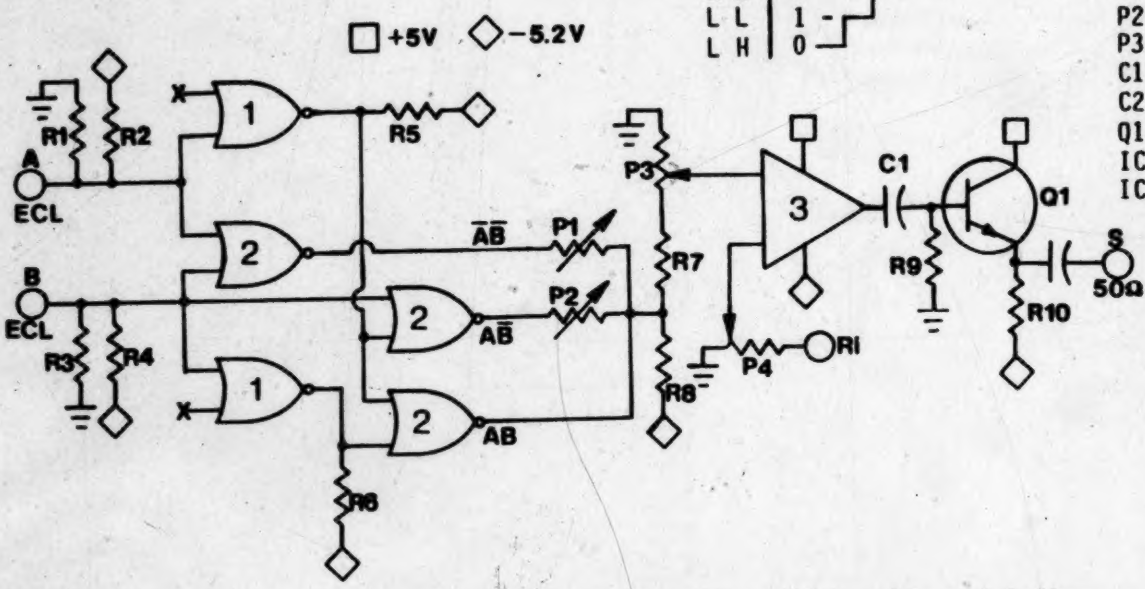
□ +5V
◇ −5.2V
A
ECL
B
ECL
R1
R2
R3
R4
R5
R6
X
X
1
2
2
2
1
$\overline{A}\overline{B}$
$A\overline{B}$
AB
P1
P2
P3
P4
R7
R8
3
C1
R9
Q1
R10
RI
S
50Ω

R1,3	- 82 ohms
R2,4,7,8	- 130 ohms
R5,6	- 470 ohms
R9	- 2.7 kilo-ohms
R10	- 1.0 kilo-ohms
P1	- 100 ohm trimpot
P2	- 500 ohm trimpot
P3,4	- 50 ohm trimpot
C1	- 0.1 uF
C2	- 0.1 uF, 6.8 nF tant.
Q1	- 2N5179
IC1,2	- MC10102
IC3	- MC1733

Fig. 4.11 Feedback Board Schematic and Coding.

Transmitted Data (2 bits)		L L	H L	H H	L H
Transmitted Signal (0-3)		3	2	1	0
Preamplifier Output		0	1	2	3
Main Amplifier Output (Ri) (0-3)		3	2	1	0
Feedback Board Output, No ISI or Feedback (0-3)		0	1	2	3
Comparator Board Output C, D		L L	L H	H H	H L
Timing Board Output (A,B) = $\overline{\text{Data}}$		H H	L H	L L	H L
Generated Feedback (0-3)		3	2	1	0

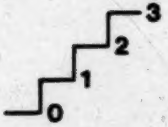

For all 4 level signals, in order of increasing positive voltage.

This table does not indicate the the relative timing between signals. For instance, ignoring the channel delay,the feedback depends on the state of the previous transmitted signal, while the timing board output depends on the state of the present transmitted signal.

Table 4.1 Overall Transmitter and Receiver Signal Coding.

CHAPTER 5. THEORETICAL EVALUATION OF THE EXPERIMENTAL SYSTEM

We are interested in the theoretical evaluation of the experimental system. Specifically, this analysis should be in terms of the system BER as a function of the received optical power and the signalling conditions. To accurately represent the communication system, the analysis should include the following:

a) Signal dependent shot noise

b) Intersymbol interference

c) Optimization of the signal levels and decoder thresholds

d) Both no equalization and DFE (including the possibility of error propagation due to decoder errors)

Several papers discuss upper and lower limits on the BER for the cases of antipodal binary or antipodal multilevel (with equally spaced signal levels) signalling over a dispersive channel with additive gaussian noise [73]. Unfortunately, the results of these papers cannot be applied to the experimental system because a) and b) above are not included in the analysis.

Others have included the possibility of DFE [27,45,74]. Their work, however, has been limited to finding the form of the optimum decision-feedback equalizer under various assumptions, much as was done in Chap. 3. None of the papers dealing with DFE thus far, to the author's knowledge, has reported an analytic solution to the system's resulting BER, as there is considerable difficulty in finding tight BER bounds even for the much simpler and mathematically more tractable problem of analyzing a system having no feedback equalization or shot noise. Error rate characterization of systems thus far has been limited to computer or hardware simulation.

Recognizing this, the theoretical evaluation of the experimental system was done through computer analysis. In this analysis, all possible signalling conditions were modelled, and the BER for each condition was solved for analytically. Consequently, the computer results are as accurate as the model used, and were not obtained through techniques such as Monte-Carlo simulation.

Appendix C contains a source listing of the system evaluation program (written in Basic). This chapter will outline the methods used in the program, as well as the program's limitations as a consequence of these methods.

5.1 Signal and Noise Levels

The analysis assumes the use of a transimpedance preamplifier in conjunction with the optical detector. Following the notation of Muoi and Hullett [20], the signal voltage at the output of the preamplifier, b_i, under the condition of no ISI, can be expressed in terms of the applied optical power P_i:

$$b_i = P_i \cdot TR \cdot R_\lambda \tag{5.1}$$

The noise present along with b_i, from Appendix B, can be expressed as

$$\sigma_i^2 = \sigma_0^2 + \xi b_i \tag{5.2}$$

Letting the ISI terms be represented by b_{ISI}, the ISI can be included in this expression:

$$\sigma_i^2 = \sigma_0^2 + \xi(b_i + b_{ISI}) \tag{5.3}$$

Even if the ISI corrupting the signal b_i is cancelled through DFE, its effect has to be included in noise calculations as the shot noise caused by it cannot be compensated for. The expected values for σ_0, ξ, and TR are stated both in Chap. 4 and in Appendix B. These values, however, are only estimates; the value for TR may be accurate to within 30%, and the values for σ_0 and ξ may be within a factor of two compared to the actual values. Since these parameters can be measured experimentally, the program allows the user to enter their values.

5.2 Channel Pulse Response Modelling

The time - domain channel response model was introduced in Chap. 3 in conjunction with the equalizer design. The channel (which includes the ODP response) is characterized by its time response at the sampling points to a single transmitted pulse. These sampling points are at time instants when the receiver's decoder compares the incoming waveform to preset levels; they are separated by time T, the reciprocal of the system baud rate. Figure 5.1 illustrates an ideal transmitted pulse and a possible channel response to it.

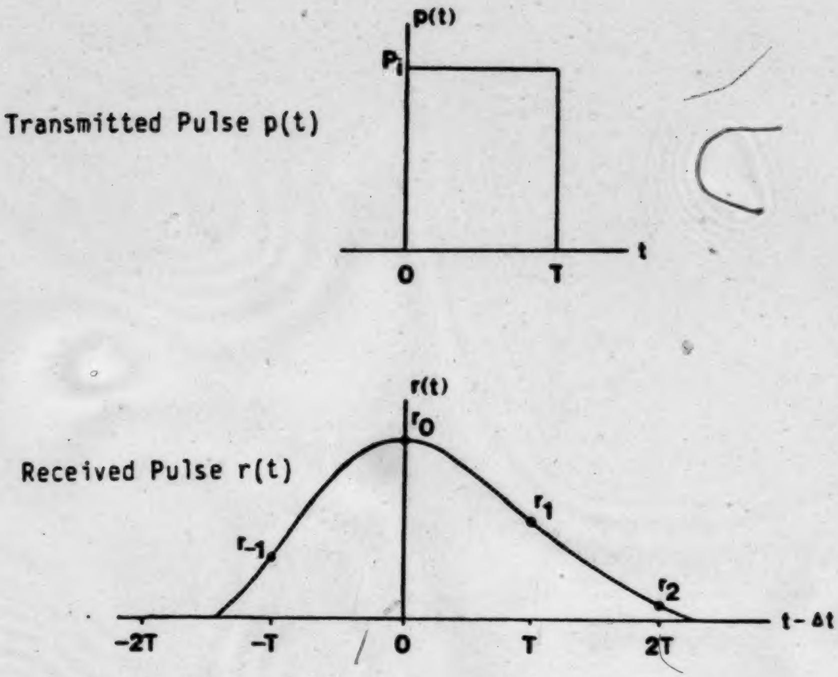
Transmitted Pulse p(t)
p(t)
P_i
0
T
t
Received Pulse r(t)
r(t)
r_0
r_1
r_{-1}
r_2
-2T
-T
0
T
2T
t-Δt

Fig. 5.1 Sampled Time Channel Response Representation.

If we define $Z = P_i \cdot L \cdot TR \cdot R_\lambda$, where L is a channel loss factor, then, using sampled - time notation,

$r(kT) = r_k = Z \cdot h_k$ where

$(h_k)_{\text{maximum}} = 1.$

The vector $H = \{h_k\} = [\ldots h_{-2}, h_{-1}, h_0, h_1, h_2, \ldots]$ defines the received pulse corresponding to a single transmitted pulse. The condition of no ISI is satisfied if

$$h_k = \begin{cases} 1, & k=0 \\ 0, & k\neq 0 \end{cases}$$

The maximum baud rate that satisfies this condition (within reasonable limits, such as H = [0.01, 0.97, 0.02]) can be found experimentally. Above this baud rate, significant ISI starts to occur, and equalization may be required.

Measurements of the appropriate h_k values corresponding to a particular baud rate above the "negligible ISI" baud rate, however, are prone to scaling errors. For normal system operation, due to ISI, there are few isolated received pulses, making the experimental determination of H more difficult. Thus, energy constraints have to be considered to correct for possible magnitude scaling.

Since the channel attenuation is constant, the ratio of the received pulse energy to the transmitted pulse energy, for isolated pulses, remains constant. It will be assumed that the pulse dispersion is primarily due to channel limitations and not due to transmitter or receiver bandwidth restriction. (This is not strictly true for the receiver, but since the receiver bandwidth will be kept higher than the channel bandwidth through adjustment of its bias conditions, this assumption is not too restricting). Then, with square-law optical detectors such as PIN diodes and APDs, the area under the received, amplified signal is directly proportional to the received pulse energy. This proportionality allows proper scaling of the measured experimental channel response.

If the system baud rate is changed from rate B1 to rate B2, the above condition implies that the corresponding received pulse shapes, H1 and H2, can be related:

$$\frac{\text{Received Energy}}{\text{Transmitted Energy}} \propto \frac{\text{Area defined by H1}}{\text{T1}} = \frac{\text{Area defined by H2}}{\text{T2}} \tag{5.4}$$

The intensity of the transmitted pulse is assumed to be constant and independent of the transmitted pulse duration T1 or T2. The area defined by the two H vectors can be found numerically, for example, by using Simpson's method. More accurate results can be obtained by including half interval points (points corresponding to $\pm T/2$, $\pm 3T/2$, ...) as well. The pulse shape that includes these half interval samples will be denoted by the vector H'. As shown by Fig. 5.2, H is a subset of H'.

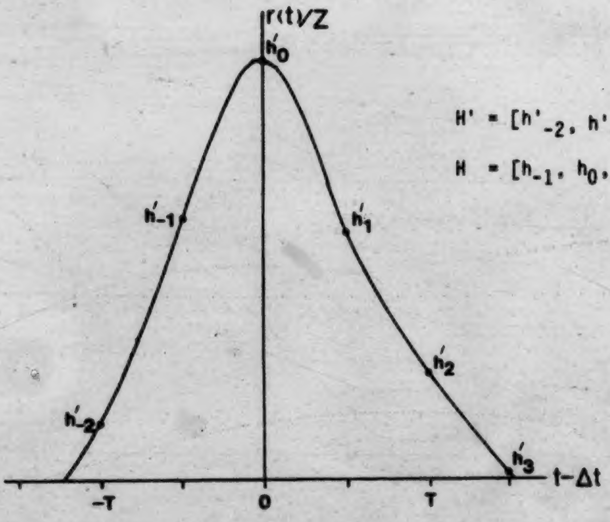

$$H' = [h'_{-2}, h'_{-1}, h'_{0}, h'_{1}, h'_{2}, h'_{3}]$$
$$H = [h_{-1}, h_{0}, h_{1}] = [h'_{-2}, h'_{0}, h'_{1}]$$

Fig. 5.2 Definition of the "Half Interval" Channel Response Vector H'.

Using Simpson's numerical integration, the pulse area, or energy, is proportional to the product

$$\text{Area} \propto T\cdot(\sum H' + \sum H) \quad \text{where}$$

$$H' = \ldots h'_{-2} + h'_{-1} + h'_{0} + h'_{1} + h'_{2} + \ldots \quad \text{and}$$

$$H = \ldots h_{-2} + h_{-1} + h_{0} + h_{1} + h_{2} + \ldots$$

With this, Eqn. 5.4 reduces to

$$(\sum H' + \sum H)_{B1} \cong (\sum H' + \sum H)_{B2}$$

This approximate equality is best illustrated in an example based on experimental data (which will be summarized in Chap. 6) measured for the 4 level system. With the receiver bandwidth set to 14 MHz (above the original design value of 10 MHz), the maximum system baud rate having negligible ISI is around 7.5 Mbaud/s. The pulse shape corresponding to this data rate is easily measured experimentally and is given by

$$H \cong [.005,\ .97,\ .01] \cong [0,\ 1,\ 0] \text{ and}$$

$$H' \cong [.005,\ .73,\ .97,\ .213,\ .01].$$

This pulse shape was determined through observation of the received pulse train under system operation. Because there is little ISI at this data rate, information regarding this shape can be deduced from most received pulses, as they are all isolated from each other. When the system baud rate is increased to 20 Mbaud/s, however, the 4 level pulses are no longer isolated from each other because of ISI, thus making determination of the H and H' vectors more difficult. The best observation-based estimates for H and H' are

$$H \cong [0.03,\ 0.68,\ 0.18] \text{ and}$$

$$H' \cong [0.03,\ 0.41,\ 0.68,\ 0.46,\ 0.18,\ 0.05].$$

For the pulse having negligible ISI, the appropriate "energy constant" is

$$\sum H + \sum H' \equiv 2.91.$$

For the 20 Mbaud/s symbol rate (which corresponds to a 40 Mb/s data rate),

$$\sum H + \sum H' \equiv 2.70.$$

The relative difference is 2.91/2.70 = 1.08. A better estimate for the channel response at 20 Mbaud/s is thus

$$(H, H')_{new} = (H, H')_{old} \cdot 1.08, \text{ or,}$$

$$H \equiv [0.03, 0.73, 0.05]$$

$$H' \equiv [0.03, 0.44, 0.73, 0.50, 0.19, 0.05]$$

This scaling is applied in the program. However, for system analysis it is much easier to consider $h_0=1.0$. This introduces artificial scaling which can be compensated for through scaling of the noise parameters σ_0 and ξ. The amount of scaling required to make $h_0=1$ is determined by energy constraints as just discussed. This requires, however, that the defining negligible ISI pulse be experimentally found before analysis of the system at other bit rates can proceed. From hereon, σ_0 and ξ will be assumed to be scaled.

5.3 Completely Equalized Pulse Analysis

The first, and easiest, case to analyze is when the pulse precursors and postcursors have been cancelled in some manner. For DFE, this is an idealistic situation because:

1. Without resorting to two communication channels, with one delayed slightly with respect to the other, it is physically impossible to cancel the pulse precursors with DFE.

2. The feedback is assumed correct, even in the presence of decoder errors.

The resulting analysis accounts for the shot noise caused by ISI, but assumes the ISI itself has been ideally eliminated. This analysis thus gives a lower limit for the performance of any form of "cancellation equalization" such as DFE. It does not present the optimum system performance using any conceivable equalization scheme, however, because not all of the available information in the received pulse is used. The Viterbi algorithm, although presently impracticable or unrealizable for most high data rate systems because of its computational burden (necessitating very high speed computations), would yield better results.

We start with the assumption that the channel response and noise parameters have been normalized so that $h_0=1$. Ignoring for now the ISI produced shot noise, the optimum signal levels and decoder thresholds can be easily found. Each level of the 4 level signal represents two bits of information. Also, these levels follow a Gray code so that only one bit of the two changes between adjacent levels. (Refer to the system coding outlined in Chapter 4). We define:

PED = overall system probability of error

PEL_i = probability of decoding a signal at level b_i as being at an adjacent level

Almost all errors will be the erroneous decoding, due to noise, of a signal as being at an adjacent signal level to its actual level. Assuming this is the case for all errors, PED can be expressed in terms of PEL:

$$PED = (1/2)\cdot(1/4)\sum_{i=1}^{4} PEL_i$$

The optimum situation is when all the PEL are equal (which implies that, because of shot noise, the levels cannot be equidistant). Then, PED = PEL/2.

For the bottom signal level, a decoding error can only be made if the noise is sufficient to cause the signal to cross the lowest decoder threshold. The probability of this occurring is made equal to 2·PED, in order that PEL_1=2·PED as desired. Likewise, the probability of noise causing the top signal to cross below the top decoder threshold is made equal to 2·PED. For the middle two signal levels, an error can be made if the noise causes the signal to fluctuate across either adjacent threshold; hence, each of these crossing probabilities is made equal to PED in order that $PEL_2 = PEL_3 = 2\cdot PED$. In total, there are 6 individual probabilities, as shown in Fig. 5.3. The "end two" of these six are optimally set to 2·PED, while the other 4 are made equal to PED.

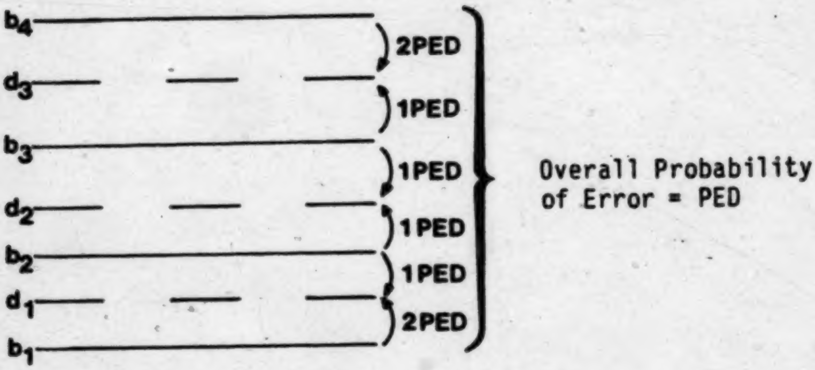

Fig. 5.3 Individual Error Probabilities for the 4 Level Pam System

In Fig. 5.3 the signal levels are designated by b_1 to b_4, and the decoder thresholds by d_1 to d_4. Associated with each signal level is a noise level, σ_i, as given by Eqn. 5.2. Referring to Appendix A, the individual error probabilities can be expressed in terms of the signal levels, decoder thresholds, and the noise levels through use of the Q function:

$$Q(x) = 0.5\ (1 - \mathrm{ERF}(x/\sqrt{2}\ )) \tag{5.5}$$

ERF(x) is the well known gaussian error function.

$PE_{i,j}$ is defined as the probability that the noise corrupting signal i will cause it to cross threshold j (with j being either i or i-1 if possible) and consequently be decoded erroneously.

$$PE_{i,j} = Q(|b_i - d_j| / \sigma_i) \tag{5.6}$$

Thus, the desired level - threshold spacing is

$$|b_i - d_j| = \sigma_i\ Q^{-1}(PE_{i,j}). \tag{5.7}$$

Use of this formula and the noise expression 5.2 allows (neglecting the ISI produced shot - noise for now) the optimum signal levels to be found. The lower signal level is set to zero. From Eqn. 5.2, its noise is simply the system's thermal noise level. Thus, the required value for d_1 is

$$(d_1 - b_1)/\sigma_1 = Q^{-1}(2 \cdot \mathrm{PED}), \text{ or}$$

$$d_1 = \sigma_0 \cdot Q^{-1}(2 \cdot \mathrm{PED}).$$

The next signal level is likewise determined:

$$(b_2 - d_2)/\sigma_2 = Q^{-1}(\mathrm{PED})$$

Substitution for σ_2 yields a quadratic expression which can be solved to obtain b_2. Repetition of the above procedure yields the other signal levels and thresholds.

Inclusion of the ISI produced shot noise is accomplished through use of Eqn. 5.3 instead of Eqn. 5.2. However, the value for b_{ISI} to be used in Eqn. 5.3 will vary for each pulse and will depend on the previous and future pulse levels. This ISI randomness causes the expected values for the noise levels to vary with the amount of ISI. A method which would yield exact results would involve setting the signal levels and decoder thresholds such that the probability of error for each level, averaged over all ISI possibilities, is 2·PED. This method, although exact, greatly increases the amount of work required. A better method, insofar as the computational burden is concerned, which yields a near - exact solution would be to use the expected noise levels in the calculations. This is achieved by using the average value of b_{ISI} in Eqn. 5.3.

There is a computational difficulty in finding the optimum signal levels and decoder thresholds. The average ISI used through Eqn. 5.3 to find these levels is itself dependent on the signal levels. This difficulty is circumvented by iteration. The value for $\overline{b_{ISI}}$ can be taken as zero initially, and the "optimum" levels and thresholds found. These levels yield a new value for $\overline{b_{ISI}}$, which can be used for recalculation of the signal levels. Repetition of this procedure 2 or 3 times ensures convergence (within 5% or closer) to the required levels and thresholds.

With H normalized so that $h_o=1$, the average amount of ISI, given the signal levels S(1) to S(4), is easily found:

$$\begin{aligned}\overline{b_{ISI}} &= (\textstyle\sum H - h_o)\cdot\sum b/4\\ &= (\textstyle\sum H - 1)\cdot(b_1 + b_2 + b_3 + b_4)/4 \qquad (5.8)\end{aligned}$$

From the signal levels required to realize a desired error rate, the required received power is easily obtained through Eqn. 5.1.

5.4 Inclusion of ISI in the System Analysis

The previous section detailed the method used to find the optimum or near optimum signal levels and decoder thresholds for the case where the ISI, but not its shot noise contribution, was eliminated. However, without this ideal equalization, ISI does occur and must be considered.

The amount of ISI present at any sampling instant can be determined by the channel response, H, and the previous and future signal levels (in order that the amplitudes of their interfering precursors or postcursors are known). All the non - zero terms in H, save for h_0, are interference terms. In the program, these terms are referred to as the "HEQ" vector. For example, if

$H = [0.1, 1.0, 0.3]$, then

$HEQ = [0.1, 0.3] = [heq_1, heq_2]$

Each of the interfering terms contributes one of four possible terms to the total ISI. The total number of ISI possibilities is thus four raised to the number of terms in HEQ, and can be enumerated. An example clarifies this concept. With HEQ having two components (as shown above), and for the 4 possible signal levels b_1 to b_4, the vector, G, of all possible ISI terms (all possible b_{ISI}), can be found:

$G = [(b_{ISI})_1, (b_{ISI})_2, (b_{ISI})_3, \ldots, (b_{ISI})_{16}]$ where

$$
\begin{aligned}
(b_{ISI})_1 &= heq_1 \cdot b_1 + heq_2 \cdot b_1 \\
(b_{ISI})_2 &= heq_1 \cdot b_1 + heq_2 \cdot b_2 \\
(b_{ISI})_3 &= heq_1 \cdot b_1 + heq_2 \cdot b_3 \\
(b_{ISI})_4 &= heq_1 \cdot b_1 + heq_2 \cdot b_4 \\
(b_{ISI})_5 &= heq_1 \cdot b_2 + heq_2 \cdot b_1 \\
&\vdots \\
(b_{ISI})_{16} &= heq_1 \cdot b_4 + heq_2 \cdot b_4
\end{aligned}
$$

To ease notation, the $(b_{ISI})_j$ will be referred to as g_j, so that $G = [g_1, g_2, g_3, \ldots]$.

Given the signal levels and decoder thresholds, the individual error probabilities for each ISI possibility can be found. The definition introduced earlier for $PE_{i,j}$ will be extended to include an ISI term:

$PE_{i,j,k}$ is defined as the probability that the received signal consisting of the desired signal bi, an ISI term g_k, and noise, will cross threshold d_j and consequently be decoded erroneously.

Extending Eqn. 5.6 to include the ISI term gives:

$$PE_{i,j,k} = Q^{-1}[|b_i + g_j - d_j| / \sigma_{i,k}] \qquad (5.9)$$

where $\sigma_{i,k}$ is identical to Eqn. 5.3 with b_{ISI} replaced with g_k:

$$\sigma^2_{i,k} = \sigma^2_o + \xi(b_i + g_k) \qquad (5.10)$$

For example, the probability of decoding a signal at level b_2 with the additive ISI term g_3, as being above the second threshold d_2 is:

$$PE_{2,2,3} = Q^{-1}[(d_2 - (b_2 + g_3))/\sigma_{2,3}]$$

where

$$\sigma_{2,3} = (\sigma_o^2 + \xi(b_2 + g_3))^{0.5}$$

The average probability of decoding a signal at level b_2 as being at level b_3, for the above example of 16 possible ISI terms, is:

$$\overline{PE}_{2,2} = [\sum_{j=1}^{16} PE_{2,2,j}]/16$$

If this average is not close to the desired value, (PED for this example), the distance between signal b_2 and threshold d_2 has to be adjusted accordingly. The above procedure can then be repeated using the new signal levels, decoder thresholds, and ISI terms (the ISI terms are dependent on the signal levels). Once all the individual error probability averages, $\overline{PE}_{i,j}$, are close to their desired values, the optimum or near optimum signal levels and thresholds have been found.

Although this method requires considerable numerical computation, it does provide a very accurate analytical solution to the optimum system power requirements for any desired error rate. For a small number of interfering ISI terms in HEQ, its computational burden on a small computer system is reasonable. When there are many terms in HEQ, however, the computational burden may become excessive and more approximate methods for analyzing the system may have to be considered. It is much faster, however, than a Monte - Carlo method of finding the near optimum signal levels.

The critical computational problem arises in adjusting the distances between the levels and thresholds. The optimum adjustment results in a very quick convergence to the required levels and thresholds. However, if the adjustment step is too large, the resulting $PE_{i,j}$ may oscillate about the desired value without converging. Too small a step results in a slow convergence of the $PE_{i,j}$ and hence excessive computations. Because of this problem, the program uses two user controllable adjustment algorithms, based on how close the $PE_{i,j}$ are to their desired values and on the severity of the ISI.

5.5 Ideal One-Tap Decision-Feedback Equalization

In the previous section, the interfering ISI possibilities were determined by cross products between HEQ and b_1 to b_4. The HEQ vector represents the interfering terms in the channel response H. Increasing the system baud rate results in an increase in both the number of terms in HEQ and in the magnitude of these terms.

Ideal one-tap DFE can be accomplished by setting the largest postcursor component of HEQ to zero. For example, if H = [0.1, 1.0, 0.3], then HEQ = [0.1, 0.3] without any equalization. The 0.3 term can be eliminated by DFE, yielding HEQ = 0.1.

The previously outlined method of finding the optimum signal levels and decoder thresholds can be applied using the new HEQ vector. However, the number of ISI possibilities is now reduced by a factor of four because the dimension of HEQ has been reduced by one. For this example, the ISI can be one of four possibilities:

$G = [g_1, g_2, g_3, g_4]$ where

$g_1 = heq_1 \cdot b_1 = 0.1 \cdot b_1$

$g_2 = 0.1 \cdot b_2$

$g_3 = 0.1 \cdot b_3$

$g_4 = 0.1 \cdot b_4$

This results in substantial computational savings, except for one difficulty. Eqns. 5.9 and 5.10 are used to find the individual error probabilities $PE_{i,j,k}$. However, the ISI terms in the noise expression (Eqn. 5.10) correspond to the unequalized HEQ. Although DFE can compensate for the ISI introduced by the postcursor terms of HEQ, it cannot compensate for the shot noise introduced by those terms.

This difficulty, if insurmountable, would result in a factor of four increase in the computational burden required to estimate each $PE_{i,j}$ in the above example because the full number of ISI terms would have to be considered in the noise calculations. However, as in section 5.3, the ISI term used in the noise expression, Eqn. 5.10, can be replaced by the average ISI term. This average ISI term will be denoted by b_{ISI}, as in Section 5.3. The approximate error probabilities are:

$$\begin{aligned} PE_{i,j,k} &\equiv Q^{-1}(|b_i + g_k - d_j|/(\sigma_o^2 + [b_i + b_{ISI}])^{0.5}) \\ &\equiv Q^{-1}(|b_i + g_k - d_j|/\sigma_i) \end{aligned}$$

where σ_i is now considered independent of the individual ISI terms but dependent on the average amount of ISI. This simplification allows a decrease in the computational burden when estimating each PE(i,j).

A trial run using experimental data was conducted to estimate the severity of this simplification. The optical power requirements to realize a 10^{-6} and a 10^{-9} error rate for the unequalized pulse shape were found using both methods. The difference came out to 0.3 dB for both error rates. This difference was considered small considering the accuracy of the experimental data. This point will be clearly illustrated in the next chapter when the theoretical and experimental system performances are given.

5.6 Non-Ideal One-Tap Decision-Feedback Equalization

The previous section considered ideal DFE in which the feedback was always correct. However, in reality, the presence of decoder errors causes erroneous feedback which in turn can cause further decoder errors. Thus, the error propagation effect of DFE has to be considered.

This can be accounted for through the expression

$$P(E|fb) = P(E|if) \cdot P(if) + P(E|cf)$$

where

$P(E|fb)$ is the probability of error with feedback

$P(E|if)$ is the probability of error with incorrect feedback

$P(E|cf)$ is the probability of error with correct feedback

$P(if)$ is the probability of incorrect feedback.

Incorrect feedback occurs whenever there is a decoding error. Thus, $P(if) = P(E|fb)$, which is the same as the system error rate. With this, the above expression simplifies to

$$P(E|fb) = P(E|cf)/[1 - P(E|if)]. \tag{5.11}$$

The methods of section 5.5 found $P(E|cf)$, the error rate given ideal feedback. If the quantity $P(E|if)$ can be found, then the overall system error rate can be found.

Eqn. 5.11 is equivalent to the geometric series:

$$P(E|fb) = P(E|cf) + P(E|cf) \cdot P(E|if) + P(E|cf) \cdot P(E|if)^2 + P(E|cf) \cdot P(E|if)^3 + \ldots$$

In words, "the probability of error given feedback is equal to the probability of error given the previous decisions have been correct, plus the probability of making an error given that the previous decision was wrong times the probability of making that previous error, plus the probability of making an error given that the two immediately previous decisions were wrong times the probability of making those two previous errors ...."

The value for P(E|if) can be analytically determined by considering the feedback error as another ISI term. Consider the earlier example where HEQ has two components, the second one being equalized to zero with DFE. The "net ISI" term given incorrect feedback is:

$$g_{i,j,k} = heq_1 \cdot b_j + heq_2 \cdot b_j - heq_2 \cdot b_k \qquad \text{with } k \neq j.$$

When k=j, the feedback is correct and the situation reduces to that for ideal feedback. Thus the condition $k \neq j$ arises.

The index k can be further restricted by realizing that decoding errors are almost always the decoding of a signal as being at an adjacent level to its actual level. If signal b_2 was received and decoded wrongly, it would be decoded as b_1 or b_3, but most likely not as b_4. Hence,

if $j = 1$, then $k = 2$
$j = 2$, then $k = 1$ or 3
$j = 3$, then $k = 2$ or 4
$j = 4$, then $k = 3$.

The ISI components including incorrect feedback can be enumerated. Using these ISI terms, the individual error probabilities, $PE_{i,j}$, can be found as in section 5.5. From these individual error probabilities, the value for P(E|if) and consequently P(E|fb) can be readily determined.

If the derived P(E|fb) is much larger than P(E|cf), the signal levels and decoder thresholds found for the ideal DFE situation can no longer be considered optimum. However, if P(E|fb) is within a factor of 2 times P(E|cf), the signal levels and thresholds used in determining P(E|fb) can be considered near optimum.

Using the experimental data and the above analysis, it was computed that the ratio of P(E|fb) to P(E|cf) is less than 1.2 for all pulse shapes, even ones possessing severe ISI. The theoretical maximum of this ratio for one - tap DFE will be shown to be four for a Gray coded 4 level system:

The feedback error can either be positive or negative. For the middle two levels, b_2 and b_3, if the feedback is large enough, this can cause a threshold crossing error irrespective of its sign. If the error is in the negative direction, level b_2 will be decoded as b_1, and level b_3 as b_2. If the feedback is large and in the positive direction, b_2 will be decoded as b_3 and b_3 as b_4. Thus,

$$P(E|\text{if}, b_2) < 1$$
$$P(E|\text{if}, b_3) < 1$$

The worst-case probability of error given incorrect feedback and either b_2 or b_2 was sent is 1.

If level b_1 was transmitted, however, the incorrect feedback will only cause b_1 to be decoded as b_2 if it is positive. Hence,

$$P(E|if, b_1) < 0.5$$

Likewise,

$$P(E|if, b_4) < 0.5.$$

Since $P(E|if) = P(E|if, S(1)) + P(E|if, S(2))$

$+ P(E|if, S(3)) + P(E|if, S(4))$,

the worst - case value for $P(E|if)$ is

$$P(E|if)_{maximum} = [0.5 + 1 + 1 + 0.5] = 0.75.$$

Consequently,

$$P(E|fb)_{maximum} = P(E|cf)/[1 - 0.75] = 4 \cdot P(E|cf).$$

With one - tap DFE, the worst case increase in the system error rate due to the error propagation effect of decoder errors is a factor of four. (This upper bound, however, is quite pessimistic; undoubtly, tighter bounds that depend on the channel characteristics can be found). For the experimentally found pulse shapes, this maximum penalty, in terms of an increase in the required optical power to realize the desired BER as compared to the ideal DFE situation, is less than 0.5 dB. (The actual penalty equivalent to the computed <20% increase in the BER is less than 0.1 dB).

The upper bound found above was for a 4 level PAM system with Gray coding and one-tap DFE. A much richer result can be obtained if the number of levels, A, and the number of feedback taps, N, are variable. With the assumption that the binary data represented by each level follows a Gray code, and if the probability of making an error given correct feedback is negligible compared to the probability of making an error given incorrect feedback (which should be true for most, if not all, communication systems employing DFE), then

$$P(E|fb)_{maximum} = P(E|cf)/(1-P(E|if))^N < P(E|cf)\cdot A^N \qquad (5.12)$$

This result is derived in Appendix D.

5.7 Limitations of the Analysis Methods

The methods used in the computer program (as discussed in Sections 5.2 to 5.6) to analyze the experimental 4 level PAM system should be accurate to within 1 dB, given accurate experimental data. This is because the analysis involved the use of an accurate system model with all possible signal combinations being considered, and with only one minor simplification. For the amount of ISI present in the experimental system, especially with only one - tap DFE being used, this exhaustive but accurate analysis is fairly quick when the program is compiled before running. (The program is written in BASIC and can be run either as is with an interpreter or compiled first before running). As was mentioned previously , for large amounts of ISI this analysis involves considerable amounts of number crunching because of the power - law increase in the number of ISI possibilities that have to be considered as well as the slower convergence of the program to the proper signal levels and decoder thresholds with increasing ISI. Thus, if enough ISI is involved to warrant the use of two or three tap DFE in the experimental system, other more approximate but faster methods of system analysis should be considered.

CHAPTER 6. THEORETICAL AND EXPERIMENTAL SYSTEM PERFORMANCE

The experimental test setup for the 4 level PAM system is shown in Fig. 6.1. With this setup, the system performance, in terms of the system BER as a function of the received optical power and data rate, was found. The measured ODP performance and the received pulse shapes were used to determine the theoretical system performance through the program discussed in Chapter 5 and listed in Appendix C. This chapter summarizes the measured and analytical results, and on the basis of these an evaluation of the usefulness of multilevel signalling with DFE over dispersive fiber channels is made.

6.1 The Experimental System Setup.

Referring to Fig. 6.1, the clock source for the system is a Wavetek 178 Programmable Waveform Synthesizer. The maximum clock frequency available from this source is 50 MHz, which limits the maximum system data rate to 50 Mb/s. This rate was above the expected maximum useful rate for the overall system.

The pseudo-random data used to test the link is generated by a HP 3762A data generator. The generated bit stream can be either $2^{10}-1$, $2^{15}-1$, or $2^{23}-1$ bits in length. With the coding performed by the transmitter, the resulting 4 level signal also has either a $2^{10}-1$, $2^{15}-1$, or a $2^{23}-1$ pattern length. It was found that, for the longer pseudo-random data streams, there is enough low frequency signal content to cause a dc level shift in the received and amplified signal. This dc drift is

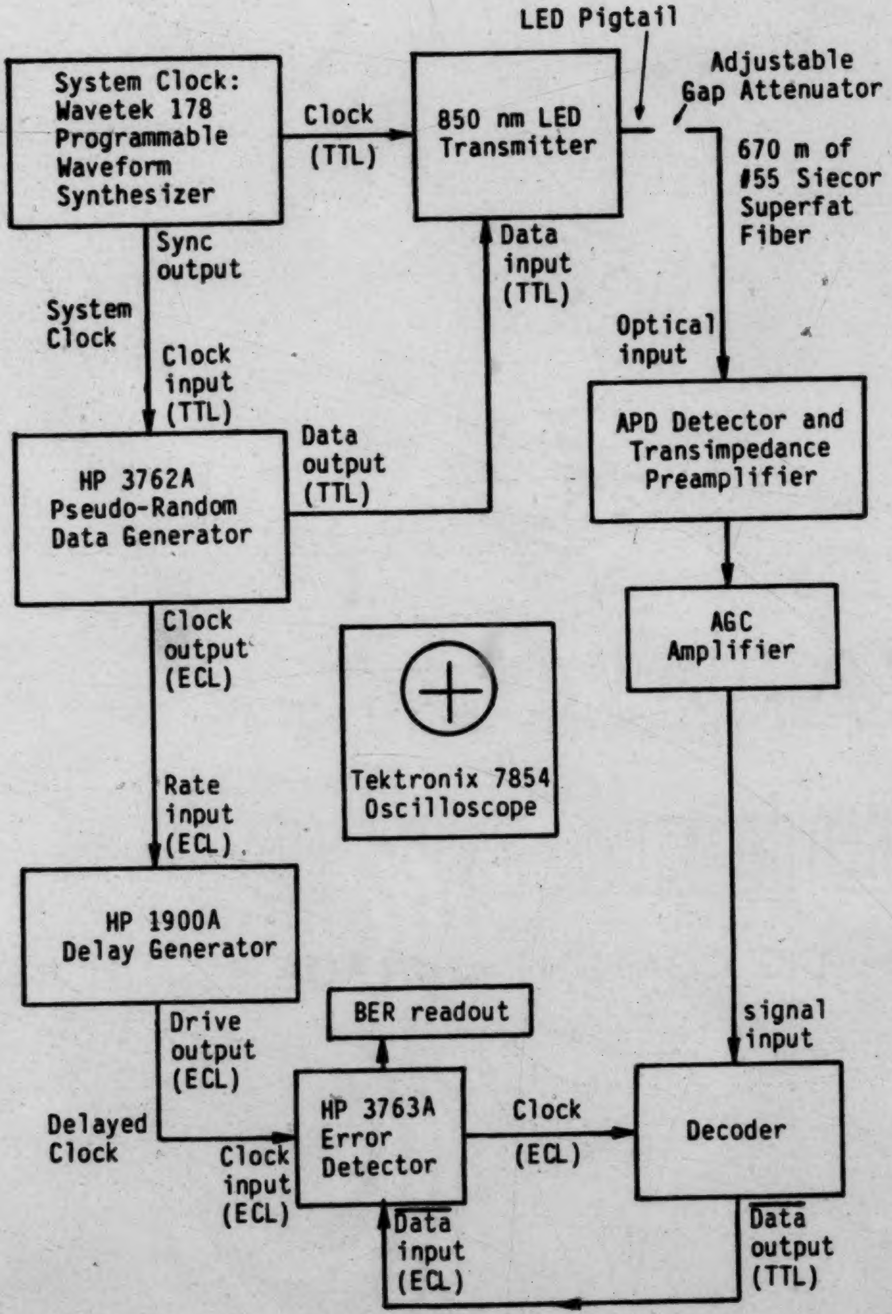
LED Pigtail
Adjustable Gap Attenuator
System Clock: Wavetek 178 Programmable Waveform Synthesizer
Clock (TTL)
850 nm LED Transmitter
670 m of #55 Siecor Superfat Fiber
Sync output
System Clock
Clock input (TTL)
Data input (TTL)
Optical input
APD Detector and Transimpedance Preamplifier
HP 3762A Pseudo-Random Data Generator
Data output (TTL)
Clock output (ECL)
AGC Amplifier
Tektronix 7854 Oscilloscope
Rate input (ECL)
HP 1900A Delay Generator
BER readout
Drive output (ECL)
signal input
Delayed Clock
Clock input (ECL)
HP 3763A Error Detector
Clock (ECL)
Decoder
$\overline{\text{Data}}$ input (ECL)
$\overline{\text{Data}}$ output (TTL)

Fig. 6.1 The Experimental 4 Level PAM System Test Setup

sufficient to adversely affect the system error rate. Although the addition of extra data coding would have removed some of this low frequency signal, the topic of coding beyond the binary to 4 level code used was not pertinent to this project. Consequently, the 2^{10}-1 bit pattern from the pseudo-random generator was used for testing the system.

The 4 level optical signal is launched into the channel by butt-coupling the Siecor fiber to the transmitter LED pigtail. By controlling the gap between the two fiber ends, the launched power can be readily controlled. Another possible method of power control would have been to control the LED drive current. However, this could result in a change in the transmitted pulse rise and fall times, as well as its signal to (clock) noise ratio, and hence was avoided. Also, it proved to be much easier to adjust the received power level with the gap attenuator.

The transmitted optical signal is detected and amplified by the ODP and main amplifier. The resulting signal is then equalized before decoding. The proper clock signal required for decoding the received signal is obtained by delaying the system clock generated by the Wavetek synthesizer. This delay is provided by a HP 1910A delay generator, and can be adjusted from 0 to 100 ns in 5 ns steps. The delayed clock signal is buffered by a HP 3763A error detector before being routed to the decoder. The error detector calculates the system BER by measuring the time required to receive either 10 or 100 errors.

By monitoring the calculated BER over several updates, the system BER, averaged over many (>1000 where possible) errors, is obtained.

At low error rates, the time required to receive 10 to 100 errors at a system data rate of 40 Mb/s or less is quite long. For example, at a data rate of 40 Mb/s and a BER of 10^{-9}, the average time required to receive 10 errors is over 4 minutes. This long time required before even a rough estimate of the system performance can be obtained resulted in three major problems at low system error rates:

1. With a long time delay before a system adjustment (such as an adjustment of the signal levels, decoder thresholds, or the amount of feedback) can be evaluated, optimization of the system is difficult. At a system BER of 10^{-7} or more, this problem does not exist, as an adjustment can be evaluated over 100 errors in 25 seconds or less (at a data rate of 40 Mb/s).

2. The laboratory environment is not conducive to system evaluation over long time periods because of the presence of RF noise. When the system is optimized for the particular operating conditions, it is quite sensitive to this RF noise. With the presence of high powered lasers and motors in the same building as the laboratory, day-time tests at low BERs are difficult, even with shielded circuits. The RF noise most probably enters the system through the power supplies and power supply connections. This noise, being burst noise in nature, causes bursts of errors as opposed to the more uniformly spaced

errors caused by the system noise. This problem was alleviated by testing the system at night.

3. It was found that the power supplies used drift slightly over time periods of several minutes to half an hour. With the decoder thresholds being determined by resistive dividers, this power supply drift causes slight, but measurable, drifts in the decoder thresholds. This usually causes the system BER to slowly increase from the optimized value by a factor of 10 to 100 over a period of 30 minutes or longer.

Whenever it was possible, the BER was measured over thousands of errors. At a data rate of 40 Mb/s and a BER of 10^{-6}, 1000 errors would occur, on the average, in 25 seconds. Thus, accurate system optimization and characterization could easily be obtained for this error rate or higher. At night, assessment of the system performance at a BER as low as 10^{-8} over several hundred errors could be made. However, because of the first and third problems mentioned above, accurate assessment of the system at error rates below 10^{-9} was difficult. The optimum received power requirements for a 10^{-9} BER are easily determined through graphical extrapolation of the higher BER results.

The overall system was operated without errors for 15 minutes at 30 Mb/s and at a received power level of -40 dBm. This corresponds to an error rate below $4 \cdot 10^{-11}$, with no discernible lower limit save those determined by power supply drift, RF noise, and transmitter and receiver limitations.

The measurements and theoretical results for the experimental system are given in the following sections. Because of the need to determine the ODP's bandwidth before the fiber bandwidth can be estimated, the ODP performance will be discussed first.

6.2 The Optical Detector and Preamplifier

In Chapter 4 and Appendix B, the design of the preamplifier used in conjunction with the RCA silicon APD was considered. The resulting circuit was analyzed to determine its bandwidth, transimpedance, noise parameters, and optimum biasing conditions. These expected results, however, are strongly dependent on the circuit component parameters, which may vary considerably from device to device. For instance, the current gain of the transistors was assumed to be 50 in the design procedure. However, the actual current gain may be anywhere from 25 to 200, according to Motorola's technical data [75]. Thus, the preamplifier circuit design allowed for adjustment of the biasing conditions to help compensate for device variations.

The initial bias current for the preamplifier cascode stage was set to the design value of 0.2 mA, and consequently the expected bandwidth for the ODP was 9.35 MHz. However, the maximum negligible ISI (as far as the effect of the ISI on the system BER is concerned) bit rate that could be obtained with this biasing current was 14 Mb/s (7 Mbaud/s). When the cascode biasing current was increased to 0.29 mA, the negligible ISI bit rate increased to 20 Mb/s. This indicates that the ODP bandwidth at the lower bias current is too low compared to the fiber bandwidth. A further increase in the bias current beyond 0.29 mA resulted in an increase in the preamplifier noise level while not significantly increasing the maximum attainable negligible ISI bit rate for the system. The 0.29 mA current resulted in the lowest possible noise level (without having to measure the parameters of the individual transistors used and optimizing the design around these parameters) while not causing too much preamplifier-introduced signal dispersion. The estimated preamplifier bandwidths for the 0.2 mA and 0.29 mA cascode biasing currents are 7.5 and 14 MHz respectively. To determine these bandwidths, the 670 m length of Siecor fiber was replaced with a much shorter length of fiber, so that the fiber bandwidth was much higher than the receiver bandwidth and hence did not contribute to the received pulse dispersion.

The expected ODP performance for a cascode biasing current of 0.2 mA was determined in Appendix B. The same analysis was applied to the 0.29 mA biasing current case for comparison with the experimental data.

The preamplifier transimpedance and noise parameters were estimated by measuring the output signal and noise levels for a known optical input power. This was done at 10 Mb/s to ensure that there was no ISI. The detector responsivity was assumed to be 77, as specified by RCA. Equations 5.1 and 5.2 were then used to estimate the preamplifier transimpedance, thermal noise level, and shot noise parameter.

Table 6.1 summarizes the theoretical and measured values for the ODP parameters for both the 0.2 mA and 0.29 mA biasing currents.

ODP Parameter		Theoretical	Measured
Bandwidth	Ic=0.20 mA Ic=0.29 mA	9.35 MHz 13.5 MHz	7.5 MHz 14 MHz
Transimpedance	Ic=0.20 mA Ic=0.29 mA	13.0 k 13.3 k	≡ 15.0 k ≡ 15.0 k
Thermal Noise	Ic=0.20 mA Ic=0.29 mA	0.07 mV RMS 0.10 mV RMS	≡0.1 mV RMS ≡0.1 mV RMS
Shot Noise Parameter	Ic=0.20 mA Ic=0.29 mA	55 uV 79 uV	≡ 60 uV ≡ 70 uV

Table 6.1 Theoretical and Measured Preamplifier Parameters.

With the exception of the lower bias current bandwidth, the measured parameters agree quite closely with their expected values, considering the possible device variations. The measured thermal noise magnitudes could only be estimated (because of their small magnitudes), and consequently they are probably only accurate to within 30%. Measurement of the thermal noise for Ic=0.29 mA was complicated by the fact that there is a small high frequency (100 MHz or higher) oscillation present in the preamplifier output at this higher bias current.

The amplitude of this oscillation is 0.5 mV RMS, and is completely swamped by shot noise except at the lowest signal level. Since this oscillation frequency is quite high, it appears as white noise to the decoder, and cannot be discerned from the actual noise when viewing the receiver eye diagrams. It does not seem to indicate preamplifier instability, since the preamplifier bias currents and hence bandwidth can be increased considerably without difficulty. Most likely, this oscillation is pickup from an undetermined source.

The system bandwidth is determined by both the ODP bandwidth and the fiber bandwidth. When the received optical power is increased above -44 dBm, with all other parameters held constant, it is noticed that the system bandwidth increases slightly. For high bit rates (40 Mb/s), this system bandwidth increase causes the ISI to decrease enough to substantially affect the BER. The reason for this bandwidth increase is apparent once the magnitude of the signal current produced by the APD is considered. This current is equal to the received optical power divided by the APD responsivity. With the preamplifier's cascode stage base bias current being slightly under 6 uA, the required received optical power to cause a signal current of the same magnitude as this bias current is

$$P_i = 6\text{uA}/(77\text{ A/W}) = 78\text{ nW, or } -41\text{ dBm.}$$

Thus, for received signal levels above -41 dBm, the APD signal current is large enough to substantially increase the cascode transistor's collector current. This causes the ODP bandwidth, and hence the system bandwidth, to increase. The nature of this increase also means that it will be largest for the highest signal levels, leading to non-uniform pulse dispersion for the different pulse levels. This non-uniformity will start when the highest received signal power is in the vicinity of -41 dBm, or when the average received power is around -44 dBm.

6.3 Transmitter Performance and Fiber Characteristics.

The maximum useful bit rate for the transmitter is 40 Mb/s, or 20 Mbaud/s for the 4 level signal. At this bit rate, the dispersion introduced by the transmitter bandwidth limitation is noticeable, but the transmitted signal eye diagram is still fully open. At 50 Mb/s, however, the transmitted eye corresponding to the lower signal levels is not fully open. The other two eyes (for a 4 level PAM signal, there are three eyes), however, are still quite wide, indicating that the dispersion is not uniform across the overall 4 level signal. More will be said about this when the received waveforms are discussed. This behavior is due to the LED characteristics. If the LED is always biased on and intensity modulated, its bandwidth is larger than if it were pulsed on and off. The lower signal eye corresponds to the LED being turned on and off. Consequently, the signal rise and fall times corresponding to this eye are larger than the rise and fall times corresponding to the other eyes, and hence this eye is the first to close as the transmitter baud rate is increased.

The transmitter-introduced dispersion for the lower eye can be compensated for at the receiver with DFE but, because the dispersion is not uniform, this DFE would result in overcompensation for the other two eyes.

The 40 Mb/s transmitter met the design specifications, and was sufficient to evaluate the effectiveness of DFE as an equalization method for the channel. The peak optical power launched into the Siecor fiber (which occurred when the gap attenuator was adjusted to provide the best possible coupling) was -13 dBm.

From the manufacturer's specifications, the expected fiber loss for the 670 m length was 20 dB, and the expected (3 dB optical) fiber bandwidth was around 7.5 MHz. The measured fiber loss is 21 dB, close to the expected value. Estimation of the fiber's actual bandwidth, however, is complicated because of the influence of the ODP's bandwidth on the overall system bandwidth.

The fiber bandwidth was estimated at a received power of less than -44 dBm, so that the ODP bandwidth stayed constant and hence could be accounted for. To estimate the 3 dB electrical bandwidth of the fiber (which is slightly lower than its optical bandwidth), the channel bandwidth (determined by both the fiber and ODP bandwidth) was estimated by observing the received pulse shapes. The received pulse's normalized peak value, h_0 (introduced in Chap. 5) represents the channel's response to a single pulse. If a square wave is transmitted instead of a single pulse, the received normalized pulse peak to peak amplitude will approximately be $1-2h_0$. When this value equals $1/\sqrt{2}$, the frequency of the square wave is at the channel's 3 dB (electrical) bandwidth. Section 6.6 summarizes the received pulse shapes. Referring to this section, the value of h_0 for a data rate of 30 Mb/s (15 Mbaud/s) is 0.9; at 40 Mb/s (20 Mbaud/s), h_0 is 0.8. Thus, at 15 Mbaud/s, (corresponding to a square wave with a frequency of 7.5 MHz), $1-2h_0 = 0.8$, and at 20 Mbaud/s (10 MHz), $1-2h_0 = 0.6$. The channel bandwidth is thus between 7.5 and 10 MHz. Using a value of 8 MHz, and with the ODP bandwidth being 14 MHz, the fiber 3 dB electrical bandwidth is estimated to be 10 MHz, somewhat above the value obtained from the manufacturer's data.

Table 6.2 summarizes the transmitter and fiber characteristics mentioned above.

Parameter	Expected	Measured
Peak Transmitter Power	-10 to -15 dBm	-13 dBm
Maximum Transmitter Bit Rate With 4 Level Signalling	40 Mb/s	40 Mb/s
Fiber Attenuation	20 dB	21 dB
Maximum Fiber Bandwidth	≡ 7.5 MHz	10 MHz

Table 6.2 Expected and Measured Transmitter and Fiber Characteristics

6.4 The AGC Amplifier

The AGC amplifier was tested by applying the binary data stream produced by the data generator through step attenuators to the amplifier. Since this data stream contained both long strings of ones and long strings of zeros (long enough to have significant spectral energy at frequencies below the amplifier's bandwidth, even for a data bit rate above the amplifier bandwidth), as well as isolated ones and zeros, the amplifier bandwidth could be determined without interference from the AGC circuitry. If a sinusoidal signal source were used, the AGC circuitry would compensate for the decrease in the amplifier gain with increasing signal frequency, and the apparent amplifier bandwidth would be much higher than its actual bandwidth. The step attenuators allowed determination of the maximum amplifier gain and dynamic range.

The amplifier output signal level can be adjusted to any desired level under 0.5 V peak to peak (p-p) by adjustment of the appropriate potentiometer in the AGC control loop (Fig. 4.7, potentiometer P2). It was found that for any given potentiometer setting, however, the output level increased slightly with an increase in the data rate. Consequently, when the output was kept below 0.5 V p-p for the 40 Mb/s 4 level signal, the output level at 10 Mb/s was 363 mV p-p. This change was of no consequence, because the decoder thresholds were optimized for each system baud rate. The reason for this behavior was due to a pole in the peak detector circuitry, which caused some partial signal integration and hence average detection at high frequencies as opposed to peak detection at low frequencies.

The signal amplitude from the data generator was 4.7 V p-p. The output level for a data rate of 10 Mb/s was set to 363 mV p-p, so that the output amplitude at higher data rates was below the maximum amplifier output amplitude of 0.5 V. This setting was used for all system tests involving the AGC amplifier. Without any signal attenuation, the amplifier "gain" required was 20log(0.363 V/4.7 V), or -22 dB. Although the amplifier can provide a signal loss, this loss is outside the useful gain control region of the MC1590 integrated circuit amplifiers used in the AGC amplifier, and thus the amplifier output had considerable distortion. The addition of 5 dB of input signal attenuation brought the required loss within the range of the amplifier.

The dynamic range of the amplifier was defined by the input signal range over which the output signal level remained within 3 dB of its maximum value without undue distortion. This range was determined to be 61 dB. The amplifier's maximum gain is 40.6 dB, and its maximum loss is approximately 17 dB. The minimum signal level required to be within 3 dB of the maximum output level (of 363 mV) is 2.4 mV. The input referred noise level, in comparison, is 0.15 mV, with the largest component of this being power-line (60 Hz) harmonics. The ratio of the input signal required to obtain the maximum (-3 dB) output to this input-referred noise is 24 dB.

The amplifier bandwidth was estimated to be 45 MHz, well above the required bandwidth. Table 6.3 summarizes the AGC amplifier performance.

Test conditions (except bandwidth test) : 50 ohm load, Vo = 363 mV (-8.8 dB) maximum, 20 Mb/s, $2^{10}-1$ bit length pseudo-random binary data.	
Maximum input signal level	2.6 V/ 8.4 dB
Minimum input signal level for Vo= -11.8 dB (3 dB down)	2.4 mV/ -52.6 dB
Maximum useful amplifier attenuation	17 dB
Maximum amplifier gain	40.6 dB
Dynamic Range	61 dB
Input referred noise level, with no signal input	0.15 mV/ -77 dB
3 dB Bandwidth, for Vi= 83 mV (-25.4 dB) Gain = 17.4 dB, Vo = 430 mV (-8.0 dB)	45 MHz

Table 6.3. Summary of the AGC Amplifier Performance.

6.5 The Decoder

The decoder can operate at data rates of 50 Mb/s with no apparent difficulty. Clock noise, although present, is low and thus not a problem. One previously mentioned problem that was observed was the drifting of the decoder thresholds with power supply drift. For continuous system operation, this problem could be solved by using temperature-compensated on-board voltage requlators.

Another difficulty encountered in the decoding operation was that of finding the optimum delay for the delayed clock. For the error measurements, the delay setting that gave the best results was used. However, because of the 5 ns maximum resolution available with the delay generator, the optimum timing usually could not be obtained. This was especially true for the 40 Mb/s signal, where the baud interval was 50 ns. The maximum eye width (for -40 dBm received optical power and DFE) was about 15 ns, and thus could be sampled at only three possible points. A delay generator with higher resolution would have aided in sampling the received signal properly.

6.6 The Channel Pulse Responses

The analysis methods discussed in Chapter 5 require the sampled time system pulse responses. These methods assume that the system response is invariant to the received power level, and that the pulse shape is identical for all possible pulse amplitudes. Experimentally, this situation did not exist, for two forenamed reasons:

1. Above a received power level of -44 dBm, the APD signal current is comparable to the base bias current of the cascode transistors. This causes the ODP bandwidth to increase enough to affect the received pulse shapes. Since this increase is greater for higher signal powers (until the ODP saturates), the highest signal level has the least amount of ODP-introduced dispersion (and a slightly increased noise level due to the bandwidth increase as well as the shot noise increase).

2. The LED turn-on and turn-off times cause the lowest signal eye to close first and, consequently, the dispersion is not linear across the whole signal. This limits the usefulness of DFE, since ideal compensation for the lowest signal level results in overcompensation for the other signal levels.

These two phenomena, especially the LED turn-on and turn-off limitation, made accurate determination of the approximate system pulse responses, for use in the analysis program, difficult. The pulse shapes used represent average pulse shapes, and were determined from the received and unequalized signal eye diagrams, as well as from the individual pulse responses observed (and averaged in order to reduce the noise variance) on the oscilloscope.

The non-uniform dispersion, as mentioned, caused some difficulties in finding the optimum amount of DFE. It also complicated the sampling process, because the three eyes in the eye diagram were fully open at slightly different times.

Thus, a sampling time that may be optimum for one of the eyes would not be optimum for the other two eyes.

In digital systems, the signal pulses are sampled at, or close to, the time they reach a maximum. This type of sample timing will be referred to as center sampling. For optimum equalization, center sampling is near optimum. However, since DFE does not compensate for the pulse precursors, center sampling is usually not optimum if DFE is being used without additional precursor equalization. For the pulse shapes found in many fiber systems, better results can theoretically be obtained if the pulse is sampled slightly before it reaches its maximum [28]. Although this results in a decrease in the sampled pulse maximum, it also decreases the precursor ISI terms. The postcursor ISI terms are increased, but these increases are of little consequence because the postcursor terms can be cancelled by DFE. For the pulse shapes found for this system, the precursor term could theoretically be made negligible through this timing shift, with a small decrease in the maximum pulse amplitude. The amount of timing shift used could be analytically varied in order to determine the optimum sampling point for the pulse.

Both center sampling and shifted sampling were analyzed by the program listed in Appendix C. In the experimental system, however, because of the lack of timing resolution, only center or near center sampling could be obtained. Hence, experimental verification of the benefits of offset sampling could not be obtained for this system. Furthermore, a lot of the benefit obtainable from shifted sampling cannot be realized when there is non-uniform pulse dispersion.

Fig. 6.2 illustrates the average received pulse shapes for the system. From these shapes, Table 6.4 was derived. This table gives the sampled pulse vectors used in the program. With this, all required parameters for the program have been given, and the expected system behavior (BER vs. received power and the data rate) can be determined and compared with the measured system behavior.

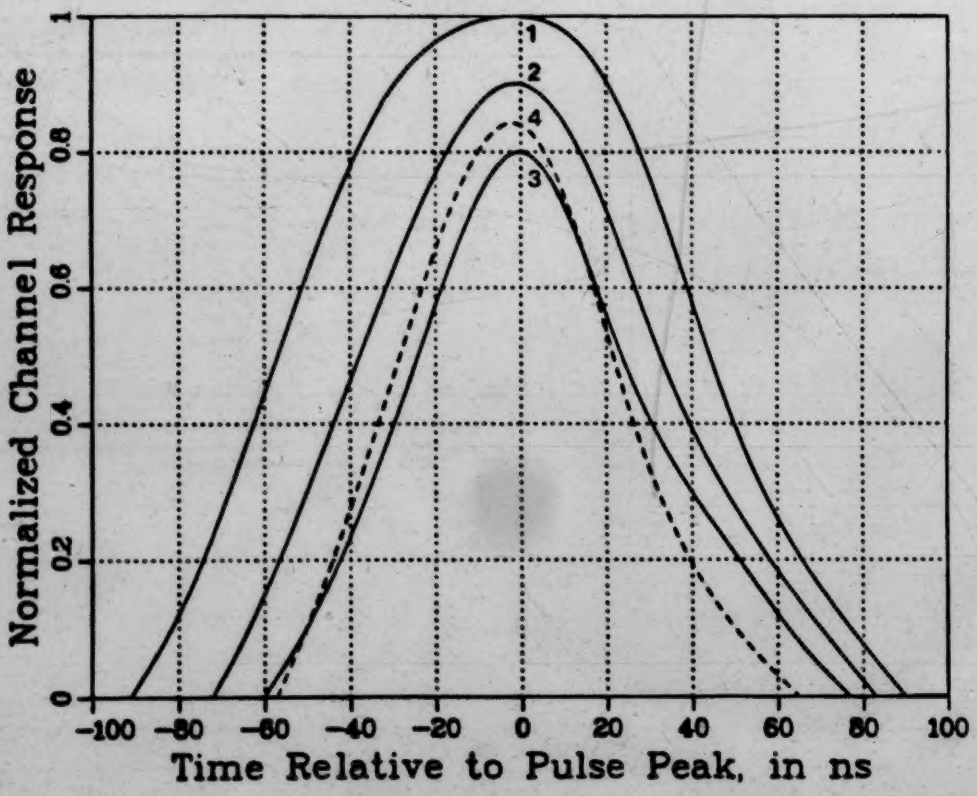

Fig. 6.2 Measured Fiber/ODP Pulse Responses

1. 20 Mb/s, low power (< -44 dBm received optical power)
2. 30 Mb/s, low power
3. 40 Mb/s, low power
4. 40 Mb/s, high power (> -44 dBm received optical power)

Data Rate / Test Conditions	H, H_2 Pulse Shapes
10 Mb/s, reduced receiver bandwidth (Ic=0.20 mA), low received power (<-40 dBm)	No ISI, pulse maximum = 1 (H=[0, 1, 0])
20 Mb/s, increased receiver bandwidth (Ic=0.29 mA) low received power	H'=[0, 0.62, 1.0, 0.40, 0] H =[0, 1, 0] No ISI. Energy Reference Pulse Shape
30 Mb/s, increased receiver bandwidth, low received power, both centered and shifted sampling	Centered Sampled: H'=[0.06,0.57,0.9,0.49,0.1,0] H =[.06, .9, .1] Shifted Sampling: H'=[0,0.47,0.89,0.58,0.18,0] H =[0, .89, .18]
40 Mb/s, increased receiver bandwidth, low received power, both centered and shifted sampling equalized pulse shape	Centered Sampled: H'=[.1,.48,.8,.48,.21,.01,0] H =[0.1, 0.8, 0.21] Shifted Sampling: H'=[0,.31,.73,.65,.3,.08,0] H =[0, 0.73, 0.3]
40 Mb/s, increased receiver bandwidth, high received power (> -40 dBm), centered sampling unequalized pulse shape	Centered Sampled: H'=[0.1,0.56,0.84,0.43,0.1,0] H =[0.1, 0.84, 0.1]

Table 6.4 Summary of the Sampled Pulse Vectors used in the System Analysis Program

6.7 Summary of the Analytic and Measured System Performance

The system was tested at data rates of 10 Mb/s, 20 Mb/s, 30 Mb/s, and 40 Mb/s. The 10 Mb/s test was with the reduced preamplifier bandwidth, and thus is not directly comparable with the other tests. It was included to show the effect of the receiver bandwidth on the system performance. All the other system tests were made with the increased receiver bandwidth, to ensure that the pulse dispersion was caused primarily by the fiber and not the receiver.

The system tests performed are listed below:

Data Rate	Equalization Condition	Remarks
10 Mb/s	No Equalization	Reduced Receiver Bw No ISI
20 Mb/s	No Equalization	Highest No ISI data rate (with increased receiver bandwidth)
30 Mb/s	No Equalization	Some ISI present
	DFE	Small Residual ISI
40 Mb/s	No Equalization	Severe ISI present at low power, significant ISI at high power
	DFE	Some Residual ISI at low power, less at higher power

Table 6.5. Performed System Tests.

The theoretical results obtained, and their appropiate conditions, are as follows:

1. 10 Mb/s, reduced receiver bandwidth (Ic=0.2 mA)
2. 20 Mb/s (increased receiver bandwidth for this and all subsequent theoretical results) (Ic=0.29 mA)
3. 30 Mb/s, ideal equalization
4. 30 Mb/s, ideal (shifted sampling) one-tap DFE
5. 30 Mb/s, centered sampled one-tap DFE
6. 30 Mb/s, no equalization
7. 40 Mb/s, ideal equalization, low power pulse shape
8. 40 Mb/s, ideal one-tap DFE, low power pulse shape
9. 40 Mb/s, centered sampled one-tap DFE, low power pulse shape (< -43 dBm)
10. 40 Mb/s, no equalization, high power pulse shape (> -43 dBm)

Figures 6.3 to 6.7 compare the theoretical and measured system performances. Fig. 6.3 summarizes all the theoretical results obtained. From this graph, it is evident that one-tap DFE with optimum timing results in a small power penalty of 1.3 dB or less (at a BER of 10^{-8}) for a two-fold increase in the system data rate. Using non-optimum center sampling, the theoretical penalty is 5.4 dB. In comparison, consider the 10 Mb/s and 20 Mb/s curves. The 10 Mb/s curve indicates the system performance with the reduced receiver bandwidth and no ISI. The maximum data rate, with negligible ISI and a reduced receiver bandwidth, is 14 Mb/s. (continued on page 169)

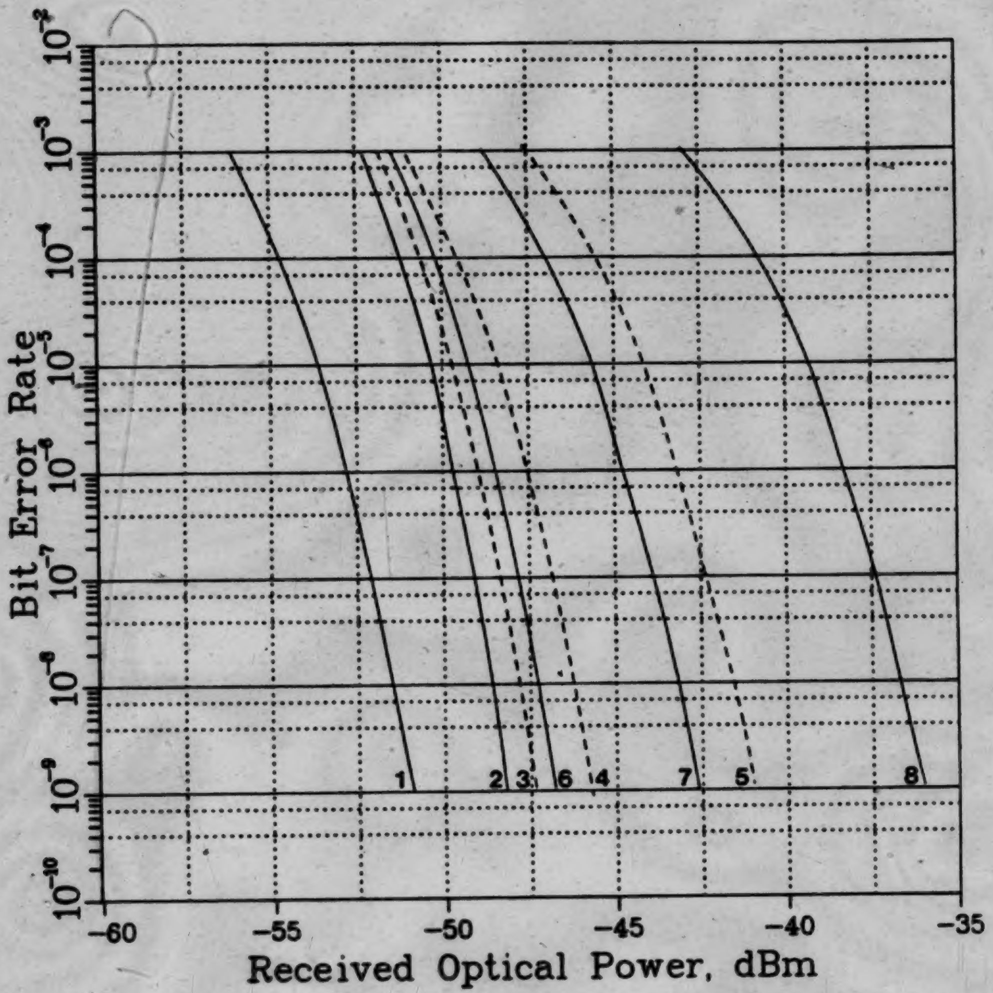

Fig. 6.3 Theoretical System Performance Summary.

1. 10 Mb/s, no equalization, lower bandwidth receiver (for the following curves, the higher bandwidth receiver is assumed.)
2. 20 Mb/s, no equalization
3. 30 Mb/s, optimum ISI cancellation and 1-tap optimum-timed DFE
4. 30 Mb/s, 1-tap centered-timed DFE
5. 30 Mb/s, no equalization
6. 40 Mb/s, optimum ISI cancellation and 1-tap optimum-timed DFE, lower power pulse shape
7. 40 Mb/s, 1-tap centered-timed DFE, lower power pulse shape
8. 40 Mb/s, no equalization, higher power pulse shape

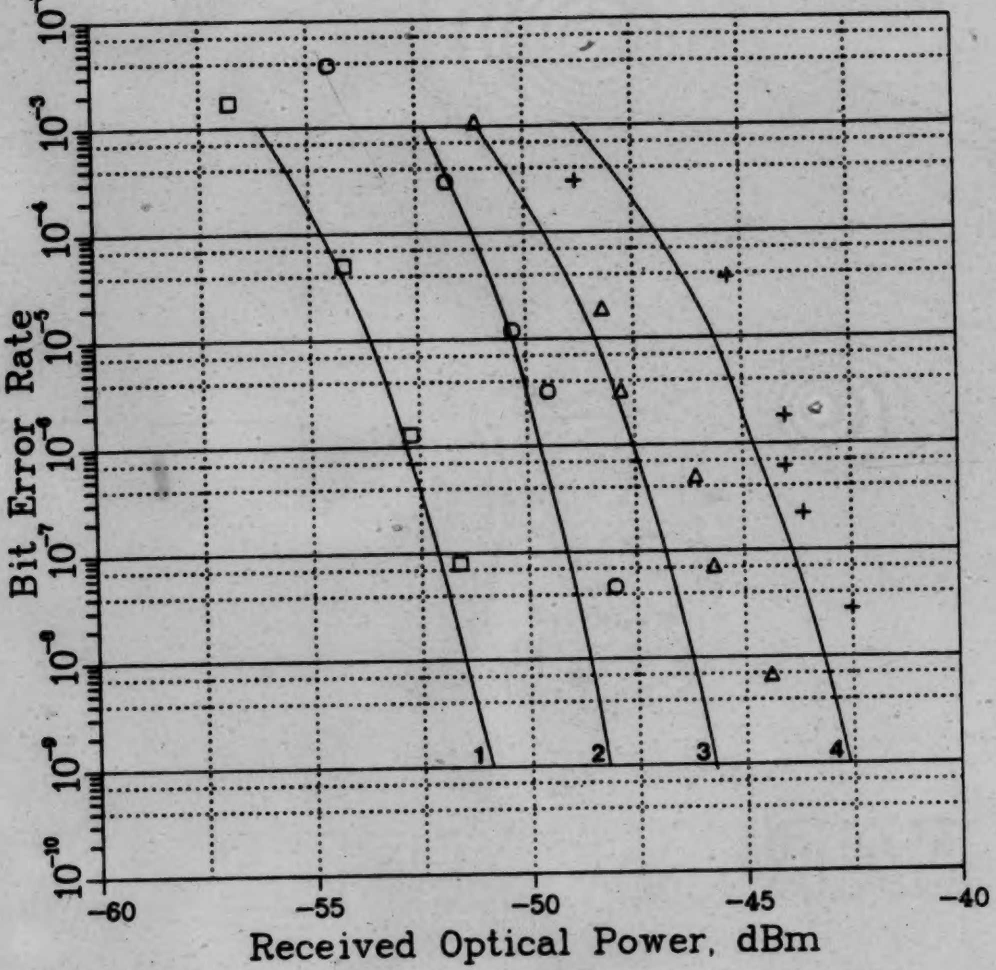

Fig. 6.4 Theoretical and Experimental System Performance with Centered-Timed DFE.

Measured Performance:

□ 10 Mb/s (no equalization required)
○ 20 Mb/s (no equalization required)
△ 30 Mb/s
+ 40 Mb/s

Theoretical Performance:

1. 10 Mb/s, no equalization, reduced bandwidth receiver (for the following curves, the higher bandwidth receiver is assumed.)
2. 20 Mb/s, no equalization
3. 30 Mb/s, DFE
4. 40 Mb/s, lower power pulse shape, DFE

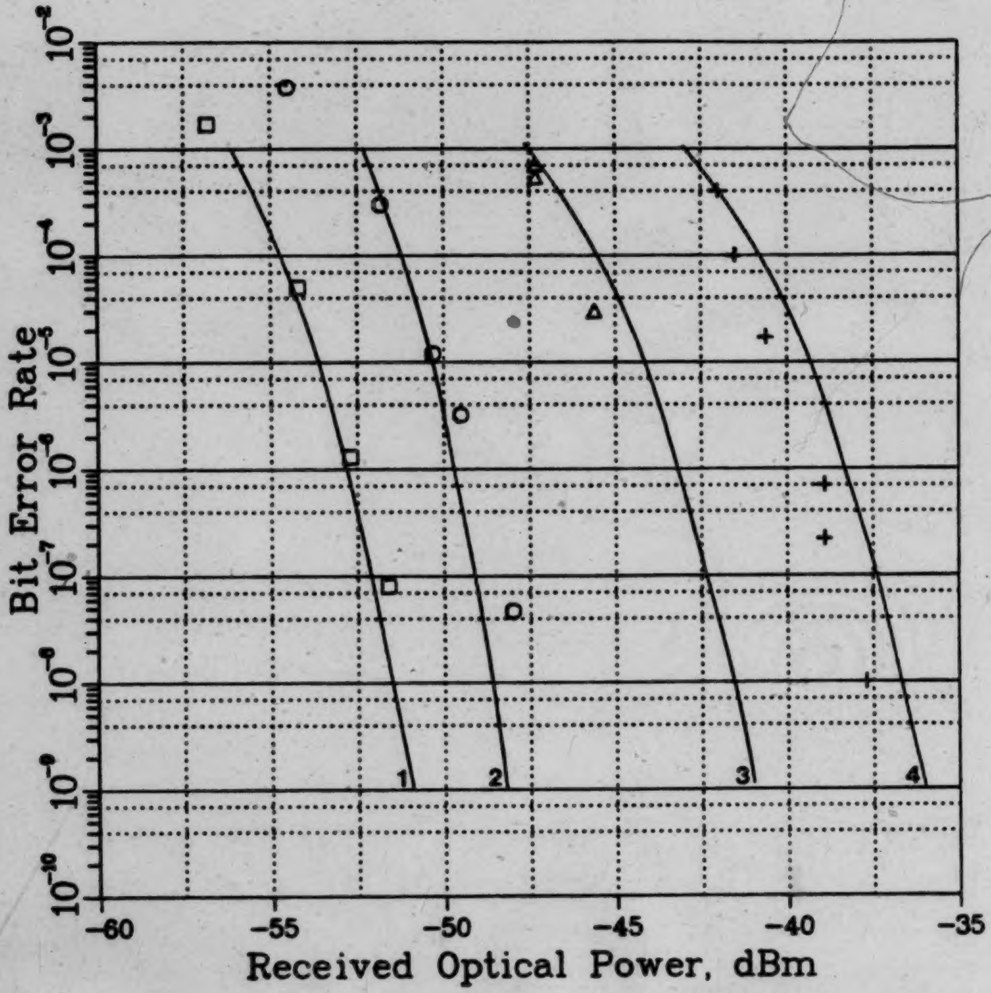

Fig. 6.5 Theoretical and Experimental System Performance with no Equalization.

Measured Performance:

□ 10 Mb/s ○ 20 Mb/s △ 30 Mb/s + 40 Mb/s

Theoretical Performance:

1. 10 Mb/s, reduced bandwidth receiver (for the following curves, the higher bandwidth receiver is assumed.)
2. 20 Mb/s
3. 30 Mb/s
4. 40 Mb/s, higher power pulse shape

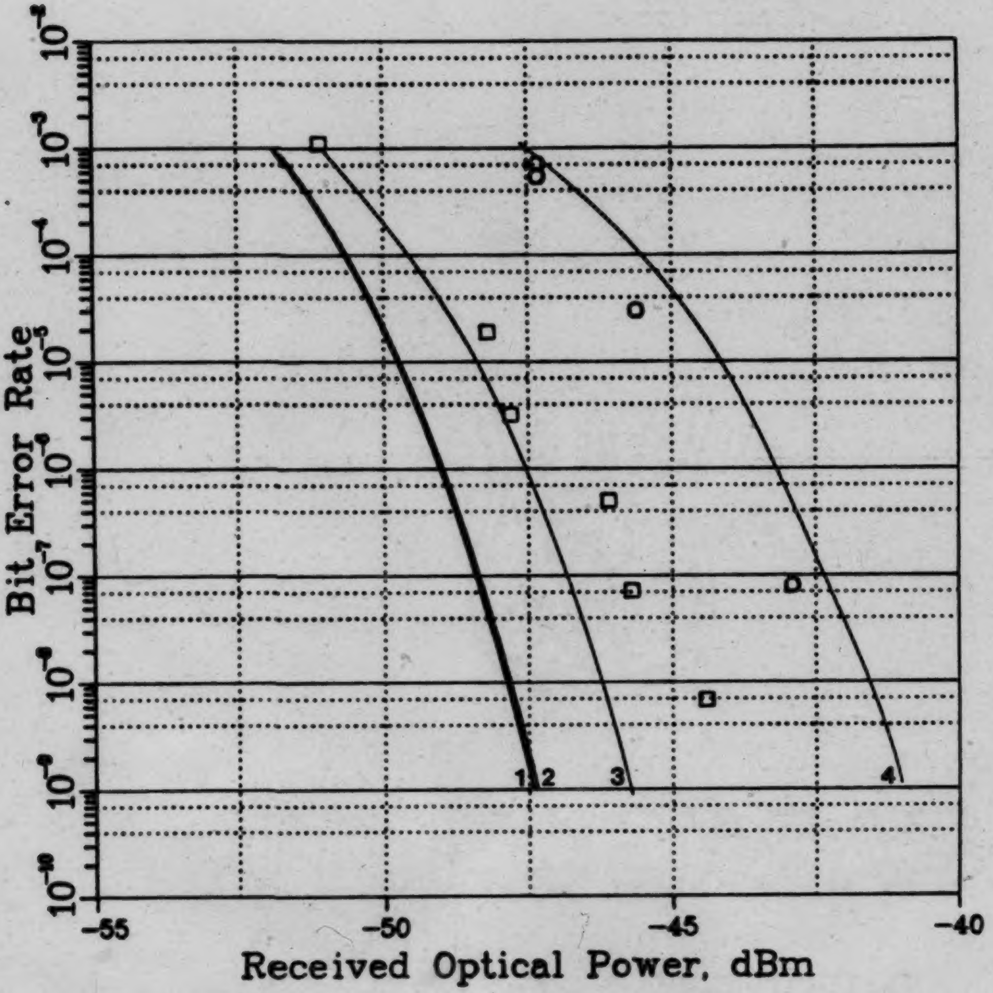

Fig. 6.6 Theoretical and Experimental System Performance at 30 Mb/s.

Measured Performance:

□ 1-tap DFE ○ no equalization

Theoretical Performance:
(with the lower bandwidth receiver)

1. Complete ISI cancellation
2. 1-tap optimum-timed DFE
3. Centered-timed 1-tap DFE
4. No equalization

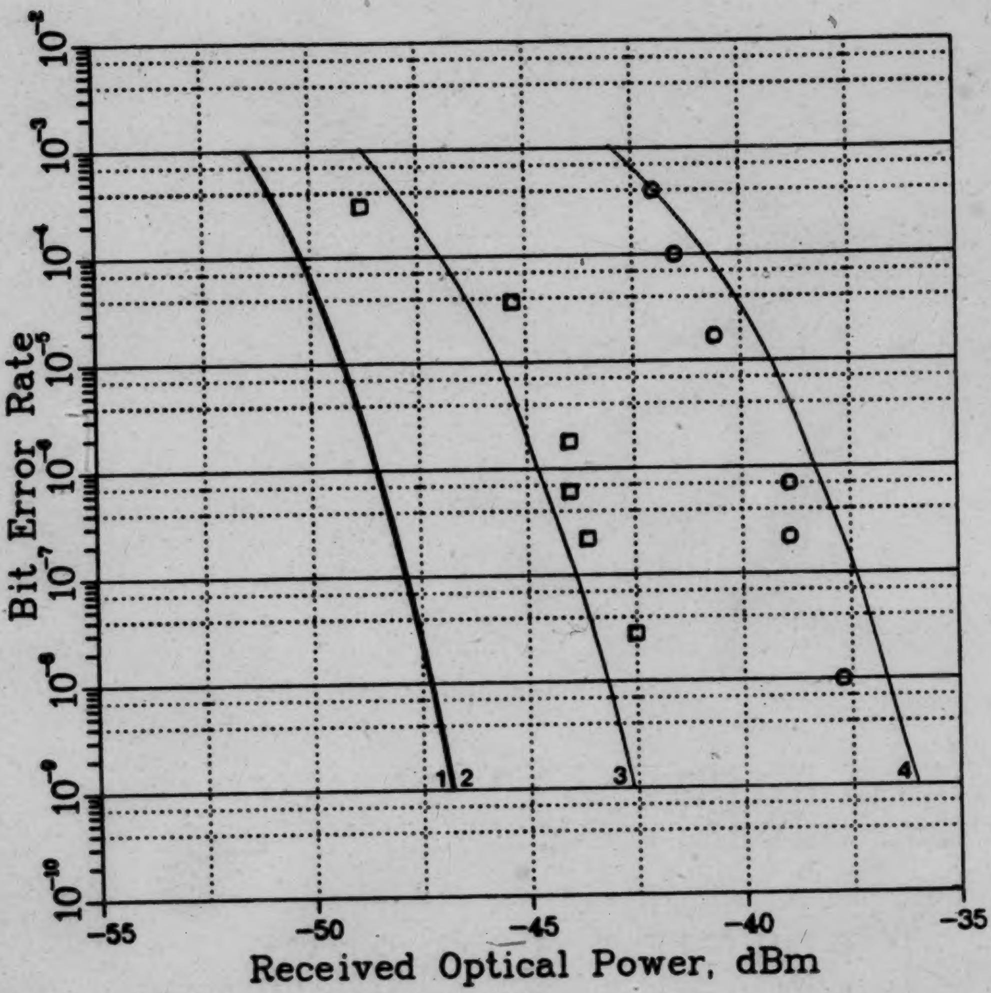

Fig. 6.7 Theoretical and Experimental System Performance at 40 Mb/s.

Measured Performance:

□ 1-tap DFE ○ no equalization

Theoretical Performance:

1. Complete ISI cancellation, lower power pulse shape
2. 1-tap optimum-timed DFE, lower power pulse shape
3. 1-tap centered-timed DFE, lower power pulse shape
4. no equalization, higher power pulse shape

The 20 Mb/s curve represents the maximum data rate with negligible ISI and an increased receiver bandwidth. The penalty incurred for this 20/14 ≅1.5 times increase in the data rate is 4.8 dB. Extending this to a two-fold increase in the data rate would give a penalty in the vicinity of 6 dB, more than the penalty incurred for non-optimum one-tap DFE.

For a data rate of 30 Mb/s, the theoretical required received optical power, for a BER of 10^{-8}, is decreased by 6.3 dB through the use of DFE. At a data rate of 40 Mb/s, the theoretical reduction is 6.3 dB and 10.3 dB for centered sampled and shifted sampled one-tap DFE respectively. These reductions would be much higher (at 40 Mb/s) if the pulse shape remained constant with increasing received power. However, they are still quite large, especially when the simplicity of the equalizer is considered.

Figure 6.4 compares the theoretical results for the tests #1, #2, #5, and #9 listed earlier to the measured data for signalling at 10 Mb/s, 20 Mb/s, 30 Mb/s with DFE, and 40 Mb/s with DFE. The results agree quite closely (within 1 dB for all data points but one), especially when the accuracy of the measured noise parameters and pulse shapes are accounted for. This graph also indicates that the DFE results measured were probably not optimum, as they agree with the centered sampled theoretical results. This was expected, again, because of the unequally distributed signal dispersion and the lack of experimental timing resolution obtainable.

Figure 6.5 compares the theoretical and measured results for the case of no equalization. (As indicated earlier, equalization was not required for the 10 Mb/s and 20 Mb/s data rates.) Again, the results compare favorably, with all measured points being within approximately 1 dB of the theoretical results. The 40 Mb/s unequalized data corresponds to the higher power, less dispersed 40 Mb/s pulse shape. The theoretical result for the low power 40 Mb/s pulse shape with no equalization is off the scale of this graph. For a BER of 10^{-8}, the required power was estimated to be -22 dBm, as opposed to the -36.7 dBm power required for the higher power pulse shape. This 15 dB difference indicates how severely a reduction in the ISI can improve the system performance.

Figures 6.6 and 6.7 summarize all the results for the data rates of 30 Mb/s and 40 Mb/s, respectively. These graphs clearly illustrate the advantage offerred by one-tap DFE. For both data rates, the optimum one-tap DFE curve is within 0.1 dB of the optimum equalization curve. This indicates that there is little need to go to a more complex multitap DFE for this fiber system at these data rates. Operation at higher data rates would be improved with multitap feedback, but only if the unequal dispersion problem can be reduced. Although the centered-sampled DFE curves are 2 to 4 dB from the optimum DFE curves, they still show large power requirement reductions, especially for the 40 Mb/s data rate, over the non-equalized curves. Again, the equalized and unequalized results shown on Fig. 6.7 correspond to two different pulse shapes. When only the low power pulse shape is considered, the theoretical power reduction realizable through center sampled one-tap DFE at a BER of 10^{-8} is 21 dB.

Finally, the system eye diagrams, as seen with an oscilloscope, are depicted in Fig. 6.8. These diagrams correspond to the output of the summing amplifier in the decoder, where the feedback signal is subtracted from the signal coming from the AGC amplifier. In these diagrams, there has been an overall signal inversion, so that the top level in each diagram corresponds to the LED being off (i.e. the lowest signal level), and the bottom level corresponds to the LED being full on (i.e. the highest signal level). The unequal signal distortion mentioned earlier can be seen clearly in the unequalized eye diagrams. In the equalized eye diagrams, the effect of this unequal dispersion resulted in both different eye widths and the eyes being fully open at slightly different times. This effect is illustrated most clearly in the 40 Mb/s, equalized diagram. It was this effect that limited the maximum system bit rate. Again, the transmitter bandwidth limitation (due to the LED turn-on and turn-off times) was probably the main cause of the unequal dispersion.

The equalized and unequalized eye diagrams were taken at the same received power level so that a fair comparison could be made between them. The only system difference was the addition or removal of the feedback. The 20 Mb/s eye diagram corresponds to a power level of -47.2 dBm. The 30 Mb/s eye diagrams correspond to -42.5 dBm, while those for 40 Mb/s

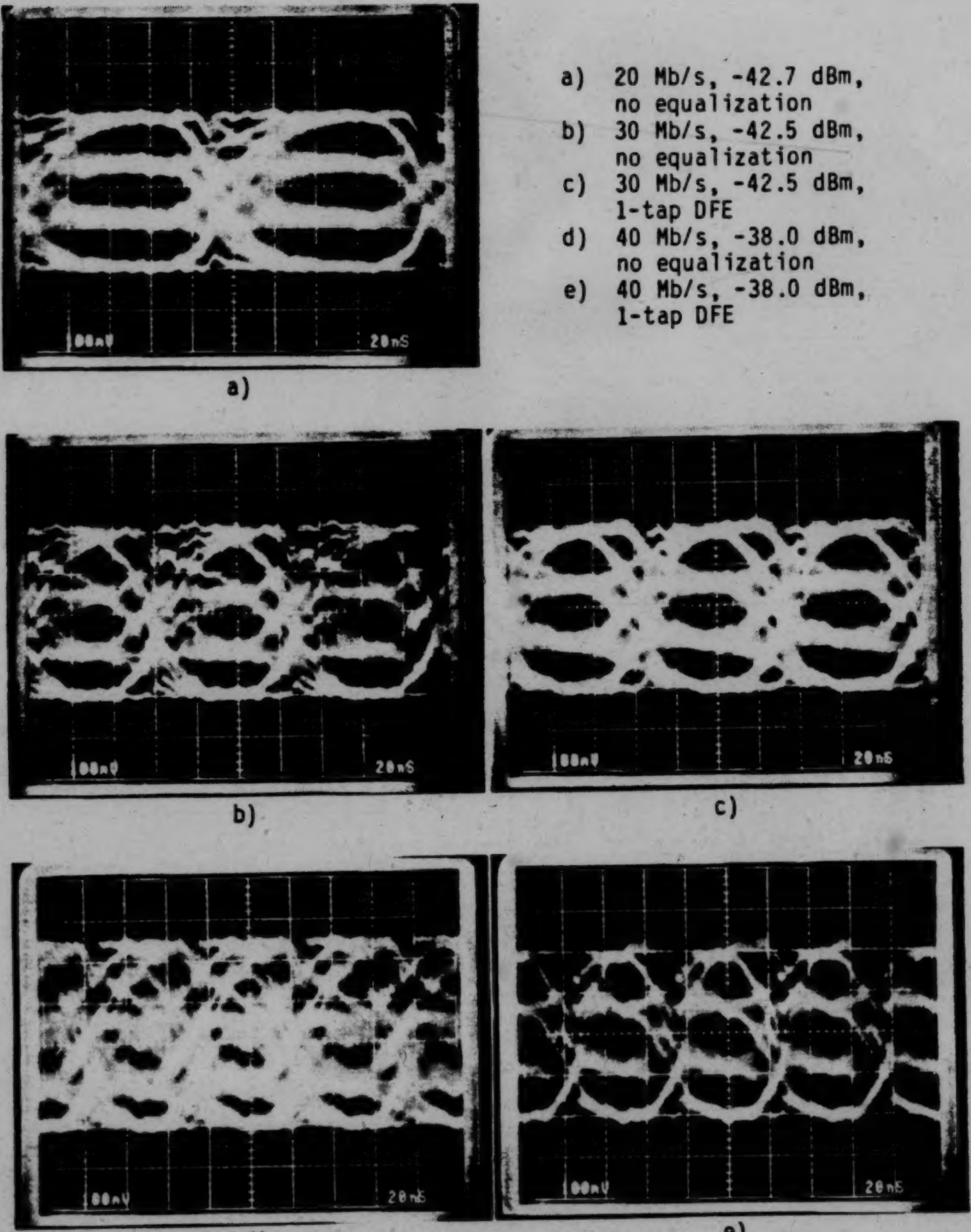

a) 20 Mb/s, -42.7 dBm, no equalization
b) 30 Mb/s, -42.5 dBm, no equalization
c) 30 Mb/s, -42.5 dBm, 1-tap DFE
d) 40 Mb/s, -38.0 dBm, no equalization
e) 40 Mb/s, -38.0 dBm, 1-tap DFE

a)

b)

c)

d)

e)

Fig. 6.9 Received Signal Eye Diagrams for the Experimental System.

correspond to -38 dBm. The 40 Mb/s results were thus taken in the "high power" region, and hence correspond to the higher power 40 Mb/s pulse shape. From the 40 Mb/s eye diagrams, the improvement in the eyes through the use of one-tap DFE is dramatic. This indicates the improvement obtainable through one-tap DFE without requiring complex wave-shaping filters and a precise knowledge of the channel characteristics. Also, with only one tap of feedback, error propagation is negligible (<20%), as indicated by the theoretical results, supported by their agreement with the measurements.

CHAPTER 7. SUMMARY AND CONCLUSIONS

In this thesis, both multilevel signalling and DFE were investigated as possible methods of increasing the data capacity of multimode fiber systems. Certainly the advantages of both methods are well recognized; however, only recently has DFE been applied to optical fiber communication systems [19]. The simultaneous application of both methods, to the author's knowledge, has not been done prior to this study.

When both multilevel signalling and DFE are used for signalling over dispersive channels, the question of what the best combination of the two is immediately arises. Kasper [28] compared binary signalling with DFE to multilevel signalling without equalization. He arrived at the conclusion that, for optical multimode fiber channels, binary signalling with DFE is superior to unequalized multilevel signalling. Kasper did not, however, consider equalized multilevel signals. Salz [27] considered this possibility, and showed that, for channels of practical interest, there is an optimum combination of the number of signal levels and the amount of equalization.

Salz's results are supported when the signalling capacities for multilevel signalling, over a bandlimited channel, are considered. These capacities (discussed by Wozencraft and Jacobs [23], and extended in Chap. 2 and Appendix A to include shot noise and one-sided signalling) indicate that the optimum number of signal levels depends on the available SNR; at a low SNR, there is little point in using a multilevel signal (except possibly for aiding in timing extraction), while at a high SNR, the capacity of a multilevel signal can be much higher than the capacity of a binary signal. Figs. 2.1 and 2.2 illustrate these capacities.

The possible improvement in signalling capacity for multimode fibers was demonstrated for hypothetical 850 nm and 1300 nm multimode fiber systems. This study indicates that, with a LD source, 4 level signalling, and DFE, it should be possible to have repeaterless transmission at a data rate of 560 Mb/s or higher over 35 km of 1300 nm multimode fiber. With binary signalling and linear equalization, this BDP could only be realized with a single-mode system (assuming the fiber zero-dispersion wavelength and the LD center wavelength mismatch by 25 nm or more). For an 850 nm fiber and a LD source, repeaterless transmission at DS-4 rates over 15 km is conceivable.

Based on fiber sales in 1982, it is estimated that telecommunications accounts for 80% of the fiber optic market [12]. Most telecommunication junction networks are not longer than 20 km; hence, any signalling method that allows the repeaterless transmission of data at DS-3 rates or higher, over a 20 km or longer length of multimode fiber, has a large market value.

The forms of the decision feedback, ZF, and MMSE equalizers were derived. These forms are similar to the results of Salz, Proakis, and others, but included the possibility of shot noise as well as stationary gaussian noise.

The design procedures were applied to a hypothetical system with a pulse response similar to that observed for the experimental system. A comparison between the resulting SNRs at the equalizer outputs clearly indicates the superiority of DFE over the linear equalization methods for typical multimode fiber channels.

An upper bound on the error propagation effect of DFE was also formulated for a general M level PAM system with N taps of DFE. This upper bound, although very pessimistic, indicates that the severity of error propagation increases as the number of signal levels or the number of feedback taps increases. This increase is quite sharp, and indicates that even nonlinear equalization, such as DFE, has a limited range of equalization ability.

In order to investigate the practicability of multilevel signalling and DFE over dispersive multimode optical fibers, a 4 level PAM system with one-tap DFE was designed and tested. Because the presence of shot noise results in the optimum signal levels and decoder thresholds being unequally spaced, the system allowed for independent adjustment of the transmitter levels and decoder thresholds.

A computer program was written to analyze the experimental system. This analysis was in terms of the required optical power needed to obtain a desired BER, for a specified data rate and equalization condition (ideal precursor and postcursor cancellation, optimum-timed one-tap DFE, center-timed DFE, or no equalization). The analysis included signal-dependent shot noise in addition to stationary (thermal) noise, and found the optimum signal levels and decoder thresholds for all signalling conditions. The effect of feedback error propagation on the system error rate was also analyzed, and for one tap of DFE, proved to be much less than the worst-case upper bound. For the maximum amount of ISI considered, error propagation increased the model system's BER by less than 20% ; in terms of power, this increase was negligible.

The measured system performance agreed quite closely (within 1 dB for all tests) with the theoretical results obtained through the computer analysis. With 4 level signalling and one-tap DFE, transmission at a data rate of 40 Mb/s over a channel with an estimated bandwidth (including the preamplifier response) of 8 MHz was achieved. This value of 5 bits/Hz clearly demonstrates the advantages of multilevel signalling in conjunction with DFE. The received eye diagrams shown in Fig. 6.8 indicate the improvement offered by just one tap of DFE. They also indicate that there was non-uniform pulse dispersion which ultimately limited the effectiveness of the DFE and determined the maximum useful bit rate for the system. The four major problems observed with the system, including the non-uniform pulse dispersion, are:

1. The transmitter LED turn-on and turn-off times limited the useful system bit rate to 40 Mb/s. Although the LED has a large enough bandwidth to transmit at higher than 20 Mbaud/s, when kept on, it is too slow to transmit above 20 Mb/s when pulsed on and off. The LED limitation caused most of the

non-uniform pulse dispersion. Use of a faster LED, or a LD, would eliminate this problem.

2. The preamplifier was designed to have the desired signal bandwidth at a low cascode stage bias current, so that its noise figure is as small as practicable. It was found that the chosen bias current was small enough to be significantly increased by optical signals having a received power above -41 dBm (peak). This caused the ODP bandwidth to increase, and consequently the pulse dispersion decreased slightly for the higher signal levels. This effect, however, did not appear except when equalization was not used for a 40 Mb/s data rate, where the received power had to be increased substantially.

3. Although the theoretical computer program indicated that DFE with shifted sampling is superior to centered-sampled DFE, this advantage could not be experimentally realized, partially because of the non-uniform pulse dispersion, and partially because of the lack of timing resolution available with the delay generator.

4. The method in which the decoder thresholds were set resulted in their drifting with power supply drift. This limited the overall error measurement period for an optimized system setting to under half an hour. A redesign of the decoder threshold setting circuitry, to make the thresholds less sensitive to the power supply voltages, would help considerably.

Although this thesis considered the topic of multilevel signalling and DFE in conjunction with multimode fiber systems quite thoroughly, it was necessarily limited in scope. Recommendations for future research in this area are:

1. With uniform pulse dispersion, both multitap DFE and shifted-time DFE can be investigated. Shifted-time DFE should be compared to DFE with a leading precursor equalizer, so that the effectiveness of precursor equalization for optical systems can be evaluated.

2. Automatic equalization would be very useful for commercial fiber systems, where the channel characteristics may change considerably from system to system. An adaptive decision-feedback equalizer has been computer modelled [74], but a high speed realization remains to be done.

3. Timing extraction was not considered in this thesis, and has to be studied for multilevel systems with DFE. Intuitively, multilevel signals would possess more timing information than an equivalent binary system because:

   a) the baud rate of a multilevel system is less than that of an equivalent binary system, and thus the pulses would have sharper edges relative to their widths, and

   b) the probability of getting a pulse level transition from one pulse time slot to the next is higher for multilevel signals.

Also, an investigation into determination of the optimum pulse sampling point for systems with DFE is required.

4. This study was limited to multimode fiber systems. There is some indication that multilevel signalling and DFE may be useful for single-mode systems as well. The power disadvantage of going to more than two levels is offset by the increase in receiver sensitivity obtained when the system baud rate is reduced, for example. Also, as was mentioned in Chap. 2, the attenuation of 1550 nm single-mode fibers is less than that of 1300 nm fibers. For a 100 km fiber, the difference may amount to 20 dB. However, the fiber dispersion at 1550 nm is higher than that at 1300 nm. Although fibers are being tailored to have a minimum dispersion at 1550 nm, these fibers thus far have a slightly higher loss and are more vulnerable to microbending losses. An alternate approach would be to use multilevel signalling and DFE to compensate for the increased fiber dispersion at 1550 nm; the power penalty of these methods is certainly going to be less than the forementioned 20 dB of extra gain required for 1300 nm fiber.

The author hopes the evaluation of multilevel signalling and decision-feedback equalization presented in this thesis stimulates further research into this area.

Appendix A. Calculation of Channel Capacities in the Presence of Shot Noise.

Consider a signal level b_i corrupted by AWGN, and a decision level d_i as shown:

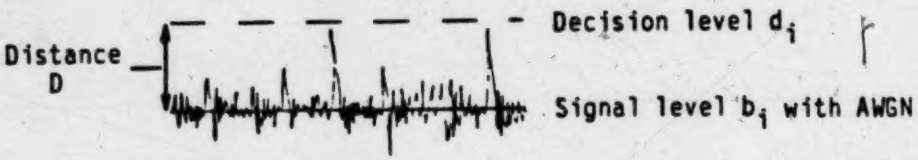
Decision level d_i
Distance
D
Signal level b_i with AWGN

Fig. A.1 Decoder threshold and adjacent signal level.

The probability that the noise will corrupt the signal enough so that it rises above the decision level will be denoted by "p", and is given from the probability-density function (pdf) for the AWGN:

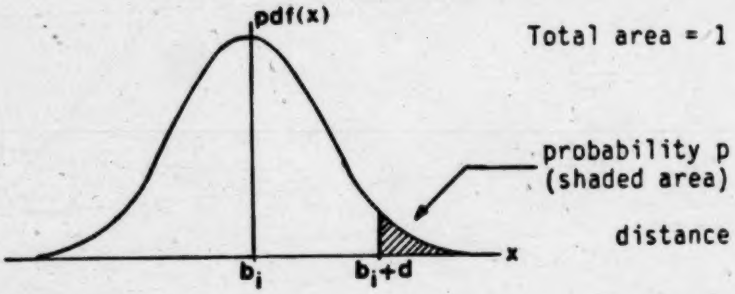
pdf(x)
Total area = 1
probability p
(shaded area)
distance
x
b_i
b_i+d

Fig. A.2 Normalized gaussian PDF centered about b_i.

The probability of error, p , can be expressed in terms of the normalized gaussian pdf:

$$p = \int_{d/\sigma_o}^{\infty} (\exp(-x^2/2)/\sqrt{2\pi})dx = Q(D/\sigma_o) \qquad (A.1)$$

where $Q(x) = (1 - \mathrm{erf}(x/\sqrt{2})/2$ (A.2)

Q(x) can be approximated or found in a table, but cannot be calculated in a closed form. From Eqn. A.1, we can find the probability of error for the 4 level situation depicted in Fig. A.2. Following the notation introduced in Chap. 3, b_1 to b_4 are the signal levels, and d_1 to d_3 are the decoder thresholds. Each signal level is corrupted by AWGN having a mean of zero and a variance of σ_o. (Shot noise will be considered later).

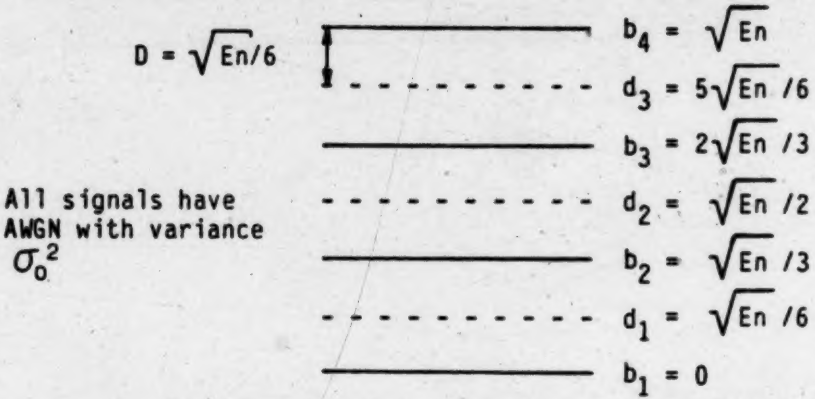
$D = \sqrt{En}/6$
$b_4 = \sqrt{En}$
$d_3 = 5\sqrt{En}/6$
$b_3 = 2\sqrt{En}/3$
All signals have AWGN with variance σ_o^2
$d_2 = \sqrt{En}/2$
$b_2 = \sqrt{En}/3$
$d_1 = \sqrt{En}/6$
$b_1 = 0$

Fig. A.3 Equidistant signal levels and thresholds for a 4 level PAM system with no shot noise

The probability of making an error, P(E), is given by

$$P(E) = (P(E|b_1) + P(E|b_2) + P(E|b_3) + P(E|b_4))/4 \qquad (A.3)$$

where $P(E|b_1)$ is the probability of making an error given the signal is at level b_1. However, if the noise at the sampling instants is denoted by n_o, where $(n_o)^2 = \sigma_o^2$, and if the signal levels are equally spaced, we have:

$$P(E|b_1) = P((b_1 + n_o) > d_1) = P(n_o > D) = p$$

$$P(E|b_2) = P((b_2 + n_o) > d_2) + P((b_2 + n_o) < d_1)$$
$$= P(|n_o| > D) = 2p$$

$$P(E|b_3) = P((b_3 + n_o) > d_3) + P((b_3 + n_o) < d_2) = 2p$$

$$P(E|b_4) = P((b_4 + n_0) < d_3) = p$$

Thus, $P(E) = (p + 2p + 2p + p)/4 = 3p/2$.

From this, it can be seen that, for multilevel signals with equiprobable signal levels, equidistant levels and decoder thresholds are not optimum (even for stationary noise only). The probability of error for each signal level is not constant; for the first and fourth signal levels it is half that of the middle two levels. However, the energy difference between this situation and the optimum situation, for the same system error probability, is small. For $P(E) = 10^{-9}$, and with four level signalling, the difference can be easily shown to be 0.05 dB.

For shot noise, however, the noise variance increases as the signal level increases. Thus, with an equally spaced multilevel system using one-sided (as opposed to antipodal) signalling, $P(E|b_i) > P(E|b_{i-1})$. The difference can be substantial, and thus unequal signal level spacing is required. Because of this, the channel capacities shown in Fig. 2.1 do not apply to PAM systems with significant shot noise. However, they can be extended to account for shot noise. Consider the two 4 level systems below:

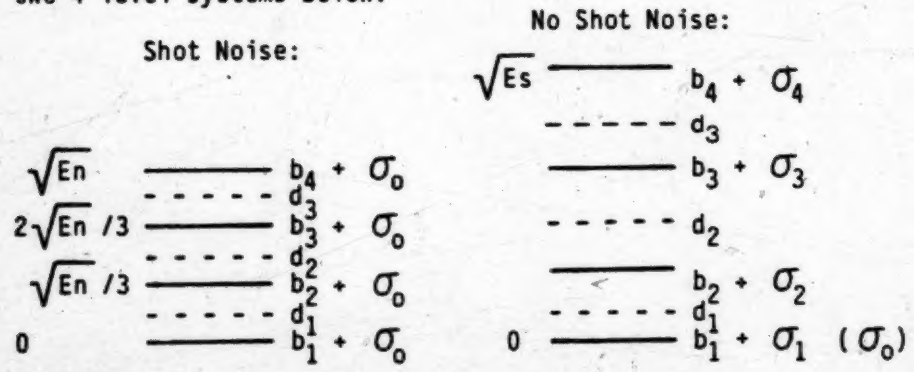
No Shot Noise:
Shot Noise:
$\sqrt{Es}$
$b_4 + \sigma_4$
d_3
$b_3 + \sigma_3$
d_2
$b_2 + \sigma_2$
d_1
0
$b_1 + \sigma_1$ (σ_0)
$\sqrt{En}$
$b_4 + \sigma_0$
d_3
$2\sqrt{En}/3$
$b_3 + \sigma_0$
d_2
$\sqrt{En}/3$
$b_2 + \sigma_0$
d_1
0
$b_1 + \sigma_0$

Fig. A.4 Signal level spacing with/without shot noise.

We want these systems to be equivalent in terms of their probability of error. Thus,

$$P(E|b_1)_{\text{no shot noise}} = P(E|b_1)_{\text{shot noise}}$$

$$P(E|b_2)_{\text{no shot noise}} = P(E|b_2)_{\text{shot noise}},$$

and so on. To extend a curve in Fig. 2.1 to include a known amount of shot noise, the procedure below was followed:

1. Suitable values for R_0 were chosen. From Fig. 2.1, the corresponding values for En/No from the desired A-level curve were obtained.

2. For Fig. 2.1, $En/No = En/2\sigma_0^2$. By substitution of an appropriate value for $_0$, the values for the En corresponding to the chosen R_0 values were found.

3. With σ_0 and the En values known, the error probabilities for the A-level system possessing no shot noise, for each value of En, could be determined. The required energies, which are denoted by Es, to realize the same error probabilities for the system possessing shot noise, were calculated.

4. The values of Es/No was were plotted against their corresponding R_0 values, thus producing the curves in Fig. 2.2. The R_0 designation was changed to R_s, to denote that the resulting capacities apply to the shot noise system.

Step 3, the analytical step, requires some explanation. Again, the noise model, from Eqn. 2.5, is

$$\sigma_i^2 = \sigma_0^2 + \xi \cdot b_i.$$

For an A-level system possessing no shot noise and with equidistant signal levels (as is the situation for Fig. 2.1), the distance between adjacent signal levels and decoder thresholds is given by $D = \sqrt{En}/2(A-1)$. The value for the signal level to adjacent threshold error probability, p, is $p = Q(D/\sigma_0)$. We want the two systems to be equivalent. Therefore,

$$Q(D/\sigma_0) = Q((d_i - b_i)/\sigma_i) = Q((b_i - d_{i-1})/\sigma_i) \qquad (A.4)$$

Consider finding the signal level b_{i+1} in terms of the previous level, b_i, with both b_i and σ_i known. We have, from Eqn. A.4,

$$(d_i - b_i)/\sigma_i = D/\sigma_0, \text{ or}$$

$$d_i = (\sigma_i D/\sigma_0) + b_i. \qquad (A.5)$$

Also,

$$(b_{i+1} - d_i)/\sigma_{i+1} = D/\sigma_0, \text{ or}$$

$$b_{i+1} = (\sigma_{i+1} D)/\sigma_0 + d_i.$$

Upon substitution for d_i from Eqn. A.4, this becomes:

$$b_{i+1} = (D\,\sigma_{i+1})/\sigma_0 + (D\,\sigma_i/\sigma_0) + b_i$$

Substitution of σ_{i+1} in terms of b_{i+1}, σ_0, and ξ into this equation yields the quadratic expression

$$b_{i+1}^2 - B \cdot b_{i+1} + C = 0,$$

where

$$B = 2(b_i + D\,\sigma_i/\sigma_0) + \xi D^2/\sigma_0^2 \text{ and}$$

$$C = b_i(b_i - 2D\,\sigma_i/\sigma_0) - D^2(1-(\sigma_i/\sigma_0)^2). \qquad (A.6)$$

Solution of this equation yields the required signal level b_{i+1} in terms of the previous level. Once b_{i+1} is known, σ_{i+1} can be solved for. Repetition of this procedure from b_2 to the highest signal level b_A allows Es to be determined. The first level, b_1, is zero, and hence provides a starting point for the level determination procedure.

The curve for C_o can be extended in the same manner as the R_o curves, to obtain the C_s curve shown in Fig. 2.2. A simpler method is to redefine the maximum channel capacity (C_o) with one-sided signalling expression. From Chap. 2 (Eqn. 2.4b),

$$C_o = (1/2)\log_2(1 + En/2No).$$

For non-stationary noise, No has to be replaced with "N_i", the signal dependent noise. If we replace En with b_i^2 and N_i with $\sigma_o^2 + \xi b_i$, we get the channel capacity with shot noise:

$$C_s = (1/2)\log_2\{1 + b_i^2/2(\sigma_o^2 + \xi b_i)\}$$

This can be simplified to yield

$$C_s = (1/2)\log_2\{1 + (b_i/\sigma_o)^2/2(1 + \xi b_i/\sigma_o^2)\}.$$

Finally, upon resubstitution of En = b_i^2 and No = σ_o^2, the final result is

$$C_s = (1/2)\log_2\{1 + (En/No)/2(1+(\xi/\sigma_o)\sqrt{En/No})\} \qquad (A.7)$$

This expression can be plotted directly. It indicates the absolute values of ξ and σ_o are not important; rather, their ratio determines the severity of the shot noise on the channel capacity. Also, the higher En/No is, the more severe the channel capacity loss due to shot noise becomes. This effect can be seen in Figs. 2.1 and 2.2.

Appendix B. Design of the Transimpedance Preamplifier

Figure 4.4 shows the ac equivalent circuit for the experimental preamplifier. As was mentioned in Chap. 4, proper design of the preamplifier involves load, bandwidth, and noise considerations. Several points pertinent to the circuit design are:

a) The biasing arrangement, shown in Fig. 4.5, has the collector current of the common-emitter (CE) transistor equal to the emitter current of the common-base (CB) transistor. Neglecting the base-current difference, these currents are equal, and will be denoted by Ic, hcascode biasing current.

b) Since the cascode transistors will have identical hybrid-pi models, the parameters relating to these transistors will be unscripted. The third (common-collector, or CC) transistor will have its parameters subscripted with a "3".

c) From El-Diwany's results [64], the optimum cascode biasing current will be small (under 1 mA).

d) The CC stage must drive a 50 ohm coaxial load, and have a signal bandwidth around 10 MHz.

e) The feedback resistor, R_f, provides both ac and dc feedback. Thus, the first transistor is biased by the voltage drop across the CC transistor's bias resistor R_e.

f) Following standard notation, all transistor model resistors will be designated by a small r, whereas all others will be designated with a large R (except where this notation may cause ambiguity).

The design procedure is concerned with finding the following parameters:

a) The cascode (stage) biasing current Ic

b) The feedback resistor R_f

c) The cascode biasing resistor R_c

d) The CC (transistor) biasing current Ic_3

e) The CC biasing resistor R_e

The transistors chosen for the circuit are Motorola's BFR90's, because of their high gain-bandwidth product of 5 GHz, low noise figure, and low input capacitance. Motorola's data for these transistors consists of S-parameters for frequencies of 200 MHz and higher, and for collector currents of 2 mA and higher. This data had to be extended to the frequency and current range of interest. To do this, a modified hybrid-pi transistor model was optimized to match the given S-parameter data (for the frequencies of 200 and 500 MHz) through the use of Compact, a computer analysis and optimization program [69]. Figure B.1 shows the transistor model. The parameters for this model are on the following page.

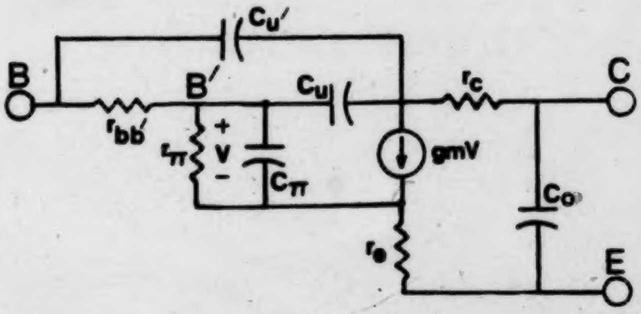

Fig. B.1 Computer-optimized modified hybrid-pi model for the BFR90 bipolar transistor.

Assumed Parameters

$\beta = 50$, $gm = Ic/V_T$ (V_T = 26 mV), $r_\pi = \beta/gm$

Computer Optimized Parameters:

(Resistor values in ohms, capacitor values in pF, unless otherwise designated)

At Ic = 2 mA: $r_{bb}' = 49$, $r_c = 14$, $r_e = 0.03$, $r_o = 73$ kilo-ohms
$C_\pi = 4.3$, $C_u = 0.02$, $C_u' = 0.58$, $C_o = 0.44$

At Ic = 5 mA: $r_{bb}' = 68$, $r_c = 12$, $r_e = 0.03$, $r_o = 55$ kilo-ohms
$C_\pi = 7.5$, $C_u = 0.04$, $C_u' = 0.57$, $C_o = 0.43$

The value for C_π satisfies the expression

$$C_\pi = \tau_F gm + C_{je} \equiv 27 \text{ ps}\cdot gm + 2.2 \text{ pF}$$

where C_{je} is the emitter-base depletion layer capacitance, and τ_F is the transistor's base transit time in the forward direction [76]. The stray capacitances Cs_1, Cs_2, Cs_3, Cs_4, and C_F, shown in Fig. 4.4, were estimated for the printed circuit board configuration used. These estimates are:

a) $Cs_1 \equiv 5$ pF
b) $Cs_2 \equiv 1.5$ pF
c) $Cs_3 \equiv 4.5$ pF
d) $Cs_4 \equiv 10$ pF
e) $C_f \equiv 0.5$ pF

From RCA's data on the CD30908E APD [67], the detector capacitance is 2 pF (maximum).

The transistor model given in Fig. B.1 is useful for computer-aided circuit analysis. However, it is too complex for hand analysis. A more suitable hybrid-pi model is obtained by neglecting the resistors r_e, r_c, and r_o. The feedthrough capacitances C_u and C_u' can be lumped as one capacitor in the position of C_u, and will be denoted by C_{uT}. With this simplified model, the ac equivalent preamplifier circuit becomes that of Fig. B.2:

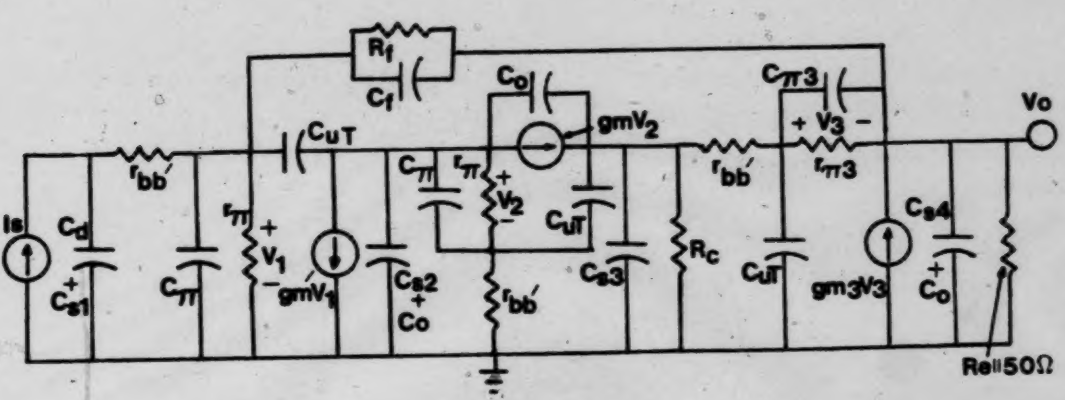
Rf
Cf
Co
gmV2
Cπ3
+ V3 −
Vo
CuT
rbb'
Cπ
rπ
+
V2
−
CuT
rbb'
rπ3
Is
Cd
+
Cs1
Cπ
rπ
+
V1
−
gmV1
Cs2
+
Co
rbb'
Cs3
Rc
CuT
gm3V3
Cs4
+
Co
Re‖50Ω

Fig. B.2 Small-signal preamplifier circuit using hybrid-pi transistor models.

Analysis of this circuit can be simplified through the following alterations:

1. For the cascode transistors, r_{bb}' is much smaller than r_π, and can be ignored (except at very high frequencies).

2. The shunt-shunt feedback can be replaced by ideal feedback, provided its loading effect in accounted for. This is accomplished by placing the feedback network in parallel with both the input and output terminals of the amplifier. The loading effect on the output, however, is negligible in comparison to the output impedances.

3. The feedthrough capacitance of the first transistor can be replaced by its Miller capacitances. For this, the voltage gain of the first transistor needs to be derived:

$Av_1 = V_2/V_1$, where

$V_2 = -(gmV_1 + gmV_2)r_\pi$, or

$Av_1 = -gm \cdot r_\pi / (1 + gm \cdot r_\pi) = -\beta/(\beta + 1) \cong -1.$

The appropriate Miller capacitances are therefore

$C_{im} = (1 - Av)C_{uT} = 2C_{uT}$, and

$C_{om} = (Av - 1)C_{uT}/Av = 2C_{uT}$

4. The CB transistor can be replaced by the equivalent model shown in Fig. B.3:

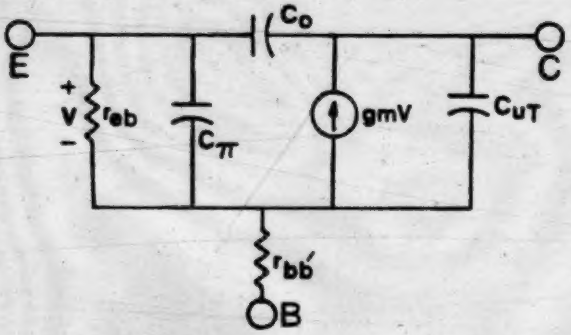

$r_{eb} = \beta/gm(\beta + 1)$

Fig. B.3 Emitter-current controlled, hybrid-pi common-base transistor model.

Although the resistor r_{bb}' in this model is negligible, it can be accounted for quite easily by the use of Miller's dual theorem. This theorem allows the replacement of r_{bb}' by series resistances in the emitter and collector leads of values

$r_{im} = r_{bb}'(1 - Ai)$, and

$r_{om} = r_{bb}'(Ai - 1)/Ai$

where Ai is the current gain of the CB stage. This current gain is given by:

$$Ai = gm \cdot r_{eb} = gm\,\beta/gm(\beta + 1) \cong 1.$$

Thus, $r_{im} = r_{om} = r_{bb}'(1-1) \cong 0$.

This result implies that the base of the CB stage does not have to be externally grounded by a capacitor, as long as the external bias resistors are kept reasonably small.

The voltage gain of this stage is simply $gm \cdot R_B$, where R_B is the parallel combination of R_c and the input resistance of the CC stage. The capacitor, C_o, of Fig. B.3, can be replaced by its Miller capacitors:

$$C_{im} = C_o(gm \cdot R_b - 1)$$

$$C_{om} = C_o(gm \cdot R_o - 1)/(gm \cdot R_b)$$

As yet, the voltage gain, $gm \cdot R_b$, is not known. However, it is almost the same as the voltage gain for the preamplifier, as both the CC stage and the CE stage have near unity voltage gain. From El-Diwany's results, the cascode stage type of transimpedance preamplifier should have a small open-loop voltage gain, in order to be stable. For a 100 MHz signal bandwidth, his derived maximum stable gain was 8. For a signal bandwidth of 10 MHz, a suitable gain for the above calculation would be 10. Then,

$$C_{im} \cong 9C_o, \text{ and}$$

$$C_{om} \cong C_o.$$

The above alterations result in the much simplified circuit for the preamplifier shown in Fig. B.4.

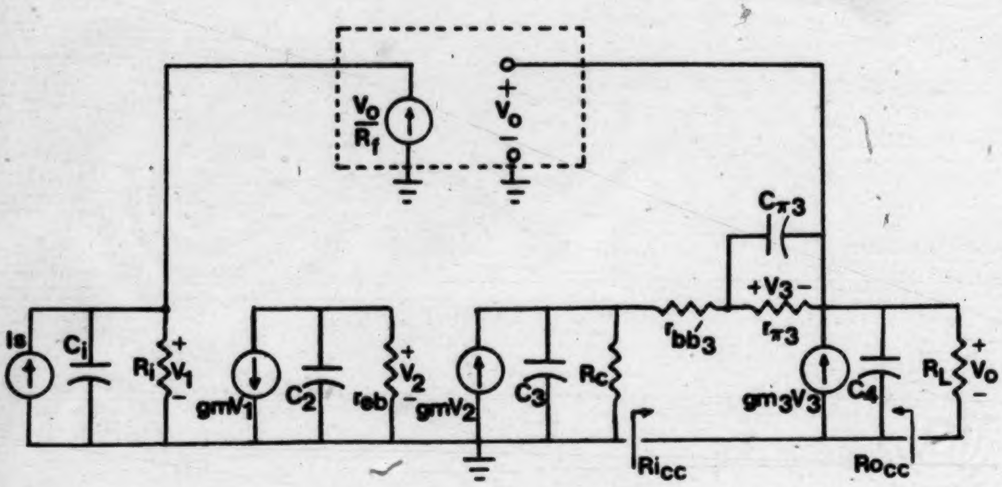

$\frac{V_o}{R_f}$
$+ V_o -$
$C_{\pi 3}$
$+V_3-$
Is
C_i
R_i
$+V_1-$
gmV_1
C_2
r_{eb}
$+V_2-$
gmV_2
C_3
Rc
$r_{bb'3}$
$r_{\pi 3}$
gm_3V_3
C_4
R_L
$+V_o-$
Ricc
Rocc

$C_i = C_d + C_\pi + Cs_1 + 2C_{uT} + C_f \cong 11.5$ pF for Ic (cascode)<1 mA.

$R_i = r_\pi \parallel R_f$

$C_2 = Cs_2 + C_o + C_\pi + 9C_o \cong 6.5$ pF for Ic < 1 mA.

$r_{eb} = \beta / gm(\beta + 1) \cong 0.98/gm$

$C_3 = Cs_3 + C_{uT} + C_o \cong 5.5$ pF

$C_4 = Cs_4 + C_f + C_o \cong 11$ pF

$R_c = R_e \parallel 50$ ohms

Fig. B.4 Simplified preamplifier circuit model.

The CC stage has to be analyzed in order to ensure proper load matching. For an estimated maximum optical launch power of -10 dBm, and an estimated channel attenuation of 25 dB including connection losses, the maximum power incident on the APD would be -35 dBm. The responsivity of the RCA APD is 77 A/W. A reasonable estimate for the preamplifier transimpedance, given the signal bandwidth required, is 10 kilo-ohms [64]. With this,

$$Vo_{maximum} = TR \cdot R_\lambda \cdot P_i = 10^4 \cdot 77 \cdot 10^{-6.5} = 240 \text{ mV}.$$

For a 50 ohm load, this would result in a 5 mA signal current. A suitable bias current for the CC stage, then, is 6 mA. With this value for Ic_3, $gm_3 = 231$ mmhos, $r_{\pi 3} = 217$ ohms, $r_{bb3}' \cong 68$ ohms, and $C_{\pi 3} = 8.5$ pF.

The first transistor is biased on by the voltage drop across R_e. Neglecting the small voltage drop across R_F, the base-emitter voltage for the CE transistor is $Vbe_1 = Ic_3 R_e$. Thus, $R_e = 0.7\text{V}/6\text{ mA} \cong 120$ ohms.

The load at the CC output is R_e in parallel with 50 ohms, or 35 ohms. To minimize the possibility of reflections at the preamplifier output, the output impedance of the CC stage should match $R_L = 35$ ohms. Thus,

$$Ro_{CC} = (r_{\pi 3} + Rs)/(1 + \beta) = 35 \text{ ohms}.$$

The source resistance, Rs, is simply R_c, as the output impedance of the CB stage is quite high. With this, the value of R_c should be 1.5 kilo-ohms. Experimentally, it was found that R_c could be made larger than this, in order to increase the preamplifier gain, without causing load reflections. A value of 2.7 kilo-ohms was used for R_c.

The input impedance of the CC stage is given by

$$Ri_{cc} = r_{\pi 3} + R_c(\beta + 1) \cong 2 \text{ kilo-ohms}.$$

The resistance seen by the common-base stage is thus

$$R_B = R_c \parallel Ri_{cc} = 1160 \text{ ohms}.$$

The voltage gain of the CC stage can be shown to be:

$$Av_{cc} = \frac{1}{1 + (r_{bb3}' + Z_\pi)/Z_L(gm_3 Z_\pi + 1)} \tag{B.1}$$

where $Z_\pi = r_{\pi 3} \parallel 1/sC_{\pi 3}$ and

$$Z_L = R_L \parallel 1/sC_4, \text{ where } s=j\omega .$$

At low frequencies,

$$Av_{CC} = \frac{1}{1 + (r_{bb3}' + r_{\pi 3})/(\beta + 1)R_L} = 0.86.$$

The CC stage has a very good frequency response, and can be operated at close to the transistor's cutoff frequency with moderate loading. An evaluation of the CC stage's frequency response, through Eqn. B.1, reveals its peak voltage gain is 1.05 at 800 MHz, and the 3 dB frequency is 1.39 GHz. Thus, in comparison to the desired signal bandwidth of 10 MHz, the CC stage can be assumed to have a flat frequency response. The preamplifier circuit can now be reduced to that of Fig. B.5:

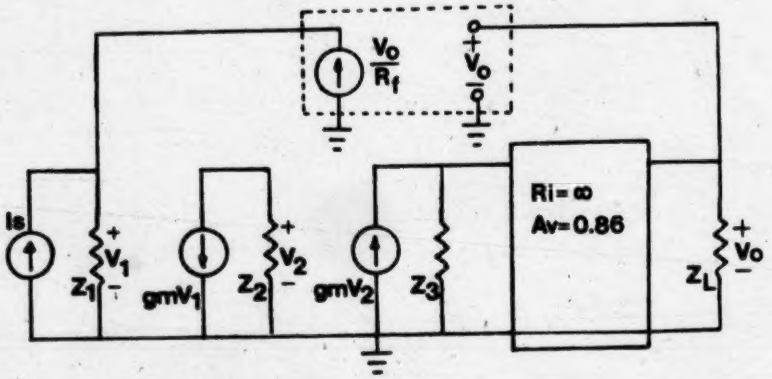

Fig. B.5 Preamplifier circuit with the CC stage completely analyzed.

In this schematic,

$Z_1 = R_i \parallel 1/sC_i = (r_\pi \parallel R_F) \parallel (1/s)\cdot 11.5$ pF

$Z_2 = r_{eb} \parallel 1/sC_2 = (0.98/gm) \parallel (1/s)\cdot 6.5$ pF

$Z_3 = R_B \parallel 1/sC_3 = 1160$ ohms $\parallel (1/s)\cdot 5.5$ pF

The open-loop voltage gain, A_o, and transimpedance, TR_o, of the preamplifier are easily found from Fig. B.5:

$$A_o(s) = A_o/(sT_2 + 1)(sT_3 + 1)$$

$$TR_o(s) = A_o \cdot R_i/(sT_1 + 1)(sT_2 + 1)(sT_3 + 1)$$

where

$A_o = -978$ gm,

$T_1 = C_i \cdot R_i$

$T_2 = C_2 \cdot r_{eb}$

$T_3 = C_3R_B = 6.4$ ns.

For $Ic < 1$ mA, $r_{eb} < 26$ ohms. Then, $T_2 < 0.17$ ns. The pole corresponding to this minimum value for T_2 is 940 MHz, and can be ignored when compared to the other two poles. The pole corresponding to T_3 is at 25 MHz.

The closed-loop transimpedance is

$$TR_c(s) = TR_o(s)/(1 + TR_o(s)/R_F)$$

$$= A_oR_i/[(sT_1 + 1)(sT_3 + 1) + A_oR_i/R_F] \qquad (B.2)$$

This expression allows the calculation of the signal bandwidth in terms of R_F and r_π. However, the relationship is not simple and hence not too useful. A much easier method of estimating the signal bandwidth is obtained by considering the preamplifier damping factor and the dominant time constant T_i. The expression for $TR_c(s)$ can be put into standard form:

$$TR_c(s) = TR_c/(s^2 + 2\zeta\omega_n s + \omega_n^2),$$

where ω_n is the natural frequency and ζ is the damping factor. This damping factor indicates how close the two dominant preamplifier poles are. The larger ζ is, the farther apart the poles are, and the stabler the circuit is. If ζ is too large, however, the circuit will have a poor rise-time.

The signal bandwidth, Bs, can be estimated through knowledge of the effective dominant pole and the damping factor:

$$Bs \cong B, \quad \zeta > 1$$

$$Bs \cong 1.29 \cdot B, \quad \zeta = 1$$

$$Bs \cong \sqrt{2}\, B, \quad \zeta = 1/\sqrt{2}$$

To allow a wide stability margin, a value of 1 for ζ is desirable. The effective dominant pole, B, is obtained by considering only the dominant pole in $TR_o(s)$:

$$TR_o'(s) = A_oR_i/(sT_1 + 1)$$

This yields

$$TR_c'(s) = A_oR_i/[(sT_1 + 1) + A_oR_i/R_f].$$

The bandwidth of $TR_c'(s)$ is defined as the effective dominant pole, B:

$$\omega_{3\ dB} \cdot T_1 = 1 + A_oR_i/R_f, \text{ or}$$

$$B = (1 + A_oR_i/R_f)/2\pi T_1$$

This can be manipulated to yield

$B = 1/2\pi C_iR_{eff}$ where the effective dominant-pole resistance, R_{eff}, is

$$R_{eff} = r_\pi \,||\, R_f/(1 + A_o).$$

The desired signal bandwidth is 10 MHz, and the desired damping factor is 1. Thus,

$$10\ \text{MHz} \cong 1.29/2\pi C_iR_{eff}, \text{ or } R_{eff} = 1785 \text{ ohms}.$$

Bandwidth considerations have yielded the relationship (with substitution of $gm = \beta/r_\pi$):

$$1781 \text{ ohms} = r_\pi \,||\, R_f/(1+A_o) = r_\pi \,||\, R_f/(1+48.9\text{k}\Omega\ /r_\pi). \quad (B.3)$$

Another relationship is required to find r_π and R_f. This relationship is obtained from noise considerations. The dominant noise sources, referred to the preamplifier input, have the following spectral current densities [64]:

a) Base-current shot noise $S_1 = 2qIb$

b) Collector-current shot noise $S_2 = 2qIc/|A_i|^2$ (k is Boltzmann's constant, and T is the absolute temperature)

c) Feedback resistor thermal noise $S_3 = 4kT/R_f$

d) Base-spreading resistance thermal noise

$S_4 = 4kTr_{bb}'[1/R_f^2 + (\omega C_i')^2]$

where $C_i' = C_d + Cs_1 + C_F$

e) APD dark-current shot noise $S_5 = 2qI_{dark}$

f) APD signal current shot noise $S_6 = 2q(\eta q/h\nu)\overline{G}^{2+x}P_i$

Only the first three of these noise sources can be controlled through the preamplifier design (for a desired signal bandwidth). Hence, they are the only ones involved in the noise minimization procedure that results in the optimum values for r_π and R_f. The input-referred noise for these three sources can be shown to be[1]: [64]

$$\overline{i_n^2} = \{4kT/R_f + 2kT/r_\pi + (2kTr_\pi/\beta)[1/R_i^2 + (2\pi C_i B_n)^2/3]]\}B_n \qquad \text{(B.4)}$$

B_n is the noise bandwidth, and can be approximated as

$$B_n = \pi B/2 \cong 12.2 \text{ MHz}.$$

From Eqn. B.4, $\overline{i_n^2}$ depends on r_π and R_f. The optimum values for r_π, in terms of R_f, are found by differentiating $\overline{i_n^2}$ with respect to r_π. The result of this is

$$r_{\pi\,opt}^2 = (\beta + 1)/[1/R_f^2 + (2\pi C_i B_n)^2/3] \qquad \text{(B.5)}$$

and $$\overline{i_n^2}_{min} = [4kT(\beta + 1)B_n/\beta][1/R_f + 1/r_\pi]. \qquad \text{(B.6)}$$

Substitution for C_i, B_n, and in Eqn. B.5 yields

$$r_\pi^2 = 51/(1/R_f^2 + 2.59\cdot 10^{-7}). \qquad \text{(B.7)}$$

This equation, in conjunction with Eqn. B.3, results in

$$r_{\pi\ opt} = 13.7 \text{ kilo-ohms}, \quad R_{f\ opt} = 9.3 \text{ kilo-ohms}.$$

This value of r_π corresponds to $Ic_{opt} \cong 0.1$ mA and $Ib_{opt} \cong 2$uA. However, this value for Ic is quite small. Since the BFR90 transistor's cutoff current is not specified, there is a possibility of reduced β at this current. The experimental results of [64] indicate the transistors should be able to operate at close to 4 uA of base current. For $\beta = 50$, this corresponds to a collector current of 0.2 mA. The final design was based around this value for Ic.

---

[1] Equation (2) in [64] should read $1/R_f'^2$ instead of $1/R_f^2$. This ommission results in the following changes:

a) Eqn. (3) should read $1/R_f'^2$ instead of $1/R_f^2$.

b)Eqns.(4)and (5) should read $\sqrt{\beta + 1}$ instead of $\sqrt{\beta}$.

c) Eqn. (6) should be multiplied by $(\beta + 1)/\beta$.

Except possibly for Eqn. (3), these changes are negligible.

For Ic = 0.2 mA, r_π is 6.5 kilo-ohms. From Eqn. B.3, the optimum feedback resistor is 20.9 kilo-ohms. A value of 20 kilo-ohms was consequently used in the experimental amplifier. With these values for r_π and R_f,

$$A_o = -978gm = -7.52$$

$$TR_o = A_oR_i = 36900 \text{ ohms (at low frequencies)}$$

$$TR_c = TR_o/(1+TR_o/R_f) = 13 \text{ kilo-ohms (at low frequencies).}$$

Also, $T_1 = C_iR_i = 56$ ns (corresponding to $f_1 = 2.8$ MHz). Eqn. B.2 can now be solved to obtain ζ and a closer estimate of the 3 dB signal bandwidth. The results are $\zeta = 0.98$ and $B_s = 9.35$ MHz. Evaluation of the noise can be done with $B_n = 1.29 \cdot B_s = 12$ MHz. This yields $\overline{i_n^2} = (5.4 \text{ nA})^2$. The signal-independent output noise voltage is then

$$\sigma_o = (5.4 \text{ nA}) \cdot TR = 70 \text{ uV}.$$

Inclusion of the base-spreading resistance thermal noise raises this figure to 71 uV.

The APD dark current is small enough that its contribution to the overall noise is negligible. The APD signal current shot noise, referred to the preamplifier output, is

$$\sigma_{i\,APD}^2 = TR^2B_n2q(\eta q/h\nu)\,\overline{(G)}^{2+x}P_i.$$

For RCA's 30908 APD, $G \cong 149$ and $\eta = 0.77$ at the recommended operating voltage. Using a value of 0.4 for x, and with an optical wavelength of 830 nm,

$$\sigma_{i\,APD}^2 \cong 55 \cdot P_i.$$

With the output signal $b_i = TR \cdot R_\lambda \cdot P_i \equiv 10^6 \cdot P_i$, the total output noise can be expressed as

$$\sigma_i^2 = (71\ \mathrm{uV})^2 + (55\ \mathrm{uV}) \cdot b_i. \qquad \text{(B.8)}$$

Appendix C. Listing of the PAM System Analysis Program

This appendix contains the 4 level PAM system analysis program discussed in Chap. 5. Because of the restrictions in the available label characters (greek, subscript, and superscript characters were not allowed), several of the parameters defined throughout the thesis have different labels in the source listing. The following list defines the important program parameters, starting with the user determined variables.

User Determined Variables

BN: The maximum "negligible-ISI" data rate the channel can support, in Mb/s.

NOISI: The sampled-time vector representing the negligible-ISI pulse shape. This vector consists of three points corresponding to the pulse response r(t) at t = -0.5T, 0, and +0.5T (where t=0 corresponds to the pulse peak; for the condition of negligible ISI, NOISI(2) ≡ 1.

BP: The data rate at which the system is to be analyzed, in Mb/s.

H2: Same as H' in Chap. 5. The vector of sampled r(t) (which now represents the BP rate pulse shape) consists of 7 points, from -T to 2T in T/2 steps. Zero values can be entered for any the points except the t=0 point, as long as there is some ISI to avoid division by zero in the program.

VT: Same as σ_0. The thermal noise level at the output of the transimpedance preamplifier, in volts.

ST: Same as ξ. The shot-noise parameter of the ODP, referred to the preamplifier output, in volts.

TR: The amplifier transimpedance, in ohms.

ER: The vector of desired BERs for which the system is to be characterized.

Program Variables

VN: Same as the normalized value of σ_0, as discussed in Chap. 5.

SN: Same as the normalized value for the shot noise parameter ξ, as discussed in Chap. 5.

S: Same as the vector b_1, b_2, b_3, b_4. Vector of the signal levels, in volts, with S(1) = 0 (corresponding to the LED being off). Dimension = 4. (Note - if there is ISI present, these levels will correspond to the minimum value of the actual signal level, plus the average amount of ISI. This is because the ISI is taken to be always positive.)

A: Same as the vector d_1, d_2, d_3, d_4. Vector of decoder thresholds, in volts. Dimension = 4.

V: Same as σ_1, σ_2, σ_3, σ_4. Vector of noise variances corresponding to the levels S(1) to S(4). With no ISI, V(1) = σ_0. Dimension = 4.

PED: The desired overall BER for the system analysis under way. One of the terms in the used determined vector ER.

PEDV: Desired vector of the individual probability of errors for each possible signal level - decoder threshold crossing. PEDV = [2PED, PED, PED, PED, PED, 2PED].

PEEQ: The final system error rates for the completely equalized pulse shape. Each term in this vector will be within 25% of the corresponding term in PEDV.

PDBMEQ: The vector of received optical powers, in dBm, required to obtain the error rates given by PEQ (for the case of complete equalization).

PEDFE: Same as PEQ, except for the case of one-tap DFE.

PEACT: Same as PEDFE, except with the error propagation effect of DFE included.

PDBMDFE: Same as PDBMEQ, except for the case of one-tap DFE.

PENEQ: Same as PEEQ except for the case of no equalization.

PDBMNEQ: Same as PDBMEQ except for the case of no equalization.

EEQ: Vector of the individual probability of errors for each possible signal level - decoder threshold crossing, for a particular set of signal levels and detector thresholds. For the final level and threshold setting, all components of EEQ should be within 25% of the corresponding components in the PEDV vector. Applies to the completely equalized case.

EDFE: Same as EEQ, except for the one-tap DFE case.

PEV: Intermediate value for the EEQ, EDFE vectors before the final result is renamed. These vectors are displayed as they are generated, for the DFE or no equalization cases, so that the user can evaluate how well the program is converging to the desired PEDV vector.

H: Same as the H defined in Chap. 5. H defines the pulse shape at the instants t = -T, 0, T, and 2T (a subset of H').

HEQ: The vector of interfering terms - the nonzero terms in H except for H(2) = H(t = 0).

ISI: Same as G in Chap. 5, but restricted to the case of no equalization. The vector of all possible ISI terms.

ISI2: Same as G in Chap. 5, but restricted to the equalized case . The vector of all possible ISI terms, given single-tap DFE is being used.

```
4 LEVEL PAM OPTICAL FIBER SYSTEM CHARACTERIZATION ROUTINE
                                                                                                  PAGE  1
                                                                                                  01-01-80
                                                                                                  00:14:02
Offset  Data    Source Line                                              IBM Personal Computer BASIC Compiler V1.00

 001A   0002    1      REM $LINESIZE: 132 $TITLE: '4 LEVEL PAM OPTICAL FIBER SYSTEM CHARACTERIZATION ROUTINE'
 001A   0002    2      REM $SUBTITLE: 'PAM - INITIALIZATION, CONTROL, AND I/O'
 001A   0002    3      REM
 001A   0002    10     REM PAM - THIS PROGRAM CALCULATES THE REQUIRED INPUT OPTICAL POWER,
 001A   0002    11     REM       DECODER SIGNAL LEVELS, AND DECODER THRESHOLDS FOR THE
 001A   0002    12     REM       EXPERIMENTAL 4-LEVEL FIBER SYSTEM. THE EXPERIMENTALLY OBTAINED
 001A   0002    13     REM       DATA REQUIRED FOR THE PROGRAM CONSISTS OF PULSE SHAPES AT
 001A   0002    14     REM       SPECIFIED BAUD-RATES, THE THERMAL-NOISE LEVEL, A SHOT-NOISE
 001A   0002    15     REM       PARAMETER, THE OPTICAL DETECTOR RESPONSIVITY, AND THE
 001A   0002    16     REM       PREAMPLIFIER TRANSCONDUCTANCE.  THE DESIRED ERROR-RATES FOR THE
 001A   0002    17     REM       SYSTEM ARE ALSO SUPPLIED, ALONG WITH THE EQUALIZATION DESIRED
 001A   0002    18     REM       (COMPLETE ISI CANCELLATION, ONE-TAP DFE, OR NO EQUALIZATION).
 001A   0002    20     CLEAR: KEY OFF: COLOR 2,0: CLS: LOCATE 25,1:COLOR 4,7:PRINT "   PAM    ";
 0042   0002    25     LOCATE 24,1: COLOR 3,0
 008C   0002    30     DEFINT F,I-L: DEFDBL X-Z,D
 00AC   0002    40     PI#=3.141592653589798#: LCOL=1
 00AD   0002    45     C1=.06: C2=.15: ON KEY (10) GOSUB 12000 'READ NEW C1 AND C2 ON KEY F10
 00D6   0014    50     DIM ISI!(64),H(3),HEQ(3),H2(7),S(4),V(4),A(4),NOISI(3),PEDV(6),PEV(6)
 00E1   01DC    55     DIM E(6),ER(10),PEDFE(10),PENEQ(10),PDBMEQ(10),PDBMDFE(10),PDBMNEQ(10)
 00E2   0300    60     DIM SEQ(4),AEQ(4),VEQ(4),EEQ(6),PEEQ(10),SDFE(4),ADFE(4),VDFE(4),EDFE(6)
 00E3   03DC    65     DIM ISI2!(8),PEACT(10)
 00E4   042C    70     OPEN "I",#1,"PAMDATA" 'READ IN DEFAULT DATA FROM THE DISK.
 00E5   042C    80     INPUT# 1,BN,NOISI(1),NOISI(2),NOISI(3),BP,H2(1),H2(2),H2(3)
 0104   042C    85     INPUT# 1,H2(4),H2(5),H2(6),H2(7),VT,ST,TR,I.ER
 0158   0434    90     FOR I=1 TO I.ER: INPUT# 1,ER(I): NEXT
 01E6   0446    100    CLOSE 'FINISHED READING THE DEFAULT DATA - NOW PRINT THE DATA
 01E6   0446    110    PRINT "BN=";BN;"  NOISI=";NOISI(1);NOISI(2);NOISI(3)
 01EC   0446    120    PRINT "BP=";BP;"  H2=    ";H2(1);H2(2);H2(3);H2(4);H2(5);H2(6);H2(7)
 0222   0446    130    AS$="THERMAL-NOISE LEVEL= ": PRINT USING "&";AS$;
 0278   0446    140    PRINT USING "##.##^^^^";VT;
 0293   044A    150    AS$="  SHOT-NOISE PARAMETER= ": PRINT USING "&";AS$;
 02A4   044A    160    PRINT USING "##.##^^^^";ST
 02BF   044A    170    PRINT "TR=";TR: PRINT "ERROR VECTOR= ";
 02D0   044A    180    FOR I=1 TO I.ER: PRINT USING "##.#^^^^  ";ER(I);: NEXT
 0329   044C    190    PRINT " ": PRINT " ": COLOR 2,0 'NOW SEE IF DEFAULT DATA IS TO BE CHANGED
 0329   044C    200    INPUT "REDEFINE THE NO-ISI PULSE-SHAPE (Y/N)"; ANS$
 036E   0450    210    IF ANS$="N" GOTO 230
 037F   0450    220    INPUT "ENTER THE NO-ISI BAUD-RATE AND VALUES:",BN,NOISI(1),NOISI(2),NOISI(3)
 03B8   0450    230    INPUT "REDEFINE THE PULSE SHAPE (Y/N)"; ANS$
 03D6   0450    240    IF ANS$="N" GOTO 270
 03E7   0450    250    INPUT "ENTER THE PULSE BAUD-RATE: ", BP
 0405   0450    252    PRINT "THE PULSE SHAPE CONSISTS OF 7 POINTS, FROM -2T/2 TO 2T/2
 0405   0450    260    INPUT "ENTER THE PULSE SHAPE:";H2(1),H2(2),H2(3),H2(4),H2(5),H2(6),H2(7)
 0467   0450    270    INPUT "REDEFINE THE NOISE PARAMETERS (Y/N)"; ANS$
 0485   0450    280    IF ANS$="N" GOTO 300
 0496   0450    290    INPUT "ENTER THE THERMAL-NOISE AND SHOT-NOISE PARAMETER: ", VT,ST
 04BD   0450    300    INPUT "REDEFINE THE PREAMPLIFIER TRANSCONDUCDANCE (Y/N)"; ANS$
 04DB   0450    310    IF ANS$="N" GOTO 330
 04EC   0450    320    INPUT "ENTER THE AMPLIFIER TRANSCONDUCTANCE: ", TR
 050A   0450    330    INPUT "REDEFINE THE DESIRED ERROR VECTOR (Y/N)"; ANS$
 0528   0450    340    IF ANS$="N" GOTO 380
 0539   0450    350    INPUT "ENTER THE VECTOR DIMENSION: ",I.ER
 0557   0450    360    FOR I=1 TO I.ER
 0564   0452    370    INPUT "ER: ", ER(I): NEXT
```

```
4 LEVEL PAM OPTICAL FIBER SYSTEM CHARACTERIZATION ROUTINE                                                    PAGE   2
PAM - INITIALIZATION, CONTROL, AND I/O                                                                       01-01-80
                                                                                                             00:14:02
Offset  Data    Source Line                                                         IBM Personal Computer BASIC Compiler V1.00

 059B   0452   380   OPEN "O",#1,"PAMDATA" 'WRITE THE DEFAULT DATA ON THE DISK
 059B   0452   390   WRITE# 1,BN,NOISI(1),NOISI(2),NOISI(3),BP,H2(1),H2(2),H2(3)
 05B1   0452   395   WRITE# 1,H2(4),H2(5),H2(6),H2(7),VT,ST,TR,I.ER
 05FA   0452   400   FOR I=1 TO I.ER: WRITE# 1,ER(I): NEXT
 067A   0454   410   CLOSE:COLOR 3,0 'FINISHED WRITING DATA TO THE DISK.
 067A   0454   420   LPRINT "BN=";BN;"  NOISI=";NOISI(1);NOISI(2);NOISI(3) 'SEND THE DATA TO PRINTER
 068F   0454   430   LPRINT "BP=";BP;"  H2=   ";H2(1);H2(2);H2(3);H2(4);H2(5);H2(6);H2(7)
 06C5   0454   440   AS$="THERMAL-NOISE LEVEL= ": LPRINT USING "&";AS$;
 071B   0454   450   LPRINT USING "##.##^^^^";VT;
 0736   0454   460   AS$="  SHOT-NOISE PARAMETER=": LPRINT USING "&";AS$;
 0747   0454   470   LPRINT USING "##.##^^^^";ST
 0762   0454   472   AS$="AMPLIFIER TRANSIMPEDANCE=":LPRINT USING "&";AS$;
 0773   0454   474   LPRINT USING "######";TR
 078E   0454   480   LPRINT "ERROR VECTOR= ";
 079F   0454   490   FOR I=1 TO I.ER: LPRINT USING "##.#^^^^  ";ER(I);: NEXT
 07E3   0456   500   LPRINT CHR$(13):COLOR 2,0:PRINT " " 'NOW FIND EQUALIZATION DESIRED
 07E3   0456   510   INPUT "OBTAIN COMPLETE EQUALIZATION RESULTS (Y/N)"; ANS$
 0830   0456   520   IF ANS$="Y" THEN FLAG.EQ=100: ELSE FLAG.EQ=0 'SET EQ FLAG-COMP EQ BIT
 0850   0458   530   INPUT "OBTAIN NO EQUALIZATION RESULTS (Y/N)"; ANS$
 086E   0458   540   IF ANS$="Y" THEN FLAG.EQ=FLAG.EQ+1 'SET EQ FLAG-NO EQ BIT
 0886   0458   550   INPUT "OBTAIN DFE EQUALIZATION RESULTS (Y/N)"; ANS$
 08A4   0458   560   IF ANS$="N" THEN IN=0: GOTO 600
 08BE   045A   570   FLAG.EQ=FLAG.EQ+10 'SET EQ FLAG-DFE EQ BIT -FIND OUT WHICH TERM IS DFE
 08BE   045A   580   INPUT "WHICH TERM IN H IS TO BE EQUALIZED (1,2, OR 3):"; IN
 08E6   045A   585   PRINT " "
 08E6   045A   590   IF IN=1 OR IN=2 OR IN=3 THEN HEQ(0)=H(IN) ELSE IN=0
 093E   045A   600   GOSUB 10000 'NORM  'NORMALIZE THE PULSE SHAPE
 0946   045A   610   FOR I.COUNT=1 TO I.ER  'SET UP LOOP TO REPEAT CALC'S FOR ALL ERROR RATES
 0953   045E   620   PED=ER(I.COUNT) 'GET THE PRESENT DESIRED ERROR RATE
 0953   045E   630   GOSUB 1000 'CRUNCH- CALCULATE THE REQUIRED LEVELS AND POWERS
 0970   0462   640   IF FLAG.EQ<100 GOTO 720 'COMP EQ RESULTS OBTAINED?
 097B   0462   650   PRINT " ": LPRINT " " 'PRINT COMP EQ RESULTS
 097B   0462   660   PRINT  "SEQ=  ";: PRINT USING "##.##^^^^ ";SEQ(1);SEQ(2);SEQ(3);SEQ(4)
 0993   0462   665   LPRINT "SEQ=  ";:LPRINT USING "##.##^^^^ ";SEQ(1);SEQ(2);SEQ(3);SEQ(4)
 09C9   0462   670   PRINT  "AEQ=  ";: PRINT USING "##.##^^^^ ";AEQ(1);AEQ(2);AEQ(3)
 09FF   0462   675   LPRINT "AEQ=  ";:LPRINT USING "##.##^^^^ ";AEQ(1);AEQ(2);AEQ(3)
 0A2D   0462   680   PRINT  "VEQ=  ";: PRINT USING "##.##^^^^ ";VEQ(1);VEQ(2);VEQ(3);VEQ(4)
 0A5B   0462   685   LPRINT "VEQ=  ";:LPRINT USING "##.##^^^^ ";VEQ(1);VEQ(2);VEQ(3);VEQ(4)
 0A91   0462   690   PRINT  "EEQ=  ";: PRINT USING "####.#";EEQ(1);EEQ(2);EEQ(3);EEQ(4);EEQ(5);EEQ(6)
 0AC7   0462   695   LPRINT "EEQ=  ";:LPRINT USING "####.#";EEQ(1);EEQ(2);EEQ(3);EEQ(4);EEQ(5);EEQ(6)
 0B0D   0462   700   PRINT  "PEEQ= ";:PRINT USING "##.##^^^^ ";PEEQ(I.COUNT); 'TOTAL PE
 0B53   0462   702   PRINT "PDBMEQ=";:PRINT USING "###.##";PDBMEQ(I.COUNT)    'TOTAL PWR
 0B7A   0462   705   LPRINT "PEEQ= ";:LPRINT USING "##.##^^^^ ";PEEQ(I.COUNT);
 0BA1   0462   707   LPRINT "PDBMEQ=";:LPRINT USING "###.##";PDBMEQ(I.COUNT)
 0BC8   0462   710   PRINT " ": LPRINT " "
 0BEF   0462   720   IF (FLAG.EQ AND 2)=0 GOTO 790 'DFEQ RESULTS OBTAINED?
 0C16   0462   730   PRINT  "SDFE= ";: PRINT USING "##.##^^^^ ";SDFE(1);SDFE(2);SDFE(3);SDFE(4)
 0C16   0462   735   LPRINT "SDFE= ";:LPRINT USING "##.##^^^^ ";SDFE(1);SDFE(2);SDFE(3);SDFE(4)
 0C4C   0462   740   PRINT  "ADFE= ";: PRINT USING "##.##^^^^ ";ADFE(1);ADFE(2);ADFE(3)
 0C82   0462   745   LPRINT "ADFE= ";:LPRINT USING "##.##^^^^ ";ADFE(1);ADFE(2);ADFE(3)
 0CB0   0462   750   PRINT  "VDFE= ";: PRINT USING "##.##^^^^ ";VDFE(1);VDFE(2);VDFE(3);VDFE(4)
 0CDE   0462   755   LPRINT "VDFE= ";:LPRINT USING "##.##^^^^ ";VDFE(1);VDFE(2);VDFE(3);VDFE(4)
 0D14   0462   760   PRINT  "EDFE= ";: PRINT USING "####.#";EDFE(1);EDFE(2);EDFE(3);EDFE(4);EDFE(5);EDFE(6)
 0D4A   0462   765   LPRINT "EDFE= ";:LPRINT USING "####.#";EDFE(1);EDFE(2);EDFE(3);EDFE(4);EDFE(5);EDFE(6)
```

```
Offset  Data    Source Line                                               IBM Personal Computer BASIC Compiler V1.00

 0D90   0462    770   PRINT  "PEDFE=";: PRINT USING "##.##^^^^ ";PEDFE(I.COUNT); 'TOTAL PE
 0DD6   0462    772   PRINT  "PDBMDFE=";: PRINT USING "###.##";PDBMDFE(I.COUNT)  'TOTAL PWR
 0DFD   0462    775   LPRINT "PEDFE=";:LPRINT USING "##.##^^^^ ";PEDFE(I.COUNT);
 0E24   0462    776   LPRINT "PDBMDFE=";:LPRINT USING "###.##";PDBMDFE(I.COUNT)
 0E4B   0462    777   PRINT  "PEACT=";: PRINT USING "##.##^^^^ ";PEACT(I.COUNT)
 0E72   0462    778   LPRINT "PEACT=";:LPRINT USING "##.##^^^^ ";PEACT(I.COUNT)
 0E99   0462    780   PRINT " ": LPRINT " "
 0EC0   0462    790   IF (FLAG.EQ AND 1)=0 GOTO 850 'NO EQ RESULTS OBTAINED?
 0EE7   0462    800   PRINT  "SNEQ= ";: PRINT USING "##.##^^^^ ";S(1);S(2);S(3);S(4)
 0EE7   0462    805   LPRINT "SNEQ= ";:LPRINT USING "##.##^^^^ ";S(1);S(2);S(3);S(4)
 0F1D   0462    810   PRINT  "ANEQ= ";: PRINT USING "##.##^^^^ ";A(1);A(2);A(3)
 0F53   0462    815   LPRINT "ANEQ= ";:LPRINT USING "##.##^^^^ ";A(1);A(2);A(3)
 0F81   0462    817   PRINT  "VNEQ= ";: PRINT USING "##.##^^^^ ";V(1);V(2);V(3);V(4)
 0FAF   0462    819   LPRINT "VNEQ= ";:LPRINT USING "##.##^^^^ ";V(1);V(2);V(3);V(4)
 0FE5   0462    820   PRINT  "ENEQ= ";: PRINT USING "####.#";E(1);E(2);E(3);E(4);E(5);E(6)
 101B   0462    825   LPRINT "ENEQ= ";:LPRINT USING "####.#";E(1);F(2);E(3);E(4);E(5);E(6)
 1061   0462    830   PRINT  "PENEQ=";:  PRINT USING "##.##^^^^ ";PENEQ(I.COUNT); 'TOTAL PE
 10A7   0462    832   PRINT  "PDBMNEQ=";:PRINT USING "###.##";PDBMNEQ(I.COUNT)   'TOTAL PWR
 10CE   0462    835   LPRINT "PENEQ=";:  LPRINT USING "##.##^^^^ ";PENEQ(I.COUNT);
 10F5   0462    837   LPRINT "PDBMNEQ=";:LPRINT USING "###.##";PDBMNEQ(I.COUNT)
 111C   0462    840   PRINT " ": LPRINT " "
 1143   0462    850   NEXT I.COUNT 'REPEAT FOR ALL DESIRED ERROR RATES
 116F   0462    860   COLOR 2,0:PRINT " "
 116F   0462    870   IF FLAG.EQ<100 GOTO 910 'SUMMARIZE ALL POWER LEVELS AND ERROR RATES
 1197   0462    880   AS$="PDBMEQ  (dBM)= ": LPRINT USING "&";AS$;
 1197   0462    890   FOR I=1 TO I.ER: LPRINT USING "+##.#    ";PDBMEQ(I);: NEXT I
 11E8   0464    892   LPRINT " ": AS$="PEEQ=            ": LPRINT USING "&";AS$;
 11E8   0464    894   FOR I=1 TO I.ER: LPRINT USING ".###^^^^ ";PEEQ(I);: NEXT I
 1246   0466    900   LPRINT " "
 1246   0466    910   IF (FLAG.EQ AND 2)=0 GOTO 950
 1263   0466    920   AS$="PDBMDFE (dBM)= ": LPRINT USING "&";AS$;
 1263   0466    930   FOR I=1 TO I.ER:LPRINT USING "+##.#     ";PDBMDFE(I);: NEXT I
 12B4   0468    932   LPRINT " ": AS$="PEDFE=           ": LPRINT USING "&";AS$;
 12B4   0468    934   FOR I=1 TO I.ER: LPRINT USING ".###^^^^ ";PEDFE(I);: NEXT I
 1312   046A    936   LPRINT " ": AS$="PEACT=           ": LPRINT USING "&";AS$;
 1312   046A    938   FOR I=1 TO I.ER: LPRINT USING ".###^^^^ ";PEACT(I);: NEXT I
 1370   046C    940   LPRINT " "
 1370   046C    950   IF (FLAG.EQ AND 1)=0 GOTO 990
 138D   046C    960   AS$="PDBMNEQ (dBM)= ":LPRINT USING "&";AS$;
 138D   046C    970   FOR I=1 TO I.ER:LPRINT USING "+##.#     ";PDBMNEQ(I);: NEXT I
 13DE   046E    972   LPRINT " ": AS$="PENEQ=           ": LPRINT USING "&";AS$;
 13DE   046E    974   FOR I=1 TO I.ER: LPRINT USING ".###^^^^ ";PENEQ(I);: NEXT I
 143C   0470    980   LPRINT " ": AS$=" ": FOR I=1 TO 80: LPRINT AS$;: NEXT I: LPRINT " "
 1476   0470    990   LPRINT " ": END 'END OF MAIN PROGRAM
 1483   0470    991   REM ---------------------------------------------------------------------
 1496   0470    992   REM
 1497   0470    993   REM $SUBTITLE: 'CRUNCH - I/O,LINKER FOR NUMBER CRUNCHING ROUTINES'
 1498   0470    994   REM $PAGE
```

```
4 LEVEL PAM OPTICAL FIBER SYSTEM CHARACTERIZATION ROUTINE                                          PAGE   4
CRUNCH - I/O,LINKER FOR NUMBER CRUNCHING ROUTINES                                                  01-01-80
                                                                                                   00:14:02
Offset  Data    Source Line                                            IBM Personal Computer BASIC Compiler V1.00

 1499   0470    1000  REM THIS SUBROUTINE IS CALLED BY PAM TO DO THE NUMBER CRUNCHING
 149A   0470    1010  LCOL=LCOL+10: LOCATE 25,LCOL: COLOR 4,7: PRINT "  CRUNCH  ";
 149B   0470    1020  GOSUB 8000 'PEDVSET - SET THE ERROR VECTOR CORRESPONDING TO PED
 14D8   0470    1030  IF FLAG.EQ<100 THEN GOTO 1070 ELSE GOSUB 2000 'COMP EQ DESIRED?
 14ED   0470    1040  PEEQ(I.COUNT)=PETOT:PDBMEQ(I.COUNT)=PDBM 'STORE COMP EQ RESULTS
 14ED   0470    1050  FOR I.C=1 TO 4
 1519   047A    1060  SEQ(I.C)=S(I.C): AEQ(I.C)=A(I.C): VEQ(I.C)=V(I.C): NEXT I.C
 1569   047A    1070  IF (FLAG.EQ AND 2)=2 THEN GOSUB 3000 ELSE GOTO 1120 'DFEQ DESIRED?
 1586   047A    1080  PEDFE(I.COUNT)=PETOT: PDBMDFE(I.COUNT)=PDBM 'STORE DFEQ RESULTS
 1586   047A    1090  FOR I.C=1 TO 4
 15B2   047A    1100  SDFE(I.C)=S(I.C): ADFE(I.C)=A(I.C): VDFE(I.C)=V(I.C): NEXT I.C
 1602   047A    1110  FOR I.C=1 TO 6: EDFE(I.C)=E(I.C): NEXT I.C
 1630   047A    1114  GOSUB 13000 'FIND ACTUAL PE GIVEN INCORRECT FEEDBACK
 1638   047A    1116  PEACT(I.COUNT)=PEACT
 1638   047A    1120  IF (FLAG.EQ AND 1)=1 THEN GOSUB 4000 ELSE GOTO 1140 'NOEQ DESIRED?
 166A   047E    1130  PENEQ(I.COUNT)=PETOT: PDBMNEQ(I.COUNT)=PDBM 'STORE NO EQ RESULTS
 166A   047E    1140  LOCATE 25,LCOL: LCOL=LCOL-10: PRINT "          ";: COLOR 3,0: LOCATE 24,1
 16BF   047E    1150  RETURN
 16D4   047E    1160  REM-------------------------------------------------------------------
 16DA   047E    1170  REM
 16DB   047E    1180  REM $SUBTITLE: 'COMPEQ - FINDS OPTIMUM LEVELS FOR COMPLETE EQ. CASE'
 16DC   047E    1190  REM $PAGE
```

```
4 LEVEL PAM OPTICAL FIBER SYSTEM CHARACTERIZATION ROUTINE                                   PAGE   5
COMPEQ - FINDS OPTIMUM LEVELS FOR COMPLETE EQ. CASE                                         01-01-80
                                                                                            00:14:02
Offset  Data    Source Line                              IBM Personal Computer BASIC Compiler V1.00

 16DD   047E    2000  REM THIS SUBROUTINE CALCULATES THE LEVELS FOR THE COMPLETE EQ. CASE
 16DE   047E    2010  LCOL=LCOL+10: LOCATE 25,LCOL: PRINT " COMP EQ  ";
 16DF   047E    2020  ISNAVG!=0: SUMS=0:FLAG.PE=1 'INITIALIZE VARIABLES
 1707   047E    2030  GOSUB 7000 'LEVELSET 'FIRST APPROX OF LEVELS FOR ESTIMATION OF ISNAVG!
 1729   0488    2040  FOR I.C=1 TO 4: SUMS=SUMS+S(I.C): NEXT I.C: SUMS=SUMS/4 'FIND SUMS
 1757   0488    2050  WHILE FLAG.PE=1 'DO UNTIL CLOSE TO DESIRED ERROR RATE
 176A   0488    2060  ISNAVG!=SUMS*SUMN 'FIND ISNAVG! FOR NOISE PURPOSES
 1774   0488    2070  GOSUB 7000 'LEVELSET - NEXT INTERATION FOR THE LEVELS - NOW FIND SUMS
 1790   048C    2080  SUMS=0: FOR I.C=1 TO 4: SUMS=SUMS+S(I.C): NEXT I.C: SUMS=SUMS/4
 17C9   048C    2090  FLAG.PE=0: PETOT=0 'CLEAR ERROR RATE TEST FLAG AND TOTAL ERROR RATE
 17D8   048C    2100  FOR I.C=1 TO 3 'FIND ERROR RATES BETWEEN ALL LEVELS/THRESHOLDS
 17F4   048C    2110  X=(A(I.C)-S(I.C))/V(I.C)
 17F4   048C    2120  GOSUB 5000 'QUE
 1830   0494    2130  PEV(2*I.C-1)=QX
 1830   0494    2140  X=(S(I.C+1)-A(I.C))/V(I.C+1)
 1847   0498    2150  GOSUB 5000 'QUE
 1883   0498    2160  PEV(2*I.C)=QX
 1883   0498    2170  NEXT I.C
 18AC   0498    2180  FOR I.C=1 TO 6 'TEST INDIVIDUAL ERROR RATES AND FIND OVERALL ERROR RATE
 18D3   0498    2190  IF PEDV(I.C)<PEV(I.C) THEN A=PEDV(I.C) ELSE A=PEV(I.C)
 18F1   049C    2200  IF (ABS(PEV(I.C)-PEDV(I.C))/A)>.2 THEN FLAG.PE=1
 1928   049C    2210  PETOT=PETOT+PEV(I.C): NEXT I.C
 1956   049C    2220  WEND: PETOT=PETOT/8: PDBM=30+10*LOG(SUMS*CONST/(TR*77))/LOG(10) 'PDBM
 195A   049C    2230  LOCATE 25,LCOL: LCOL=LCOL-10: COLOR 4,7: PRINT "          ";
 19DA   04A0    2240  RETURN
 19F0   04A0    2250  REM-----------------------------------------------------------------------
 19F6   04A0    2260  REM
 19F7   04A0    2270  REM $SUBTITLE: 'DFEQ - ROUTINE TO FIND OPTIMUM LEVELS FOR THE DFE CASE'
 19F8   04A0    2280  REM $PAGE
```

```
4 LEVEL PAM OPTICAL FIBER SYSTEM CHARACTERIZATION ROUTINE                                              PAGE   6
DFEQ - ROUTINE TO FIND OPTIMUM LEVELS FOR THE DFE CASE                                                01-01-80
                                                                                                      00:14:02
Offset  Data    Source Line                                          IBM Personal Computer BASIC Compiler V1.00

 19F9   04A0    3000  REM THIS SUBROUTINE CALCULATES THE LEVELS FOR THE DFE CASE
 19FA   04A0    3010  LCOL=LCOL+10: LOCATE 25,LCOL: PRINT "   DFEQ   ";
 19FB   04A0    3020  HEQ(1)=H(1): HEQ(2)=H(2): HEQ(3)=H(3) 'INITIALIZE EQ. PULSE SHAPE
 1A23   04A0    3030  HEQ(IN)=0: GOTO 4030 'PROCEED AS IN NO EQ CASE
 1A45   04A0    3040  REM-----------------------------------------------------------------------
 1A5D   04A0    3050  REM
 1A5E   04A0    3060  REM $SUBTITLE: 'NO EQ - ROUTINE TO FIND OPTIMUM LEVELS FOR THE NO EQ CASE'
 1A5F   04A0    3070  REM $PAGE
```

```
4 LEVEL PAM OPTICAL FIBER SYSTEM CHARACTERIZATION ROUTINE                                           PAGE   7
NO EQ - ROUTINE TO FIND OPTIMUM LEVELS FOR THE NO EQ CASE                                            01-01-80
                                                                                                     00:14:02
Offset  Date    Source Line                                          IBM Personal Computer BASIC Compiler V1.00

 1A60   04A0    4000  REM THIS SUBROUTINE CALCULATES THE LEVELS FOR THE NO EQ CASE
 1A61   04A0    4010  LCOL=LCOL+10: LOCATE 25,LCOL: PRINT "  NO EQ   ";
 1A62   04A0    4020  HEQ(1)=H(1): HEQ(2)=H(2): HEQ(3)=H(3) 'INITIALIZE THE PULSE SHAPE
 1A8A   04A0    4030  REM THIS PORTION IS USED BY DFEQ AND NOEQ.
 1AAC   04A0    4035  RATIO=(HEQ(1)+HEQ(2)+HEQ(3))/H2(3) 'USED FOR E-VECTOR CONVERGENCE CONTROL
 1AAD   04A0    4036  RATIO=RATIO^.7
 1AD1   04A4    4040  ISNAVG!=0: SUMS=0: FLAG.PE=1 'INITIALIZE VARIABLES
 1AE4   04A4    4050  GOSUB 7000 'LEVELSET - APPROX LEVELS FOR ESTIMATION OF ISNAVG!
 1B06   04A4    4060  FOR I.C=1 TO 4 'FIND SUMS
 1B0D   04A4    4070  SUMS=SUMS+S(I.C): NEXT I.C: SUMS=SUMS/4
 1B35   04A4    4080  WHILE FLAG.PE=1 'DO UNTIL CLOSE TO DESIRED ERROR RATES
 1B48   04A4    4085  FOR I.4=1 TO 3
 1B59   04A6    4090  ISNAVG!=SUMS*SUMN 'FIND ISNAGV! FOR NOISE CALCULATIONS
 1B59   04A6    4100  GOSUB 7000 'LEVELSET- APPROX. SET THE LEVELS AND FIND SUMS
 1B75   04A6    4110  SUMS=0:FOR I.C=1 TO 4: SUMS=SUMS+S(I.C): NEXT I.C: SUMS=SUMS/4
 1BAE   04A6    4115  NEXT I.4
 1BCF   04A6    4120  GOSUB 9000 'ISI CALC - CALCULATE ALL ISI TERMS
 1BD7   04A6    4130  GOSUB 11000 'PEISI - CALCULATE ERROR RATES FOR EACH ISI TERM
 1BDF   04A6    4140  COLOR 3,0: LOCATE 24,1: PRINT USING "##.##^^^^ ";PEV(1);PEV(2);PEV(3);PEV(4);PEV(5);PEV(6)
 1BDF   04A6    4145  PRINT USING "####.##   ";E(1),E(2),E(3),E(4),E(5),E(6): COLOR 4,7
 1C37   04A6    4150  WEND  'IF OVERALL ERROR RATE BETWEEN THRESHOLDS/LEVELS NOT GOOD, REDO
 1C84   04A6    4160  PETOT=PETOT/8: PDBM=30+10*LOG(SUMS*CONST/(TR*77))/LOG(10) 'PRW
 1C84   04A6    4170  LOCATE 25,LCOL: LCOL=LCOL-10: PRINT "          ";
 1CE5   04A6    4180  RETURN
 1D0B   04A6    4190  REM------------------------------------------------------------------------
 1D11   04A6    4200  REM
 1D12   04A6    4210  REM $SUBTITLE: 'QUE - ROUTINE FOR EVALUATION OF THE ERROR FUNCTION'
 1D13   04A6    4220  REM $PAGE
```

```
4 LEVEL PAM OPTICAL FIBER SYSTEM CHARACTERIZATION ROUTINE                                                  PAGE   8
QUE - ROUTINE FOR EVALUATION OF THE ERROR FUNCTION                                                          01-01-80
                                                                                                            00:14:02
Offset  Data    Source Line                                                IBM Personal Computer BASIC Compiler V1.00

 1D14    04A6    5000  REM THIS PROGRAM EVALUATES THE FUNCTION QX=QUE(X), USING 1 OF 2 FORMULAS
 1D15    04A6    5010  LCOL=LCOL+10: LOCATE 25,LCOL: PRINT "   QUE    ";
 1D16    04A6    5020  IF X<0 THEN Z.Q=1 ELSE Z.Q=0  'ENABLE THE EVALUATION FOR NEGATIVE X
 1D65    04AE    5030  X.Q=ABS(X)
 1D65    04AE    5040  IF X.Q <12! THEN GOTO 5050 ELSE QX=3E-39: LOCATE 25,LCOL: LCOL=LCOL-10
 1DAA    04B6    5045  COLOR 4,7: PRINT "                    ";: RETURN 'X TOO LARGE - QX~0
 1DAA    04B6    5050  IF X.Q<4! GOTO 5090 'USE THE SERIES FORMULA FOR X<3
 1DDE    04B6    5060  Y.Q=-X.Q*X.Q 'FOR X>3, USE SIMPLE EXPONENTIAL FORMULA
 1DDE    04B6    5065  IF X.Q<4.7 THEN Q.Z=.865# ELSE IF X.Q<6.7 THEN Q.Z=.91# ELSE Q.Z=.96#
 1E3E    04C2    5070  QX=EXP(.5*Y.Q)*(1+Q.Z/Y.Q)/(X.Q*SQR(2#*PI#))
 1E3E    04C2    5080  GOTO 5170
 1EA9    04C2    5090  Y.Q=X.Q/SQR(2!) 'SERIES FORMULA FOR X<3
 1EAD    04C2    5100  X.Q=-Y.Q*Y.Q
 1EC8    04C2    5110  QX=Y.Q
 1EE3    04C2    5120  FOR I.Q=1 TO 25 'SERIES CHOPPED AFTER 30 TERMS
 1EFB    04C4    5130  Y.Q=X.Q*Y.Q*(2*I.Q-1)/((2*I.Q+1)*I.Q)
 1EFB    04C4    5140  QX=QX+Y.Q
 1F3E    04C4    5150  NEXT I.Q
 1F6C    04C4    5160  QX=.5*(1-(2#/SQR(PI#))*QX)
 1F6C    04C4    5170  QX=ABS(Z.Q-QX)
 1FAD    04C4    5180  LOCATE 25,LCOL:LCOL=LCOL-10:PRINT "          ";
 1FD1    04C4    5190  RETURN
 1FF7    04C4    5200  REM-----------------------------------------------------------------------
 1FFD    04C4    5210  REM
 1FFE    04C4    5220  REM $SUBTITLE: 'IQUE - ROUTINE FOR EVALUATING THE INVERSE ERROR FUNCTION'
 1FFF    04C4    5230  REM $PAGE
```

```
4 LEVEL PAM OPTICAL FIBER SYSTEM CHARACTERIZATION ROUTINE                                          PAGE   9
IQUE - ROUTINE FOR EVALUATING THE INVERSE ERROR FUNCTION                                         01-01-80
                                                                                                  00:14:02
Offset  Data    Source Line                                       IBM Personal Computer BASIC Compiler V1.00

 2000   04C4    6000  REM THIS PROGRAM CALCULATES X=IQUE(QX) USING NEWTON ROOT FINDING
 2001   04C4    6005  REM WITH A SECOND-DERIVATIVE (APPROX) CORRECTION
 2002   04C4    6010  LCOL=LCOL+10: LOCATE 25,LCOL: PRINT "   IQUE    ";
 2003   04C4    6020  Q.X=QX: I.I=1: DX.I=1: X=3! 'INITIAL GUESS FOR X=IQUE(QX)
 202B   04C4    6030  WHILE (ABS(DX.I)>.1) AND (I.I<10) 'TEST CRITERION
 2054   04D2    6040  GOSUB 5000 'QUE- EVALUATE THE FUNCTION QUE(X)
 2086   04D2    6050  IF QX=3E-39 THEN X=10: I.I=10 'QX IS VERY SMALL - RETURN A LARGE X VALUE
 20A8   04D2    6060  X.I=-EXP(-X*X/2#)/(QX*SQR(2#*PI#)): DY.I=LOG(Q.X/QX)
 20AB   04D2    6070  DM.I=DY.I*(X+X.I) 'SECOND DERIVATIVE-BASED SLOPE CORRECTION
 2127   04E2    6080  DX.I=DY.I/(X.I-DM.I*.5#)
 2143   04EA    6090  X=X+DX.I
 2167   04EA    6100  I.I=I.I+1
 217A   04EA    6110  WEND
 2186   04EA    6120  LOCATE 25,LCOL:LCOL=LCOL-10: PRINT "          ";
 21A6   04EA    6130  RETURN
 21AC   04EA    6140  REM----------------------------------------------------------------------
 21B2   04EA    6150  REM
 21B3   04EA    6160  REM $SUBTITLE: 'LSET - SETS OPTIMUM LEVELS FOR GIVEN E VECTOR AND NO ISI'
 21B4   04EA    7000  REM THIS SUBR. SETS THE OPT. LEVELS/THRESHOLDS FOR NO ISI BUT ISI NOISE
 21B5   04EA    7010  LCOL=LCOL+10: LOCATE 25,LCOL: PRINT "   LSET    ";
 21B6   04EA    7020  S(1)=0# 'CLEAR THE FIRST LEVEL
 21BE   04EA    7030  V(1)=SQR(VN+SN*(S(1)+ISNAVG!)) 'FIND NOISE LEVEL FOR S(1) - GIVEN ISNAVG!
 21EA   04EA    7040  FOR I.L=1 TO 3 'FIND THE OTHER LEVELS AND THRESHOLDS
 2210   04F4    7050  A(I.L)=S(I.L)+V(I.L)*E(2*I.L-1) 'FIND THE NEXT THRESHOLD
 221D   04F4    7060  B=2*A(I.L)+SN*(E(2*I.L))^2 'USE A QUADRATIC FORMULA FOR THE NEXT LEVEL
 225C   04F4    7070  C=(A(I.L))^2-(VN+ISNAVG!*SN)*(E(2*I.L))^2
 22A1   04F8    7080  S(I.L+1)=.5*(B+SQR(B*B-4*C))
 2300   04FC    7090  V(I.L+1)=SQR(VN+SN*(S(I.L+1)+ISNAVG!))
 2350   04FC    7100  NEXT I.L 'REPEAT UNTIL ALL THRESHOLDS,LEVELS ARE FOUND
 23A0   04FC    7110  LOCATE 25,LCOL:LCOL=LCOL-10:PRINT "          ";
 23A0   04FC    7120  RETURN
 23C6   04FC    7130  REM----------------------------------------------------------------------
 23CC   04FC    7140  REM
 23CD   04FC    7150  REM $SUBTITLE: 'PEDVSET - ROUTINE TO SET E VECTOR FROM PRESENT PED'
 23CE   04FC    7160  REM $PAGE
```

```
4 LEVEL PAN OPTICAL FIBER SYSTEM CHARACTERIZATION ROUTINE                                        PAGE  10
PEDVSET - ROUTINE TO SET E VECTOR FROM PRESENT PED                                               01-01-80
                                                                                                 00:14:02
Offset  Data    Source Line                                       IBM Personal Computer BASIC Compiler V1.00

 23CF   04FC    8000  REM THIS SUBROUTINE FINDS E AND PEDV FROM PED.
 23D0   04FC    8010  LCOL=LCOL+10: LOCATE 25,LCOL: PRINT "  PEDVSET  ";
 23D1   04FC    8020  QX=2*PED: FOR I.EV=2 TO 5: PEDV(I.EV)=PED: NEXT I.EV
 2433   04FE    8025  PEDV(1)=QX: PEDV(6)=QX 'ENDLEVELS CAN HAVE 2*PED ERROR RATES
 2433   04FE    8030  GOSUB 6000 'IQUE - FIND DISTANCE CORRESPONDING TO 2*PED
 244F   04FE    8040  X.E=X: QX=PED 'FIND DISTANCE CORRESPONDING TO PED
 244F   04FE    8050  GOSUB 6000 'IQUE 'NOW CAN SET THE DISTANCE VECTOR E.
 246E   0506    8060  FOR I.EV=2 TO 5: E(I.EV)=X: NEXT I.EV: E(1)=X.E: E(6)=X.E
 249C   0506    8070  LOCATE 25,LCOL: LCOL=LCOL-10:PRINT "          ";
 24B4   0506    8080  FOR I.EV=1 TO 6: EEQ(I.EV)=E(I.EV):NEXT I.EV 'SAVE AS EEQ VECTOR ALSO
 2508   0506    8090  RETURN
 2508   0506    8100  REM------------------------------------------------------------------------
 250E   0506    8110  REM
 250F   0506    8120  REM $SUBTITLE: 'ISI CALC - ROUTINE TO FIND ALL THE POSSIBLE ISI TERMS'
 2510   0506    8130  REM $PAGE
```

```
4 LEVEL PAM OPTICAL FIBER SYSTEM CHARACTERIZATION ROUTINE                                        PAGE  11
ISI CALC - ROUTINE TO FIND ALL THE POSSIBLE ISI TERMS                                            01-01-80
                                                                                                 00:14:02
Offset  Data   Source Line                                           IBM Personal Computer BASIC Compiler V1.00

 2511   0506    9000  REM THIS SUBROUTINE CALCULATES ALL THE ISI TERMS FOR HEQ.
 2512   0506    9010  LCOL=LCOL+10: LOCATE 25,LCOL: PRINT " ISI CALC "; 'SORT HEQ- MIN TO MAX:
 2513   0506    9012  IF HEQ(1)>HEQ(2) THEN HEQ(0)=HEQ(2): HEQ(2)=HEQ(1): HEQ(1)=HEQ(0)
 256C   0506    9014  IF HEQ(2)>HEQ(3) THEN HEQ(0)=HEQ(3): HEQ(3)=HEQ(2): HEQ(2)=HEQ(0)
 259D   0506    9016  IF HEQ(1)>HEQ(2) THEN HEQ(0)=HEQ(2): HEQ(2)=HEQ(1): HEQ(1)=HEQ(0)
 25CE   0506    9020  IF HEQ(1)=0 THEN FLAG.H=1: ELSE FLAG.H=0 'FIND OUT HOW MANT NONZERO TERMS
 25EB   0508    9030  IF HEQ(2)=0 THEN FLAG.H=FLAG.H+1 'AND SET H FLAG ACCORDINGLY
 2600   0508    9040  IF HEQ(3)=0 THEN FLAG.H=FLAG.H+1 'SO THAN THE MIN. OF ISI TERMS ARE CALC.
 2615   0508    9060  ON FLAG.H GOTO 9150,9220,9250 'EITHER 0,1,2, OR 3 ISI TERMS
 2626   0508    9070  FOR I.1=1 TO 4 '3 INTERFERING ISI TERMS - 64 ISI POSSIBILITIES
 262D   050A    9090  FOR I.2=1 TO 4
 2634   050C    9100  FOR I.3=1 TO 4
 263B   050E    9110  ISI!(I.1*I.2*I.3)=S(I.1)*HEQ(1)+S(I.2)*HEQ(2)+S(I.3)*HEQ(3)
 263B   050E    9130  NEXT I.3: NEXT I.2: NEXT I.1
 26E1   050E    9140  FLAG.H=64: GOTO 9280 'SET H FLAG TO INDICATE # OF ISI POSSIBILITIES
 26E1   050E    9150  FOR I.1=1 TO 4 '2 INTERFERING ISI TERMS - 16 ISI POSSIBILITIES
 26F2   050E    9170  FOR I.2=1 TO 4
 26F9   050E    9180  ISI!(I.1*I.2)=S(I.1)*HEQ(2)+S(I.2)*HEQ(3)
 26F9   050E    9200  NEXT I.2: NEXT I.1
 2764   050E    9210  FLAG.H=16: GOTO 9280 'SET H FLAG TO INDICATE # OF ISI POSSIBILITIES
 2764   050E    9220  FOR I.1=1 TO 4: ISI!(I.1)=S(I.1)*HEQ(3): NEXT I.1 '1 ISI TERM
 27A8   050E    9230  REM
 27A8   050E    9240  FLAG.H=4: GOTO 9280 'SET H FLAG TO INDICATE 4 ISI POSSIBILITIES
 27A9   050E    9250  ISI!(1)=0: FLAG.H=1 'NO ISI TERMS - ISI=0, H FLAG SET TO 1.
 27B3   050E    9280  LOCATE 25,LCOL: LCOL=LCOL-10: PRINT "          ";
 27C5   050E    9290  RETURN
 27E0   050E    9300  REM-----------------------------------------------------------------------
 27F1   050E    9310  REM
 27F2   050E    9320  REM $SUBTITLE: 'NORM - NORMALIZATION OF PULSE SHAPE ROUTINE'
 27F3   050E    9330  REM $PAGE
```

```
4 LEVEL PAM OPTICAL FIBER SYSTEM CHARACTERIZATION ROUTINE                                         PAGE 12
NORM - NORMALIZATION OF PULSE SHAPE ROUTINE                                                       01-01-80
                                                                                                  00:14:02
Offset  Data    Source Line                                          IBM Personal Computer BASIC Compiler V1.00

 27F4   050E    10000 REM THIS SUBROUTINE NORMALIZES THE PULSE SHAPES AND NEQ
 27F5   050E    10010 LCOL=LCOL+10: LOCATE 25,LCOL: COLOR 4,7: PRINT "   NORM   ";
 27F6   050E    10020 SUMN2=0: NO=N2(3) 'NORMALIZE N'S SO THAT N2(3)=1.0 - MAXIMUM
 282E   050E    10030 FOR I.N=1 TO 7
 284C   0518    10040 N2(I.N)=N2(I.N)/NO:SUMN2=SUMN2+N2(I.N): NEXT I.N
 288D   0518    10050 N(1)=N2(1): N(2)=N2(5): N(3)=N2(7) 'DEFINE N(nT) TERMS
 288D   0518    10070 SUMN=N(1)+N(2)+N(3) 'FIND SUM OF N(nT) TERMS
 28AF   0518    10080 ENOISI=NOISI(1)+NOISI(3)+2*NOISI(2) 'FIND NOISI ENERGY
 28C8   0518    10090 CONST=ENOISI/(SUMN2+SUMN+1) 'CONST NEEDED TO MEET ENERGY RESTRAINTS
 28ED   051C    10100 VN=(VT/CONST)^2: SN=ST/CONST  'SCALE NOISE FACTORS ACCORDINGLY
 2911   051C    10110 LOCATE 25,LCOL: LCOL=LCOL-10: COLOR 4,7: PRINT "          ";
 2941   051C    10120 RETURN
 2977   051C    10130 REM-----------------------------------------------------------------
 297D   051C    10140 REM
 297E   051C    10150 REM $SUBTITLE: 'PEISI - ROUTINE TO DETERMINE ERROR RATE GIVEN ISI'
 297F   051C    10160 REM $PAGE
```

```
4 LEVEL PAM OPTICAL FIBER SYSTEM CHARACTERIZATION ROUTINE                                                   PAGE  15
PEACT - DFE ERROR RATE ESTIMATION GIVEN FEEDBACK ERRORS                                                     01-01-80
                                                                                                            00:14:02
Offset  Data    Source Line                                                   IBM Personal Computer BASIC Compiler V1.00

 2DAF   0520    13000 REM THIS SUBROUTINE CALCS PE GIVEN INCORRECT FEEDBACK (AFTER DFEQ CALL)
 2DB0   0520    13010 LCOL=LCOL+10: LOCATE 25,LCOL: PRINT "  PEACT   ";
 2DB1   0520    13020 FOR I.C=1 TO 6: PEV(I.C)=0: NEXT I.C 'CLEAR PEV
 2E02   0520    13030 PETOT=0 'CLEAR PETOT
 2E02   0520    13040 ISI2!(1)=H(IN)*(S(2)-S(1)): ISI2!(2)=ISI2!(1)
 2E0E   0520    13050 ISI2!(3)=-ISI2!(1): ISI2!(4)=H(IN)*(S(3)-S(2))
 2E41   0520    13060 ISI2!(5)=-ISI2!(4): ISI2!(6)=H(IN)*(S(4)-S(3))
 2E7A   0520    13070 ISI2!(7)=-ISI2!(6): ISI2!(8)=ISI2!(7)
 2EB3   0520    13100 FOR J.PE=1 TO 8  'EIGHT CASES FOR ISI2!
 2ED5   0522    13110 FOR I.PE=1 TO FLAG.N  'ALL ISI TERMS
 2EE2   0524    13120 FOR I.C=1 TO 3
 2EE9   0524    13130 X=(A(I.C)-S(I.C)-ISI!(I.PE)-ISI2!(J.PE))/V(I.C)
 2EE9   0524    13140 GOSUB 5000 'FIND ERROR RATE FOR THIS CASE OF ISI
 2F47   0524    13150 PEV(2*I.C-1)=QX+PEV(2*I.C-1)
 2F47   0524    13160 X=(S(I.C+1)+ISI!(I.PE)+ISI2!(J.PE)-A(I.C))/V(I.C+1)
 2F67   0524    13170 GOSUB 5000 'FIND ERROR RATE FOR THIS CASE OF ISI
 2FC5   0524    13180 PEV(2*I.C)=PEV(2*I.C)+QX
 2FC5   0524    13190 NEXT I.C: NEXT I.PE: NEXT J.PE
 3018   0524    13200 FOR I.C=1 TO 6 'FIND THE AVERAGES FROM THE SUMS
 3022   0524    13210 PEV(I.C)=PEV(I.C)/(FLAG.N*8)
 3022   0524    13220 PETOT=PETOT+PEV(I.C) 'FIND THE TOTAL ERROR RATE
 304C   0524    13230 NEXT I.C
 3075   0524    13240 PETOT=PETOT/4 'FIND THE AVERAGE FROM THE SUM
 3075   0524    13250 PEACT=PEDFE(I.COUNT)/(1-PETOT) 'GET PEAVG FROM PWR SERIES FORMULA
 3088   0524    13260 LOCATE 25,LCOL: LCOL=LCOL-10: PRINT "          ";
 30B1   0524    13270 RETURN
 30D7   0524    13280 REM-----------------------------------------------------------------
 30DD   0524
 30E3   0524

22151 Bytes Available
14287 Bytes Free

    0 Warning Error(s)
    0 Severe  Error(s)
```

```
4 LEVEL PAM OPTICAL FIBER SYSTEM CHARACTERIZATION ROUTINE                                                    PAGE  14
INTERACTIVE CONVERGENCE CONTROL ROUTINE (KEY F10)                                                            01-01-80
                                                                                                             00:14:02
Offset  Data    Source Line                                                 IBM Personal Computer BASIC Compiler V1.00

 2CE3   0520    12000 REM THIS SUBROUTINE READS THE CONVERGENCE PARAMETERS C1 AND C2 FROM KBRD.
 2CE4   0520    12010 COLOR 2,0: LOCATE 24,1
 2CE5   0520    12015 PRINT " " 'PRINT PRESENT C1,C2, AND RATIO
 2D05   0520    12020 PRINT "C1= ";C1,"C2= ";C2,"RATIO= ";:PRINT USING "#.###";RATIO
 2D13   0520    12030 INPUT "ENTER C1 AND C2:",C1,C2 'GET DESIRED C1,C2 FROM KEYBOARD
 2D78   0520    12040 PRINT " ": LOCATE 25,1:COLOR 4,7
 2D78   0520    12050 RETURN
 2DA6   0520    12060 REM-----------------------------------------------------------------
 2DAC   0520    12070 REM
 2DAD   0520    12080 REM $SUBTITLE: 'PEACT - DFE ERROR RATE ESTIMATION GIVEN FEEDBACK ERRORS'
 2DAE   0520    12090 REM $PAGE
```

```
4 LEVEL PAM OPTICAL FIBER SYSTEM CHARACTERIZATION ROUTINE                                    PAGE  13
PEISI - ROUTINE TO DETERMINE ERROR RATE GIVEN ISI                                            01-01-80
                                                                                             00:14:02
Offset  Data    Source Line                              IBM Personal Computer BASIC Compiler V1.00

 2980   051C    11000 REM THIS SUBROUTINE CALCULATES PEV FOR THE INDIVIDUAL ISI CASES
 2981   051C    11010 LCOL=LCOL+10: LOCATE 25,LCOL: PRINT "  PEISI   ";
 2982   051C    11015 KEY (10) ON 'ALLOW USER CHANGING OF CONVERGENCE VARIABLES DURING RUNNING
 29AB   051C    11020 FOR I.C=1 TO 6: PEV(I.C)=0: NEXT I.C 'CLEAR PEV
 29DC   051C    11030 PETOT=0: FLAG.PE=0 'CLEAR TOTAL PE, PE FLAG
 29DC   051C    11040 FOR I.PE=1 TO FLAG.H 'DO THE CALCULATIONS FOR ALL THE ISI POSSIBILITIES
 29F8   0520    11050 FOR I.C=1 TO 3 'FIND THE INDIVIDUAL ERROR RATES BETWEEN LEVELS/THRESHOLDS
 2A02   0520    11060 X=(A(I.C)-S(I.C)-ISI!(I.PE))/V(I.C)
 2A02   0520    11070 GOSUB 5000 'QUE - FIND A PARTICULAR ERROR RATE
 2A4F   0520    11080 PEV(2*I.C-1)=QX+PEV(2*I.C-1)
 2A4F   0520    11090 X=(S(I.C+1)+ISI!(I.PE)-A(I.C))/V(I.C+1)
 2A6F   0520    11100 GOSUB 5000 'QUE - FIND A PARTICULAR ERROR RATE
 2ABC   0520    11110 PEV(2*I.C)=PEV(2*I.C)+QX
 2ABC   0520    11120 NEXT I.C:NEXT I.PE
 2B01   0520    11125 KEY (10) OFF  'DISABLE CHANGING OF CONVERGENCE VARIABLES FOR NOW
 2B02   0520    11130 FOR I.C=1 TO 6 'SCALE PEV SUMS TO GET AVG. PEV'S
 2B11   0520    11140 PEV(I.C)=PEV(I.C)/FLAG.H: PETOT=PETOT+PEV(I.C) 'FIND OVERALL PE.
 2B11   0520    11150 QX=PEV(I.C): GOSUB 6000 'IQUE - FIND DISTANCES CORRESPONDING TO PEV'S
 2B68   0520    11155 IF X<.1 THEN X=.1 'IF QX IS NEGATIVE, MAKE IT CLOSE TO ZERO
 2B80   0520    11160 X=(EEQ(I.C)/X):IF (PEV(I.C)/PEDV(I.C))>10 THEN C=C2/RATIO ELSE C=C1/RATIO
 2BEA   0520    11162 REM- SCALE THE E VECTOR USING CONVERGENCE FACTORS -
 2BEA   0520    11164 REM- IF C.F'S ARE TOO LARGE - OSCILLATE - IF TOO SMALL - SLOW CONVERGENCE
 2BEB   0520    11170 E(I.C)=E(I.C)*(X^C) 'RATIO IS USED IN CONV - HIGH ISI, LOWER C
 2BEC   0520    11180 IF PEDV(I.C)<PEV(I.C) THEN A=PEDV(I.C) ELSE A=PEV(I.C)
 2C68   0520    11190 IF (ABS(PEV(I.C)-PEDV(I.C))/A)>.25 THEN FLAG.PE=1 'TEST CLOSENESS
 2CA2   0520    11200 NEXT I.C 'OF THE ERROR TO THE DESIRED ERROR FOR EACH LEVEL/THRESHOLD
 2CB4   0520    11210 LOCATE 25,LCOL: LCOL=LCOL-10: PRINT "          ";
 2CB4   0520    11220 RETURN
 2CDA   0520    11230 REM-------------------------------------------------------------------
 2CE0   0520    11240 REM
 2CE1   0520    11250 REM $SUBTITLE: 'INTERACTIVE CONVERGENCE CONTROL ROUTINE (KEY F10)'
 2CE2   0520    11260 REM $PAGE
```

Appendix D. An Upper Bound on the Propagation Effect of DFE

In this appendix, an upper bound on the error propagation effect of an N-tap decision-feedback equalizer will be presented. The notation used throughout the bound derivation is an extension of the notation introduced in Chap. 5:

P means " the probability of making "

E means " (decoding) error "

f means " feedback "

C means " correct decoding decision (or similar) "

c means " correct "

i means " incorrect "

| means " given "

The subscripts 1,2,3,...,N denote the feedback tap numbers; the first tap (1) being derived from the immediately previous decoded data, and the N^{th} tap being the feedback derived from the N^{th} previously decoded data. With this notation, for example, P(E|cf) means " the probability of making a decoding error given correct feedback " (as defined in Chap. 5), and $P(C|c_1, c_2, c_3, \ldots, c_{n-1}, c_n)$ means " the probability of making a correct decoder decision given all the feedback taps are correct, except for the N^{th} tap ".

We are interested in expressing the probability of making an error given feedback, P(E|f), in terms of the probability of making an error given correct feedback, P(E|cf). P(E|f) is the same as the overall probability of making a decoder error, and will thus be designated by Pe. P(E|cf) is the error probability with ideal DFE. The ratio of Pe to P(E|cf) indicates the error propagation effect of the DFE.

We have

$$Pe = P(E|if)\cdot P(if) + P(E|cf)\cdot P(cf)$$

$$= P(E|if)\cdot[1 - P(cf)] + P(E|cf)\cdot P(cf)$$

Although P(E|if) depends on the magnitude of the erroneous feedback tap, as well as many other factors, an upper bound for is exists, and will be found later. For N taps of feedback, the probability of correct feedback is equal to the probability of having made the last decoder decision correctly, given that all its feedback values were correct, plus the probability of having made the last decoder decision correctly, given that all its feedback values, except for the Nth one, were correct:

$$P(cf) = P(C_{previous}|c_2,c_3,\ldots,c_N,c_{N+1})\cdot P(c_2,c_3,\ldots,c_N,c_{N+1})$$

$$+ P(C_{previous}|c_2,c_3,\ldots,c_N,i_{N+1})\cdot P(c_2,c_3,\ldots,c_N,i_{N+1})$$

This is equivalent to

$$P(cf) = P(C|cf)\cdot P(cf) + P(C|if)\cdot P(c_1,c_2,\ldots,c_{N-1},i_N).$$

However,

$$P(C_1,C_2,\ldots,C_{N-1}|i_N)\cdot P(i_N) = P(C|if)^{N-1}\ Pe.$$

Also, $P(C|cf) = 1 - P(E|cf)$, and $P(C|if) = 1 - P(E|if)$.

Thus,

$$P(cf) = [1 - P(E|cf)]\cdot P(cf) + P(C|if)\cdot P(C|if)^{N-1}\ Pe$$

$$= [1 - P(E|cf)]\cdot P(cf) + [1 - P(E|if)]^N\ Pe.$$

Solving this for P(cf) gives

$$P(cf) = [1 - P(E|if)]^N\ Pe/P(E|cf).$$

Consequently, the total decoder error prabability can be written as:

$$Pe = P(E|if)\cdot[1 - P(E|cf)] + P(E|cf)\cdot P(cf)$$

$$= P(cf)\cdot[P(E|cf) - P(E|if)] + P(E|if)$$

$$= [1 - P(E|if)]^N\ Pe\cdot[P(E|cf) - P(E|if)]/P(E|cf) + P(E|if)$$

By letting

$R = P(E|cf)$, (correct or "right" feedback)

$W = P(E|if)$, ("wrong" feedback)

this reduces to

$$Pe = RW/[R + (1-W)^N(W-R)] = R/[R/W + (1-W)^N(1 - R/W)]. \quad (D.1)$$

Usually, $R \ll W$ ($P(E|cf) \ll P(E|if)$, and Eqn. D.1 reduces to

$$Pe \doteq R/(1-W)^N. \quad (D.2)$$

If a bound on $W = P(E|if)$ can be found, a bound on Pe is also found.

Consider an A-level system. Assuming the feedback errors, when they occur, are large, then for the lowest signal level:

$$P(E|if,\ \text{lowest level})_{max} = P(\text{feedback error is positive}) = 1/2$$

In words, the bottom level is decoded incorrectly if the feedback error causes the equalized signal to rise above the lowest threshold.

Similarily, for the highest signal level,

$$P(E|if,\ \text{highest level})_{max} = P(\text{feedback error is negative}) = 1/2.$$

For the middle levels, a large positive or negative feedback error can cause a decoding error. Hence,

$$P(E|if,\ \text{middle level})_{max} = 1.$$

Consequently,

$A \cdot P(E|if)_{max} = 1/2 + 1/2 + (A-2) \cdot 1.0,$

or $P(E|if)_{max} = (A-1)/A.$ (D.3)

For example, a 4 level system has

$P(E|if)_{max} = (4-1)/4 = 0.75.$

For any reasonable system BER (e.g. 10^{-9}), this 0.75 value is much larger than the system error rate, and hence the assumption that W >> R made earlier is valid. From Eqns. D.2 and D.3, we get

$Pe \equiv R/[1 - (A-1)/A]^N = R\, A^N/[A - (A-1)]^N = R \cdot A^N.$

The upper bound on the error propagation effect is consequently

$Pe/P(E|cf) = A^N.$ (D.4)

For an A-level PAM system, where $A = 2^n$, each level represents n bits of information. Also, Pe is the probability of making a decoding error. For each decoding error, up to n bits may be in error. Hence, with

$BER_{max} = n \cdot Pe$ and $R_{max} = BER_{ideal\ DFE}$,

$BER_{max} = n \cdot A^N.$ (D.5)

This applies to a multilevel system regardless of the coding scheme used. If Gray - coding is used, however, a tighter bound is obtained. Assuming that all decoder errors will be the decoding of a signal level as being at an adjacent level (which is a valid assumption except possible when there is popcorn noise or random signal spikes, as opposed to the more "uniform" stationary noise such as that found for the experimental system), with Gray coding, a decoding error results in only one bit being in error. Consequently,

$$BER_{max} = Pe_{max}, \text{ or } BER_{max} = (BER_{ideal\ DFE}) \cdot A^{N}. \qquad (D.7)$$

References

[1] Technical Staff of CSELT (Centro Studi e Laboratori Telecomunicazioni), Optical Fiber Communication, Torino, Italy. McGraw-Hill, U.S.A., 1981, pp. 1-6.

[2] A. N. Hall, G. E. Fenner, T. D. Kingsley, T. J. Soltyo, R. O. Carlson, "Coherent light emission from GaAs junctions", Phys. Rev. Lett., Vol. 1, Nov. 1962, pp. 366-378, cited in Technical Staff of CSELT, op. cit., p. 3.

[3] H. I. Nathan, W. P. Dumbe, G. Burns, F. H. Dill, G. J. Lasher, "Stimulated emission of radiation from GaAs p-n junctions", Appl. Phys. Lett., Vol. 1, Nov. 1962, pp. 62-64, cited in Technical Staff of CSELT, loc. cit.

[4] I. Hayashi, M. B. Panish, P. W. Foy, S. Sumelay, "Junction lasers which operate continuously at room temperature", Appl. Phys. Lett., Vol. 12, No. 12, 1976, pp. 310-312, cited in Technical Staff of CSELT, loc. cit.

[5] H. Kressel, ed., "Laser Diodes and LEDs for Fiber Optic Communications", Semiconductor Devices for Optical Communications, Springer-Verlag, 1980, pp. 54-59.

[6] K. C. Kao, G. A. Hockam, "Dielectric fiber surface waveguides for optical frequencies", Proc. IEEE, Vol. 113, 1966, pp. 1151-1158, cited in Technical Staff of CSELT, op. cit., p. 2.

[7] F. P. Kapron, D. B. Keck, "radiation losses in glass optical waveguides", Trunk Telecommunications by Guided Waves, London, Sept. 29 - Oct. 2, 1970, cited in Technical Staff of CSELT, op. cit., p. 3.

[8] R. D. Maurer, First European Electro-optics Market and Technology, Geneva, Sept. 12-15, 1972, cited in Technical Staff of CSELT, loc. cit.

[9] M. Horiguchi, H. Osanai, "Spectral losses of low-OH-content optical fibers", Electronics Letters, Vol. 12, No. 12, 1976, pp. 310-312, cited in Technical Staff of CSELT, op. cit., pp. 4.

[10] T. Miyashita, T. Miya, M. Nakahara, "An ultimate low loss single mode fiber at 1.55 um", Optical Fiber Communication, Washington, D.C., Mar. 6-8 1979, cited in Technical Staff of CSELT, loc. cit.

[11] G. Antell, K. Hess, W Muska, J. Rozenbergs, Electrical Communication, the Technical Journal of the International Telephone and Telegraph Corporation, Vol. 56, No. 4, 1981, pp. 349-357.

[12] D. A. Duke, "The Fiberoptic Industry in 1983: A Status Report", Laser Focus (incl. Electro-Optics) Magazine, Vol. 19, No. 9, Sept. 1983, pp. 155-164.

[13] Yasuhara Suematsu, "Long-Wavelength Optical Fiber Communication", Proc. IEEE, Vol. 71, No. 6, June 1983, pp. 692-721.

[14] Li Tingye, "Advances in Optical Fiber Communications: An Historical Perspective", IEEE Journal on Selected Areas in Communications (hereafter cited as JSAC), Vol. SAC-1, No. 3, April 1983, pp. 356-372.

[15] Detlef Gloge, Li Tingye, "Multimode-Fiber Technology for Digital Transmission", Proc. IEEE, Vol. 68, No. 10, Oct. 1980, pp. 1269-1274.

[16] K. Ogawa, "Considerations for Single-Mode Fiber Systems", Bell System Technical Journal (hereafter cited as BSTJ), Vol. 61, No. 8, Oct. 1982, pp. 1919-1931.

[17] D. B. Keck, "Single-mode fibers outperform multimode cables", IEEE Spectrum, Vol. 20, No. 3, Mar. 1983, pp. 30-37.

[18] P. R. Ball, M. J. Bennett, "Extending the range of long wavelength multimode optical fiber transmission using decision feedback", Eighth European Conference on Optical Communication (hereafter cited as ECOC-8), Cannes, France, 21-24 Sept. 1982, pp. 406-410.

[19] M. Dippold, "Receivers for High Bit-rate Digital Transmission on Graded Index Fibres with Decision Feedback Equalization", AEU, Vol. 37, 1983, pp. 15-24. In German.

[20] T. V. Muoi, J. L. Hullett, "Receiver Design for Multilevel Digital Optical Fiber Systems", IEEE Transactions on Communications, Vol. 23, No. 9, Sept. 1975, pp. 987-994.

[21] R. Petrovic, "Multilevel Signalling over Step-Index Fibers", IEEE Transactions on Communications, Vol. COM-28, No. 2, Feb. 1980, pp. 294-297.

[22] R. Petrovic, "Multilevel Signals in Digital Optical-Fiber Communications", Electron. Lett., Dec. 7 1978, Vol. 14, No. 25, pp. 806-808.

[23] J. Wozencraft, I. Jacobs, Principles of Communication Engineering, John Wiley and Sons, Inc., 1965, pp. 285-323.

[24] J. Proakis, Digital Communications, McGraw-Hill Co., 1975, pp. 240-322.

[25] R. Ziemer, W. Tranter, Principles of Communications: Systems, Modulation, and Noise, Houghton Mifflin Co., 1976, pp. 337-338.

[26] Technical Staff of CSELT, op. cit., pp. 723-775.

[27] J. Salz, "Optimum Mean-Squared Decision Feedback Equalization", BSTJ, Vol. 52, No. 8, Oct. 1973, pp. 1341-1373.

[28] B. L. Kasper, "Equalization of Multimode Optical Fiber Systems", BSTJ, Vol. 61, No. 7, Sept. 1982, pp. 1367-1388.

[29] J. E. Midwinter, "First-Generation Trunk Transmission Systems: Capabilities and Limitations", JSAC, op. cit., pp. 356-372.

[30] Federico Tosco, "Optical-fiber communications in the 0.8 - 0.9 um wavelength region: applications and perspectives", ECOC-8, op. cit., pp. 9-16.

[31] Product information on Corguide First Window Fiber #2710F, Telecommunication Products Dept., Corning Glass Works, Corning, New York, 14831, May 1, 1982.

[32] R. W. H. Engelmann, "Bandwidth Formulas for Chromatic Limitation in Optical Fibers", Electron. Lett., Vol. 17, No. 9, Apr. 30 1981, pp. 333-334.

[33] D. Gloge, K. Ogawa, L. G. Cohen, "Baseband Characteristics of Long-Wavelength LED Systems", Electron. Lett., Vol. 16, No. 10, May 8 1980, pp. 366-368.

[34] Kiyoshi Nakagawa, "Second-Generation Trunk Transmission Technology", JSAC, op. cit, pp. 387-393.

[35] C. J. Lilly, "The state of the art, and applications of optical fiber systems operating at the longer wavelengths of 1300-1600 nm", ECOC-8, op. cit., pp. 17-24.

[36] S. D. Personick, "Review of Fundamentals of Optical Fiber Systems", JSAC, op. cit., pp. 373-380.

[37] H. Yonezu, S. Kalayama, N. Fujine, I. Sakuma, K. Nishida, "Reliability of Light Emitters and Detectors for Optical Fiber Communication Systems", JSAC, op. cit., pp. 508-514.

[38] R. H. Saul, "Recent Advances in the Performance and Reliability of InGaAsP LEDs for Lightwave Communication Systems", IEEE Transactions on Electronic Devices, Vol.xED-30, No. 4, Apr. 1983, pp. 285-295.

[39] K. Ogawa, "Considerations for Optical Receiver Design", JSAC, op. cit., pp. 524-532.

[40] S. R. Forrest, G. F. Williams, O. K. Kim, R. G. Smith, "Excess-noise and Receiver Sensitivity Measurement of InGaAs/InP Avalanche Photodiodes", Electron. Lett., Vol. 17, No. 24, Nov. 26, 1981, pp. 917-919.

[41] T. Mikawa, S. Kagawa, T. Keneda, T. Sakurai, H. Ando, O. Mikami, "A Low-Noise n^{+}np Germanium Photodiode", Journal of Quantum Electronics, Vol. QE-17, 1981, p. 210.

[42] T. P. Lee, C. A. Burrus, A. G. Dentai, K. Ogawa, "Small Area InGaAs/InP p-i-n Photodiodes: Fabrication, Characteristics, and Performance of Devices in 274 Mb/s and 45 Mb/s Lightwave Receivers at 1.31 um Wavelength", Electron. Lett., Vol. 16, Feb. 14 1980, pp. 155-156.

[43] D. R. Smith, A. K. Chattergee, M. A. Z. Wake, B. R. White, "Pin-Fet Hybrid Optical Receiver for 1.1-1.6 um Optical Communication Systems", Electron. Lett., Vol. 16, No. 19, 11 Sept. 1980, p. 750.

[44] T. Mikawa, T. Kaneda, H. Nishimoto, M. Motegi, H. Okushima, "Small-Active-Area Germanium Avalanche Photodiode for Single-Mode Fiber at 1.3 um Wavelength", Electron. Lett., Vol. 19, No. 12, June 9 1983, pp. 452-453.

[45] J. Proakis, Digital Communications, McGraw-Hill Co., 1983, pp. 334-386.

[46] A. Bruce Carlson, Communication Systems - An Introduction to Signals and Noise in Electrical Communication, McGraw-Hill, 2nd. Ed., 1975, pp. 376-387.

[47] W. F. McGee, "Coding, equalization, and feedback of digital cable pair signals", Canadian Electronics Engineering Journal, Vol. 7, No. 1, 1982, pp. 4-8.

[48] R. Ziemer, W. Tranter, op. cit., pp. 337-338.

[49] Technical Staff of CSELT, op. cit., pp. 703-721.

[50] D. G. Messerschmidt, "Zero-Forcing and Decision-Feedback Equalization of Digital Fiber Optic Systems", IEEE 1980 International Symposium on Circuits and Systems, Vol. 1, Apr. 28-30 1980, pp. 943-946.

[51] D. Messerschmidt, "Minimum MSE Equalization of Digital Fiber Optic Systems", IEEE Transactions on Communications, Vol. COM-26, No. 7, July 1978, pp. 1110-1118.

[52] M. S. Mueller, J. Salz, "A Unified Theory of Data-Aided Equalization", BSTJ, Vol. 60, No. 9, Nov. 1981, pp. 2023-2038.

[53] Product infomation on Siecor Super Fat Fiber Cable #155, Siecor Optical Cables, Inc., Hickory, North Carolina, 155FR(9/80 MA)

[54] Product information on Northern Telecom's High Radiance Infrared LEDs # NT 40-3-30-2 and NT 40-3-30-3. Data Sheet No. 14012/01, Sept. 1978

[55] C. H. Roth, Jr., Fundamentals of Logic Design, 2nd edition, West Publishing Co., 1979, p. 13.

[56] U. Mengali, E. Pezzani. "Tracking Properties of Phase-Locked Loops in Optical Communication Systems", IEEE Transactions on Communications, Vol. COM-26, No. 12, 1978, pp. 1811-1818.

[57] U. Mengali, "Timing Recovery in Optical Data Transmission", Optical and Quantum Electronics, Vol. 9, 1977, pp. 383-391.

[58] R. Doglioti, A. Luvison, G. Pirani, "Timing Error Tolerant Waveforms in Optical Fiber Systems", Optical and Quantum Electronics, Vol. 11, 1979, pp. 541-550.

[59] S. D. Personick, "Receiver Design fpr Digital Fiber Optic Communication Systems, part 1.", BSTJ, Vol. 52, No. 6, July - Aug. 1973, pp. 843-875.

[60] S. D. Personick, "Receiver Design for Optical Fiber Systems", Proc. IEEE, Vol. 65, No. 12, 1977, pp. 1670-1678.

[61] J. E. Goell, "An Optical Repeater with High-Impedance Input Amplifier", BSTJ, Vol. 53, Apr. 1974, pp. 629-643.

[62] D. R. Smith, I. Garrett, "A simplified approach to digital optical receiver design", Optical and Quantum Electronics, Vol. 10, 1978, pp. 211-221.

[63] W. Albrecht, C. Baach, "A Broad-Band Opto-Electronic Receiver with Bipolar Transistors", Journal of Optical Communications, Vol. 2, No. 1, 1981, pp. 24-25.

[64] M. H. El-Diwany, D. J. Roulston, S. G. Chamberlain, "Design of low-noise bipolar transimpedance preamplifiers for optical receivers", IEE Proc., Vol. 128, Pt. G, No. 6, Dec. 1981, pp. 299-305.

[65] M. J. N. Sibley, R. T. Unwin, "Transimpedance Optical Preamplifier having a Common-Collector Front End", Electron. Lett., Vol. 18, No. 23, 11 Nov. 1982, pp. 985-986.

[66] T. Pearsall, "Photodetectors for Optical Communication", Journal of Optical Communications, Vol. 2, No. 2, 1981, pp. 42-48.

[67] Product information on RCA Electro-Optics and Devices, Photodiodes No. C30904E, C30905E, C30908E (developmental types), 2-1978.

[68] P. Gray, R. Meyer, Analysis and Design of Analog Integrated Circuits, 2nd. Edition, John Wiley and Sons, Inc., 1984, pp. 412-452.

[69] Compact User Manual, Version 4.75, Compact Engineering, Inc., 1978.

[70] Motorola Linear Integrated Circuits, Series C, 2nd printing, Motorola Inc., 1979, pp. 6-51 to 6-59.

[71] S. D. Personick, "Comparison of Equalizing and Nonequalizing Repeaters for Optical Fiber Systems", BSTJ, Vol. 55, No. 7, Sept. 1976, pp. 957-971.

[72] J. Cartledge, "Receiver Sensitivity of Optical Fiber Communication Systems: The Effects of Channel Characteristics and Receiver Filter Design", IEEE Transactions on Communications, Vol. COM-26, No. 7, July 1978. pp. 1103-1109.

[73] L. E. Franks, ed., Data Communication: Fundamentals of Baseband Transmission, Benchmark Papers in Electrical Engineering and Computer Science, Vol. 9, Dowden, Hutchinson and Ross, Inc., 1974, pp. 213-254.

[74] Ibid., pp. 380-392.

[75] Motorola RF Data Manual, 2nd. Ed., 3rd. printing, Motorola Inc., 1982, pp. 17-80 to 17-82.

[76] P. Gray, R. Meyer, op. cit., pp. 31-44.

[77] B. Owen, "PIN - GaAs FET Optical Receiver with a Wide Dynamic Range", Electron. Lett., Vol. 18, No. 14, 8 July 1982, pp. 626, 627.